Computational Studies of Carboxylate-Assisted C-H Activation and Functionalization at Group 8-10 Transition Metal Centers.

David L. Davies,*[,a] Stuart A. Macgregor*[, b] and Claire L. McMullin[b,c]

[a]Department of Chemistry, University of Leicester, Leicester, LE1 7RH, UK

[b]Institute of Chemical Sciences, Heriot-Watt University, Edinburgh, EH14 4AS, UK

[c]Present address: Department of Chemistry, University of Bath, Bath, BA2 7AY, UK

*Corresponding Authors: dld3@leicester.ac.uk; s.a.macgregor@hw.ac.uk

Abstract: Computational studies on carboxylate-assisted C-H activation and functionalization at Group 8-10 transition metal centers are reviewed. The review is organised by metal and will cover work published from late 2009 until mid-2016. A brief overview of computational work prior to 2010 is also provided and this outlines the understanding of carboxylate-assisted C-H activation in terms of the 'ambiphilic metal-ligand assistance' (AMLA) and 'concerted metalation deprotonation' (CMD) concepts. Computational studies are then surveyed in terms of the nature of the C-H bond being activated (C(sp^2)-H or C(sp^3)-H), the nature of the process involved (intramolecular with a directing group or intermolecular) and the context (stoichiometric C-H activation or within a variety of catalytic processes). The review aims to emphasize the connection between computation and experiment and to highlight the contribution of computational chemistry to our understanding of catalytic C-H functionalisation based on carboxylate-assisted C-H activation. Some opportunities where the interplay between computation and experiment may contribute further to the areas of catalytic C-H functionalisation and applied computational chemistry are identified.

1. Introduction

Contemporary computational chemistry provides a major means by which insight into the mechanisms of organometallic reactions and catalysis can be gained. This utility derives from the ability of computational chemistry to routinely characterise reactive intermediates and transition states, thus providing an ideal complement to experiment where data on such species are either extremely difficult or impossible to obtain. Computational chemistry has made a particularly strong contribution to our understanding of the mechanisms of C-H bond activation and progress in this area was the focus of several major reviews published at the end of the last decade.[1,2,3,4,5,6] The importance of computational work in this area reflects the range of mechanistic possibilities that are associated with the C-H activation step: oxidative addition, σ-bond metathesis and electrophilic activation are all available at late transition metal centers, and which mechanism will be active for a given scenario can depend subtely on the metal, its oxidation state and the immediate coordination environment. Carboxylate-assisted C-H activation has added to this landscape, by providing a means of breaking C-H bonds through the combination of an electron-deficient metal center and efficient deprotonation by a carboxylate base. The privileged status of carboxylate bases is in many cases related to their chelating ability which allows them to remain bound to the metal center whilst facilitating an efficient deprotonation through a pendant basic carbonyl arm. Related examples where carboxylates are proposed to act as efficient external bases are also increasing in number.

The last ten years have not only greatly enhanced our mechanistic understanding of C-H activation, but also seen several important developments in computational methodology that have profoundly impacted on the modelling of transition metal reactivity. Although density functional theory (DFT)

remains the most widely used method, the possibility of modelling larger systems has highlighted the known difficulties that DFT has in describing long-range stabilizing dispersion interactions. Although an isolated pairwise dispersion interaction is individually weak, the cumulative effect of many such interactions in larger systems can be very considerable. Dispersion interactions can be taken into account through their separate computation, for example with Grimme's D3 parameter set,[7,8] through the use of functionals such as B97D[9] or ωB97X-D[10] that incorporate dispersion, or by employing a Minnesota functional, such as M06 or its variants,[11] where dispersion effects are captured within the parameterisation scheme. Using these approaches can lead to greatly improved computed energetics, a classic example being L_nM-PR_3 dissociation energies.[12,13,14,15,16,17] These developments highlight the importance surrounding the choice of functional for a computational study, and in particular when larger models are to be employed in the calculations.[18, 19]

More recently, the focus of experimental work has moved toward integrating C-H activation processes into catalytic cycles for organic transformations.[20,21,22,23,24,25,26,27,28,29,30,31,32,33] Computational work has mirrored this trend[34,35,36,37,38,39,40,41,42] with studies on catalytic cycles featuring both C-H activation *and* functionalization becoming increasingly the norm. Such studies reveal the complexity of these multiple-step processes, both from a mechanistic viewpoint, as well as the speciation of the active species performing the catalysis. In principle, calculations are ideally placed to assess different mechanistic possibilities; however, the complexity of the reaction systems often means that computational studies are most effective when they are conducted in close collaboration with experiment. Such studies, when coupled with the advances in computational chemistry, can then permit a more quantitative assessment of a computed reaction mechanism.

2. Scope and Nomenclature

This review will cover computational studies on carboxylate-assisted C-H activation and functionalization at Group 8-10 transition metal centers. The scope of the review will be broadened to cover reactions exploiting other chelating bases that act in a similar way to carboxylates (i.e. they

are potential κ^2-ligands such as carbonate or phosphates). The review will be organised by metal, with Group 10 metals covered first, reflecting the propensity of Pd catalysis in this area, followed by Group 9 and then Group 8. The review will focus on the literature published since the major computational reviews on C-H activation published in 2009/early 2010,[1,3] i.e. from late 2009 to mid-2016. A brief overview of computational work prior to 2010 will be given to provide appropriate context. Some aspects of this review have been summarised elsewhere, but are included here for completeness.[43,44]

Most studies reported in this review have employed DFT calculations and in each case the main computational protocol used to arrive at the final reported energetics will be highlighted. This will include the functional employed for optimisation, with any corrections to the energies being noted in parenthesis. Thus BP86(toluene, D3) indicates use of the BP86 functional for optimisation with single-point energy corrections for toluene solvent and dispersion effects using the D3 parameter set. In cases where one functional is used for optimisation and a second for the energy calculation the // convention will be used, e.g. BP86(toluene, D3)//B3LYP indicates initial optimisation with B3LYP followed by a single point energy calculations with BP86 with corrections for toluene solvent and dispersion effects. Any exceptions to these approaches will be highlighted in the text and the original literature should be consulted for full computational details.

As mentioned in the Introduction, the trend in the period covered in this review has been towards the use of dispersion-corrected functionals; however this does not mean that results obtained in studies that neglect dispersion effects are necessarily invalid. The computed trends and the mechanistic ideas obtained in such studies can still give valuable insight, especially if focussed on electronic effects arising from small models. However, the dramatic effect of the dispersion correction on reaction energetics – particularly those steps featuring ligand dissociation – means that studies purporting a quantitative assessment of computed energetics that do not include dispersion in the protocol should be viewed with caution.

In general the reported 'energy' will be a free energy computed at standard conditions (298.15 K and 1 atm) and usually corrected for solvent and possibly dispersion effects as detailed above. If relevant, cases where other temperatures are employed will be highlighted in the text. The multi-step processes involved in catalysis mean that different scenarios arise when describing the associated energetics. Firstly, the term 'energetic span' will be used to denote the overall activation barrier associated with a catalytic cycle, as recommended by Kozuch and Shaik.[45] The energetic span corresponds to the difference in energy between the lowest lying intermediate and the highest lying transition state and will generally be abbreviated to $\Delta G^{\ddagger}_{span}$. The activation barriers or thermodynamic changes associated with a series of consecutive steps that do not themselves correspond to the energetic span will be referred to as an 'overall $\Delta G^{\ddagger}$', or 'overall ΔG' respectively, and this is distinct from the use of '$\Delta G^{\ddagger}$' or 'ΔG' to describe the energetics of a single step between two minima linked by a single transition state. In diagrams the energies of transition states will be denoted in square brackets and dashed arrows will be used to denote multi-step processes; in the latter case the transition state energy provided will be the highest point between the two minima indicated.

The vast majority of the work covered in this review features computational studies that refer directly to specific experimental systems. Increasingly both these aspects are contained within a single paper and in such cases the details of the experimental system being modelled will be provided. Otherwise the cited computational work should be consulted for details of the original experimental work. In many cases the computed reaction profiles can be viewed qualitatively in terms of the efficiency of an experimental process; for example, a computed energy span may reflect the reaction conditions that are required for efficient catalysis. Such an assessment can be challenging, however, not only because of the multiple-step nature of catalysis, but also because under catalytic conditions the substrates will be in large excess and so can significantly bias equilibria and hence overall rates. Studies that include kinetic data both from experiment and from kinetic simulations fed by computed energetics are therefore particularly valuable.

3. Overview of pre-2010 Studies on Carboxylate-Assisted C-H activation at Group 8-10 Metals

The first computational work on carboxylate-assisted C-H activation was reported by Sakaki in 2000 who reported an MP4(SDQ) study of the intermolecular C-H activation of both benzene and methane at [M(κ^2-$O_2CH)_2$] (M = Pd, Pt).[46] For both substrates the mechanism involved a two-step process with the initial κ^2-κ^1-displacement of one formate ligand to give intermediate σ-complexes featuring short M···C-H and C-H···O contacts (see **2a,b** for M = Pd, Figure 1). These interactions facilitate the subsequent heterolytic cleavage of the C-H bonds. This remarkable study presages much of the subsequent computational work in this area. In particular, the similar mechanisms of activation for both aromatic and aliphatic C-H bonds are seen, as well as the greater kinetic and thermodynamic accessibility of aromatic C(sp^2)-H activation at Pd. While this is also true for the thermodynamics of C-H activation at Pt, in that case benzene forms a particularly stable σ-complex at -21.1 kcal/mol from which the barrier for C-H cleavage is 21.3 kcal/mol. A similar two-step process was subsequently characterised by Goddard and Periana with B3LYP calculations for benzene activation at [Pt(bpym)$(TFA)_2$] and [Pt(pic)$(TFA)_2]^-$ species (bpym = 2,2'-bipyrimidyl, pic = κ^2-N,O-picolinate; TFA = trifluoroacetate).[47] In this case the TFA derived from the trifluoroacetic acid (TFAH) solvent facilitates the C-H activation.

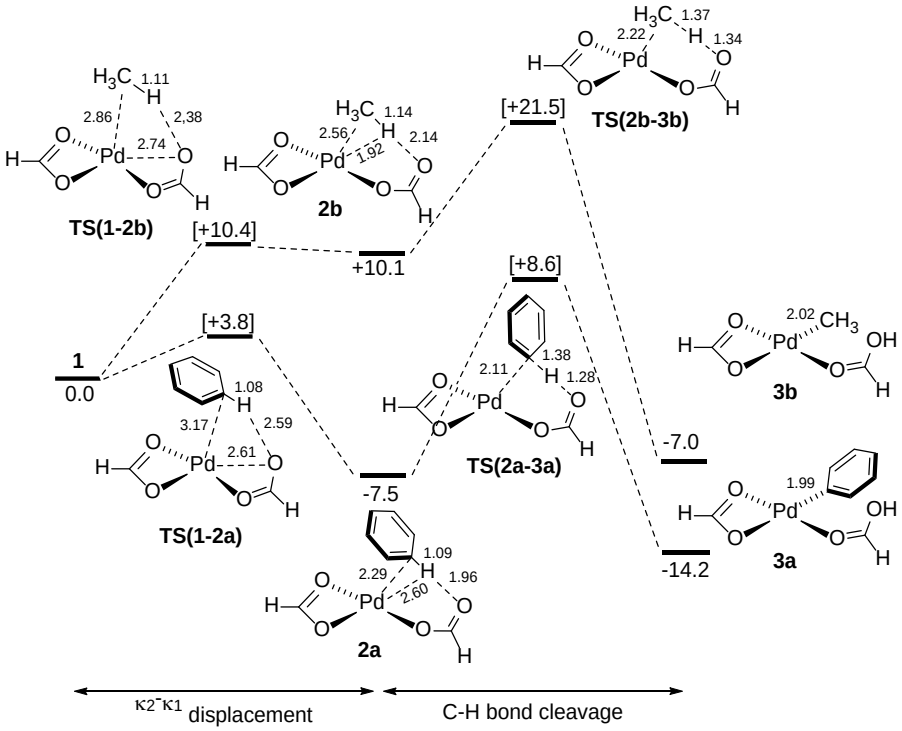

Figure 1. Computed reaction profiles for C-H activation of CH_4 and C_6H_6 at [Pd(κ^2-$CO_2H)_2$]; MP4(SDQ) energies are in kcal/mol and are quoted relative to a non-covalent precursor complex, **1**, at 0.0 kcal/mol in each case; selected distances in Å. Adapted with permission from Ref. 46. Copyright 2000 American Chemical Society.

The first computational study of intramolecular C-H activation featuring a directing group was reported in 2005 by Davies and Macgregor who used BP86 calculatons to model the cyclometalation of dimethylbenzylamine at [$Pd(OAc)_2$],[48] a system that had been extensively studied experimentally in the 1980s by Ryabov and co-workers (Figure 2).[49] Starting from a [$Pd(OAc)_2(Me_2NCH_2Ph)$] precursor, **4**, a two-step C-H activation process was again computed, with the first step involving the κ^2-κ^1 displacement of the OAc ligand by the *ortho*-C-H bond of the benzyl group via **TS(4-5)**. This leads to the formation of an agostic intermediate, **5**, which features a polarised C-H bond that is, as a consequence, able to engage in H-bonding with the free arm of the κ^1-OAc ligand. Cleavage of this C-H bond then proceeds with a minimal barrier via a 6-membered transition state, **TS(5-6)**, and forms the cyclometallated product, **6**, as an HOAc adduct. An overall barrier of 13 kcal/mol was computed with **TS(4-5)** being the highest point on the profile. Other mechanisms based on either H^+ transfer

onto the Pd-bound acetate oxygen (i.e. via a 4-membered transition state) or oxidative addition to form a Pd(IV) intermediate exhibited much higher computed barriers. This study is important in highlighting the central role played by an agostic intermediate in carboxylate-assisted C-H activation. A Wheland (or arenium) species was specifically ruled out, indicating that a fundamentally different mechanism to electrophilic aromatic substitution (S_EAr) is operative in this case. This type of mechanism was later termed 'ambiphilic metal-ligand assistance' (AMLA), a description that emphasizes how an electron-deficient metal center can combine with an adjacent intramolecular base to promote facile C-H bond activation.[3] This mechanism also modelled the small rate-enhancement associated with an electron donating meta-substituent on the DMBA ring. As AMLA involves an agostic intermediate it should not (unlike S_EAr) be restricted to the C-H activation of aromatic C-H bonds; indeed a computed barrier of only 20 kcal/mol was computed for the analogous C(sp^3)-H activation of $Me_2NCH_2CH_2CH_3$. This ability to activate C(sp^3)-H bonds was prefaced in even earlier work by Kragten and co-workers who postulated that the acetate ligand in $[Pd(OAc)(CH_2CH_2OH)(H_2O)_2]$ could assist in β-H transfer from the β-hydroxyethyl ligand, a key step in vinylacetate formation.[50]

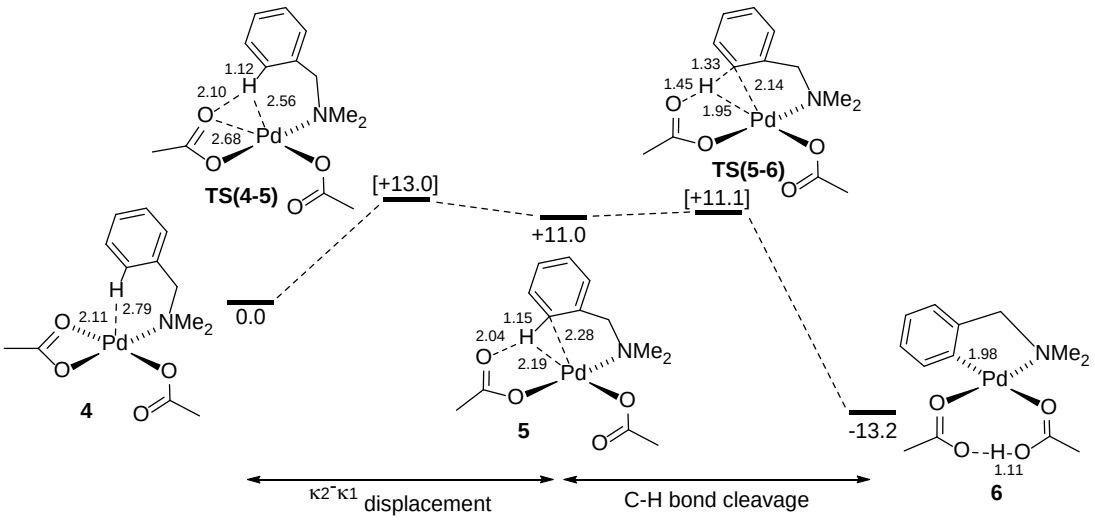

Figure 2. Computed reaction profile for C-H activation in $[Pd(OAc)_2(Me_2NCH_2Ph)]$. Energies are in kcal/mol and include a correction for zero-point energies; selected distances in Å.[48] Adapted with permission from Ref. 43. Copyright 2016, John Wiley and Sons.

Shortly afterwards Maseras and Echavarren reported B3LYP calculations on C-H activation in [Pd(2-phenethylphenyl)(X)(PH_3)] species (**7**, X = Br or HCO_3, Figure 3), as model intermediates for intramolecular C-C coupling catalysed by [$Pd(OAc)_2$].[51] Initial oxidative addition of an aryl bromide precursor forms the Pd-aryl bond which subsequently acts as a directing group for C-H activation. With X = HCO_3 this proceeds by proton abstraction *via* **TS7A** in a similar fashion to that described above for [$Pd(OAc)_2(Me_2NCH_2Ph)$], although in this case a one-step process was defined and no agostic intermediate was located. When X = Br, proton abstraction by the bromide ligand proved inaccessible, however, deprotonation by external bicarbonate (**TS7B**) was competitive. Both the internal and external deprotonation mechanisms were subsequently shown to be consistent with reactivity enhancements seen experimentaly when electron-withdrawing substituents (F, Cl) were introduced into the aryl ring.[52] This trend would clearly be at odds with a traditional S_EAr mechanism.

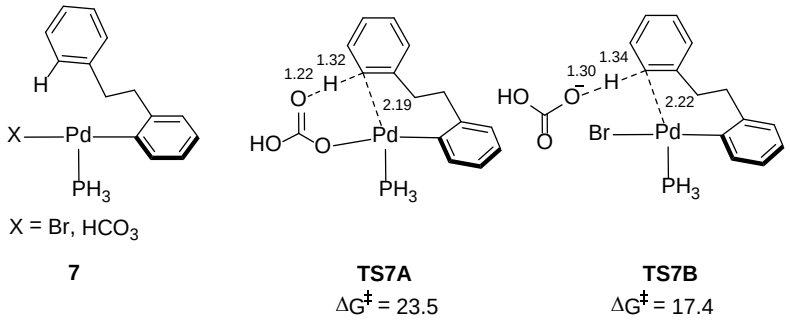

Figure 3. C-H activation in **7** via internal (**TS7A**) or external (**TS7B**) proton abstraction. Computed relative SCF energies in kcal/mol and key distances in Å.[52] Adapted with permission from Ref. 43. Copyright 2016, John Wiley and Sons.

Further evidence for the significance of agostic interactions in carboxylate-assisted C-H activation was provided by Fagnou who characterized C(sp^3)-H bond cleavage as a key step in the Pd-catalysed synthesis of dihydrobenzofurans (**8** → **9**, Figure 4(a)).[53] Using a [Pd(Ar)(OAc)(PMe_3)] model system and B3LYP calculations, the three distinct C(sp^3)-H bonds of the 2-methylbutoxy substituent were all shown to react via a concerted, inner-sphere deprotonation mechanism (Figure 4(b)). Reaction *via*

TS8a forms a 6-membered palladacycle and this has a lower barrier than C-H activation of either the ethyl CH_2 (*via* **TS8b**) or CH_3 (*via* **TS8c**) groups, where the latter leads to a 7-membered palladacycle. Such one-step C-H activation processes are consistent with 'concerted metalation deprotonation' (CMD) that Fagnou later put forward. Clot and Baudoin also demonstrated intramolecular C(sp^3)-H activation at [PdAr(CO_3^-)(PR_3)] (Ar = 2-^{t}BuC_6H_4) species with carbonate as the internal base (B3PW91(DMF) calculations).[54] In this case the carbonate was situated trans to the agostic interaction but the geminal C-H bond was sufficiently protic to enable an intramolecular C-H cleavage via **TS10** (Figure 4(c)). Lledós and Urriolabeitia also found that related computed processes could account for selectivities seen in the cyclometalation of stabilised iminophosphoranes, Ar_3P=NC(O)Ph at [Pd($OAc)_2$] (B3LYP(CH_2Cl_2) calculations).[55]

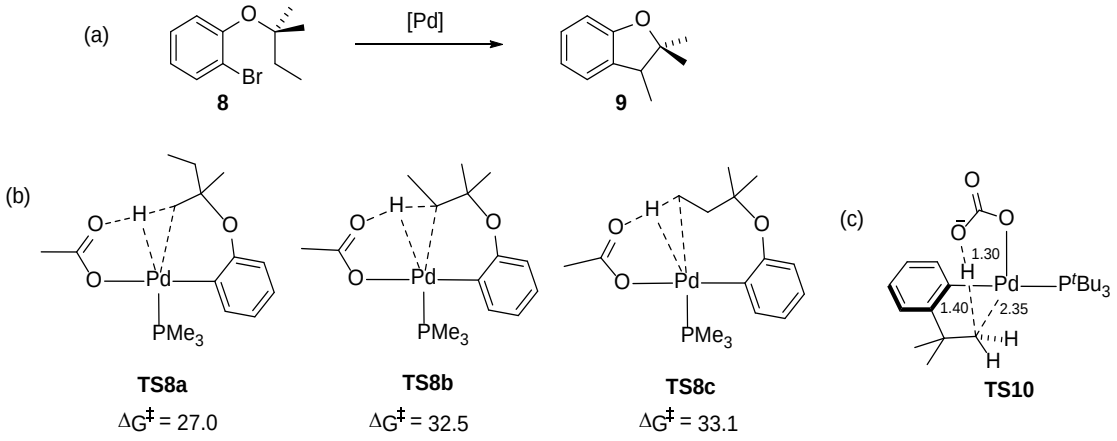

Figure 4. (a) Pd-catalysed reaction of **8** to form dihydrobenzofuran, **9**; (b) alternative C(sp^3)-H activation transition states with computed free energies quoted relative to [Pd(Ar)(OAc)(PMe_3)];[53] (c) computed C(sp^3)-H activation transition state for [Pd(2-^{t}Bu-C_6H_4)(CO_3^-)(P^tBu_3)] with selected distances in Å.[54] Adapted with permission from Ref. 43. Copyright 2016, John Wiley and Sons.

Returning to intermolecular C-H activation, the efficacy of fluorinated arenes in [Pd($OAc)_2$]-catalyzed direct arylations led Fagnou to model their C-H activation reactions.[56] Using [Pd(Ph)(X)(PH_3)] model species (X = Br, HCO_3) B3LYP calculations probed several different mechanisms, the most accessible of which was a one-step non-directed process in which metalation and proton abstraction by the

intramolecular bicarbonate base occurred in a concerted manner (see Figure 5 for the reaction of C_6F_5H via **TS11** in which a P^tBu_2Me ligand is employed and $\Delta G^{\ddagger}$ = 9.9 kcal/mol). Attempts to characterise an S_EAr mechanism were unsuccessful and this, in combination with the enhanced reactivity exhibited by the more acidic fluoroarene C-H bonds, led this group to propose the term 'concerted metalation deprotonation', CMD, to describe such reactions.[2,57] A later report on the C-H activation of benzene gave a reduced barrier of 24.9 kcal/mol when pivalate (OPiv, Piv = $C(O)^tBu$) was employed as the base, compared to a value of 26.2 kcal/mol with HCO_3.[58]

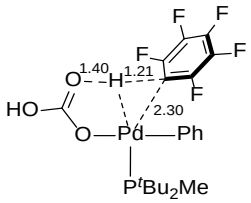

TS11

Figure 5. C-H activation transition state computed for the reaction of C_6F_5H at [Pd(HCO_3)(Ph)(P^tBu_2Me)], with selected distances in Å.[56] Adapted with permission from Ref. 43. Copyright 2016, John Wiley and Sons.

In 2008 Gorelsky and Fagnou generalised the CMD concept by studying the C-H activation of a broad spectrum of (hetero)aromatic substrates (B3LYP calculations). Significantly, the CMD mechanism was shown to be operative even for electron-rich arenes that had previously been considered to react through an S_EAr mechanism.[57] The CMD pathway also accounted for the experimentally observed selectivities, including the reaction at the 2-position of thiophene and *ortho*-C-H activation in pyridine *N*-oxide (Figure 6). Electron-withdrawing substituents again lead to reduced computed barriers, as exemplified in the C2-H activation of 3-fluorobenzothiophene ($\Delta G^{\ddagger}$ = 22.8 kcal/mol) *vs*. the equivalent process in benzothiophene ($\Delta G^{\ddagger}$ = 26.5 kcal/mol). The predicted reactivity trends and regioselectivities were later validated experimentally.[59]

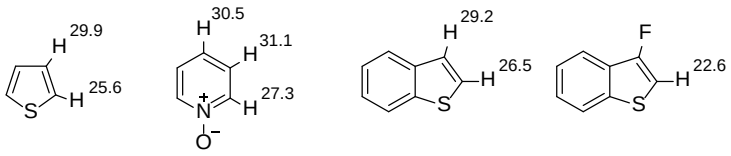

Figure 6. Free energy activation barriers (kcal/mol) computed for C-H activation of selected heterocycles at [Pd(OAc))Ph)(PMe_3)].[57] Reproduced with permission from Ref. 43. Copyright 2016, John Wiley and Sons.

Many of the features described above for carboxylate-assisted C-H activation at Pd(II) species have also been shown to be operative in Rh(III) and Ir(III) systems. In 2006 Davies and Macgregor reported an initial computational study of the cyclometallation of Me_2NCH_2Ph at $[IrCl_2Cp^*]_2$ in the presence of NaOAc.[60,61] Acetate plays two critical roles in this process: first, in promoting opening of the chloro-bridged dimer to access monomeric active species and, second, as an intramolecular base in the C-H activation step. BP86 calculations using a model $[Ir(\kappa^2\text{-OAc})(Me_2NCH_2Ph)Cp]^+$ species characterised a one-step C-H activation in which the κ^2-κ^1 displacement of acetate and deprotonation of the ortho-C-H bond by the free acetate arm occur in a concerted fashion via a single 6-membered transition state. These features are all characteristic of an AMLA/CMD C-H activation and this "AMLA-6" process was clearly favored over either an "AMLA-4" alternative (i.e. where the Ir-bound oxygen effects the deprotonation via a 4-membered transition state) or a concerted oxidative addition pathway that yields an Ir(V)-hydride. In a later study[60] a two-step pathway was characterised featuring an agostic intermediate. This process had a slightly lower barrier of 13.4 kcal/mol in which the κ^2-κ^1 displacement of acetate was rate-limiting. Replacing acetate with a weaker carboxylate base, RCO_2^-, resulted in further reduced barriers to C-H activation (R = CF_3 < CCl_3 < HO < Ph < Me). As weaker bases are also poorer ligands, these will tend to facilitate the rate-limiting κ^2-κ^1 displacement step. The cyclometalation of *N*-methyl-2-pyrrole-imine was also considered around this time and also adhered to the AMLA/CMD mechanistic scheme.[62]

Ess, Periana and Goddard subsequently reported on the C-H activation of benzene and methane at [Ir(acac')$_2$(X)] species (X = OH, OAc, Figure 7; B3LYP calculations).[63] With X = OAc C–H activation is most accessible via a two-step process in which the initial κ^2- κ^1-displacement of OAc is rate-limiting. Overall barriers of 32.6 kcal/mol were computed for both benzene and methane, with C-H bond cleavage occurring via the 6-membered transition states **TS12** and **TS13** respectively. Use of the activation strain model (see Section 4.3) showed these processes were associated with a low ΔE_{dist} term; in comparison the alternative 4-membered transition states (in which proton transfer involves the Ir-bound oxygen) are more constrained and lie approximately 19 kcal/mol higher in energy. The 4-membered transition states computed for acetate and hydroxide are very similar geometrically and, although technically not within the remit of this review on carboxylate-assisted C-H activation, such processes that involve the 1,2 addition of a C-H bond across a M-X single bond (X = OR, NR_2) are worth highlighting as being related to an AMLA/CMD process: in both cases the availability of a lone pair of electrons on the ligand is central to facilitating an intramolecular deprotonation.[64] Ess, Goddard and Periana[65, 66, 67] and Gunnoe and Cundari[68] have all contributed significantly to this area.

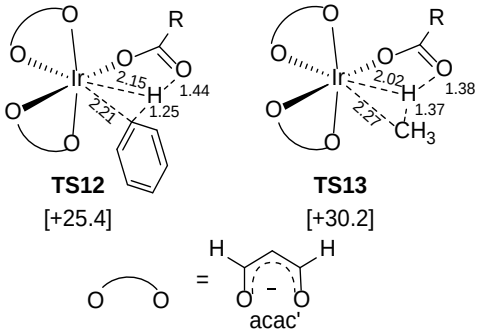

Figure 7. Computed transition states for C-H activation of benzene and methane at [Ir(acac')$_2$(κ^2-OAc)] with computed free energies (kcal/mol) and selected distances in Å. Adapted with permission from Ref. 63. Copyright 2000 American Chemical Society.

The only computational study on carboxylate-assisted C-H activation at a Group 8 metal to predate the period of this review was reported by in 2008 by Maseras and Dixneuf who modelled the

cyclometalation of 2-phenylpyridine (**ppy**) at $[RuCl_2(p\text{-cymene})]_2$ in the presence of *N*-heterocyclic carbene (NHC) co-ligands.[69] B3LYP calculations on a *cis*-$[RuCl_2(IMe)(\mathbf{ppy})]$ model system (IMe = 1,3-dimethylimidazol-2-ylidene) indicated a strong agostic interaction that developed *trans* to the IMe ligand. Despite this the energetics associated with a concerted oxidative addition to form a Ru(IV)-hydride were very unfavourable. Instead initial coordination of bicarbonate was preferred and from this structure a low energy deprotonation was defined *via* **TS14** (Figure 8). This proceeds with a barrier of only 13.9 kcal/mol and involves C-H bond cleavage concomitant with the dissociation of bicarbonate, which leaves the coordination sphere as H_2CO_3.

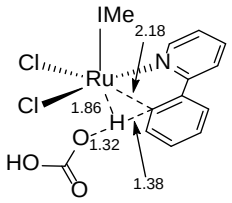

TS14

Figure 8. Computed transition state for C-H activation of 2-phenylpyridine at {*cis*-$Ru(Cl)_2(IMe)$} in the presence of bicarbonate; selected distances in Å.[69] Adapted with permission from Ref. 43. Copyright 2016, John Wiley and Sons.

Overall, these early studies of carboxylate-assisted C-H activation highlight a number of key common features. These include the combination of an electron-deficient metal center and a carboxylate base that act in concert to facilitate C-H bond cleavage. Computationally, this is most evident when an agostic intermediate is located as this allows the polarisation (and hence enhanced acidity) of the C-H bond to be defined, which is thus readily abstracted by the pendant arm of the carboxylate base. Under these circumstances C-H activation becomes a simple acid-base reaction. This picture also rationalises how these systems can perform $C(sp^3)$-H bond activation.

An important component of the overall C-H activation process is the need to make a vacant coordination site available at the metal center. In the above examples this involves the κ^2- κ^1-

displacement of the carboxylate base by the incoming substrate and in many cases this contributes significantly to (or may actually be the major component of) the overall barrier. Whether C-H activation is achieved as a one- or two-step process appears rather system-dependent and for intramolecular C-H activation the associated energy surface is generally rather flat. This suggests that any agostic intermediates would not have a significant lifetime. While the two transition states involved can be distinguished computationally, whether the first (carboxylate κ^2-κ^1-displacement) or the second transition state (C-H bond cleavage) is the higher could be viewed as corresponding to either an early or a late transition state, respectively. Although energetically this distinction may not be significant, these transition states have very different degrees of C-H bond elongation and so will impact on the interpretation of experimental observables such as k_H/k_D kinetic isotope effects (KIEs).[70]

One particular strength of computational chemistry is its ability to probe different mechanistic scenarios. Thus the possibility of carboxylates acting as an external base after dissociation from the metal coordination sphere has been considered. Other mechanisms (concerted oxidative addition, proton transfer onto a halide or the metal-bound oxygen of the carboxylate) have consistently been shown to be less accessible. Likewise, with aromatic substrates no evidence for an S_EAr process was reported. Experimentally, such a mechanism is often invoked for aromatic C-H bond activation on the basis of empirical ring substituent effects, i.e. where the reaction is enhanced by electron-donating groups. However, as described above[57,48] computational studies have shown that such groups can also promote C-H activation via the AMLA/CMD pathways. Computational evidence for the alternative S_EAr mechanism in carboxylate-assisted C-H activation would rely on the computed structure and charge distribution of any putative Wheland-type stationary point, as well as capturing any experimental substituent effects through changes in activation barriers. To date no convincing computational evidence for such a process has been reported when carboxylate assistance has been involved in the C-H activation.

What do we call carboxylate-assisted C-H activation? The two terms, 'ambiphilic metal-ligand assistance' (AMLA) and 'concerted metalation deprotonation' (CMD), provide similar interpretations of the mechanism of carboxylate-assisted C-H activation. 'AMLA' stresses the dual role of metal and base in promoting the C-H activation. Being a ligand, the base is necessarily bound to the metal center and this is a significant point, as in many cases the use of simple monodentate bases such as amines does not permit the C-H activation. This chelating ability of carboxylates probably lies behind the dominance of such bases in practical schemes for C-H activation and functionalization. This behaviour is also readily generalised to other chelating bases, several examples of which will be given below. 'CMD' captures the processes that occur during the C-H bond activation: a metal-carbon bond forms as the C-H bond is deprotonated. This description can encompass cases where the carboxylate is bound as a ligand at the metal (an internal base) or where it has fully dissociated (an external base). In the following we shall refer to the former mechanism as AMLA/CMD and to the latter as 'external CMD'. For AMLA it can be taken that a 6-membered transition state is involved unless otherwise stated.

The above survey highlights the emphasis of early work on Pd(II) and Ir(III). This has now dramatically expanded, in particular to Rh(III), but also to Ru(II) metal centers. Little work has been reported on either osmium or platinum, and the first computational studies on carboxylate-assisted C-H activation at cobalt and nickel systems have also only appeared during the period of this review. We are not aware of any work on carboxylate-assisted C-H activation at iron.

Recently the emphasis of computational work has moved from the C-H activation step to the modelling of processes that integrate this into catalytic cycles for C-H functionalisation. The complexity of the catalytic systems used experimentally presents many challenges. In response, the computational state-of-the-art will model the full catalyst and substrates used experimentally (i.e. without any truncation of ligands or recourse to model systems) and include the effects of implicit solvation (via continuum methods) and dispersion. Conformational searching would also be included

for large flexible systems. An additional level of complexity arises from the use of additives - generally simple inorganic metal salts, MX - in experimental protocols, the presence of which enhances catalytic efficiency. An accurate treatment of such species as separate ions in solution would require the use of explicitly solvated models, necessitating many solvent molecules in the calculation and requiring molecular dynamics techniques. The use of such methods is currently impractical for the sorts of systems under study here. Efforts to model additive effects have, in many cases, considered these salts to be present as discrete molecular ion-pairs, 'MX'. This may be somewhat unrealistic, especially in higher polarity solvents. In the following when additives are included and modelled in this way, they will be placed in inverted commas in the text to highlight the uncertainly of their true speciation in solution.

4. Palladium

4.1 Intramolecular C(sp^2)-H Activation

Since the initial work outlining the key features of carboxylate-assisted C-H activation a number of studies have proposed variations on the AMLA/CMD theme. Other factors that may affect these processes have also been considered, including the non-innocent roles of solvent, additives and alternative bases within the metal inner- and outer-coordination sphere. The precise details of the mechanism can therefore vary depending on the circumstances.

Given the above, the electrospray ionisation-mass spectrometry (ESI-MS) study reported by Roithova on the C-H activation of 2-phenylpyridine (**ppy**) at [$Pd(OAc)_2$] is important as it occurs in the gas-phase in the absence of any external factors.[71] After reaction in acetonitrile a mixture with a parent ion at *m*/*z* 475 is produced and formulated as either [Pd(OAc)(**ppy**)$_2$]$^+$ and/or [Pd(HOAc)(**ppy**)(**ppy**')]$^+$ (where here and throughout the prime will indicate a cyclometallated ligand). Collision induced dissociation (CID) of HOAc occurs with an energy of 15.5 ± 0.7 kcal/mol, suggesting either facile C-H activation already in solution, or a combination of facile C-H activation and HOAc loss in the CID

experiment. B3LYP(D2) calculations based on a $[Pd(\kappa^2\text{-}OAc)(\mathbf{ppy})_2]^+$ precursor locate an intermediate at +10.5 kcal/mol with short contacts from Pd to one *ortho*-C-H bond which undergoes a subsequent AMLA/CMD C-H activation with an overall barrier of 19.8 kcal/mol. C-H activation is slightly exothermic (ΔH = -1.9 kcal/mol), in contrast to the $[Ru(OAc)(\mathbf{ppy})(\eta\text{-}C_6H_6)]^+$ (ΔH = +3.3 kcal/mol) system also reported in this work. B3LYP(D2) gives a computed HOAc dissociation enthalpy from $[Pd(HOAc)(\mathbf{ppy})(\mathbf{ppy}')]^+$ of 18.9 kcal/mol, which falls to 15.3 kcal/mol with B3LYP(D3), in good agreement with experiment. In contrast, B3LYP gives a value of 6.9 kcal/mol, emphasizing the importance of dispersion effects in describing this dissociative process. Note that the gas-phase MS method necessarily results in the detection of charged species such as $[Pd(\kappa^2\text{-}OAc)(\mathbf{ppy})_2]^+$ and that neutral precursors analogous to $[Pd(OAc)_2(Me_2NCH_2Ph)]$ proposed by Ryabov may still be present.[48, 49]

Substrate substituent effects were probed by Martínez and Urriolabeitia in a joint kinetic and computational study on the $[Pd(OAc)_2]$-mediated C-H activation of methyl-phenylglycinate derivatives, **15**, in acetone and toluene.[72] Cyclometalation is promoted by non-H substituents at the N- or C^α-positions, while the outcome is insensitive to the aryl substituents, X. These observations are more consistent with an AMLA/CMD process over S_EAr. B3LYP(toluene or acetone) calculations on selected $[Pd(OAc)_2(\mathbf{15})]$ species define a two-step C-H activation mechanism with overall barriers around 20 kcal/mol, variations in which reproduce the observed reactivity trends. The effect of *N*-methylation is particularly marked as this creates more electron-rich substrates that facilitate the initial $\kappa^2\text{-}\kappa^1$-OAc displacement step. Experimentally, hydrochloride salts are more efficient than the simple amines and this is seen computationally in lower computed barriers associated with a $[PdCl(OAc)(\mathbf{15})]$ precursor. In this case C-H activation proceeds in a single step with no agostic intermediate. The aminophosphonate substrate, **16**, also exhibits a reduced barrier and this system proved amenable to alkoxylation, halogenation and CO insertion processes that were pursued experimentally.

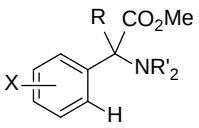

15

R = H, Me, Ph, Bn, ^{t}Bu; R' = H, Me
X = 4-OMe, 4-Br, 3-Br, 3-NO_2, 2-Br

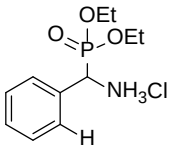

16

Directing group effects were also considered by Fang as part of a study of $MeOCH_2Ph$ and $MeSCH_2Ph$ olefination with methyl acrylate.[73] The thioether is more reactive experimentally and B3LYP(DCE) calculations (where DCE = 1,2-dichloroethane) suggest this reflects its greater coordination ability. This would also aid the κ^2-κ^1 displacement of OAc in the CH activation step. The coordinating abilities of other sp^3- and sp^2-hybridised heteroatom directing groups were compared and found to follow the trends PMe_2 > SMe > NMe_2 > OMe and PMe > NMe > S > O, respectively.

Korenaga has considered the effects of the ancillary phosphine ligand on the energetics of C-H activation at [Pd((2-phenoxymethyl)phenyl)(κ^2-CO_3^-)(PR_3)] species.**[74]** In this study CO_3^{2-} was placed cis to the activating C-H bond rather than the trans arrangement suggested previously with bulky PR_3 ligands.[54] Computed activation barriers (M06-2X//B3LYP) follow the trend PPh_3 (26.8 kcal/mol) > PCy_3 (24.5 kcal/mol) > $P(BFPy)_3$ (23.3 kcal/mol) and so reproduce the accelerating effect of the electron withdrawing $P(BFPy)_3$ ligand ($P(BFPy)_3$ = *tris*-{2,6-bis-CF_3-4-pyridyl}phosphine). $P(BFPy)_3$ is proposed to lower the barrier relative to PPh_3 by promoting a stronger Pd···C interaction. On the other hand NBO analysis indicates that stronger donation from PCy_3 enhances C-H···O H-bonding. Thus C-H activation can be promoted either by creating a more electron-deficient metal center or by enhancing ligand basicity, features that are consistent with the synergy of metal/ligand contributions inherent in the AMLA model.

Granell and Martínez observed accelerated cyclometalation of *N*-methylbenzylimine at $Pd(OAc)_2$ when performed in acetic acid solvent.[75,76] $[Pd(HOAc)_3(MeN{=}CHPh)]^{2+}$ was proposed as the key intermediate and B3LYP(MeOH) calculations (with MeOH chosen to model the dielectric of acetic acid) suggest C-H activation proceeds via initial substitution of one acetic acid ligand by the

approaching *ortho*-C-H bond to form an agostic intermediate with the free acetic acid then performing an external deprotonation to form an H_2OAc^+ cation (see **TS17**, Figure 9). The overall barrier for this process is only 6.8 kcal/mol, with C-H cleavage *via* **TS17** the highest point on the profile. The magnitude of this computed barrier also proved insensitive to the choice of solvent (toluene: $\Delta G^{\ddagger}$ = 6.2 kcal/mol; water: $\Delta G^{\ddagger}$ = 6.7 kcal/mol)

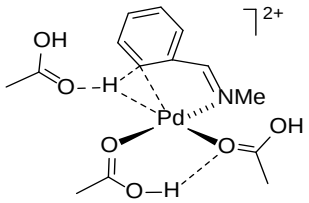

TS17

Figure 9. Transition state for the cyclometallation of *N*-methylbenzylimine at $[Pd(OAc)_2]$ in acetic acid.[75] Adapted with permission from Ref. 43. Copyright 2016, John Wiley and Sons.

Martínez and Urriolabeitia have also compared the alternative C-H activation reactions of (*Z*)-2-aryl-4-arylidene-5(4H)-oxazolones, **18**, at $[Pd(OAc)_2]$ under acidic conditions.[77] The C-H^a arylidene position is favored, giving 6-membered palladacycles that are isolated as carboxylate-bridged dimers. B3LYP(HOAc) calculations (X = Y = H) showed that protonation of the Pd precursors to C-H activation gives reduced barriers, with reaction via a dicationic intermediate, $[Pd(HOAc)_3(\kappa\text{-}N\text{-}\mathbf{18})]^{2+}$, being most in line with experimental activation data. This proceeds by a HOAc loss/external deprotonation pathway, similar to that seen above with *N*-methylbenzylimine.[75] The kinetic preference for activation of the C-H^a bond (and the unusual preference for a 6- over a 5-membered palladacycle) reflects the reduced geometric reorganisation in this case. Replacing HOAc with TFAH gives lower barriers, and the latter system is indeed more reactive experimentally. The detailed energy landscape of these processes varies, C-H bond cleavage being rate-limiting in TFAH, while in acetic acid this corresponds to the dissociation of HOAc.

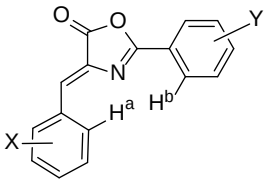

18

Larionov has described the [Pd(OAc)$_2$]-catalysed C8-arylation of quinoline *N*-oxides (**19**) in acetic acid (Figure 10).[78] B3LYP(HOAc) calculations favor reaction via [Pd(HOAc)$_3$(κ-*O*-**19**)]$^{2+}$ and a 5-membered transition state, **TS20**, corresponding to external deprotonation by HOAc. The energetics of this process (overall $\Delta G^{‡}$ = 24.7 kcal/mol, ΔG +14.2 kcal/mol) accord with the H/D exchange seen experimentally. Reaction at the 2-position proves much less accessible (overall $\Delta G^{‡}$ = 40.4 kcal/mol) as it entails a 4-membered transition state. In contrast **19** undergoes C2-H bond activation at [Pd(κ^2-OAc)(Ph)(PMe$_3$)] (overall $\Delta G^{‡}$ = 29 kcal/mol), although this proceeds by an intermolecular C(sp^2)-H activation rather than via using the *N*-oxide moiety as a directing group (see Section 4.3).

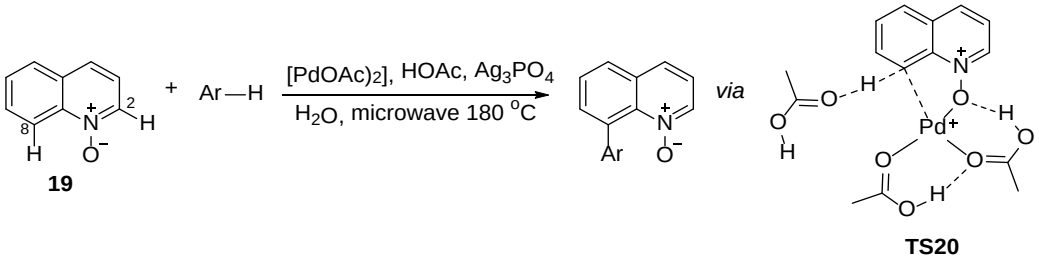

19 **TS20**

Figure 10. (a) Direct, C8-selective arylation of quinoline *N*-oxide, **19**, via **TS20**.[78] Adapted with permission from Ref. 43. Copyright 2016, John Wiley and Sons.

The [Pd(OAc)$_2$]-catalysed hydroxylation of the *N*-bound phenyl group in *N*-methyl-*N*-phenylbenzamide, **21**, indicates selective C-H^a activation to form a 6-membered metallacycle.[79] This reaction proceeds in acidic medium (9:1 TFAH:trifluoroacetic anhydride), although neutral [Pd(TFA)$_2$(**21**)$_2$], formed from [Pd(OAc)$_2$]$_3$, was considered as the active species. M06(HOAc)//B3LYP calculations suggest C-H activation involves loss of TFA followed by external CMD at an agostic intermediate. The overall barrier is computed to be 27.3 kcal/mol, 1.7 kcal/mol lower than for C-H^b activation, a difference that is related to the less electron-rich character of the benzoyl phenyl

group. Details of the alternative inner-sphere AMLA/CMD C-H activation at Pd were not presented, although intramolecular C-H activation of this type is computed to be favored at [Ru(TFA)(**21**)(*p*-cymene)]$^{+}$, leading to hydroxylation at the benzoyl position, as observed experimentally.

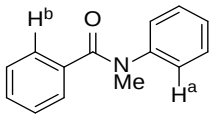

21

The potential non-innocence of protic solvents has also been highlighted by Sunoj in a study of the alkoxylation of *N*-methoxybenzamide at [Pd(OAc)$_2$].[80, 81] Using M06(MeOH)//B3LYP calculations a mechanism in which a methanol solvent molecule intervenes as a proton shuttle in both the *N*-deprotonation and subsequent C(sp^2)−H activation steps is proposed (see **TS22**, Figure 11). The HOAc formed is then deprotonated by the amide ligand to regenerate acetate, which subsequently aids the C-OMe bond forming step by deprotonating the methanol molecule involved in this process.

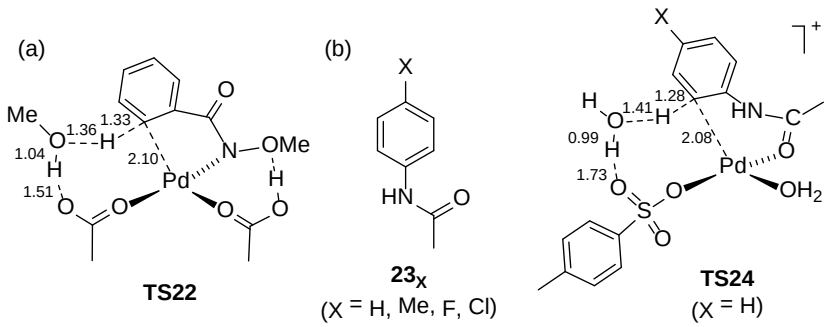

TS22

23$_X$
(X = H, Me, F, Cl)

TS24
(X = H)

Figure 11. (a) Computed transition state **TS22** for the solvent-assisted C-H activation of *N*-methoxybenzamide at [Pd(OAc)$_2$] in MeOH;[80, 81] (b) Computed transition state, **TS24**, for the water-assisted C-H activation of *p*-X-C$_6$H$_4$-NHC(O)Me, **23$_X$**, at [Pd(OTs)(H$_2$O)$_3$]$^{+}$.[82] Selected distances are given in Å; for **TS24** X = H.

Brown has defined a related process involving water in a M06-2X(acetone) study of the C-H activation of substituted acetanilides (**23$_X$**), at [Pd(OTs)(H$_2$O)$_3$]$^{+}$.[82] Substrate binding (with X = H) with displacement of two waters permits an AMLA/CMD C-H activation in which one S=O bond of the OTs

ligand accepts the proton with an overall barrier of 22.9 kcal/mol. Replacing OTs by OAc gives a similar overall barrier of 23.7 kcal/mol. An alternative general base catalysis in which an intervening water molecule relays the proton to the tosylate S=O group (via **TS24**, Figure 11) has a barrier of only 14.3 kcal/mol, and this value is more consistent with the efficient room temperature process observed experimentally. Transition state energies proved sensitive to substituents, X, in the 4-position and followed the trend X = Me < H < F < Cl. A classical S_EAr process was inferred, however, with the 4-Me and 4-F substrates a significant stabilisation of the *O*-bound precursors is also computed meaning that the overall barrier in both these cases is higher than when R = H. C-H activation of $\mathbf{23_H}$ (X = H) was also modelled by Stirling and Novák in their study of the coupling with benzaldehyde/^{t}BuOOH mediated by [Pd(OAc)$_2$] in water/TFAH.[83] M06(water) calculations identify [Pd(κ^2-OAc)($\mathbf{23_H}$)]$^+$ as the immediate precursor to C-H activation, this charged species being more stable in water than neutral [Pd(OAc)$_2$] + free $\mathbf{23_H}$ or [Pd(OAc)$_2$($\mathbf{23_H}$)] (by 19.3 kcal/mol and 22.1 kcal/mol, respectively). C-H activation then proceeds with a barrier of *ca*. 15 kcal/mol, to ultimately form an acetate-bridged dimer, [Pd(OAc)($\mathbf{23_H'}$)]$_2$. Addition of a benzoyl radical gives a Pd(III)/Pd(II) species from which C-C reductive coupling is computed to readily occur.

The nature of the active species during catalysis by "Pd(OAc)$_2$" has also been considered. Musaev assessed both dimeric and monomeric intermediates in the C-H activation of a range of *N*- and *O*-donor substrates, including benzo[*h*]quinoline (**bzq**) and several *N*-deprotonated *N*-arylbenzamides, where the latter are considered as ion-pairs with a Cs^+ cation.[84,85] B3LYP(DMF, D3)//M06 calculations with optimisation in DMF formulate [Pd(OAc)$_2$]$_2$ as a paddlewheel structure which reacts via a kinetically facile and exergonic associative substitution of one acetate arm by the incoming substrate. C-H activation requires a vacant site and thus entails full dissociation of an OAc ligand which occurs concurrently with the C-H activation via **TS25** (Figure 12). Repeating this process at the second Pd center produces a dimeric 'clam-shell' structure with two cyclometalated ligands. The first C-H activation has the higher barrier (e.g. for **bzq** these are 18.1 and 11.9 kcal/mol respectively) but both processes have higher barriers than the equivalent step at monomeric [Pd(κ^2-OAc)$_2$] (8.7

kcal/mol). Direct comparison requires the energy to break up the $[Pd(OAc)_2]_2$ dimer to be taken into account (+24.3 kcal/mol) and on this basis the reaction via the dimer has the lower overall barrier, although specific ligation (e.g. by solvent) or concentration effects may also play a role. The dimeric cyclometallated intermediate is significantly more stable than two separate monomers, by 25.4 kcal/mol for **bzq**. The stability of the dimers may also be enhanced by π–π stacking between appropriate cyclometallated ligands although the more natural 'bite angle' provided for the bridging acetates by the dimeric motif may also be a factor in stabilizing this form over monomers featuring a κ^2-OAc with a tight O-Pd-O angle of *ca*. 80°. In an earlier study Sakaki had characterised the C-H activation of **bzq** at monomeric $[Pd(OAc)_2]$ as proceeding via a $[Pd(\kappa^2\text{-OAc})(\kappa^1\text{-OAc})(\eta^2\text{-}\mathbf{bzq})]$ intermediate rather than the alternative *N*-bound form.[86] This led to a transition state more similar to an intermolecular AMLA/CMD C-H activation (see Section 4.3) with a computed barrier at the MP4(SDQ)//B3PW91(C_6H_6) level of 18.3 kcal/mol.

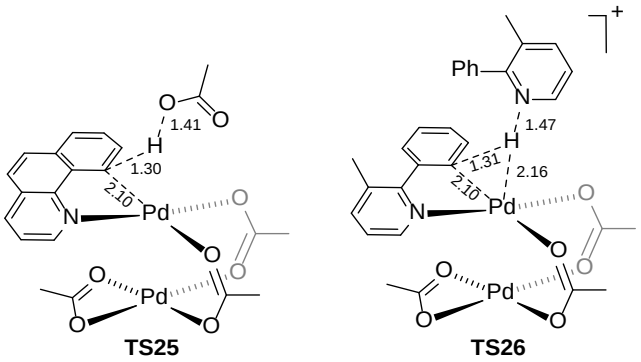

Figure 12. Computed transition states for C-H activation of benzo[*h*]quinoline (**bzq**) and 3-Me-2-phenylpyridine (**mppy**) at $\{Pd(\mu\text{-}OAc)_2Pd(\kappa^2\text{-}OAc)\}$; selected distances are given in Å. Adapted with permission from Refs [84,85] and 87. Copyright 2014 and 2013, respectively, American Chemical Society.

The nature of the second C-H activation step in forming dimeric clam-shell cyclometallated intermediates had in fact been discussed previously by Canty, Sanford and Yates in the context of the catalytic arylation of 3-Me-2-phenylpyridine (**mppy**) by $[Pd(OAc)_2]_3$ in acetic acid.[87] The free

energy barrier to an acetate-assisted C-H activation analogous to **TS25** is 11.0 kcal/mol (M06(CH_2Cl_2) level) compared to 12.3 kcal/mol at monomeric [Pd(κ^1-OAc)$_2$(**mppy**)]. However, under catalytic conditions (5 mol% [Pd(OAc)$_2$]) it is argued that free OAc would not be available in sufficiently high concentrations and that the large excess of the **mppy** substrate makes this an attractive alternative, especially as C-H activation can proceed via an external CMD. This process (see **TS26**, Figure 12) has a barrier of only 5.7 kcal/mol and is also consistent with the rate-determining step lying elsewhere in the cycle, namely the oxidation with PhI(OAc)$_2$ (see Section 4.3.2).

Defining the nature of the active species involved in C-H activation is further complicated by the presence of additives. Sunoj and Schaefer assessed the effects of AgOAc and CsF in the [Pd(OAc)$_2$]-catalysed amination of *N*-arylbenzamides with *N*-oxy- and *N*-chloromorpholines[88] (**27** to **28**, Figure 13(a)).[89] M06(DCE) calculations were used to define C-H activation at monomeric, homobimetallic and heterobimetallic species in the presence of both additives. 'CsF' first promotes *N*-deprotonation of the benzamide substrate to yield HF which, in combination with the acetate, interacts with the Cs^+ cation to facilitate C-H activation. The most accessible process is via heterobimetallic **TS27**, although all the structures surveyed retained the core features of AMLA/CMD C-H activation, *i.e*. C-H interaction at electron deficient Pd^{2+} and efficient intramolecular deprotonation by a proximate carboxylate base. In the case of **TS27** this begins to resemble an external CMD with the base positioned by the adjacent metal center.

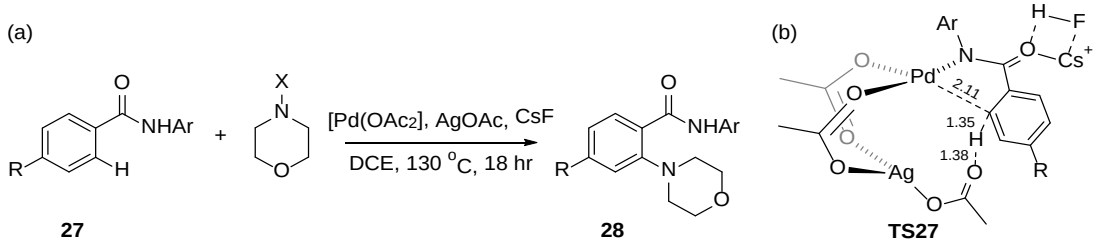

Figure 13. (a) Pd-catalysed amination of *N*-arylbenzamides (experiment, R = ^{t}Bu, Ar = 4-$C_6F_4CF_3$, X = Cl, OAc,O_2CPh); (b) Computed transition state **TS27** (R = H, Ar = 4-$C_6F_4CF_3$), with selected distances in Å. Adapted with permission from Ref 89. Copyright 2014, American Chemical Society.

Subsequently the full cycle for the direct amination of **27** to **28** (R = ^{t}Bu, Ar = 4-$C_6F_4CF_3$) with *O*-benzoyl hydroxypiperidine was modelled.[90] C-H activation via **TS27** (Figure 13(b)) has an overall barrier of 20.3 kcal/mol and is exergonic, giving an intermediate at -26.1 kcal/mol. After displacement of HOAc by the piperidine, N-O bond activation and C-N reductive coupling proceed via transition states that are 30.3 and 32.1 kcal/mol respectively above this precursor. In this case the AgOAc and CsF additives were initially modelled as the solvent adducts $AgOAc(DCE)_2$ and $CsF(DCE)_6$ and different degrees of microsolvation were assessed in the key transition states along the pathway. In the absence of the additives a pathway with an energetic span, $\Delta G^{\ddagger}_{span}$, of 31.2 kcal/mol is computed, with C-H activation now being rate determining. This energy span is actually slightly lower than that computed in the presence of the AgOAc/CsF additives: experimentally, these additives induce a higher yield (from ca. 40% to 97 %; 18 hr at 130 ^{o}C), emphasizing the challenge of computing these complex reaction systems.

A heterobimetallic $[PdAg(OAc)_3]$ system is also proposed to be central to the *meta*-selective C-H activation of **29** by $[Pd(OAc)_2]$/[AgOAc] (Figure 14).[91] Here, the remote CN group binds to Ag and directs the {Pd(OAc)} moiety to a *meta*-C-H bond which proceeds via **TS29** with overall $\Delta G^{\ddagger}$ = 24.8 kcal/mol (M06(DCE)//B3LYP). This proves more accessible than either *ortho*- or *para*-C-H activation (overall $\Delta G^{\ddagger}$ = 27.8 kcal/mol and 28.3 kcal/mol respectively). Reaction via $[Pd(OAc)_2]$, $[Pd_2(OAc)_4]$ and $[Pd_3(OAc)_6]$ all entailed higher barriers for *meta*-C-H activation and actually predicted *ortho*-selectivity with the mono- and trimeric systems.

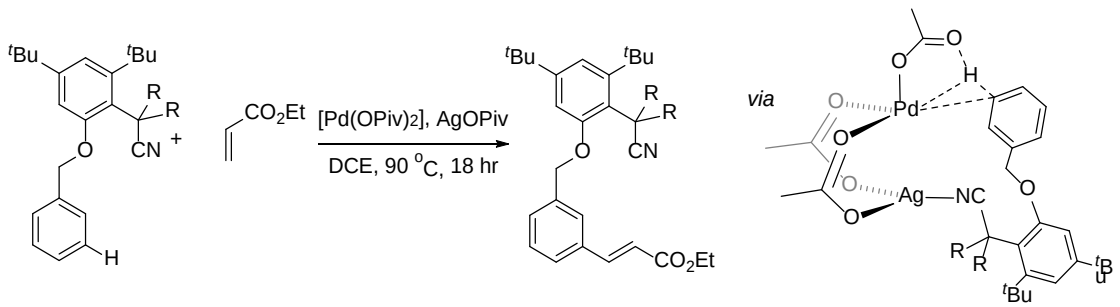

Figure 14. *Meta*-selective Pd/Ag-catalysed alkenylation of **29** to **30** *via* **TS29**. Adapted with permission from Ref 91. Copyright 2014, American Chemical Society.

Removable bidentate directing groups have been developed to address challenging C-H functionalisation processes and the efficiency of *N*,*N*-bidentate directing groups in promoting C(sp^2)-H activation at [$Pd(OAc)_2$] has been assessed by Huang, Wang and Chen with B3LYP(toluene, D3) calculations.[92] Using *N*-(quinolin-8-yl)benzamide (**31**, P_x = NH; D_s = N) and *N*-(pyridin-2-ylmethyl)-benzamide (**32**, P_x = NH; D_s = N, n = 1) as reference species, this and related studies,[93] emphasize the importance of a protic substituent at the proximal position, P_x. These promote access to vacant sites at the metal via displacement of the acetate ligands, one via protonation and loss as acetic acid and the second via κ^2-κ^1 displacement by the approaching C-H bond of the strongly anchored bidentate substrate. C-H bond activation then involves a characteristic AMLA/CMD process. The greater acidity of the quinoline-based ligands therefore makes them particularly effective. Donor groups in the distal position (D_s) aid substrate coordination and so also promote C-H activation. For **32** (P_x = NH, D_s = N) a shorter ligand backbone (*n* = 0) increases the barrier to C-H cleavage by over 14 kcal/mol due to greater strain in the transition state and elongation of the proximal Pd-N bond. Similar trends were also seen in a related study on C(sp^3)-H activation which included a 2-thiomethylaniline *N,S* bidentate group.[93] These trends appear to be broadly transferable to other metal centers with similar results obtained in this study for the reactions of [$Ni(OAc)_2$] and [$Ru(OAc)_2(PH_3)_3$] (see Sections 5 and 8 respectively).

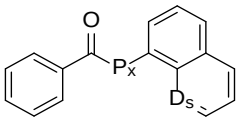

31
P_x = NH, NMe, O
D_s = N, CH

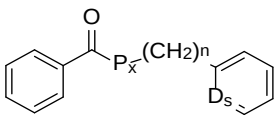

32
P_x = NH, NMe, O
D_s = N, CH
n = 0-2

The C-H activation of naphthalene, substituted at the C1-position with a bidentate *N,N*-pyridylarylimine (**33**), at [$Pd(OAc)_2$] has been assessed with BP86(toluene, D3) calculations.[94] C-H

activation involves a two-step AMLA/CMD and favors reaction at C8 over C2 ($\Delta\Delta G^{\ddagger}$ = 1.8 kcal/mol, $\Delta\Delta G$ = 3.5 kcal/mol). In this case a 6-membered palladacycle is formed; however with 2-naphthylpyridine reaction at the 2-position is favoured and gives a 5-membered *C,N*-chelate. This change is also seen experimentally and suggests the change in selectivity is linked to use of the bidentate imine.

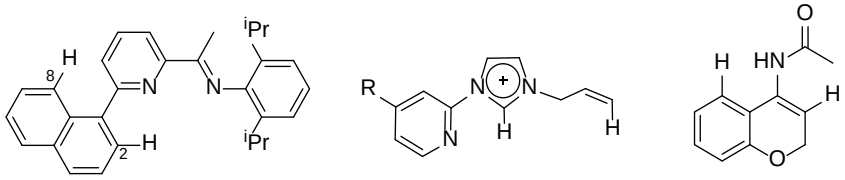

33 **34** **35**

The sequential C(sp^2)-H activations of 1-(pyridin-2-yl)-3-allyl-1H-imidazoliums, **34**, at [$Pd(OAc)_2$] have been characterised by M06 calculations by Willans and Ariafard where optimisations were carried out in MeCN solvent.[95] The pyridine moiety acts as a directing group for the initial imidazolium C-H activation to form [Pd(κ^2-OAc)(MeCN)(κ-*N,C*-**34'**)]$^+$. In this case a MeCN solvent molecule is retained throughout making this an unusual example of C-H activation at a 5-coordinate Pd center, with the pyridyl arm dissociating after the C-H activation. An overall barrier of 23.1 kcal/mol is computed (with R = OMe). The *N,C*-chelate can then act as a bidentate directing group for the second C(sp^2)-H activation which has an overall barrier of 24.3 kcal/mol. This C-H activation generates a 6-membered ring and a tridentate *N,C,C*-palladacycle, and this process is computed to be competitive with the binding and C-H activation of a second imidazolium ligand. Experimental evidence is seen for both processes when R = OMe. Competition between the [$Pd(OAc)_2$]-mediated intramolecular aromatic and vinylic C(sp^2)-H activation in enamide **35** was studied by Fang with B3LYP(dioxane) calculations.[96]

The development of *N*-acyl mono-protected amino acids (MPAA, e.g. **36**) in promoting enantioselective C-H functionalisations has attracted a number of computational studies. MPAAs act as chiral auxiliaries and with [$Pd(OAc)_2$] they enter the coordination sphere as mono-anionic *O*-deprotonated *N,O*-chelates (see **Int36**). In doing so, protonation and loss of one acetate as HOAc

creates a vacant site for a substrate to bind. In their initial work in this area Musaev and Yu used B3LYP(THF) calculations to model C-H activation of substrates **37** and **38** with the *R*-enantiomer of an MPAA (PG = $CO_2{}^tBu$, R = ^iPr) and R^1 = H.[97] A key outcome of this study is that *N*-deprotonation of the initial *N,O*-chelate by $R^1CO_2^-$ occurs prior to the C-H activation. In this case the C-H activation occurs via an external CMD, with the recycled $R^1CO_2^-$ acting as base. Formation of the new Pd-C bond is favored trans to O. With **37**, depending on the orientation of the $-CHPh_2$ group the C-H activation can be either pro-*R* or pro-*S* and in this study the former process is favored in agreement with experiment.

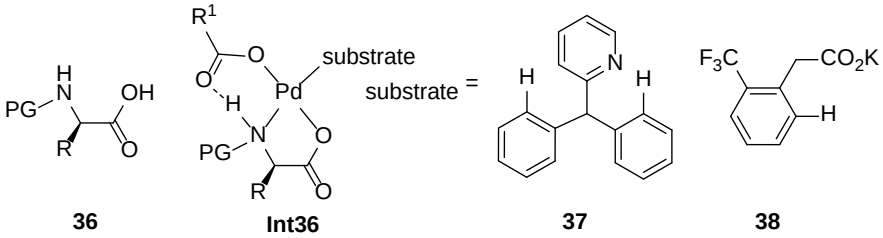

36 **Int36** **37** **38**

More recently Musaev has assessed the general features of MPAA-assisted C(sp^2)–H activations in **Int36** by systematically varying R (H ^iPr, ^iBu), PG (H, CO_2Me, Boc, C(O)Me, TFA) and substrate (**37**, **38**).[98] B3LYP-D3(THF) calculations emphasize the importance of having an electron withdrawing PG, with ΔG for this step with **37** varying by over 27 kcal/mol. C-H activation again proceeds via an external CMD by acetate and this is favored over an intramolecular process at the PG carbonyl that had been suggested by Houk, Yu and Wu (see below). The barriers for this external CMD step fall in a narrow range (6-8 kcal/mol), indicating the dominance of the *N*-deprotonation step in determining the overall barriers. With R = ^iPr both pathways favor formation of the *R*-enantiomer. The substrate also determines which pathway is favored. Thus with **38** (with PG = TFA, R = ^iPr) the inner and outer sphere processes become competitive. With β-MPAAs (i.e. with a second backbone CH_2 group) 6-membered *N,O*-chelates are formed in a boat conformation making the steric impact of the backbone substituent more significant as it is in close proximity to the metal.

An additional role of the MPAA in which a pendant *N*-acyl protecting group acts as an internal base in the C-H activation process was proposed by Houk, Yu and Wu in their M06(generic solvent, ε = 16.7) study of the *meta*-olefination of **39** with ethyl acrylate to give **40** (Figure 15).[99, 100] MS and computational data indicate the active species to be monomeric in nature and identify reaction *via* **TS39** to be most accessible ($\Delta G^{\ddagger}$ = 23.6 kcal/mol, *cf*. 24.5 kcal/mol and 24.1 kcal/mol for reaction at the *ortho*-C-H and *para*-C-H bonds respectively).

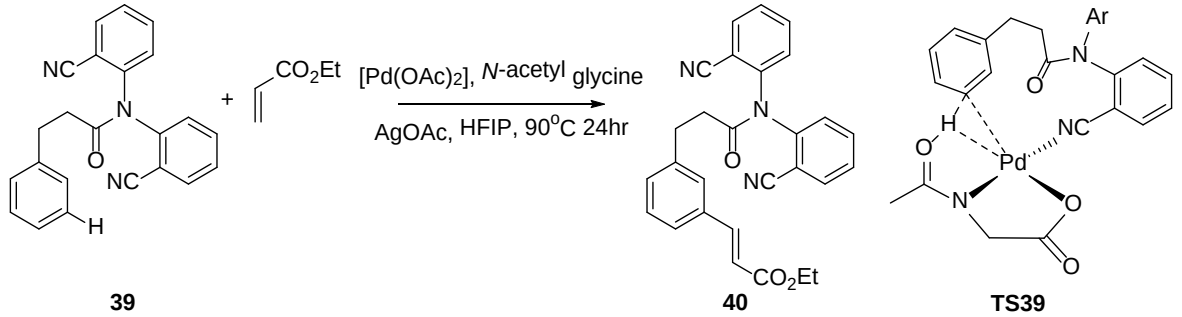

Figure 15. Pd-catalysed alkenylation of **39** to **40** *via* **TS39** in which the *N*-acyl group of an MPAA co-ligand acts as an internal base (Ar = 2-C_6H_4-CN). Adapted with permission from Ref 99. Copyright 2014, American Chemical Society.

Subsequently Yu and Wu also combined MS data with computation to probe the C-H activation event with α,α-diphenylacetic acid, **41**, as the substrate (see Figure 16).[101] Initial MS studies on a 1:1:1:1 mixture of [$Pd(OAc)_2$], KOAc, MPAA (with PG = C(O)Me and R = Me) identified species corresponding to [Pd(MPAA)(**41**), K,-2H]$^+$ in the gas phase, characterised as a mixture of C-H activated and C-H non-activated species. Isolation of the non-activated component then permitted C-H activation to be demonstrated in the gas-phase and hence in the absence of an external base. M06 calculations on this reaction starting from **Int41** (PG = $CO_2{}^t$Bu, R = ^{i}Pr) confirmed the feasibility of the *N*-PG group to act as an internal base and showed the formation of the *R*-enantiomer to be kinetically favored via **TS41(*R*)** over the *S*-form via **T41(*S*)** by 1.3 kcal/mol. This preference is traced to (i) the approach of the reacting C-H bond from below the coordination plane: this aligns it with the preferred position of the *N*-Boc internal base which lies anti to ^{i}Pr substituent on the MPAA

backbone and (ii) minimised repulsion between the reacting and spectator Ph groups of the substrate in the pro-*R* attack. This 'gearing' mechanism for control of enantioselectivity was then confirmed with a range of other substrates and MPAA combinations.

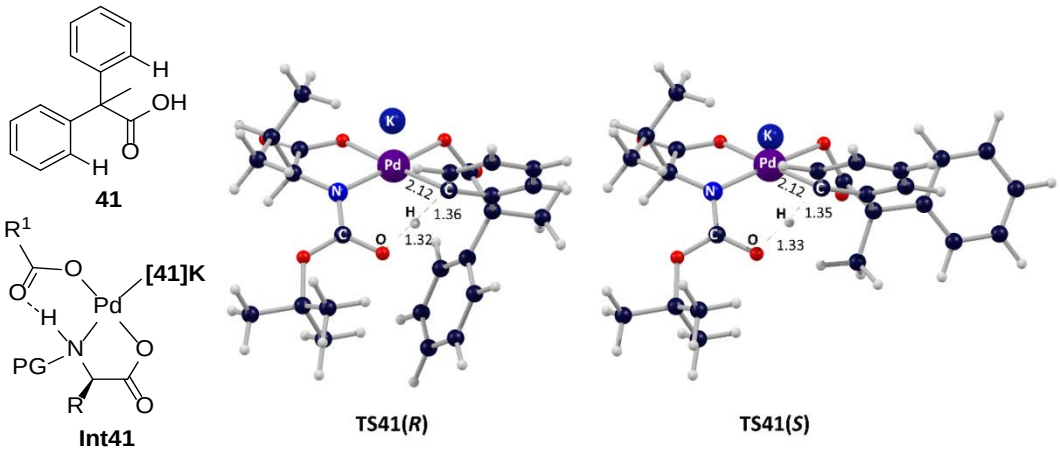

Figure 16. Substrate **41** and the lowest energy pro-*R* and pro-*S* C-H activation transition states in its reaction *via* **Int41** (PG = $CO_2{}^tBu$ and R = ^{i}Pr) where the substrate is present as its potassium salt and selected distances are in Å. Adapted with permission from Ref. 101. Copyright 2015 John Wiley and Sons.

MPAAs are also finding application as supporting ligands for catalytic C-heteroatom bond formation. Sunoj and Maiti combined an MPAA co-ligand with a 2-cyanophenyl methanesulfonate meta-directing group to perform aromatic C(sp^2)-H meta-acetoxylation at 70 °C in hexafluoroisopropanol (HFIP).[102] Experimental studies indicate a rate-limiting C-H activation with a k_H/k_D KIE of 3.0 and proposed an intermediate, **42**, by NMR. M06 calculations (with optimisations run in solvent with ε = 16.7 to mimic HFIP) locate **42** as a minimum and show this to undergo *meta*-selective C-H activation with amide carbonyl assistance with an overall barrier of 16.4 kcal/mol. Oxidative addition with $PhI(TFA)_2$ forms a 5-coordinate Pd(IV) species in which the MPAA exhibits a κ^1-*O*-binding mode. C-O reductive coupling then leads to the *meta*-functionalised product via a transition state that is 1.3 kcal/mol below that for C-H activation. Dang has also studied the Pd-mediated C–H iodination of benzylamine **43** in which an MPAA ligand (R' = ^{i}Bu, R = Ph *cf*. that in **42**) both promotes the reaction

and controls enantioselectivity (M06(DMSO)//B3LYP calculations).[103] In this case AMLA/CMD C-H activation is proposed to involve the carboxylate of the MPAA as the internal base with an overall barrier of 20.5 kcal/mol. Oxidative addition of I_2 and C-I bond forming reductive coupling is rate-limiting and forms the *R*-enantiomer with $\Delta G^{\ddagger}_{span}$ = 22.8 kcal/mol, 5.0 kcal/mol below that for the equivalent pathway to form the *S*-enantiomer.

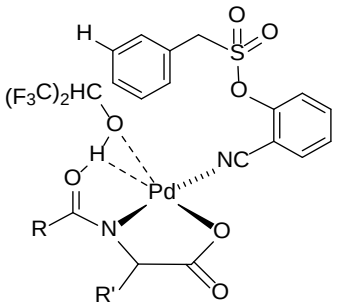

42

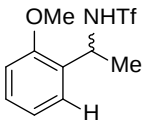

43

The iodination of *N*-arylbenzylamides has also been studied by Yu and Musaev with M06(DMF) calculations to model a $[Pd(OAc)_2]$/CsOAc catalyst system.[104] C-H activation of the *N*-deprotonated benzamide (formulated as an ion-pair with Cs^+) has a barrier of 14.3 kcal/mol. After HOAc loss the iodination proceeds via an end-on bound I_2 adduct with a Pd-mediated transfer of I^+ onto the *ortho*-carbon. This has a barrier of only 7.7 kcal/mol, 12.9 kcal/mol below an alternative route involving a concerted oxidative addition. A similar sequence may also take place on the cyclometalated dimer.

The protic character of a phosphoryl directing group also accounts for the greater reactivity of methylbenzylphosphonate, $PhCH_2P(O)(OMe)(OH)$ (**44$_{OH}$**) over dimethylbenzylphosphonate, $PhCH_2P(O)(OMe)_2$ (**44$_{OMe}$**) toward alkenylation with styrene (Figure 17).[105] Modelling a $[Pd(OAc)_2]$/[AgOAc] catalyst system B3PW91(1,4-dioxane) calculations show that **44$_{OH}$** can first protonate one OAc ligand and thus facilitate substrate binding via the P=O bond. The free oxygen of the phosphonate group can now act as an internal base for the C-H activation which is rate-limiting with $\Delta G^{\ddagger}_{span}$ = 25.7 kcal/mol (see **TS44$_{OH}$**). Subsequent H^+ transfer to OAc facilitates the formation of a coordination site for styrene to bind and undergo a 2,1-insertion. The regenerated phosphonate

anion also facilitates the subsequent β-H transfer step *en route* to the coupled product **45$_{OH}$**. With **44$_{OMe}$** the lack of a protic hydrogen means C-H activation occurs at a [Pd(OAc)$_2$] moiety via an AMLA/CMD process with an increased $\Delta G^{\ddagger}_{span}$ of 30.0 kcal/mol.

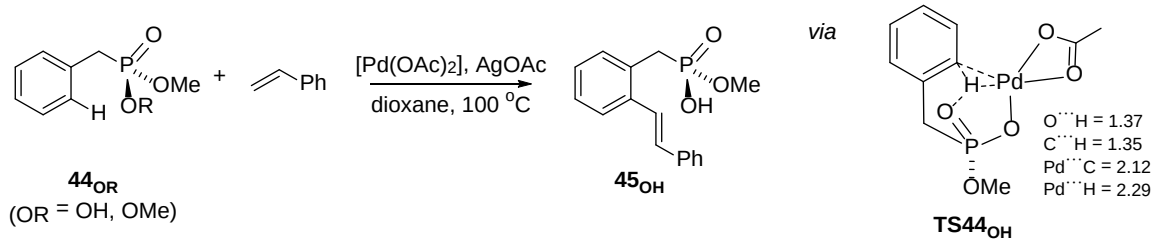

Figure 17. Pd-catalysed alkenylation of **44$_{OR}$** showing the computed phosphonate-assisted C-H activation transition state **TS44$_{OH}$** with selected distances in Å. Adapted with permission from Ref. 105. Copyright 2014, American Chemical Society.

Jiao has used M06(DCE) calculations to model the Pd-catalysed formation of phenanthridinone, **47**, from 2-iodotoluene and methylcarbamic chloride **46** (Figure 18).[106] This system exploits the Catellani protocol and constructs two C(sp^2)-C(sp^2) bonds each of which are accessed after directed C(sp^2)-H activations. Oxidative addition of *o*-iodotoluene and insertion of norbornene sets up an AMLA/CMD C-H activation facilitated by carbonate (modelled as '$CsCO_3^-$' see **TS46a**) which is *meta* to the Me substituent derived from 2-iodotoluene. This forms an initial cyclometallated intermediate at which rate-limiting C-Cl oxidative addition of **46** proceeds with a computed barrier of 30.3 kcal/mol. C-C coupling and de-insertion of the norbornene auxiliary leads to a further C-H activation via **TS46b** with a final C-C reductive coupling to form **47.**

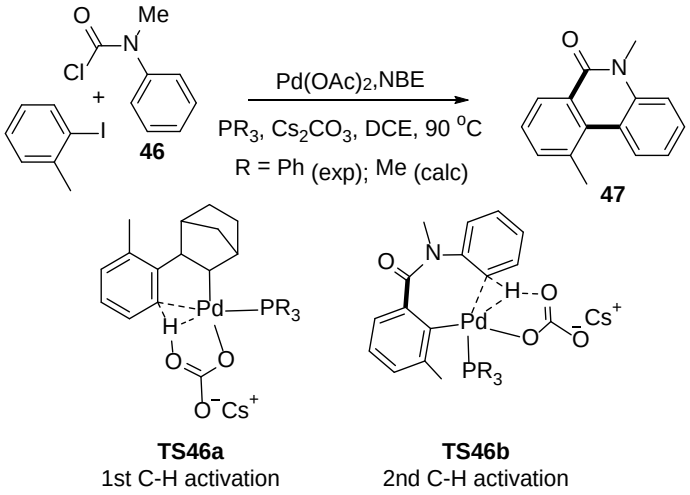

Figure 18. Pd-catalysed formation of phenanthridinone from 2-iodotoluene and methylcarbamic chloride highlighting the two C-H activation transition states.Adapted from Ref. 106.

The Pd-catalysed coupling of CO and isonitriles with benzamidines[107] and of isonitriles with benzamides have been modelled.[108] In the latter case, Wang reported M06L(dioxane)//B3LYP calculations on the reaction of *N*-methoxyiso-nicotinamide, **48**, with ^{t}BuNC at $Pd_2(dba)_3$ with O_2 as oxidant to give **49** (see Figure 19). The cycle commences with the formation of $[Pd(^{t}BuCN)_2(\eta^2\text{-}O_2)]$ that can deprotonate two molecules of **48** in its imidic acid tautomer to form **Int48a** and H_2O_2. Importantly, this anionic form of the substrate promotes binding through the amide rather than the pyridyl nitrogen. ^{t}BuCN insertion followed by a 1,3-acyl migration then generates **Int48b**. This can then undergo an AMLA/CMD C-H activation of the pyridyl *ortho*-C-H bond in which the pendant oxygen of the second imidate acts as the intramolecular base. C-C coupling from **Int48c** provides the final product. The C-H activation is involved in the rate determining process with $\Delta G^{\ddagger}_{span}$ = 27.3 kcal/mol and although similar C-H activations can in principle occur earlier in the cycle (e.g. at **Int48a**) these have overall barriers in excess of 30 kcal/mol. This study reiterates the generality of the chelating base in AMLA/CMD C-H activation and further work replacing the pyridyl moiety with a range of *p*-substituted phenyl groups showed C-H activation is promoted by electron donating groups that enhance the basicity of the pendant C=O group.

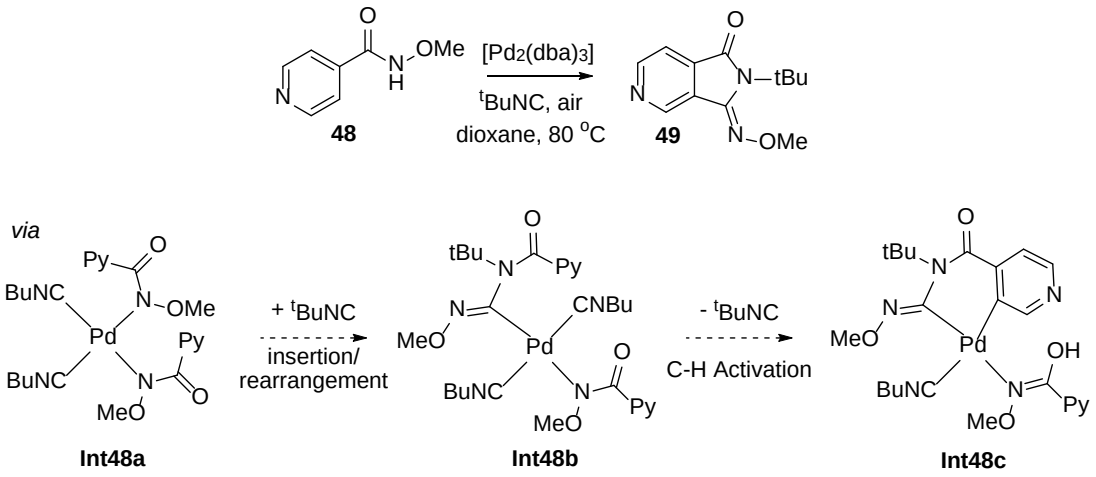

Figure 19. Pd-catalysed coupling of ^{t}BuNC with benzamide **48** with selected computed key intermediates. Adapted with permission from Ref. 108. Copyright 2016, American Chemical Society.

Fang has modelled the cyclisation of $PhCH_2CMe_2OH$ at $[Pd(OAc)_2]$,[109] a reaction that initially appears to be a heteroatom analogue of indane formation reported by Clot and Baudoin (see Section 4.2).[110] However, in this case B3LYP(C_6F_6) calculations (with free energies at 100 °C) show a Pd(II)-Pd(IV)-Pd(II) cycle is necessary. After substrate binding, C-H activation proceeds through a 2-step AMLA/CMD C-H activation with an overall barrier of 20.2 kcal/mol. Direct C-O reductive coupling at this stage entails a high barrier of 41.0 kcal/mol; instead, oxidation with $PhI(OAc)_2$ gives $[Pd(\kappa^1\text{-}OAc)_3(HOAc)(\kappa\text{-}C,O\text{-}C_6H_4CH_2CMe_2OH)]$ from which C-O bond formation has a barrier of only 11.6 kcal/mol. The oxidation to Pd(IV) is rate determining with $\Delta G^{\ddagger}_{span}$ = 30.9 kcal/mol and this barrier is lower than those computed with other $PhI(O_2R)_2$ species (R = CF_3, ^{t}Bu). The energetics of the oxidation to Pd(IV) were found to be sensitive to whether the Pd center was described with a pseudopotential and basis set or with an all-electron basis set.

4.2 Intramolecular C(sp^3)-H Activation

The role of agostic intermediates in AMLA/CMD C-H activation indicates that such processes are not restricted to aromatic C-H bonds but will also apply to C(sp^3)-H bonds. In early computational studies Clot and Baudoin modelled the cyclisation reactions of 2-halo-alkylbenzenes, starting with the

conversion of 2-bromo-*tert*-butylbenzene, **50**, to benzocyclobutane, **51**. This process involves initial C-Br oxidative addition at a bulky [Pd(PR_3)] species (R = ^{t}Bu[54, 111] or Cyp[112]) to generate a Pd-aryl bond that then acts as a directing group for intramolecular C(sp^3)-H activation. Experimentally, carbonate bases proved most efficient, however B3PW91(DMF) calculations comparing OAc, HCO_3^- and CO_3^{2-} at a model PMe_3 system failed to capture this; moreover, C-H activation was computed not to be rate-limiting, in contrast to the significant k_H/k_D KIE observed experimentally. Instead, calculations on a [Pd(2-^{t}Bu-phenyl)(CO_3^-)(P^tBu_3)] model posited a novel variation on the AMLA/CMD mechanism in which the bulky P^tBu_3 ligand precludes the carbonate from sitting adjacent to the substrate's agostic C-H bond (Figure 20). Deprotonation of one of the geminal C(sp^3)-H bonds is, however, still possible as this position exhibits enhanced acidity due to the neighboring agostic interaction.[113] C-H activation via **TS50** now becomes rate-limiting and is more accessible with CO_3^{2-} than with OAc or HCO_3^-.

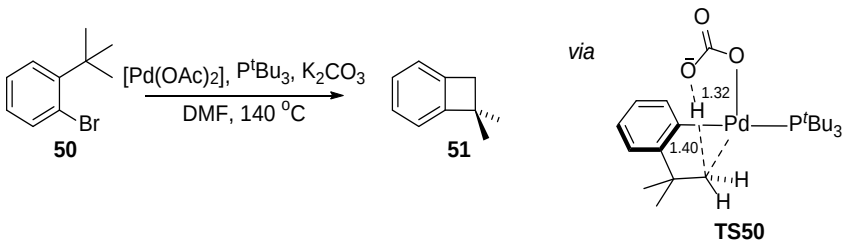

Figure 20. Pd-catalysed formation of benzocyclobutane, **51** via **TS50** with selected distances in Å.[111] Adapted with permission from Ref. 43. Copyright 2016, John Wiley and Sons.

These intramolecular cyclisations have been extended to the diastereo- and enantioselective syntheses of indanols[114] and indanes.[110] With **52-Br** (Figure 21, R = ^{i}Pr) reaction proceeds via the C-Br activated [Pd(**52**)(CO_3^-)L] intermediate, where L is a chiral binepine-based phosphine ligand and carbonate is again sited *trans* to the vacant site. With R = ^{i}Pr indane formation is observed and PBE0-D3BJ(DMSO) calculations locate the eight diastereo- and enantio-distinct C-H activation transition states, the most accessible of which corresponded to formation of the *R,R*-product **53**. This is 1 kcal/mol more stable than the nearest competing process that led to the *S,S*-product, a difference

that equates to an enantiomeric ratio of 77:23, in good agreement with experiment. A non-covalent interaction (NCI) plot highlighted a network of ligand-substrate interactions that promote the *R,R*-process.

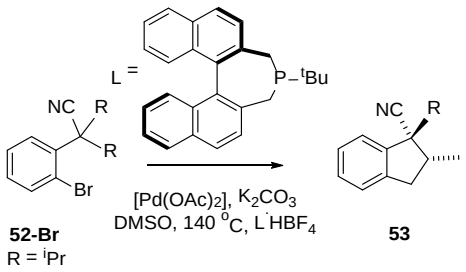

Figure 21. Indane formation via a Pd-catalysed enantioselective intramolecular cyclisation. Adapted with permission from Ref 110. Copyright 2015, American Chemical Society.

With **52-Br** (R = Et) C-H activation of the methylene adjacent to the benzylic positon is favored and the system reverts to benzocyclobutane formation. In this case, however, competition with β-H elimination is also seen.[115] B3PW91(DMF, D3BJ) calculations link this to the protonolysis of the Pd-Ar bond by the HCO_3^- formed in the initial cyclometallation (see **54**, Figure 22). This has a barrier of 24.3 kcal/mol and yields Pd-alkyl **Int54a** from which a carbonate-assisted β-H transfer gives **Int54b**. Alternatively HCO_3^- dissociation leads to C-C coupling, giving **Int54d** via **Int54c**. The rate of HCO_3^- loss via **TS54c** is therefore the key to controlling the reaction outcome, but a reliable barrier for this process is difficult to compute. Instead a kinetic model was set up in which the product distribution was monitored as a function of the inputted barrier to HCO_3^- dissociation. When this is set to 6 kcal/mol benzocyclobutane formation is favored, but at 12 kcal/mol β-H elimination via **Int54a** dominates. This demonstrates the importance of such kinetic modelling in interpreting complex, multi-step catalytic cycles that may also have competing reaction pathways. Moreover, the bicarbonate loss step here is not rate-limiting, and yet still plays a crucial role in determining the product distribution. Martin has also recently shown that these palladacycles such as **Int54c** can be

intercepted with diazocarbenes to form indanes; calculations suggest the carbene moiety inserts preferentially into the Pd-C(sp^3) bond prior to C-C reductive coupling.[116]

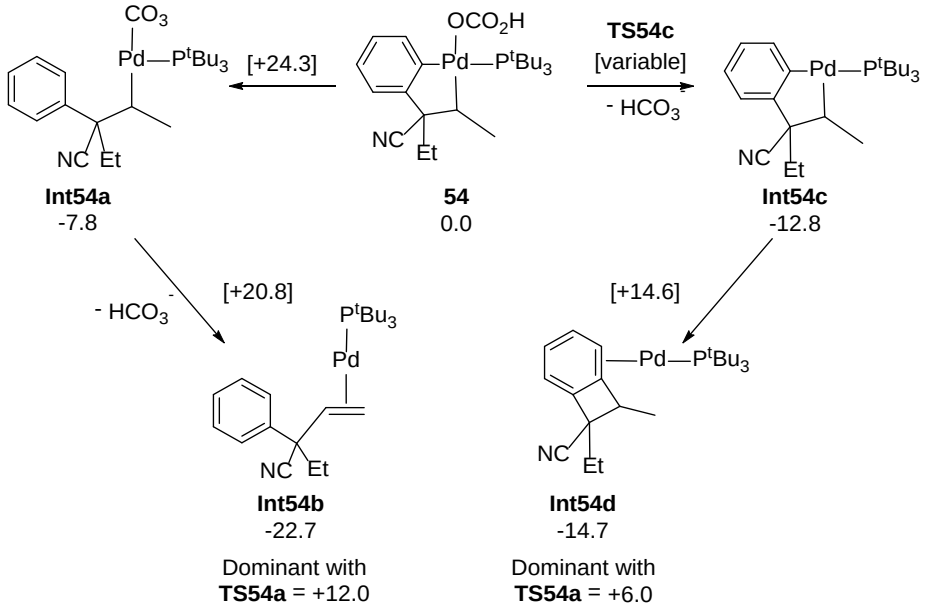

Figure 22. Competing pathways upon C-Br and C-H activation of **52-Br** (R = Et) at [Pd(P^tBu_3]; relative free energies are given in kcal/mol. Adapted with permission from Ref. 115. Copyright 2014, American Chemical Society.

A related intramolecular C(sp^2)-C(sp^3) cyclisation of **55-Cl** to form indolone **56** was investigated by Fu with M06(mesitylene)//B3LYP calculations (Figure 23).[117] After C-Cl oxidative addition at [Pd(PAd_2Bu)] the exchange of Cl with a base at [Pd(**55**)(Cl)(PAd_2Bu)] was assessed for $CsCO_3^-$, HCO_3^- and PivNHO, with the *N*-hydroxypivalamide forming the most stable intermediate when bound in a κ^2-*O,O* form. C(sp^3)-H activation of the 2-methyl substituent now proceeds via **TS55** ($\Delta G^‡$ = 23.7 kcal/mol), and is significantly more stable than the alternative C(sp^2)-H activation at the 8-position of the naphthyl moiety ($\Delta G^‡$ = 30.2 kcal/mol). C-C coupling then forms the indolone product. In this case the benzylic nature of the C(sp^3)-H bond facilitates reactivity and the rate-limiting process corresponds to the initial C-Cl activation ($\Delta G^‡_{span}$ = 26.3 kcal/mol). The utility of the PivNHO additive is ascribed to its greater solubility. Solé and Fernández have characterised the mechanism of the intramolecular arylation of sulfone **57-I** using B3LYP-D3(THF) calculations.[118] After C-I oxidative

addition, C(sp^3)-H activation proceeds via a carbonate-assisted AMLA/CMD. The rate-limiting process is the final C-C reductive coupling to form the indoline intermediate **58** which then reacts on with a vinylsulfone to form **59**.

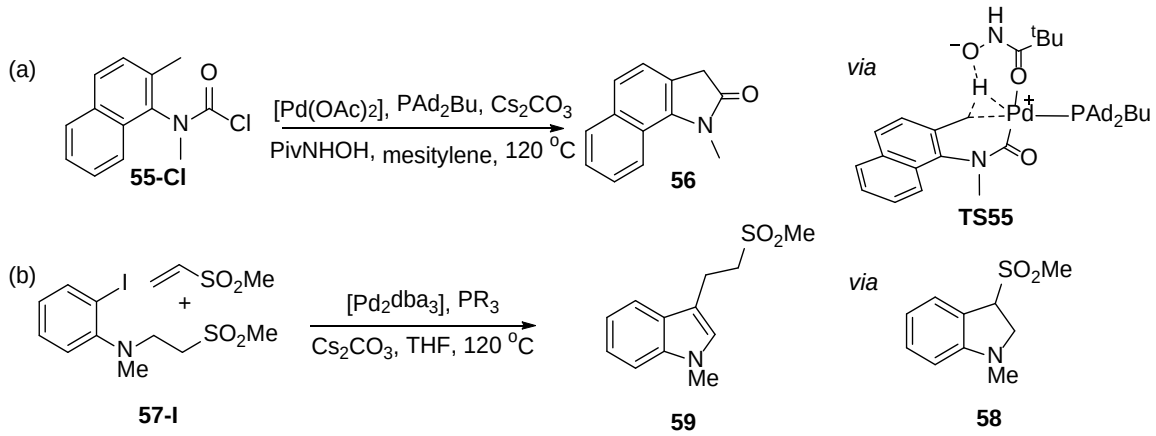

Figure 23. (a) Indolone formation via the intramolecular C(sp^2)-C(sp^3) cyclisation of **55-Cl**; the computed C-H activation transition state **TS55** is also shown. Adapted with permission from Ref 117. Copyright 2013, American Chemical Society. (b) Synthesis of 3-[2-(phenyl/methylsulfonyl)ethyl]indole, **59** (PR_3, experiment: = 2,2′-Bis(diphenylphosphino)-1,1′-binaphthalene (BINAP) or 1,1′-Bis(diphenylphosphino)ferrocene (dppf); computation: PMe_3. Adapted with permission from Ref 118. Copyright 2016, American Chemical Society.

C-N cyclisation has been modeled by Gaunt in a joint experimental and computational mechanistic study of the aziridination of cyclic amine **60** to **61** via the intramolecular activation of a C(sp^3)-H bond (Figure 24).[119] Experimentally, the reaction rate shows an inverse dependence on [**60**], is first order in [$Pd(OAc)_2$] and zero order in $PhI(OAc)_2$. A significant k_H/k_D of 3.8 is also observed and a mechanism based on BLYP-D3(toluene) calculations successfully captures these features. Initial binding of **60** at [$Pd(OAc)_2$] is supported by intramolecular NH···OAc H-bonding and is followed by an AMLA/CMD C-H activation of a Me group at the 3-position with a barrier of 20 kcal/mol. This is facilitated by enhanced C-H acidity due to the proximity of the carbonyl moiety: C-H activation at the 5-position has a higher barrier of 24.9 kcal/mol. Oxidation with $PhI(OAc)_2$ gives a Pd(IV) tris-acetate

intermediate from which HOAc loss occurs with deprotonation of the amine. The resultant intermediate **Int60** features a formally anionic amide ligand and can undergo C-N reductive coupling leading to **61** with an overall barrier of 17.2 kcal/mol, i.e. lower than that associated with the C-H activation process and hence consistent with the observed KIE. Shortly afterwards Liu and Wang published a related B3LYP(toluene) study probing selectivity in the 3,3-ethylmethyl- and 3,3-diethyl analogues of **60**.[120] In both cases activation of the 1° Me C-H bonds was preferred, and in the case of the diethyl species this results in a 5-membered palladacycle. C-O reductive coupling with an OAc ligand was then preferred over C-N cyclisation.

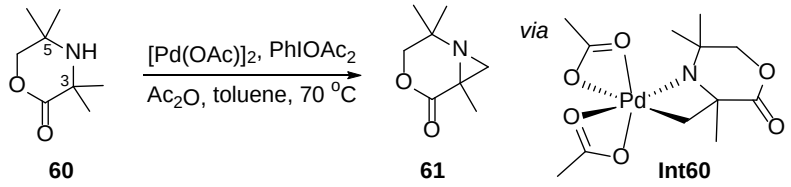

Figure 24. Pd-catalysed aziridination of cyclic amine **60** gives **61** via Pd(IV) species **Int60**. Adapted with permission from Ref 119. Copyright 2015, American Chemical Society.

Stereoselective C(sp^3)-H activation was considered by Houk and Yu in the context of the Pd(II)-catalyzed iodination and acetoxylation of oxazoline derivatives **62** (see Figure 25, M06//B3LYP calculations).[121] The resting state was found to control reactivity; thus with sterically encumbered **62a** ($R^1 = R^2 = {}^t$Bu) this is the $[Pd(OAc)_2]_3$ trimer from which a C-H activation process with an overall barrier of 26.2 kcal/mol via **TS62a** is characterised. In this case the diastereomeric excess, de, of 82 % seen experimentally can be linked to the *anti* arrangement of the ^{t}Bu substituents in the transition state. This is preferred over the alternative syn forms that lie 2.3 kcal/mol higher in energy, the difference in energy implying a 96 % de. In contrast when R^1 = Et and $R^2 = {}^i$Pr (**62b**) the trimer is opened up to give a monomeric precursor, $[Pd(OAc)_2(\kappa\text{-}N\text{-}\mathbf{62b})_2]$, from which C-H activation entails an overall barrier of 38.4 kcal/mol. $\Delta\Delta G^{\ddagger}$ in this case reduces to -0.2 kcal/mol (*cf*. a de of 0% experimentally) and a much reduced overall yield is also obtained.

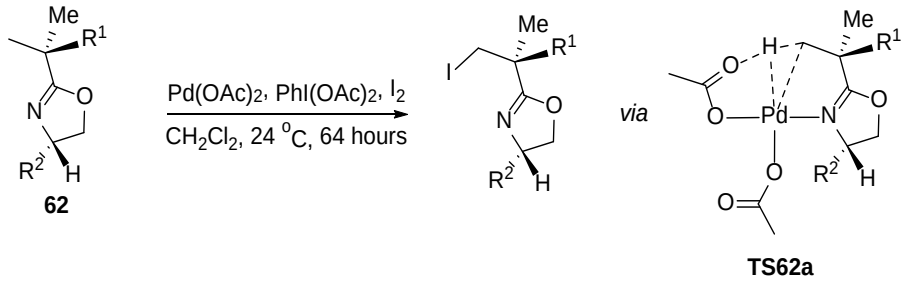

Figure 25. C(sp^3)-H iodination of oxazolines (R^1 = R^2 = ^{t}Bu, **62a**; R^1 = Et, R^2 = ^{i}Pr, **62b**) and **TS62a**. Adapted with permission from Ref 121. Copyright 2012, American Chemical Society.

Kündig has provided further evidence of the ability of DFT calculations to model the small energy differences associated with enantioselectivity through two M06-L(xylenes) studies of the [Pd(NHC)]-catalysed asymmetric synthesis of indolines (see Figure 26).[122,123] With *R*-**63-Br** initial Ar-Br activation and Br/OPiv exchange yields **Int*R*-63**, from which C-H activation occurs preferentially at the methylene group, and in particular that leading to the product as its *trans* isomer, *trans*-**64**. Methyl C-H bond activation that leads to **65** is preferred over formation of *cis*-**64** which involves reaction of the second methylene C-H bond. Analogous studies based on **Int*S*-63** and a benzyl analogue also reflect the observed experimental outcomes. The high degree of enantioselectivity can be related to unfavourable interactions involving the NHC ligand, a result that was confirmed with the B97-D functional.

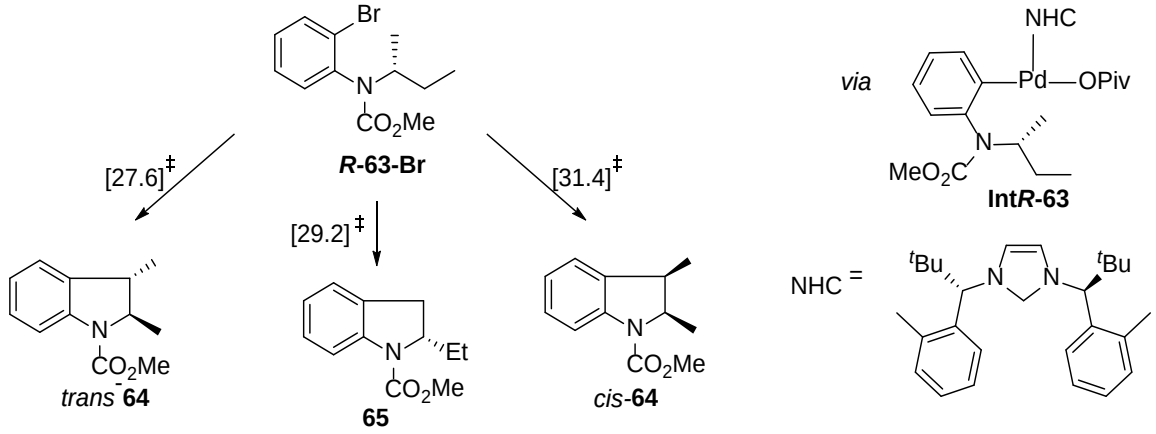

Figure 26. Reactions of ***R*-63-Br** to give alternative indoline products via **Int*R*-63**; transition state free energies (computed at 413 K) are indicated in kcal/mol.[122] Adapted with permission from Ref. 43. Copyright 2016, John Wiley and Sons.

The role played by a carbonate base was further probed by Rousseaux in a combined experimental/computational study of $[Pd(Ar)(Br)(PR_3)_2]$ species (**Int66a,** Ar = 2-(dimethylcarbamoyl)phenyl), Figure 27).[124] Both carboxylate and carbonate additives are required for efficient catalysis and B3LYP(toluene) calculations (R = Me) indicate that the carboxylate promotes both the C-H activation, as well as initial phosphine dissociation from the Pd center (i.e. **Int66a** → **Int66b**, ΔG = -0.6 kcal/mol). Formation of the initial HOAc adduct, **Int66c**, is endergonic and so this species should rapidly revert back to **Int66b**. The carbonate additive is proposed to circumvent this via a rapid deprotonation, thus trapping out the cyclometallated intermediate and allowing this to react on to products. The fact that the carbamoyl moiety is only weakly coordinating is also significant, as with more basic amines displacement of the κ^2-OAc ligand in **Int66b** is predicted to form stable bidentate *C,N*-adducts which render any subsequent C-H activation far less accessible.

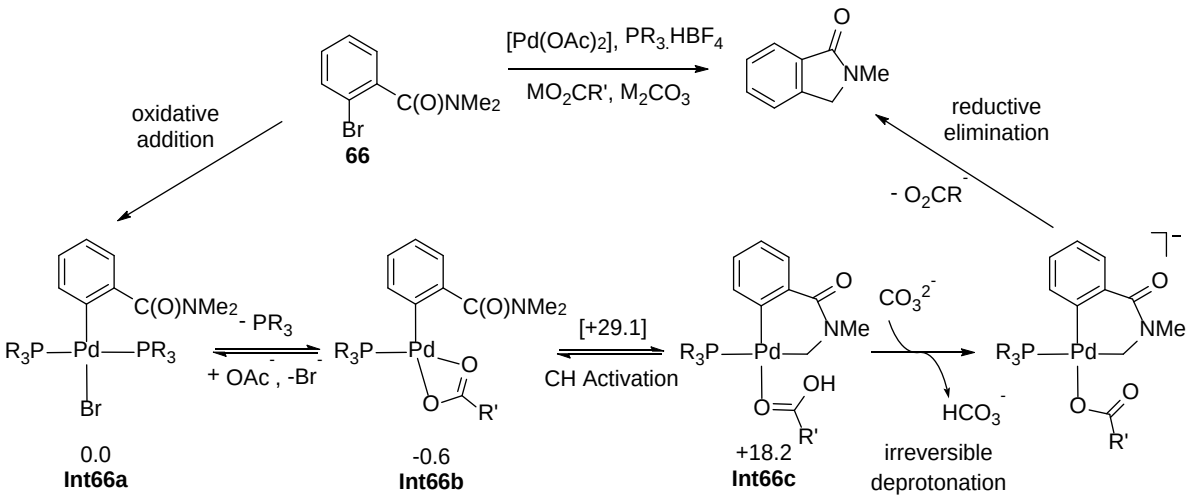

Figure 27. Pd-catalysed indolinone formation (experiment, R = Cy, R' = ^{t}Bu) with selected computed intermediates (R = Me, R' = Me, relative free energies in kcal/mol).[124] Adapted with permission from Ref. 43. Copyright 2016, John Wiley and Sons.

The roles of substrate substituents and additives have been dissected by Morokuma in a comprehensive study of the stereoselective C(sp^3)-H arylation of alanine derivatives **67$_R$** at [Pd(TFA)$_2$] (Figure 28).[125] Starting from *trans*-[Pd(TFA)$_2$(2-picoline)$_2$] B3LYP-D3(DCE) calculations suggest that substitution of 2-picoline by **67$_H$** involves an initial *N*-deprotonation by 'CsF', a process facilitated by the greater acidity of the *N*-aryl group. This leads to a contact ion-pair in which Cs^+ is associated with both the amide nitrogen and one C=O group of the succinimide substituent. C-H activation then proceeds via intermediate **Int67$_H$** in which displacement of one of the TFA ligands creates a vacant site for an agostic interaction. Importantly the TFA is retained in the outer coordination sphere, aided by electrostatic interactions with the Cs^+ cation and the low dielectric of the DCE solvent. From **Int67$_H$** the C(sp^3)-H activation step proceeds via an external CMD with a barrier of 7.9 kcal/mol which contributes to a free energy span of 23.9 kcal/mol. C-C coupling was then modeled from a *bis*-2-picoline intermediate (isolated experimentally) with substitution of one 2-picoline ligand being facilitated by protonation (with TFAH). Ph-I oxidative addition ($\Delta G^{\ddagger}$ = 22.3 kcal/mol) then gives a Pd(IV) intermediate which can access a facile reductive elimination to generate **67$_{Ph}$**. This species can itself act as a substrate and undergoes activation of a secondary C(sp^3)-H bond via an equivalent external CMD pathway in which the TFA anion approaches from above the metal coordination plane. This is favored kinetically by 9.1 kcal/mol due to reduced steric hindrance between the Ph and the succinimide groups and leads to the *S,R*-product seen experimentally. Electronic effects on the C-H activation step at the –CH_2R group depend significantly on R. With R = H, C-H activation is predicted to be aided by a stronger agostic interaction which can be promoted by a more electron-withdrawing co-ligand (e.g. 2-trifluoromethylpyridine) or moving to the Pt analogue. In contrast for R = Ph the electron withdrawing effect means that a more electron donating co-ligand is preferred (e.g. 2-methoxypyridine). These trends are mirrored experimentally.

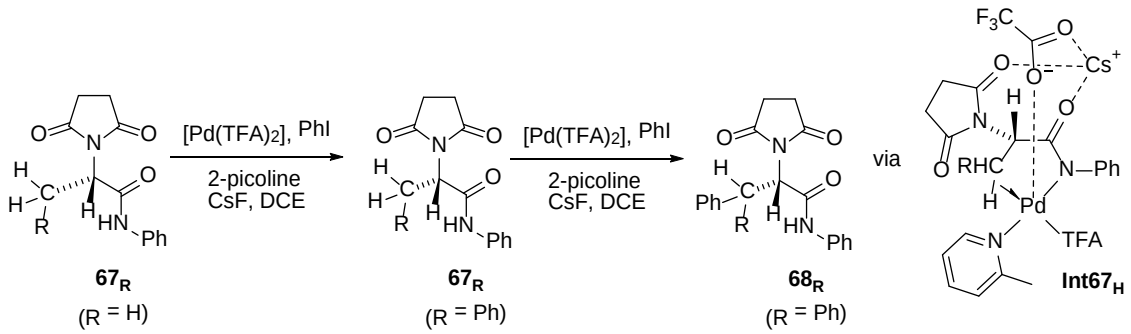

Figure 28. Pd-catalysed stereoselective C(sp^3)-H arylation of alanine derivatives $\mathbf{67_R}$ (R = H, Ph) at [$Pd(TFA)_2$] showing key intermediate $\mathbf{Int67_H}$. Adapted with permission from Ref 125. Copyright 2015, American Chemical Society.

The use of a bidentate 8−aminoquinolinyl directing group in assisting the intermolecular arylation of a 2° C(sp^3)-H bond in **69** at [$Pd(TFA)_2$] has been modelled by Wu and Zeng with B3LYP(2-butanol) calculations.[126] Substrate binding and *N*-deprotonation accesses a Pd(II)-Pd(IV)-Pd(II) pathway involving initial C-H activation following by rate-limiting Ph-Br activation ($\Delta G^{\ddagger}_{span}$ = 27.5 kcal/mol). This is clearly favored over the alternative featuring oxidative addition of Ph-Br prior to C-H activation ($\Delta G^{\ddagger}_{span}$ = 53.9 kcal/mol). This large difference primarily reflects the much easier oxidative addition step at the more electron-rich cyclometalated intermediate: both C-H activations proceed via AMLA/CMD pathways with more similar barriers of 19.6 kcal/mol and 24.5 kcal/mol at Pd(II) and Pd(IV) respectively. The C-H activation step is endergonic at Pd(II) by 9 kcal/mol, but exergonic by 12.4 kcal/mol at Pd(IV). Related reports on directed C(sp^3)-H bond activation processes at Pd^{2+} centers include an external CMD with HCO_3^- proposed by Wang and Wang for an anionic alanine amide (M06-L(DCE)//BP86, with optimisation including the DCE solvent),[127] the stereoselective C(sp^3)-H arylation of a 2-pyridylsulfonyl derivative of valine reported by Alonso and Ferńandez-Ibáñez (M06(MeCN)//B3LYP) that captures the preferred activation of the pro-*R* Me of the iPr substituent,[128] and the C(sp^3)-H bond activation of alkylamides featuring a 2-pyridylisopropyl directing group (**70**) which has been characterised by Shi (M06-L//BP86 calculations).[129] Zhu and Zhang found use of a novel bidentate directing group fitted with a dioxo-dihydro-anthracenyl

substituent leads to C-H activation adjacent to the amide C=O group to form a 4-membered palladacycle, **71**.[130] Formation of this species has an overall barrier of 33.2 kcal/mol, 3.0 kcal/mol lower than the alternative C-H activation of one of the terminal methyl C-H bonds. Reaction with $PhI(OAc)_2$ leads to the acetoxylation product.

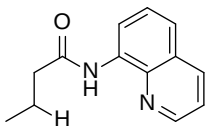

69

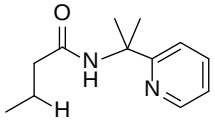

70

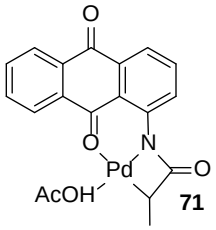

71

The carboxylate-assisted activation of allylic C(sp^3)-H bonds has also been modelled computationally. In such processes the alkene moiety could be considered as a directing group, although the intrinsic reactivity of allylic C(sp^3)-H bonds and the large geometric rearrangement required to form an η^3-allyl ligand result in reported transition states being dominated by interaction with the carboxylate base and long Pd···C distances in excess of 3 Å that imply limited interactions.[131,132,133] While these processes literally involve a concerted metalation and deprotonation they do not feature the synergic involvement of the metal and carboxylate ligand that CMD might imply but that AMLA makes explicit.

4.3 Intermolecular C(sp^2)-H activation

Many computational studies of intermolecular C(sp^2)-H activation have been performed in the context of so-called direct arylation reactions. These involve C(sp^2)-C(sp^2) bond formation via the coupling of two aryl groups, one of which is derived from an intermolecular C(sp^2)-H activation while the other generally involves C-X oxidative addition with a leaving group, X. The order of these events can vary, with implications for the pattern of the Pd oxidation states involved. In oxidative coupling reactions both partners derive from C-H bond activation and so avoid any leaving groups, making such processes particularly desirable from an atom economy point of view. Examples include reactions where one partner is derived from an intramolecular (directed) C-H activation and the

other via an intermolecular C-H activation process. Most challenging of all is to combine two coupling partners that are both supplied by intermolecular C-H activation. The nature of these oxidative coupling reactions means that such processes require an oxidant to complete the catalytic cycle. One other process that formally involves C(sp^2)-H-C(sp^2)-H coupling is C-H alkenylation, the C-H activation analogue of the Mizoroki-Heck reaction. In the following, after covering some key general papers in the area, the discussion is structured in terms of the nature of the coupling reactions involved and, within that, by substrate type.

Building on the CMD concept,[57] Gorelsky has made use of the activation strain model[134] to analyse B3LYP-computed barriers to C-H activation for a range of aromatic and heteroaromatic substrates reacting at [Pd(κ^2-OAc)(Ph)(PMe_3)].[135,136,137] In this approach, illustrated in Figure 29 for benzene, the activation energy, ΔE_{act}, is split into two terms: ΔE_{dist}, the sum of the energies associated with distorting the two reaction partners into the geometries they each adopt in the transition state, and ΔE_{int}, the interaction energy between these two distorted fragments. Through this approach a wide range of substrates can be categorized into three different classes depending on which energy term dominates the overall barrier. In Class I substrates ΔE_{dist} is dominant, and in particular the energy required to distort the C-H bond. This destabilising term is lower with more acidic C-H bonds, for example electron-deficient substrates such as C_6F_5H, fluoro(hetero)aromatics and heterocyclic *N*-oxides. In Class II species the stabilising ΔE_{int} term dominates and this is enhanced by more nucleophilic substrates. Finally, in Class III substrates the variations in both ΔE_{dist} and ΔE_{int} must be taken into account. Computed reaction profiles indicate that precursors featuring the substrate bound at Pd may occur, either as π-bound, heteroatom-bound or C-H-bound adducts. No Wheland intermediates were seen and with C_6F_5H no precursor was located at all. Gorelsky has provided an overview of this area, including work on azoles, Cl- and F-substituted arenes, heterocyclic *N*-oxides, and thiophenes.[135] A key outcome of this body of work is the ability of the AMLA/CMD concepts to accommodate *both* electron deficient *and* electron rich substrates.

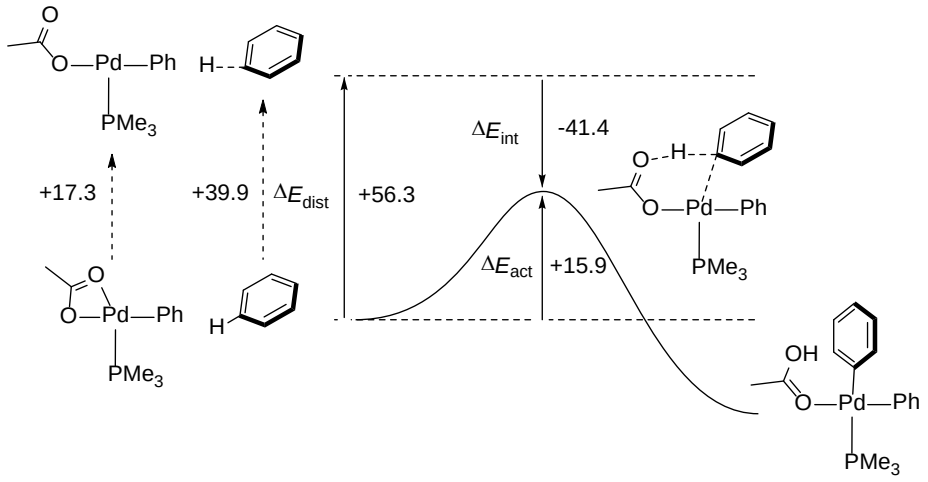

Figure 29. Illustration of the activation strain model based on C-H activation of benzene at [Pd(κ^2-OAc)(Ph)(PMe_3)]. Contributing energies terms are provided in kcal/mol.[137] Reproduced with permission from Ref. 43. Copyright 2016, John Wiley and Sons.

The nature of the active species derived from [$Pd(OAc)_2$] in such reactions has come under scrutiny. Hartwig showed that the direct arylation of 2-bromotoluenes and benzene is more efficient in dimethylacetamide (DMA) solvent in the absence of added phosphines and that a preformed dimer, $[PdArBr_2]_2^{2-}$, was a competent catalyst.[138] B3LYP calculations showed a barrier of 31 kcal/mol for C-H activation of benzene at [Pd(κ^2-OPiv)(Ph)(DMA)], and this compared to 42 kcal/mol for the same reaction at [Pd(κ^2-OPiv)(Ph)(P^tBu_3)]. The increased barrier is due to the bulky phosphine that results in greater steric hindrance around the Pd center. 'Ligandless' C-H activation may therefore be possible, even for these unactivated substrates.

4.3.1. Catalytic Direct Arylation. Eisenstein and Perutz have reported work on the direct arylation of polyfluorinated arenes, Ar^F-H.[139] Starting from a [Pd(κ^1-OAc)(Ph)(DMA)(PMe_3)] adduct (with DMA trans to PMe_3) B3PW91(DMA) calculations (with free energies at 100 °C) assessed the initial DMA/arene exchange and C-H activation steps, as well as the subsequent steps involving HOAc dissociation, C-C reductive coupling and dissociation of the biaryl product. The computed trends show a marked dependency on the number of fluorines that are *ortho* to the reacting C-H bond. Thus DMA/arene exchange is always endergonic, but is least so with substrates featuring no *ortho*-F

which can form π-adducts. Substrates with two *ortho*-F form Pd···H-C adducts, this interaction being enhanced by H-bonding to the free arm of the κ^1-OAc . The C-H bond cleavage is also promoted by two *ortho*-F substituents and as a result these substrates have the lowest overall barriers to C-H activation. In contrast, C-C reductive coupling is disfavored by *ortho*-F substituents. The trends in C-H activation reflect both the C-H bond acidities (related to the computed heterolytic BDEs) and the homolytic BDE of the Pd-Ar^F bond formed in the [Pd(Ar^F)(Ph)(HOAc)(PMe_3)] intermediates. A stronger Pd-Ar^F bond also increases the barrier to C-C coupling which is accessed after HOAc dissociation. Overall, the C-H activation is more sensitive to the number and location of the F-substituents as the trends in C-H bond acidity and the Pd-Ar^F bond strength reinforce each other; in contrast while a strong Pd-Ar^F bond will tend to increase the barrier to C-C coupling this effect is counter-balenced by the greater stability of the [Pd(Ar^F)(Ph)(PMe_3)] intermediate. The importance of the Pd-Ar bond strength on the regioselectivities of (hetero)arene activation at [Pd(κ^2-OAc)(Ph)(PMe_3)] has also been discussed by Ess and co-workers (M06 calculations).[140] Gorelsky has questioned this[135] and re-emphasized the role of the ΔE_{int} term, due to the poor correlation between ΔE_{int} and the computed Pd-Ar^F heterolytic BDEs. However, as ΔE_{int} may depend on other factors than just the Pd-Ar^F bond strength, these two interpretations may not be mutually exclusive. A role for 'Ag_2CO_3' in deprotonating C_6F_5H has also been suggested in a B3LYP study of the [Pd($OAc)_2$]-catalysed oxidative coupling with benzene.[141]

A novel approach to the activation of fluorobenzene was reported by Larossa who used [$Cr(CO)_3$(η^6-C_6H_5F)] as a substrate for C-H activation at [Pd(κ^2-OAc)(Ph)(PMe_3)].[142] B3LYP calculations indicate the barrier to C-H activation *ortho* to F is 25.0 kcal/mol, 5.7 kcal/mol lower than that for free fluorobenzene. An activation strain analysis indicates that distortion of the C-H bond is significantly reduced in the complexed C_6H_5F, reflecting the enhanced acidity induced by the {$Cr(CO)_3$} moiety.

Gorelsky has probed the effect of the *N*-bound CuCl additive on the computed barriers to C-H activation of azoles at [Pd(κ^2-OAc)(Ph)(PMe_3)] (B3LYP, see Figure 30).[136] Free azoles favor reaction at

C5 but this changes to C2 in the presence of the Cu(I) salt; for *N*-methylimidazole and oxazole this mirrors the swap in regioselectivity seen experimentlaly. The Lewis acidic CuCl moiety shifts the azole from a Class II substrate (nucleophilicity dominant)[143] to a Class I substarte (C-H bond acidity dominant). Similarly the thiazole *N*-oxide has a much lower barrier to C2-H bond activation (16.7 kcal/mol) than in the free thiazole (26.3 kcal/mol). The C-H activation of *N*-alkylindoles has also been studied and an AMLA/CMD mechanism found to be applicable to a range of substituents in the C6 position.[144] Computed barriers could be understood if these species are considered as Class II substrates, while regioselectivities correlated with the distribution of the HOMOs of these species.

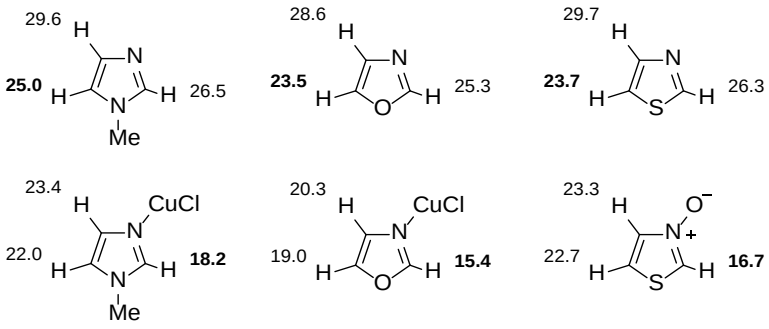

Figure 30. Computed activation barriers (free energies, kcal/mol) for C-H activation for *N*-methylimidiazole and oxazole (and their *N*-bound CuCl adducts), thiozole and thiazole *N*-oxide at [Pd(κ^2-OAc)(Ph)(PMe_3)].[136] Reproduced with permission from Ref. 43. Copyright 2016, John Wiley and Sons.

Due to their importance in synthesis a number of studies have considered the reactivity of heterocyclic *N*-oxides. Campeau reported kinetic studies, supported by B3LYP calculations on the direct arylation of pyridine *N*-oxide.[145] Experimental studies show the catalytic coupling of *para*-nitropyridine *N*-oxide with 5-bromo-*m*-xylene involves initial P^tBu_3 loss and Ar-Br activation to form a dimeric resting state. This must then open up in order to access the rate-determining C-H activation of the pyridine *N*-oxide. B3LYP calculations show that C-H activation at the 2-position of the pyridine *N*-oxide at [Pd(κ^2-O_2CR)(Ph)(PMe_3)] involves an AMLA/CMD inner-sphere process with computed

barriers of 34.9 kcal/mol or 34.1 kcal/mol for R = OH^- or CH_3 respectively. Pyridine ring substituent effects were also rationalised computationally. Although [Pd(κ²-OAc)(Ph)(P^{t}Bu$_3$)] (**72**) was proposed as the catalytically active species, this was later questioned by Hartwig who showed that **72** does not react with pyridine *N*-oxide. A cyclometallated dimer, [Pd(OAc)(^{t}Bu$_2$PCMe$_2$CH$_2$)]$_2$, **73**, was instead implicated (see Figure 31)[146] that opens to give a cyclometalated monomer, [Pd(κ²-OAc)(^{t}Bu$_2$PCMe$_2$CH$_2$)], **74**, that then effects the C-H activation. The bromo-analogue, [Pd(Br)(^{t}Bu$_2$PCMe$_2$CH$_2$)], is inactive and so C-H activation is suggested to proceed *via* an AMLA/CMD pathway with the intimate involvement of acetate, rather than, for example, a σ-bond metathesis with Pd-C bond of the cyclometallated phosphine ligand. B3LYP calculations gave a reduced barrier of 27 kcal/mol for C-H activation at **74** compared to 33 kcal/mol at **72**. Overall a cooperative mechanism is proposed featuring C-H activation of pyridine *N*-oxide at **74** to generate **75** (Figure 31). Exchange with the OAc ligand in **72** reforms **74** along with [Pd(Ar)(Ar')(P^{t}Bu$_3$)], **76**, from which reductive elimination yields the biaryl product and [Pd(P^{t}Bu$_3$)]. Under catalytic conditions the latter goes on to reform **73**/**74**. Gorelsky subsequently confirmed that the computed selectivities of C-H activation for a range of heterocycles are the same at cyclometalated species **74** as seen previously at **72**, and that these trends can be understood by the activation strain model.[147]

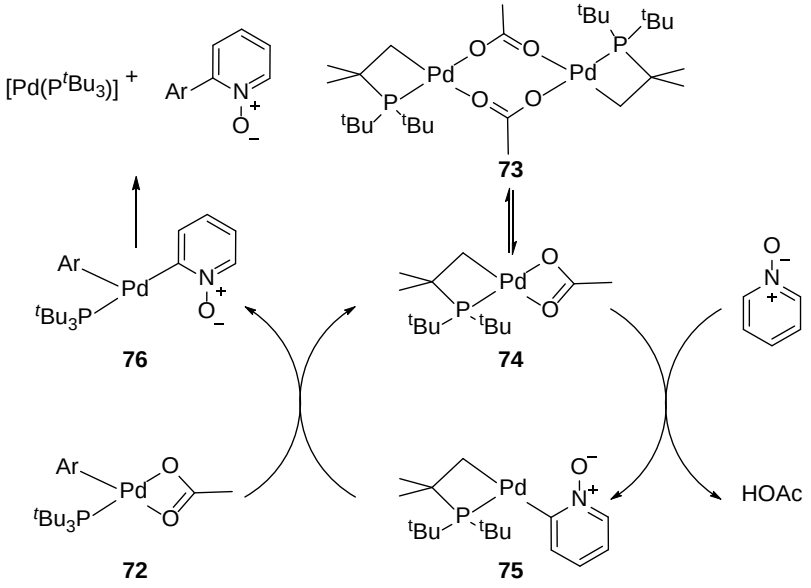

Figure 31. Proposed mechanism for the direct arylation of pyridine *N*-oxides in the $[Pd(OAc)_2]/P^tBu_3$ system. Adapted with permission from Ref 146. Copyright 2012, American Chemical Society.

The C-H activation of 2-substituted thiophenes at the 5-position was modelled by Gorelsky and Lapointe using a $[Pd(\kappa^2\text{-}OAc)(Ph)(PMe_3)]$ model system and B3LYP calculations.[137] Computed barriers showed a correlation with the nucleophilicity of the substrate and additional correlations between σ_p and both ΔE_{act} and ΔE_{dist} were established. Substrates featuring both electron-withdrawing substituents (CN, CO_2Me) and certain electron-donating groups (*N*-pyrrolidine) both displayed lower computed barriers than the unsubstituted thiophene, and this enhanced reactivity was confirmed in experimental competition studies. The fact that both electron-withdrawing and electron-donating groups can be more reactive reflects the counter-balancing effects of enhanced acidity (less favorable ΔE_{int}, more favorable ΔE_{dist}) *vs*. enhanced nucleophilicity (more favorable ΔE_{int}, less favorable ΔE_{dist}). A negative gradient in a Hammett plot is often taken as evidence of S_EAr character, however, and so this study is particularly significant in showing that σ_p can show a similar correlation with the components of the activation strain model and that a negative Hammett gradient can therefore also be compatible with mechanisms based on AMLA/CMD C-H activation. An earlier B3LYP study of substituted thiophenes and *N*-methylindoles had also indicated rate enhancement upon introduction of an electron-withdrawing Cl substituent, as well as highlighting useful regioselectivities that could be exploited synthetically.[148]

Ozawa has studied mechanistic variations seen experimentally for the stoichiometric direct arylation of thiophenes and benzothiazoles with $[PdAr(\mu\text{-}OAc)(PPh_3)]_n$ (Figure 32).[149] M06-2X(1,4-dioxane)//B3LYP calculations on a simple $[Pd(\kappa^2\text{-}OAc)(Ph)(PH_3)]$ model reproduced the observed change in rate-determining step, from AMLA/CMD C-H activation with benzothiazole ($\Delta G^{\ddagger}_{span}$ = 23.8 kcal/mol) to C-C coupling with 2-methylthiazole ($\Delta G^{\ddagger}_{span}$ = 25.2 kcal/mol). Calculated k_H/k_D KIEs also aligned well with experiment. The same workers then assessed the effect of *para*-substituents in the

triarylphosphine co-ligands, P(4-$C_6H_4R)_3$ (R = H, OMe, F and CF_3), on these processes.[150] The rates of reaction observed for [Pd(Ar)(κ^2-OAc){P(4-$C_6H_4R)_3$}] intermediates (Ar = 2,6-$C_6H_3Me_2$) follow opposite trends between benzothiazole (R = CF_3 > F > H > OMe) and 2-methylthiophene (R = OMe > H > F > CF_3). M06-2X(THF)//B3LYP calculations (Ar = Ph, Figure 32) again show the identity of the rate-determining step change depending on the substrate. Benzothiazole reacts via rate-limiting C-H activation (see **TS77**, Figure 32), with larger computed barriers arising from a stabilisation of the *N*-bound precursors when more electron-withdrawing phosphines are employed. For 2-methylthiophene the C-C reductive coupling step becomes rate-limiting (**TS78**) and this becomes more accessible with more electron-donating phosphines. Jing also found C-H activation of 6-Ph-imidazo[2,1-b]thiazole at [Pd(κ^2-OAc)(C_6H_4R)(PPh_3)] to be favored at C5 over C2 or C3 (B3LYP calculations).[151]

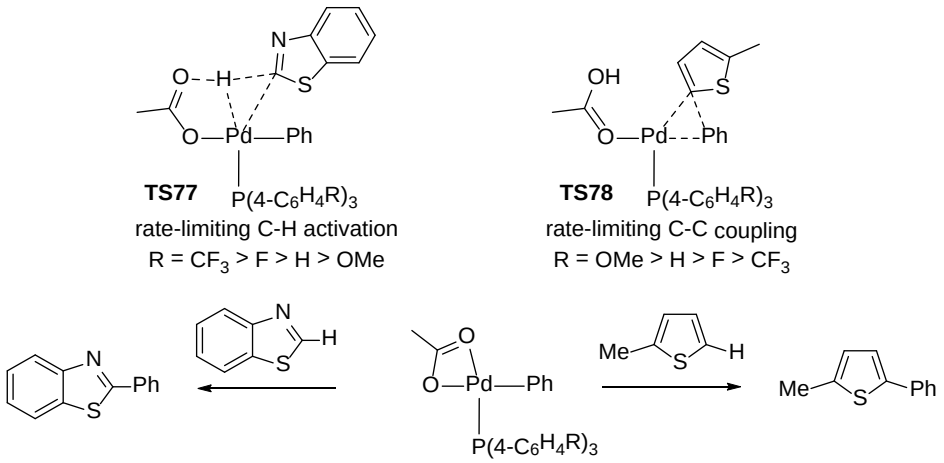

Figure 32. Phosphine-dependence in the direct arylation of benzothiazole and 2-methylthiophene.[150] Adapted with permission from Ref. 43. Copyright 2016, John Wiley and Sons.

With 2,3-disubstituted thiophenes the regioselectivity of the direct arylation has been shown to depend on the choice of co-ligand: with 2,2'-bipyridine (bpy) C5-arylation is seen, whereas with P{$OCH(CF_3)_2$}$_3$ arylation at the C4 postion dominates.[152,153] Using dispersion-corrected double hybrid DFT (B2PLYP-D3//TPSS-D3) Grimme, Itami and Studer modelled the reaction of $[PdPh(bpy)]^+$ with thiophene and showed a kinetic preference for insertion into the Pd-Ph bond with phenyl transfer

onto C3; however this step is reversible and product selectivity is governed by the deprotonation following insertion that favours C2.[154] Fu considered the reactions of 3-methoxy-2-phenylthiophene at [Pd(κ^1-HCO_3)(Ph)(bpy)] and [Pd(κ^2-HCO_3)(Ph){P(OR)$_3$}] (R = Me, $CH(CF_3)_2$) with M06(toluene)//B3LYP calculations.[155] With the bpy co-ligand activation at the C5-H bond proceeds via **TS79** with $\Delta G^{\ddagger}$ = 29.9 kcal/mol (see Figure 33). In this case the non-labile, bidentate bpy mandates the initial displacement of HCO_3^- by the thiophene substrate, with the liberated base then completing the C-H activation via an external CMD mechanism. Alternatively, thiophene may undergo a Heck-type insertion but this has a higher barrier of 31.6 kcal/mol (and in fact favors Ph-transfer onto the 4 position). Calculations with [Pd(Ph)(κ^2-HCO_3){P($OCH(CF_3)_2$)$_3$}] did capture the change in regioselectivity, with C5-H bond activation having a computed barrier of 36.7 kcal/mol while insertion with Ph transfer to C4 is more accessible *via* **TS80** with a barrier of 34.4 kcal/mol. Experimentally the reaction proceeds at 130 °C in 12 hours. The use of P{$OCH(CF_3)_2$}$_3$ in the calculated model was important as specific H-bonding interactions involving this ligand in the transition state are suggested to control the selectivity. With a simpler P(OMe)$_3$ model the change in selectivity was not reproduced.

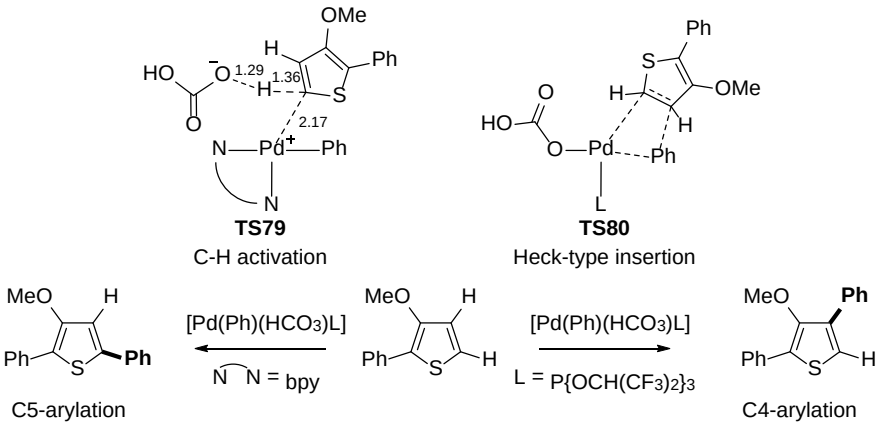

Figure 33. Different outcomes of the direct arylation of 3-methoxy-2-phenylthiophene with selected distances in Å for the C-H activation transition state **TS79**.[155] Adapted with permission from Ref. 43. Copyright 2016, John Wiley and Sons.

4.3.2. Oxidative coupling. Several studies have considered the Pd-mediated arylation of cyclometallated ligands that themselves have been formed by C-H activation. Using MP4(SDQ)//B3PW91(C_6H_6) Sakaki modelled the reaction of benzo[*h*]quinoline (**bzq**) with benzene occurring at monomeric [$Pd(OAc)_2$] with a focus on the promoting effect of a benzoquinone additive (**bq**).[86] After formation of the cyclometallated intermediate (see Section 4.1) substitution of HOAc by **bq** leads to [Pd(**bzq'**)(κ^2-OAc)(η^2-**bq**)] at -34.6 kcal/mol. C-H activation of benzene then proceeds with a barrier of 26.7 kcal/mol to give [Pd(**bqz**')(Ph)(HOAc)(η^2-**bq**)] from which the final C-C coupling occurs with a very low barrier of only 0.4 kcal/mol. The major role of the **bq** additive is to promote this C-C coupling, as in its absence the barrier rises to 34.7 kcal/mol.

Sanford and Schoenebeck were the first to define an intermolecular AMLA/CMD C-H activation at a dimeric Pd system in their study of the role of base in the selective arylation of **bzq** with 1,3-dimethoxybenzene (DMB) in the presence of **bq**. This leads to coupling at either the 5- or the 4-position of DMB depending on whether acetate or carbonate is used.[156] Starting from the cyclometalated dimers, [Pd(**bzq'**)(μ-O_2CR)]$_2$, M06L(DMSO or DMB)//ωB97X-D calculations considered C-H activation directly at the dimer or via the [Pd(**bzq'**)(κ^2-O_2CR)] monomer. For acetate, C-H activation at the 4-/5-positions via the monomer proceeds with overall barriers of 35.5/42.2 kcal/mol. This involves a regular AMLA/CMD transition state and compares with barriers of 35.9/41.8 kcal/mol at the dimer. The latter process involves opening the bridged dimer structure to permit C-H bond cleavage via a Pd-supported external CMD (**TS81**, *cf*. **TS27**, Figure 13 where Ag^+ plays a similar role[89]). For carbonate (modelled by '$NaCO_3^-$') the equivalent data are 32.5/39.0 kcal/mol and 32.2/36.5 kcal/mol respectively. Thus C-H activation is clearly favored at the 4-position with both bases and for '$NaCO_3^-$' the C-H activation is also the selectivity determining process. For acetate, however, C-C reductive elimination becomes the highest lying transition state and this favors the 5-position. The reversibility of C-H activation under these circumstances was tested experimentally by use of an insoluble MgO base to act as an acid trap; arylation at the 4-position was then observed.

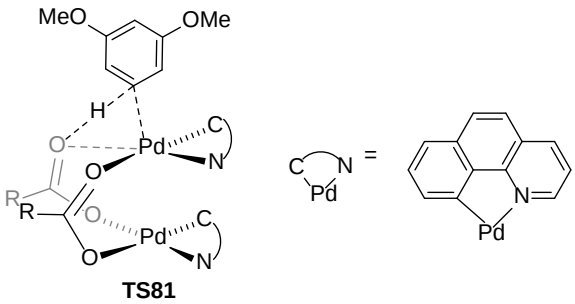

TS81

In their 2013 paper Canty, Sanford and Yates modelled the arylation of 3-methyl-2-phenylpyridine (**mppy**) with $[Ph_2I][BF_4]$ at the [Pd(**mppy'**)(μ-OAc)]$_2$ dimer, where the latter is formed by a facile external deprotonation by the basic substrate (see Section 4.1).[87] The reaction then proceeds via Ph^+ transfer from Ph_2I^+ to Pd(II) with a barrier of 20.7 kcal/mol to give [Pd(Ph)(**mppy'**)(μ-OAc)$_2$Pd(**mppy'**)]$^+$ from which C-C reductive coupling has a barrier of 7.0 kcal/mol. The retention of Pd···Pd interactions in these processes is thought to be important, as much higher barriers are computed with more open dimer structures. Overall, oxidation of the [Pd(**mppy'**)(μ-OAc)]$_2$ dimer by Ph_2I^+ is rate determining and this is in agreement with the lack of any experimental k_H/k_D KIE. A computational study on the arylation of enamide **35** with $PhSi(OMe)_3$ with a $Pd(OAc)_2$/AgF catalyst has been previously highlighted in Section 4.1.[96]

Oxidative coupling based on two intermolecular C(sp^2)-H activations has also been considered**.** In an insightful study, Peng, Paton and Hong used ωB97X-D(HOAc) calculations to model selectivity in the oxidative cross coupling reactions of heterocycles **82$_x$** with benzene and **bq** (Figure 34).[157] Modeling a [Pd(TFA)$_2$] catalyst in pivalic acid H/D exchange studies show enolone **82$_o$** undergoes reversible C-H activation at C3 for which calculations provide an overall barrier of 18.9 kcal/mol relative to a [Pd(κ^2-TFA)(κ^1-TFA)(η^2-C_6H_6)] adduct formed in benzene solution. This is 9.2 kcal/mol more accessible than C-H activation at C2, reflecting the more π-electron rich character of the C3 position. However, in this case C-H activation of the benzene solvent is more accessible ($\Delta G^{‡}$ = 17.7 kcal/mol) and should dominate due to the excess of benzene present, as well as the availability of six C-H bonds for reaction. A [Pd(Ph)(TFA)(κ^1-*O*-**82$_o$**)] intermediate is therefore formed. However C-H activation of **82$_o$**

at this species would still favour reaction at C3 ($\Delta G^{\ddagger}$ = 24.1 kcal/mol); instead, insertion of the alkene moiety into the Pd-Ph bond proved more accessible ($\Delta G^{\ddagger}$ = 16.8 kcal/mol) and this does result in Pd-C3 bond formation. This regioselectivity again reflects the more electron rich-character of the C3 position but now it leads to the C2 functionalised product, **83**. In the reaction with **bq**, the initial C3-H bond activation of $\mathbf{82_O}$ will dominate as this is 8.7 kcal/mol more accessible than that of **bq**. This step therefore determines the formation of product **84** with C3 selectivity.

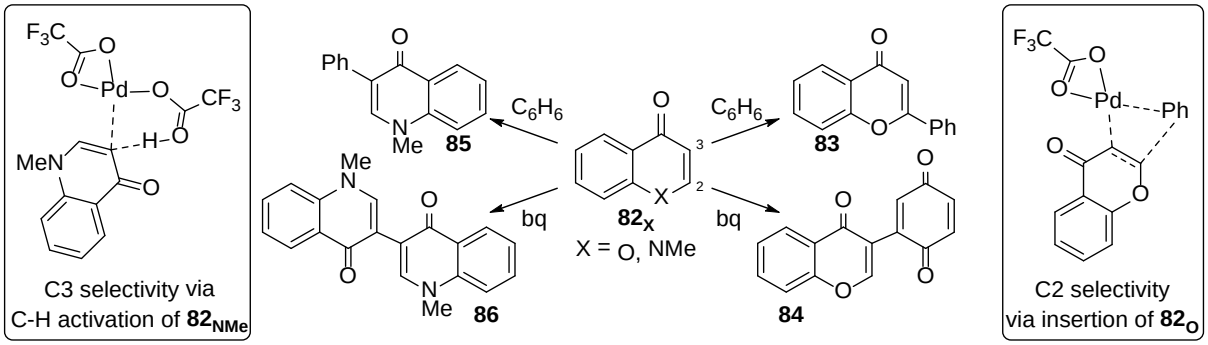

Figure 34. Selectivity in the oxidative cross coupling reactions of heterocycles $\mathbf{82_X}$ (X = O, NMe) with benzene and **bq**. Adapted from Ref. 157.

With enaminone $\mathbf{82_{NMe}}$, C-H activation at C3 is again preferred over C2 and is now significantly more accessible than the C-H activation of benzene ($\Delta\Delta G^{\ddagger}$ = -4.4. kcal/mol). Thus C3-H activation leads to a [Pd($\mathbf{82_{NMe}'}$)(κ^2-TFA)(η^2-C_6H_6)] intermediate from which the C-H activation of benzene and subsequent C-C reductive coupling forms **85**. The higher reactivity of $\mathbf{82_{NMe}}$ makes its C-H activation competitive with that of benzene and so some homocoupling is also observed that results in **86**. All the C-H activations in this study were characterised as AMLA/CMD processes and no evidence for a Wheland intermediate or an external CMD process was seen. Good correlations between the C-H activation barriers and certain transition state metrics were noted - in particular the developing Pd···C distance and the distortion of the C–H bond out of the ring-plane. This reflects the greater reactivity of the more electron rich-substrates in this system and, within a given substrate, the more

electron-rich site. These benefit from a greater degree of Pd···C interaction in the transition state and the resultant increase in C–H acidity due to the out-of-plane distortion of the reacting C–H bond.

Hu and You have used B3LYP calculations to model the [$Pd(OAc)_2$]-catalysed coupling of *N*-methylimidazole with thiophene, were the former is a model for xanthines (see Figure 35).[158] Thiophene is computed to readily undergo C-H activation at [$Pd(OAc)_2$] with a barrier (based on SCF energies) for reaction at the 2-position of only 9.6 kcal/mol. Although described as proceding via S_EAr, the computed transition state appears typical for an intermolecular AMLA/CMD process. Displacement of HOAc by *N*-methylimidazole gives **87**, which then undergoes C-H activation at the 2-position with a barrier of 43.2 kcal/mol to yield **88**. Alternatively, a second thiophene may bind to give **89** which can access a Heck-type insertion of the C2=C3 bond into the Pd-thiophenyl bond with a slightly lower barrier (relative to **87**) of 39.4 kcal/mol. The resultant formation of **90** would imply homocoupling, although this is not seen experimentally under the reaction conditions (20 hours at 120 °C in 1,4-dioxane). A follow-up study used M06(1,4-dioxane) calculations to model the oxidative coupling of caffeine and 2-formylfuran.[159] Shaik and Kozuch have highlighted the role of concentration effects in dictating the balance of homo- *vs.* hetero-coupling in oxidative coupling reactions.[160]

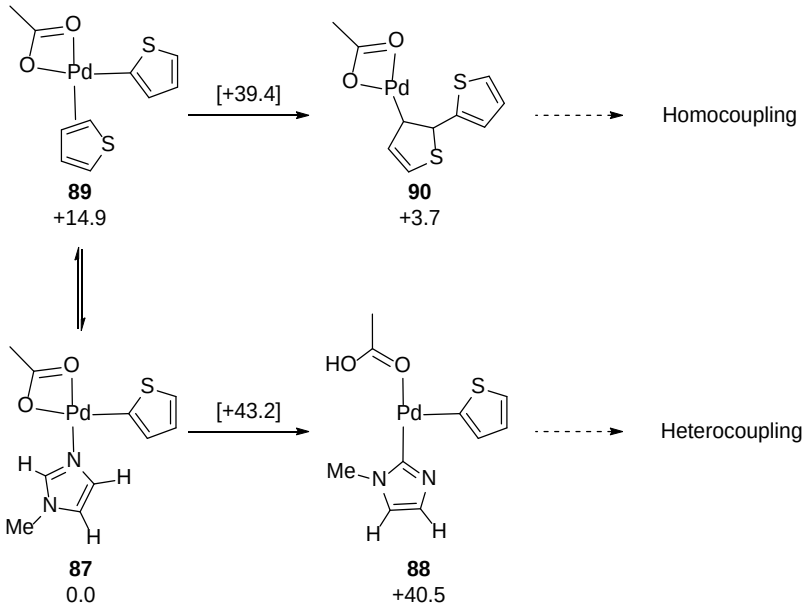

Figure 35. Computed key stationary points with for the reactions of thiophene and *N*-methylimidazole at [$Pd(OAc)_2$]; relative SCF energies are reported in kcal/mol.[158] Adapted with permission from Ref. 43. Copyright 2016, John Wiley and Sons.

4.3.3. Alkenylation Reactions. Benzene alkenylation by enolone **82$_o$** has already been discussed in the context of oxidative coupling in Section 4.3.2.[157] A related example was reported by Wu and Zeng for the *meta*-selective C-H functionalisation of pyridine (py) at [$Pd(OAc)_2$] in the presence of an MPAA ligand and using B3LYP(1-pentanol) calculations (see Figure 36).[161] The key intermediate formed prior to the C-H activation is [Pd(κ^1-OAc){κ-*N,O*-{AcNCH(^{i}Pr)CO_2}(py)] which is formed upon the double deprotonation of *N*-acetyl-valine and which features an *N*-bound pyridine ligand. Isomerisation to a π-bound form costs 17.1 kcal/mol and is necessary to access C-H activation via the AMLA/CMD transition state **TS91** (overall $\Delta G^{\ddagger}$ = 31.0 kcal/mol). C-H activation at either the *ortho*- or *para*-positions proves to be less accessible (overall $\Delta G^{\ddagger}$ = 32.4 kcal/mol and 31.9 kcal/mol, respectively). The possibility that the *N*-acetyl group may be implicated in the C-H activation step (that was later proposed by Houk[99]) was not considered (see **TS39**, Figure 15). Reprotonation promotes the *N*-decoordination of the MPAA ligand, which allows access to the subsequent reaction steps with ethyl acrylate. Zhang has published a related study with mono-substituted arenes.[162]

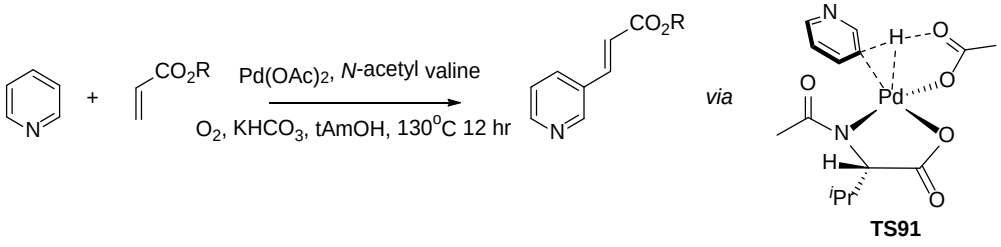

Figure 36. Pd-catalysed alkenylation of pyridine facilitated by an MPAA co-ligand (experiment R = ^{n}Bu; computed R = Et).[161] Adapted with permission from Ref. 43. Copyright 2016, John Wiley and Sons.

The Lewis acid-promoted alkenylation of indoles has been studied by Liao and Yin.[163] Starting from the $[Pd(OAc)_2]_3$ trimer B3LYP(MeCN, D3) calculations indicate $\Delta G^{\ddagger}_{span}$ = 28.4 kcal/mol for the favored C3-H activation via an initial $[Pd(OAc)_2(\eta^2_{CC}\text{-indole})]$ intermediate at +14.5 kcal/mol. In contrast addition of $[Sc(OTf)_3]$ serves to break up the trimer to give a bimetallic paddlewheel complex, $[Pd(\mu\text{-}OAc)_2(\mu\text{-}OTf)_2Sc(OTf)]$ at -20.9 kcal/mol from which C-H activation has a much reduced barrier of 14.5 kcal/mol. As a result the rate-determining step of the alkenylation moves from C-H activation to the alkene insertion ($\Delta G^{\ddagger}_{span}$ = 25.4 kcal/mol). β-H transfer and deprotonation of the resultant hydride produces a [Pd(HOAc)(alkene)] species which is then reoxidised by O_2 with formation of H_2O_2. The O_2 addition corresponds to the highest lying transition state in this latter half of the cycle and has an overall barrier of 20.3 kcal/mol.

4.3.4. C-S bond formation. Wang and Liu have proposed a mechanism for the arylthiolation of benzene with *N*-thiophenylsuccinimide, **92**, at a $[Pd(OAc)_2]$/TFAH catalyst system (Figure 37).[164] Using M06(TFAH)//B3LYP calculations they propose *trans*-$[Pd(TFA)_2(HOAc)_2]$ is initially formed at which the AMLA/CMD C-H activation of benzene proceeds with an overall barrier of 22.3 kcal/mol. **92** then binds in a κ^2-*O,S* fashion from which N-S activation occurs via **TS92** with a barrier of 23.6 kcal/mol. This process occurs with concomitant Ph-SPh bond formation, with this product being released after rearrangement and reprotonation of the succinimide ligand. The alternative sequence involving S-N activation then C-H activation is considerably less accessible.

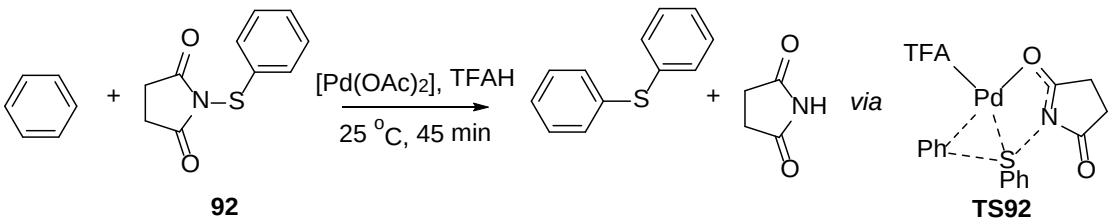

Figure 37. Pd-catalysed C-S coupling to form diphenylsulfide highlighting the N-S bond forming transition state. Adapted with permission from Ref. 164. Copyright 2016, The Royal Society of Chemistry.

4.4 Intermolecular C(sp^3)-H Activation

In a series of papers Strassner has considered the C-H functionalisation of simple alkanes in acidic media promoted by a [$PdBr_2$(L-L)] complex, **93**, featuring a chelating bis-NHC ligand (see Figure 38). B3LYP(TFAH, D3BJ) calculations suggest that the reaction proceeds from a [$Pd(TFA)_2$(L-L)] precursor from which TFA dissociation forms [$Pd(TFA)(L\text{-}L)(CH_4)]^+$ at +16.1 kcal/mol .[165] Intramolecular AMLA/CMD then proceeds with a barrier of 23.4 kcal/mol via **TS93**, and this is 8.3 kcal/mol more accessible than an external CMD involving the outer-sphere TFA counterion. Simple oxidative addition lies to even higher energy. The overall energy span is therefore 39.5 kcal/mol and forms, after deprotonation, an [$Pd(CH_3)(TFA)$(L-L)] intermediate at +30.5 kcal/mol. The preference for intramolecular AMLA/CMD over an external CMD in the C-H activation is a reversal of the situation computed by Morokuma in their study of C-H functionalisation of substituted alanines.[125]

After C-H activation, oxidation by dithionate leads to a $[PdMe(TFA)_2(L\text{-}L)]^+$ cation from which C-O reductive coupling readily occurs. An alternative pathway featuring C-H activation at a Pd(IV) species, $[PdBr_2(TFA)(L\text{-}L)]^+$, formed via facile oxidative addition of Br_2, lies only 3.6 kcal/mol higher in energy. The computed $\Delta G^{\ddagger}_{span}$ for C-H activation at the acetate analogue, [$Pd(OAc)_2$(L-L)], is slightly higher (40.7 kcal/mol) but this is composed of a much harder OAc dissociation (+25.0 kcal/mol) followed by a more facile C-H cleavage (+15.7 kcal/mol). Knowledge of the C-H activation step is in itself not sufficient to understand the overall C-H activation process: putting in place the circumstances for C-H activation to occur, e.g. by prior ligand dissociation, can be equally if not more important and will reflect a balance between the favorable effects of greater basicity against the unfavorable consequences of stronger coordination. The resting state of the system was subsequently proposed to be [$PdBr_4$(L-L)] which is computed to lie 14.8 kcal/mol below [$PdTFA_2$(L-L)].[166]

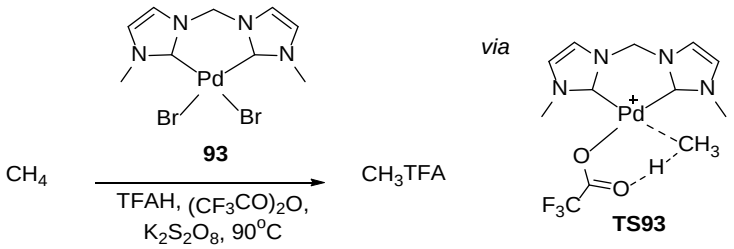

Figure 38. C-H functionalisation of methane catalysed by [$PdBr_2$(L-L)] **93** via C-H activation transition state **TS93**. Adapted with permission from Ref. 165. Copyright 2013 American Chemical Society.

The reaction of propane at [$Pd(TFA)_2$(L-L)] proceeds via a similar mechanism with $\Delta G^{\ddagger}_{span}$ for activation of a primary C-H bond being 38.1 kcal/mol, 5.0 kcal/mol below that for a secondary C-H bond.[167] Experimentally, however, the formation of $^{i}PrOC(O)CF_3$ is observed and this is explained by the facile isomerisation of [$Pd^{n}Pr$(L-L)]$^{+}$ to the more stable 2^{o} alkyl, [$Pd^{i}Pr$(L-L)]$^{+}$, which is stabilised by the stronger donating ability of the ^{i}Pr ligand. This also favors the subsequent oxidation by Br_2 and ultimately the formation of the observed product.

5. Nickel and Platinum

Relatively few computational studies of carboxylate-assisted C-H activation at nickel have been reported, the first being within the 2014 B3LYP(toluene, D3) general study by Huang, Wang and Chen into *N*,*N*-bidentate directing groups.[92] The transition state computed for C(sp^2)-H activation of *N*-(pyridin-2-ylmethyl)-benzamide at [$Ni(OAc)_2$], **TS94**, exhibits a geometry characteristic of an AMLA/CMD process. A subsequent study considered C(sp^3)-H activation in related systems.[93]

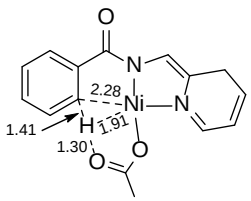

TS94
(distances in Å)

Fu has studied the alternative selectivities seen for the [Ni(COD)$_2$]/dcype-catalysed arylation of azole **95** using different aryl carboxylate reactants, RCO$_2$Ph (R = 2-thiophenyl, ^{t}Bu; COD = cyclooctadiene; dcype = 1,2-bis-(dicyclohexylphosphino)ethane, see Figure 39).[168] For R = 2-thiophenyl M06L(dioxane)//B3LYP calculations suggest initial oxidative cleavage of the C(acyl)-O bond at {Ni(dcype)} is favored over C(phenyl)-O bond activation. 'K_3PO_4'/OPh exchange then liberates 'KOPh' and installs '$K_2PO_4^-$' at the Ni center. This acts as an intramolecular base for C-H activation via **TS95b** after which rate-limiting decarbonylation and C-C reductive elimination yield the coupled products. This mechanism has an energy span of 30.1 kcal/mol and is consistent with the absence of a k_H/k_D KIE and the inverse dependency on [CO] seen experimentally. For R = ^{t}Bu the greater steric bulk makes the decarbonylation step prohibitively high in energy. Instead the reaction starts with cleavage of the C(phenyl)-O bond at Ni(0) to give [Ni(κ^1-OPiv)(Ph)(dcype)]. OPiv is not however used in the subsequent C-H activation, but rather exchange with 'K_3PO_4' leads to a 'K_2PO_3'-assisted C-H activation of the azole via **TS95a**. C-C coupling then gives the final product. In this case the C-H activation is rate-limiting with $\Delta G^{\ddagger}_{span}$ = 30.6 kcal/mol.

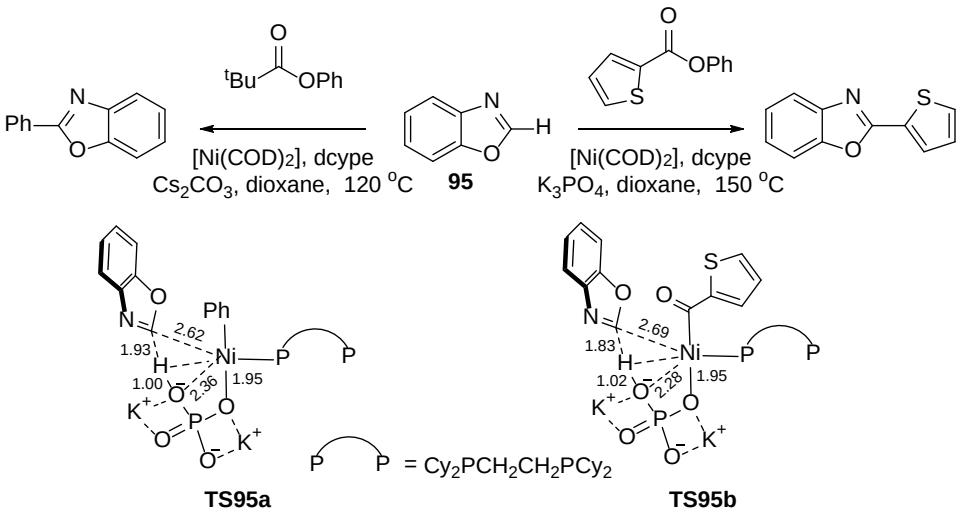

Figure 39. Alternative outcomes in the [Ni(COD)$_2$]/dcype-catalysed arylation of azole, **95**, with aryl carboxylates; computed C-H activation transition states are shown with selected distances in Å. Adapted with permission from Ref. 168. Copyright 2014 American Chemical Society

Itami and Musaev have considered the related coupling of azoles with naphthalen-2-yl pivalates at the {Ni(dcype)} fragment with M06L calculations with optimisations including the effect of the 1,4-dioxane solvent.[169] C(naphthyl)-O activation forms [Ni(dcype)(2-naphthyl)(κ^1-OPiv)] at which intermolecular C-H bond cleavage of the azole is effected by the dissociating OPiv anion with concomitant Ni-C bond formation. Facile C-C reductive coupling then gives the final product. $\Delta G^{\ddagger}_{span}$ for this process is 34.7 kcal/mol with C-H activation involved in the rate-limiting transition state. Experimentally the reaction requires heating at 120 ^{o}C for 12 hrs, but up to 3-fold rate enhancements and improved yields were seen when a Cs_2CO_3 additive was employed. To account for this, a '$Cs_2CO_3(OPiv)^-$' cluster is proposed to be the active base in the C-H activation step; with this $\Delta G^{\ddagger}_{span}$ = 31.1 kcal/mol, while with '$K_2CO_3(OPiv)]^-$' an intermediate value of 32.5 kcal/mol is determined. This is therefore postulated to account for the differential effects of M_2CO_3 salts on the efficiency of C-H activation. Alternatively such salts are considered to be proton sinks that reduce the reversibility of C-H activation and so enhance the rate of the onward functionalisation reaction.[124, 145, 170] The relative efficiencies of different salts may also reflect their solubility.[156] On the other hand, Clot and Baudoin have shown that CO_3^{2-} can be intimately involved in the C-H activation step.[54] Identifying the species active in the C-H activation step, whilst often challenging, would help clarify these issues and in the Itami/Musaev study the computed stability of the proposed active species, [(dcype)Ni(Cs_2CO_3{OPiv})]$^+$, would make it an ideal target for experimental characterisation.

Since Goddard and Periana's initial characterisation of an AMLA/CMD C-H activation transition state for benzene activation at [Pt$(TFA)_2$(bpym)] and [Pt(pic)$(TFA)_2]^-$ (bpym = 2,2'-bipyrimidyl, pic = κ^2-N,O-picolinate; TFA = trifluoracetate),[47] very few studies have considered carboxylate-assisted C-H activations at Pt. This may reflect the greater capacity of this metal to undergo the alternative oxidative addition: for example, Goddard showed that CH_4 prefers oxidative addition at [PtCl(OSO_3H)(H-bpym)]$^+$ (featuring a protonated bpym ligand) over an external CMD by bisulfate.[171] Similarly in Morokuma's study of stereoselective C(sp^3)-H arylation of alanine derivatives at Pd$(TFA)_2$,

C-H activation at the Pt analogue of **Int67$_H$** (Section 4.2) was characterised but found to involve proton transfer to Pt, rather than the external TFA base as was seen with Pd.[125]

6. Rhodium and Iridium

6.1. Intramolecular C(sp^2)-H Activation

Davies and Macgregor have modelled the cyclometalation of *N*-alkylimines (**96-100**) and 2-phenylpyridine (**ppy**) at $[MCl_2Cp^*]_2$/NaOAc (M = Rh, Ir, see Figure 40(a)).[172] Experimentally, H/D exchange studies show C-H activation to be reversible at Rh while this process is irreversible at room temperature at Ir. Competition studies also gave trends in the substrate reactivities. Reaction profiles were computed at the BP86(solvent, D3) level (solvent = MeOH for M = Rh or CH_2Cl_2 for M = Ir) and are exemplified by those shown for the 2-thiophenyl derivative **98** in Figure 41. Opening of the $[MCl_2Cp^*]_2$ dimer in the presence of acetate followed by substitution of either Cl in $[MCl(\kappa^2\text{-}OAc)Cp^*]$ or OAc in $[M(\kappa^2\text{-}OAc)(\kappa^1\text{-}OAc)Cp^*]$ by **98** leads to the formation of **Int98a$_M$**. For Rh, a two-step AMLA/CMD C-H activation *via* an agostic intermediate, **Int98b$_{Rh}$**, gives the cyclometallated HOAc adduct **Int98c$_{Rh}$**; HOAc/Cl substitution then yields the observed product **101$_{Rh}$**. The energetics of this process (ΔG = -4.0 kcal/mol; $\Delta G^{\ddagger}$ = 11.8 kcal/mol) are consistent with reversible C-H activation and hence H/D exchange. For Ir the reaction has a higher overall barrier ($\Delta G^{\ddagger}$ = 17.4 kcal/mol) and is more exergonic (ΔG = -11.9 kcal/mol), consistent with an irreversible process under kinetic control. In this case C-H activation is a one-step process and corresponds to κ^2-κ^1 displacement of OAc. The lack of H/D exchange also indicates that HOAc/Cl exchange in **Int98c$_{Ir}$** must be faster than H/D exchange at the HOAc ligand and the back reaction to **Int98a$_{Ir}$**. Experimentally the Rh reactions are slower, taking much longer to achieve reasonable yields. However, the calculations show that this is due to a slow approach to equilibrium with Rh, with the reverse reaction being much more significant than for Ir.

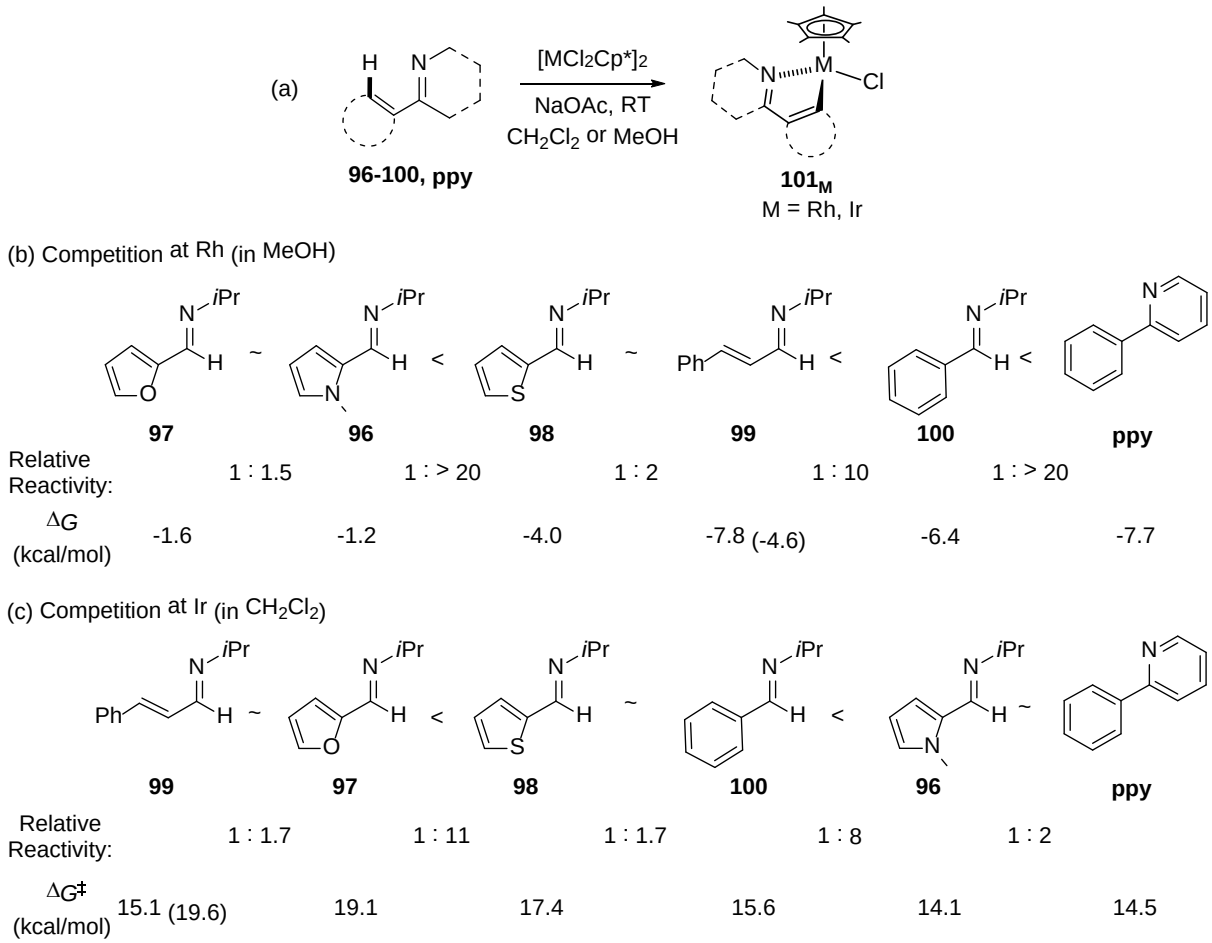

Figure 40. (a) Cyclometalation of *N*-alkylimines (**96-100**) and 2-phenylpyridine (**ppy**) at $[MCl_2Cp^*]_2$ (M = Rh, Ir) to give $\mathbf{101_M}$; (b) experimental reactivity trends and computed overall free energy changes (ΔG, kcal/mol) at $[RhCl_2Cp^*]_2$; (c) experimental reactivity trends and computed overall activation barriers, $\Delta G^{\ddagger}$, at $[IrCl_2Cp^*]_2$.[172] Data in parenthesis are for the modified ligand **99*** (see text for details). Adapted with permission from Ref. 43. Copyright 2016, John Wiley and Sons.

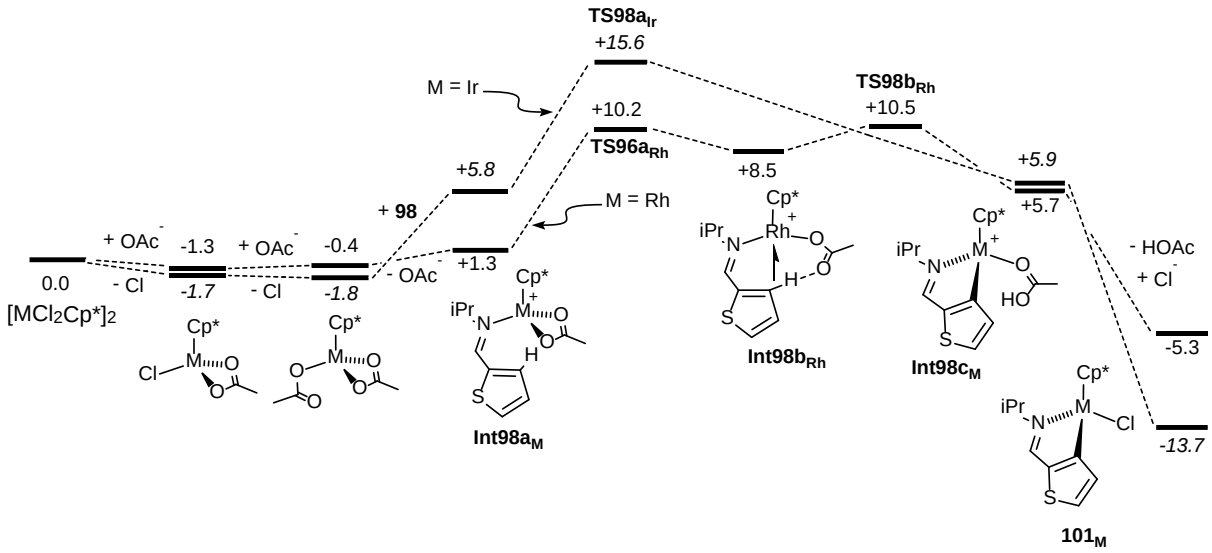

Figure 41. Free energy profiles (kcal/mol) computed for the reactions of **98** with $[MCl_2Cp^*]_2$ (M = Ir, Rh) to give cyclometallated **101$_M$**; data for M = Ir are in CH_2Cl_2 (italics) and for M = Rh in MeOH (plain text). Adapted with permission from Ref. 43. Copyright 2016, John Wiley and Sons.

Importantly, use of both the D3 correction and an extended basis set (with diffuse functions to ensure a reasonable description of the loosely held electron density of the free anions) was the key to reproducing the favorable thermodynamics that were expected for all the combinations of metal and substrate in this study. The stabilization due to dispersion becomes particularly significant when the bulky substrate is placed close to the {MCp*} fragment, and this also reiterates the need to employ the full experimental system in the calculations. Use of this protocol reproduces the more subtle trends in the substrate reactivities reasonably well. Thus for Rh (Figure 40(b), operating under thermodynamic control) the trend in ΔG largely mirrors the increase in substrate reactivity, whereas for Ir (Figure 40(c), under kinetic control) an increase in substrate reactivity is reflected in reduced overall barriers, $\Delta G^{\ddagger}$. One exception was **99**, for which the calculations overestimated the reactivity for both metals. Here the increased size of the vinyl CH=CHPh substituent compared to the aromatic substituents in **96-98** and **100** was postulated to lead to an anomalously high dispersion stabilization. This is because the chemical model, which is based on isolated molecules, tends to emphasize intramolecular stabilization over interaction with the environment, *i.e.* explicit solvent molecules, that are absent in the calculation. Hence, the degree of dispersion stabilization upon binding the

larger substrate **99** to the metal fragment is particularly overestimated. The behavior of a model substrate, **99***, which featured a smaller $CH{=}CH_2$ substituent was therefore assessed (data in parentheses, Figure 40). This gave both a reduced ΔG at Rh and an increased $\Delta G^{\ddagger}$ at Ir and is therefore more consistent with the experimental results for **99**. Shortly afterwards Zheng also compared Rh(III) and Ir(III) in a study of the cyclometalation of *N*-phenylbenzaldimines at $[MCl_2Cp^*]_2$ dimers in the presence of acetate.[173] B3LYP(MeOH) calculations again indicated that reaction at Ir was thermodynamically favored (Rh: ΔG = -0.5 kcal/mol; Ir: ΔG = -8.4 kcal/mol); however the barrier to C-H activation was now computed to be higher with Rh (Rh: $\Delta G^{\ddagger}$ = 26.4 kcal/mol; Ir: $\Delta G^{\ddagger}$ = 19.7 kcal/mol). Experimentally the reaction is indeed slower with Rh and the computational results suggest this may be due to either the higher barrier or, as in the Davies/Macgregor study, the reversibility of the process (and hence a slow approach to equilibrium) with Rh.[174] This study also assessed the effect of phenyl substituents, R, introduced *meta* to the directing group. With R = CF_3 or Me steric effects dominate, while for R = OMe and F reaction at the adjacent *ortho*-C-H bond becomes competitive; this change in selectivity is also seen experimentally.

Chen has also highlighted the importance of dispersion corrections in a benchmarking study of 19 different functionals against the results of CCSD(T)-F12 calculations.[175] The AMLA/CMD C-H activation step in $[Rh(\kappa^1\text{-}O_2CH)(\kappa^1\text{-}O_2CPh)Cp]$ was one of several bond activation processes considered, with optimisations performed at the B3LYP level. The CCSD(T)-F12//B3LYP energetics are $\Delta E^{\ddagger}$ = 11.7 kcal/mol and ΔE = -5.8 kcal/mol and the best overall performing functionals were B3LYP-D3 and ωB97X-D. Note this study did not consider the initial κ^2- κ^1 displacement of the carboxylate ligand that is usually a key component of the AMLA/CMD C-H activation process.

Cyclometallation of the *tris*-(2-thienyl)phosphine ligand in $[(HOAc)(P\{2\text{-thienyl}\}_3)Rh(\mu\text{-}OAc)_3Rh(OR')]$ dimers (**$102_{OR'}$**, OR' = OAc, OTf) has been studied by Lahuerta and Pérez-Prieto with B3PW91 calculations (see Figure 42).[176] For the OTf adduct cyclometalation proceeds from an *S*-bound precursor **102_{OTf}** which first rotates to a π-bound intermediate. This then undergoes rate-limiting

AMLA/CMD C-H bond cleavage ($\Delta G^{\ddagger} \approx 20$ kcal/mol; $\Delta G \approx +0.1$ kcal/mol) with the marginal endergonicity being consistent with facile H/D exchange. This pathway implies that the thienyl moiety never leaves the Rh coordination sphere and so H/D exchange is confined to one of the thienyl substituents, as is observed experimentally. For the OAc adduct calculations indicate a κ^2-precursor, **102_{OAc}**, from which C-H activation proceeds with a similar overall barrier, but within which the κ^2-κ^1 displacement is now rate-limiting. This reflects the greater coordinating ability of OAc *cf*. OTf. The reaction is now significantly exergonic (ΔG = -16 kcal/mol) and so consistent with irreversible cyclometalation in the presence of NaOAc and the experimental observation of **103_{OAc}**.

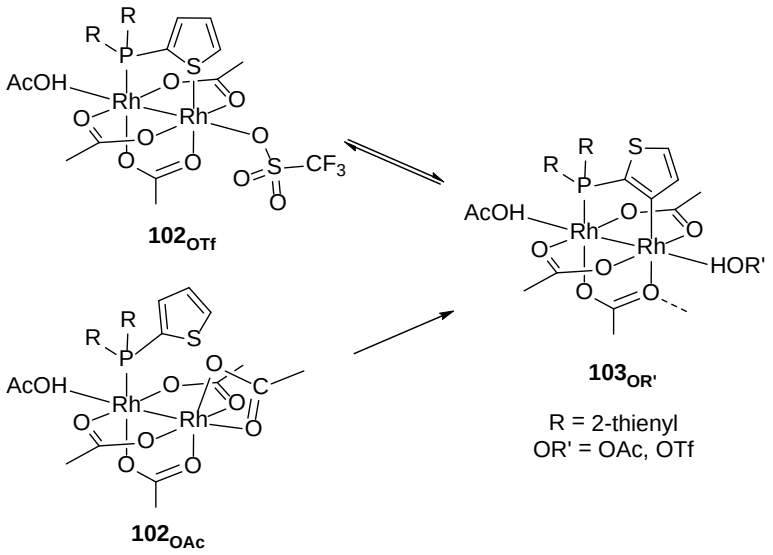

Figure 42. Cyclometallation of a *tris*-(2-thienyl)phosphine ligand in [(HOAc)(P(2-thienyl)$_3$)Rh(μ-OAc)$_3$Rh(OR')] (**$102_{OR'}$**, OR' = OAc, OTf). Adapted with permission from Ref. 176. Copyright 2009, John Wiley and Sons.

Carboxylate-assisted C-H activation has now been widely incorporated into cycles for Rh(III)-catalysed C-H functionalisation reactions. The $[RhCl_2Cp^*]_2$ dimer is the near-ubiquitous precursor in this chemistry and opening of this dimer by acetate (or another carboxylate) is usually assumed in computational studies to form $[Rh(OAc)_2Cp^*]$ or a related species as the catalyst precursor. One acetate ligand must then be removed to create a vacant site for an intramolecular AMLA/CMD C-H activation. Substrates bearing protic hydrogens can facilitate this by inducing loss of HOAc. The large

number of studies that have modelled AMLA/CMD C-H activation at Rh(III) indicate this occurs with modest barriers and with the endergonic formation of an initial cyclometallated HOAc adduct. Compared to Pd, fewer examples of direct C-H functionalisation have been reported with Rh; however, oxidative coupling reactions with unsaturated partners that result in the formation of heterocylic rings are more prevalent and this will be the initial focus below. A more limited number of related studies on Ir(III) catalytic C-H functionalisation have also appeared.

6.1.1. Catalytic Heterocycle Formation with Internal Oxidants. The use of benzamides, ArC(O)NHOR, and their coupling with alkynes, alkenes or carbenes has been extensively studied. In this process the OR group (OR = OMe, OPiv) acts as an internal oxidant via the oxidative cleavage of the N-O bond. This may occur either after a reductive coupling event in which case a Rh(III)-Rh(I)-Rh(III) cycle is involved. Alternatively N-O bond cleavage prior to coupling gives a Rh(III)-Rh(V)-Rh(III) cycle, typically with the formation of a Rh(V)-nitrene intermediate.

In 2011, Guimond published B3LYP(MeOH) calculations on the coupling of acetylene with *N*-acetoxybenzamide at $[Rh(OAc)_2Cp]$ to form isoquinolone, the first computational study of Rh(III)-catalyzed heterocycle formation based on a C-H activation and functionalization strategy (see Figure 43).[177] *N*-deprotonation followed by HOAc loss and directed C-H activation give $\mathbf{I_{OAc}}$ with an overall barrier of 20.5 kcal/mol, and this proved to be much more accessible than an alternative route based on the C-H activation of the neutral (i.e. *N*-protonated) substrate ($\Delta G^{‡}$ = 34.7 kcal/mol). Energetically accessible HOAc/HCCH exchange, insertion and N(sp^3)-C(sp^2) reductive coupling then form $\mathbf{IV_{OAc}}$, with the isoquinolone bound to a Rh(I) center (Rh-N = 2.13 Å) and the *N*-acetate group also chelates the Rh (Rh-O = 2.21 Å). N-O bond cleavage and simultaneous transfer of acetate to Rh then proceed with a minimal barrier ($\Delta G^{‡}$ = 0.8 kcal/mol) to form Rh(III) intermediate $\mathbf{V_{OAc}}$. The isoquinolone product is released via protonolysis by HOAc, which also completes the catalytic cycle. The calculations suggest that C-H activation is rate-limiting, consistent with the large k_H/k_D KIE observed experimentally with ArC(O)NHOPiv substrates. However, with *N*-methoxybenzamide no KIE was

observed indicating that the nature of the rate-limiting step is substrate dependent. Note that in this early paper a small model was employed and no dispersion correction was applied. A similar mechanism was recently characterised by Fang for the oxidative coupling of a MIDA boronate alkyne with PhC(O)NHOPiv using B3LYP(D3) calculations with optimisation in MeCN solvent and free energies at 313 K.[178] These show alkyne insertion is preferred with the boronate substituent adjacent to the metal on steric grounds. This study proposed that OPiv transfer to Rh(I) could be facilitated by prior binding of '[$Cu(OAc)_2$]' to the metal center.

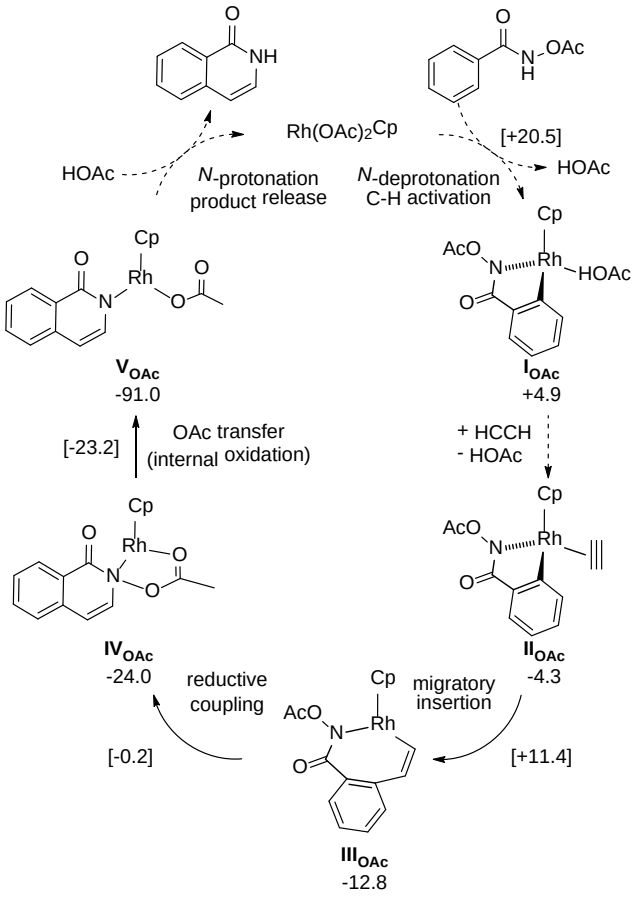

Figure 43. Catalytic cycle computed for the model reaction coupling acetylene with *N*-acetoxybenzamide at [$Rh(OAc)_2Cp$];[177] computed free energies (kcal/mol) are quoted relative to the reactants at 0.0 kcal/mol. Adapted with permission from Ref. 43. Copyright 2016, John Wiley and Sons.

In 2012 Xia published an important complementary study on the coupling of alkenes with PhC(O)NH(OR), where the outcome depends on the OR group: when OR = OMe β-H elimination is seen, whereas with OR = OPiv the alternative N(sp^3)-C(sp^3) coupling to give the 3,4-dihydroquinolone is observed (see Figure 44(a) for the case of ethene).[179] M06(MeOH) calculations on the reactions of both benzamides with ethene at [$Rh(OAc)_2Cp^*$] gave very similar *N*-deprotonation/C-H activation profiles in each case ($\Delta G^{\ddagger} \approx +18$ kcal/mol; $\Delta G \approx +4$ kcal/mol). HOAc/ethene substitution then allows insertion to form a conformationally flexible 7-membered rhodacycle, $\mathbf{I}_{OR}$, in which a weak interaction with the π-system of the original cyclometallated phenyl is maintained (Figure 44(b)). For OR = OPiv, however, the pendant oxygen can also coordinate to the metal center and this produces a more stable isomer in this case ($\mathbf{I'}_{OPiv}$, Figure 44(c)).

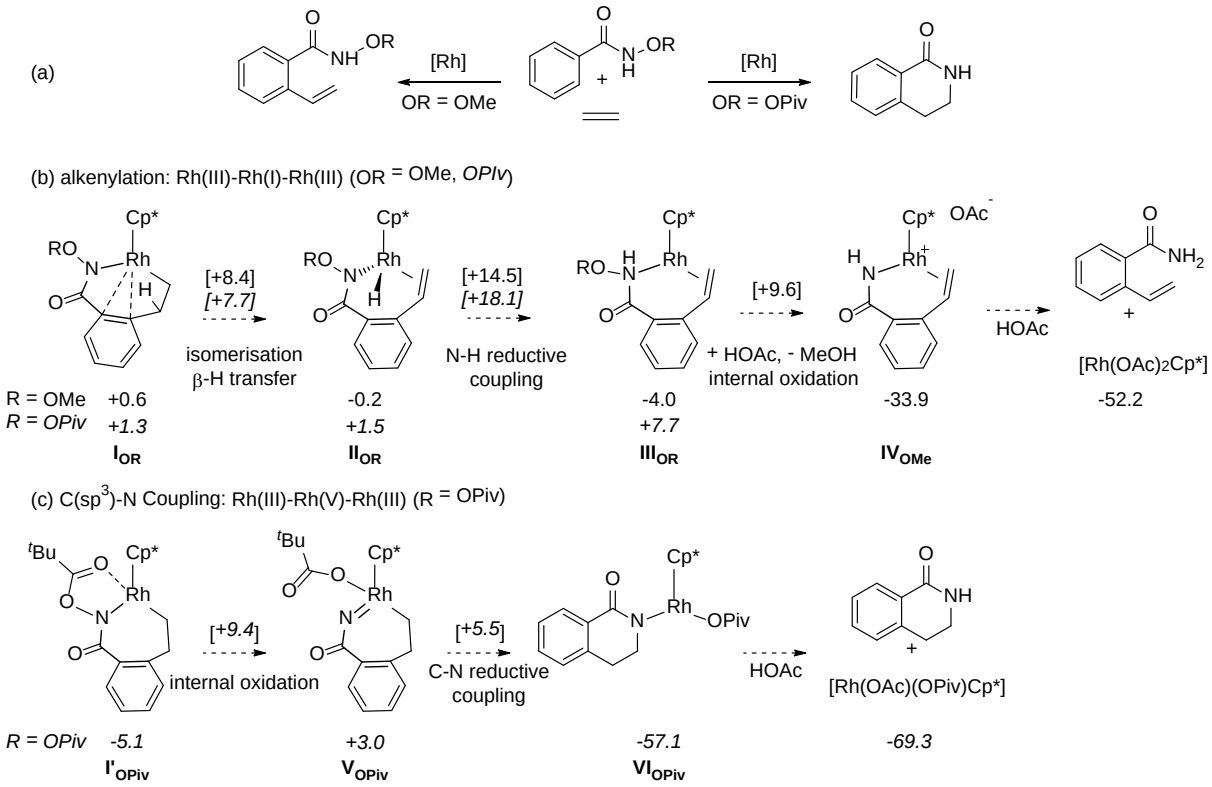

Figure 44. (a) Alternative reactions of ethene with PhC(O)NH(OR) (OR = OMe, OPiv) at [$Rh(OAc)_2Cp^*$].[179] (b) Key stationary points for the alkenylation pathway for OR = OMe and (in italics)

OPiv, with data for the onward reaction of **III$_{OR}$** for R = OMe only; and (c) C(sp^3)-N coupling for OR = OPiv. Free energies (kcal/mol) are quoted relative to the reactants at 0.0 kcal/mol. Adapted with permission from Ref. 43. Copyright 2016, John Wiley and Sons.

The fate of the 7-membered rhodacycles now depends on the *N*-substituent. For OR = OMe (Figure 44(b)), facile β-H elimination is followed by formal N-H reductive coupling to give Rh(I) intermediate **III$_{OMe}$**. This reacts with HOAc via cleavage of the N-O bond with a barrier of 13.6 kcal/mol to form MeOH and the Rh(III) species **IV$_{OMe}$**. The barrier to re-oxidation via OMe transfer onto Rh in **III$_{OMe}$** is 22.4 kcal/mol higher in energy. Product release and catalyst regeneration then occur by a second protonation with HOAc at the amide nitrogen in **IV$_{OMe}$**. Direct C-N coupling in **I$_{OMe}$** is too high to be competitive as it involves a transition state at +43.8 kcal/mol. In contrast, in **I'$_{OPiv}$** migration of the OPiv from N to Rh (Figure 44(c)) readily occurs to give Rh(V) nitrene **V$_{OPiv}$** ($\Delta G^{\ddagger}$ = 14.5 kcal/mol, Rh-N = 1.871 Å) and is now favored over β-H elimination and N-H reductive coupling (i.e from **I'$_{OPiv}$** to **III$_{OPiv}$**, $\Delta G^{\ddagger}$ = 23.2 kcal/mol). **V$_{OPiv}$** then undergoes facile C-N reductive coupling and protonolysis to complete the cycle. The OPiv group is thought to play several roles in this mechanistic swap: the extra Rh-O interaction stabilises the 7-membered rhodacycle **I'$_{OPiv}$** increasing the barrier to β-H transfer, while increased repulsion between the OPiv and the Cp* also destabilises the alkene intermediate, **III$_{OPiv}$**, making β-H transfer significantly endergonic. The Rh-O interaction in **I'$_{OPiv}$** is also key to the internal oxidation to give the Rh(V) nitrene intermediate **V$_{OPiv}$**,.

The regioselectivity of the insertion of styrene with PhC(O)NHOBoc (OBoc = $CO_2{}^tBu$) has been studied with PBE0(dDsC, MeOH)//ωB97X-D calculations by Corminboeuf and Cramer (Figure 45).[180] Experimentally, {RhCp*}-based catalysts favor the 4-isomer whereas those with {RhCp^{Cy}} groups promote formation of the 3-isomer. Calculations based on the pathways in Figure 44 indicate that the transition state energies for the insertion and internal oxidation steps are very similar. Hence, quantitative predictions of regioselectivity were difficult and so the computed data were used for kinetics simulations. These predicted the 3-isomer is favoured by a 76:24 ratio with {RhCp^{Cy}}, in

excellent agreement with experiment. For {RhCp*} the computed ratio is essentially 1:1, indicating a relative increase in the 4-isomer, although experimentally a 16:84 ratio is observed. The authors point out that this discrepancy equates to a 0.5 kcal/mol shift in energy and this highlights the computational challenge when such subtle selectivities are being modelled.

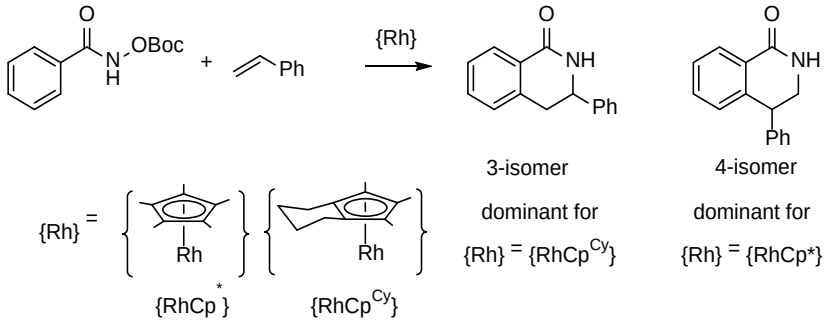

Figure 45. Dihydroisoquinolone formation with Rh-cyclopentadienyl catalysts.[180] Reproduced with permission from Ref. 43. Copyright 2016, John Wiley and Sons.

Xia subsequently used this mechanistic picture to rationalise the different outcomes of the Rh(III)-catalyzed C-H activation/cycloaddition of ArC(O)NHOPiv (Ar = Ph or 2-furanyl) with methylenepropenes (see Figure 46).[181] M06(MeOH) calculations characterise a similar sequence of *N*-deprotonation/C-H activation and alkene insertion for both substrates, although for Ar = Ph the C-H activation is rate-limiting ($\Delta G^{\ddagger}_{span}$ = 23.1 kcal/mol) while for Ar = 2-furanyl this is the alkene insertion ($\Delta G^{\ddagger}_{span}$ = 26.3 kcal/mol). These steps form 7-membered rhodacycles (*cf*. **I'$_{OPiv}$**, Figure 44(c)) from which the chemoselectivity is determined by a competition between OPiv transfer or β-C elimination. When Ar = Ph, OPiv transfer is favored ($\Delta G^{\ddagger}$ = 15.1 kcal/mol *cf*. 15.9 kcal/mol for β-C elimination) and the resultant Rh(V) intermediate readily undergoes C-N coupling with formation of **104**. In contrast with Ar = 2-furanyl, β-C elimination intervenes ($\Delta G^{\ddagger}$ = 10.5 kcal/mol *cf*. 13.3 kcal/mol for OPiv transfer) and forms an expanded 8-membered rhodacycle. OPiv transfer ($\Delta G^{\ddagger}$ = 14.6 kcal/mol) then accesses a Rh(V) species that undergoes C-N coupling to **105**. The more favorable β-C elimination computed with Ar = 2-furanyl reflects the ability of the furan moiety to accommodate strain in the transition state due to the intrinsically wider $C^1{=}C^2$-C and C-$C^1{=}C^2$ angles.

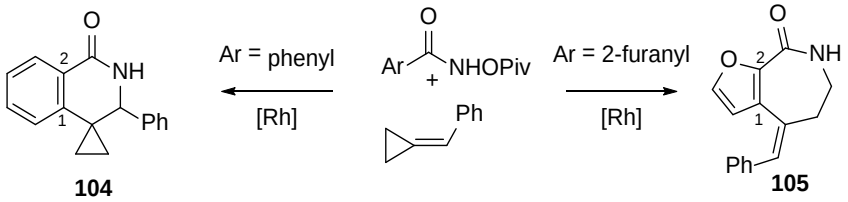

Figure 46. Different outcomes of the reaction of ArC(O)NHOPiv (Ar = Ph or 2-furanyl) with a methylenepropene. Adapted with permission from Ref. 181. Copyright 2015 American Chemical Society

Ma studied the related formation of 8-membered lactams (**106**, Figure 47) via coupling of allene-enes with *N*-acetoxybenzamide.[182] M06(MeOH) calculations based on a [Rh(κ^2-CO_3^-)Cp*] active species indicate that the carbonate can both deprotonate the substrate and (as HCO_3^-) effect the subsequent C-H activation. The latter C-H activation was found to be rate-limiting with ($\Delta G^{\ddagger}_{span}$ = 20.8 kcal/mol, ΔG = +5.4 kcal/mol) and this is consistent with the observations of efficient room temperature catalysis and a significant k_H/k_D KIE. In contrast, no H/D exchange was seen experimentally, even in the absence of the coupling partner, and this is at odds with the computed endergonic C-H activation. After coordination of the allene-ene insertion of the distal allenic double bond precedes that of the terminal alkene to form the rhodacyclic intermediates **107** and **108** respectively. The reaction is then analogous to that in Figure 44(c), with formation of a Rh(V) nitrene via OAc transfer again preferred to β-H transfer/N-H reductive coupling. Huang and Chen reported a related M06(MeOH)//B3LYP study on the Rh(III)-catalysed coupling of both cyclohexylallene and 1,1-dimethylallene with PhC(O)NHOR (OR = OPiv, OMe).[183] The computed results are consistent with the swap in selectivity seen experimentally, with the 4-isomer (*cf*. Figure 45) being favored with cyclohexylallene while the greater steric hindrance of 1,1-dimethylallene favors the alternative insertion that leads to the 3-isomer.

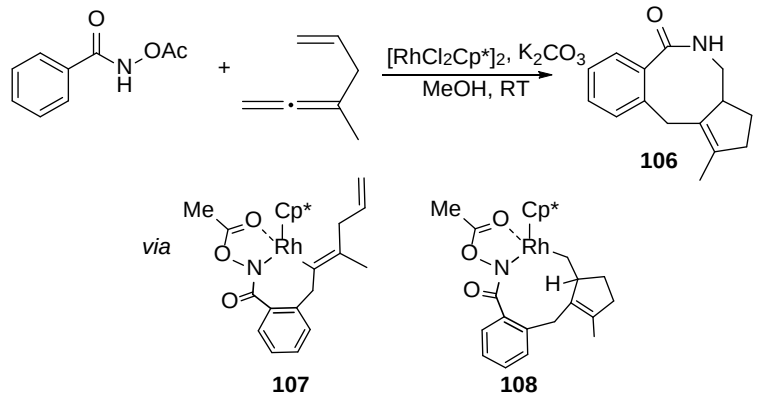

Figure 47. Rh(III)-catalysed formation of lactam **106** via coupling of *N*-acetoxybenzamide with 3-methylhexa-1,2,5-triene.[182] Adapted with permission from Ref. 43. Copyright 2016, John Wiley and Sons.

A further example of *N*-substituent control of selectivity was modeled by Li for the reactions of benzamides PhC(O)NHOR (OR = OMe, OPiv) with cyclohexadienone-containing 1,6-enynes, **109**, catalysed by $[RhCl_2Cp^*]_2$ (Figure 48).[184] M06(DMF) (OR = OPiv) and M06(DCE) (OR = OMe) calculations characterise accessible *N*-deprotonation and AMLA/CMD C-H activation with overall barriers of ca. 21 kcal/mol. Alkyne insertion then forms the 7-membered rhodacyclic intermediates $\mathbf{110_{OR}}$. The most stable isomer of $\mathbf{110_{OPiv}}$ has a pivalate bridging across the Rh-N bond and this facilitates C-N bond coupling (see Figure 48(a)). Cleavage of the Rh-OPiv bond effects the internal oxidation to give **111** from which an intramolecular Michael addition forms **112**. Experimentally a significant k_H/k_D KIE of 6.1 is observed, while computationally the C-N bond coupling is found to be rate-determining. However, this has a very similar barrier to that associated with the *N*-deprotonation/C-H activation (21.8 kcal/mol *cf*. 20.3 kcal/mol). With OR = OMe (Figure 48(b)) one site at Rh remains accessible in $\mathbf{110_{OMe}}$ and so insertion of the cyclohexadienone into the Rh-vinyl bond can form **113** from which rearrangement and protonolysis with 2 equiv of HOPiv gives **114** and $[Rh(OPiv)_2Cp^*]$ ($\Delta G^{\ddagger}_{span}$ = 27.3 kcal/mol). The use of a weakly coordinating solvent such as DCE may be significant as a more coordinating solvent might block alkene binding and insertion.

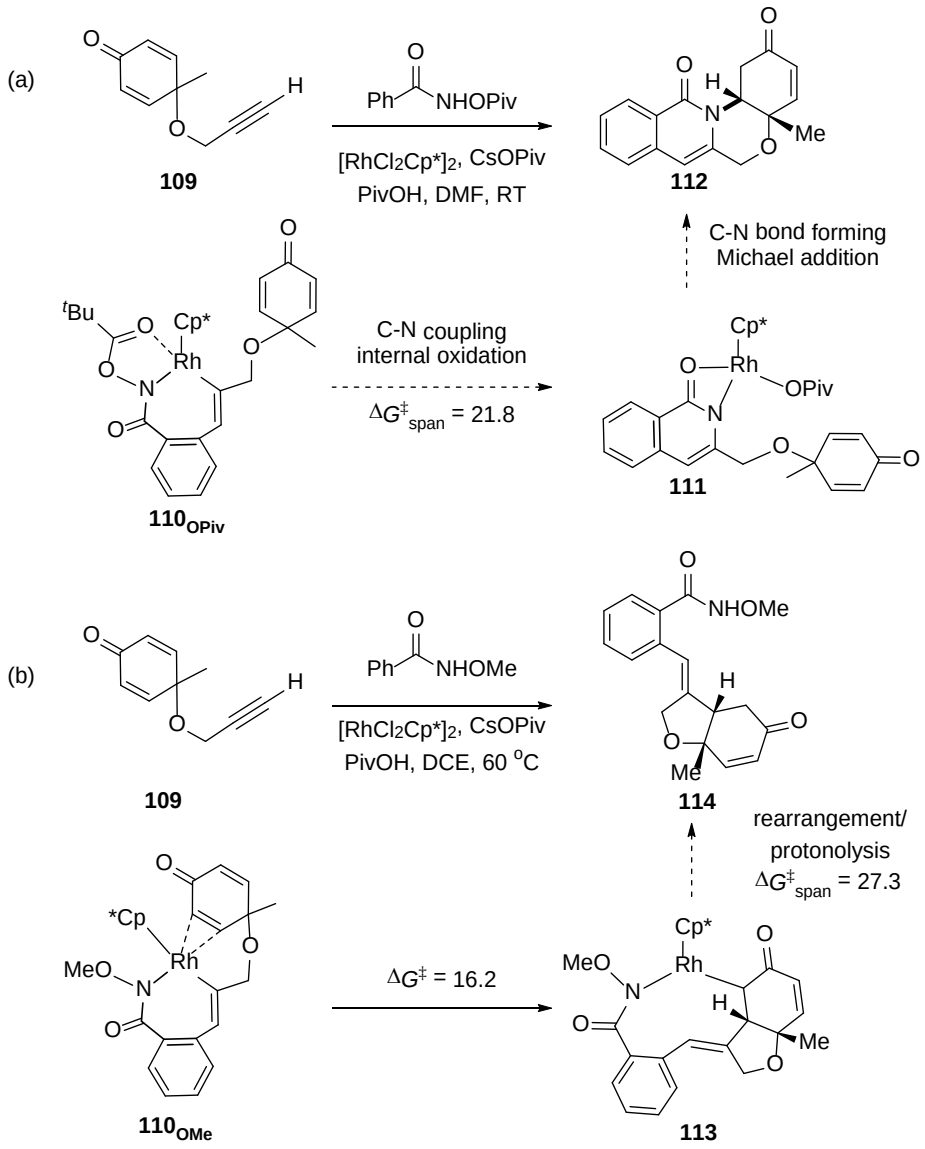

Figure 48. Reactions of PhC(O)NHOR with cyclohexadienone-containing 1,6-enynes, showing intermediates involved in the selectivity-determining steps; (a) OR = OPiv; (b) OR = OMe. Adapted with permission from Ref. 184. Copyright 2016 American Chemical Society

The different outcomes of the coupling of *N*-pivaloxybenzamide with diazocarbenes, $MeO_2CC(N_2)R$ (R = vinyl, Ph), have been rationalised by Xia with M06(MeCN) calculations (see Figure 49).[185] In this case after the initial cyclometalation, binding of the diazocarbene followed by N_2 loss and insertion into the Rh-aryl bond produces 6-membered rhodacycle intermediates of the type **115**. With R = Ph the expected oxidative cleavage of the N-O bond accesses a Rh(V)-nitrene, **116**, from which C-N reductive coupling and protonolysis give the 5-membered iso-indolinone product **117**. In contrast

when R = vinyl rearrangement via a 1,3-allylic migration permits expansion to a 8-membered rhodacycle. N-O oxidative cleavage then forms the Rh(V)-nitrene intermediate **118** from which C-N reductive coupling forms a 7-membered cyclic lactam **119**.

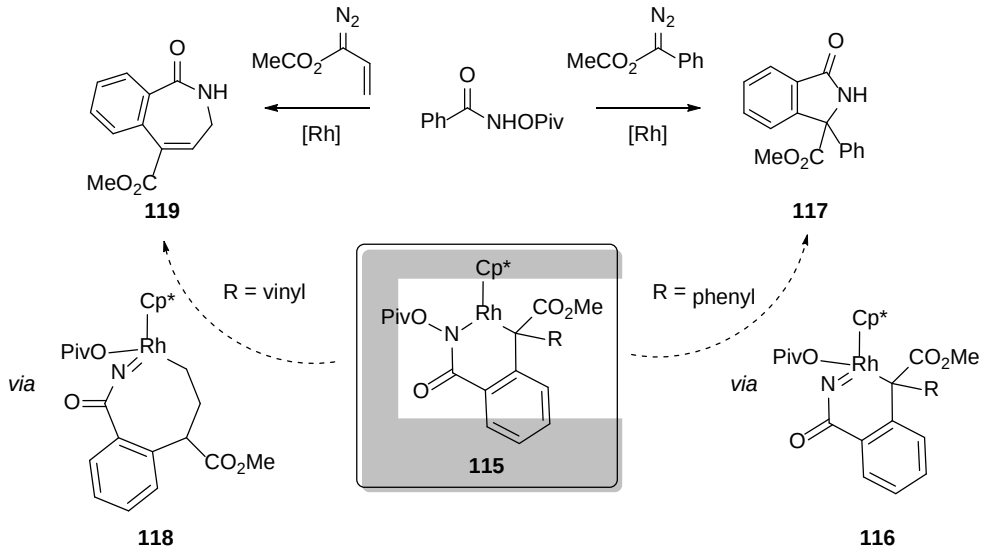

Figure 49. Different outcomes of the reaction of PhC(O)NHOPiv with diazocarbenes, $MeO_2CC(N_2)R$ (R = vinyl, Ph) showing key intermediates involved in the selectivity-determining steps. Adapted with permission from Ref. 185. Copyright 2015 John Wiley and Sons

A number of studies have considered the Rh(III)-catalysed functionalisation of *N*-phenoxyacetamide, PhONHAc, **120**, in which oxidative cleavage of the O-N bond again serves as an internal oxidant. Houk and Wu used M06(solvent)//B3LYP calculations to rationalise the solvent-dependent coupling with PhCCPh that forms either enamides **121** (in MeOH) or benzofurans **122** (in CH_2Cl_2, see Figure 50).[186] Reaction at $[Rh(OAc)_2Cp^*]$ again involves sequential *N*-deprotonation and AMLA/CMD C-H activation and is computed to be readily accessible in both solvents (MeOH/CH_2Cl_2: $\Delta G^{\ddagger}$ = 21.0/16.9 kcal/mol). The subsequent insertion of PhCCPh is rate-limiting ($\Delta G^{\ddagger}_{span}$ = 25.4/28.7 kcal/mol) and forms a 7-membered rhodacycle **Int120b** at -3.3/-5.7 kcal/mol. Internal oxidation then forms a Rh(V)-nitrene **Int120c**. C-N reductive coupling from this species forms a new 7-membered rhodacycle **Int120d** with barriers (relative to **Int120c**) of only 4.3/5.1 kcal/mol; protonolysis then releases the enamide product (**121**). Alternatively addition of HOAc to **Int120c** protonates the

nitrene (**Int120e**) and permits C-O coupling with barriers (relative to **Int120e**) of 4.2/3.8 kcal/mol after which protonolysis releases benzofuran **122**. The very similar barriers for the competing C-N and C-O reductive couplings suggest a close competition between the two pathways and show C-O coupling and furan formation becomes more competitive in the less polar CH_2Cl_2 solvent. Alternative pathways including C-N reductive coupling at **Int120b** or C-O bond coupling at **Int120c** to give the furan directly were shown to be uncompetitive. A further route to the furan has been proposed by Li for the reaction with MeCCPh which inserts to form an analogue of intermediate **Int120b** with the Ph substituent adjacent to Rh (M06(CH_2Cl_2) calculations).[187] A concerted C-O bond coupling/ N-O bond cleavage then forms the furan with a barrier of 21.5 kcal/mol, 1.6 kcal/mol lower than for the formation of the Rh(V)-nitrene intermediate.

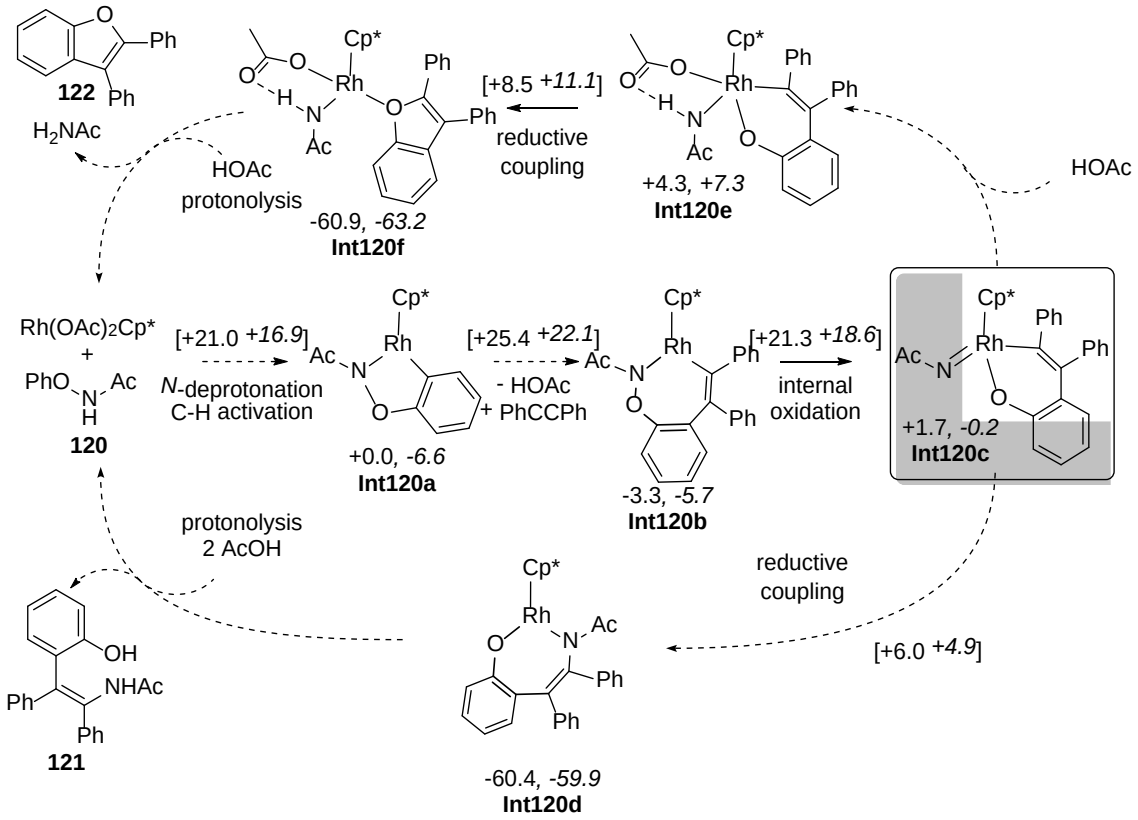

Figure 50. Key stationary points computed for the coupling of PhONHAc, **120**, with PhCCPh at [$Rh(OAc)_2Cp$]. Computed free energies (kcal/mol) are quoted relative to the reactants at 0.0

kcal/mol. Values in plain text are computed in MeOH, those in italics are in CH_2Cl_2. Adapted with permission from Ref. 186. Copyright 2016 American Chemical Society

Xia has compared the couplings of *N*-pivaloxybenzamide and *N*-phenoxyacetamide (**120**) with 3,3-dimethylcycloprop-1-ene at [Rh(OPiv)$_2$Cp*] (see Figure 51(a)).[188, 189] M06(MeOH) calculations provide similar profiles for *N*-deprotonation/C-H activation with overall barriers of 21.9 kcal/mol and 21.3 kcal/mol, respectively, and this is then followed by facile alkene insertion to form 7-membered rhodacycle intermediates. With *N*-pivaloxybenzamide an analogous path to that shown in Figure 44(c) is followed and forms the cyclic lactam **123**. With *N*-phenoxyacetamide, however, the 7-membered rhodacyclic intermediate **125** (Figure 51(b)) undergoes a preferential β-C elimination to form an allylic intermediate **126**. Protonation of the amide nitrogen then releases cyclohexa-2,4-dienone **127** that subsequently rearranges, facilitated by the [Rh(OPiv)$_2$Cp*] catalyst, to the *2H*-chromene **124**. The β-C elimination step is shown to be favored when the Rh center interacts with the C^2 and C^1 positions in the transition state, as this orientates the bulky disubstituted C^3 position away from the {RhCp*} unit; a higher barrier of 24.3 kcal/mol is computed with the alternative arrangement when Rh interacts with C^1-C^3. This pathway, in which the Rh(III) oxidation state is maintained throughout, also pertains with related 3-Me-3-phenylethylcycloprop-1-ene and updates earlier work by Li on that system.[187]

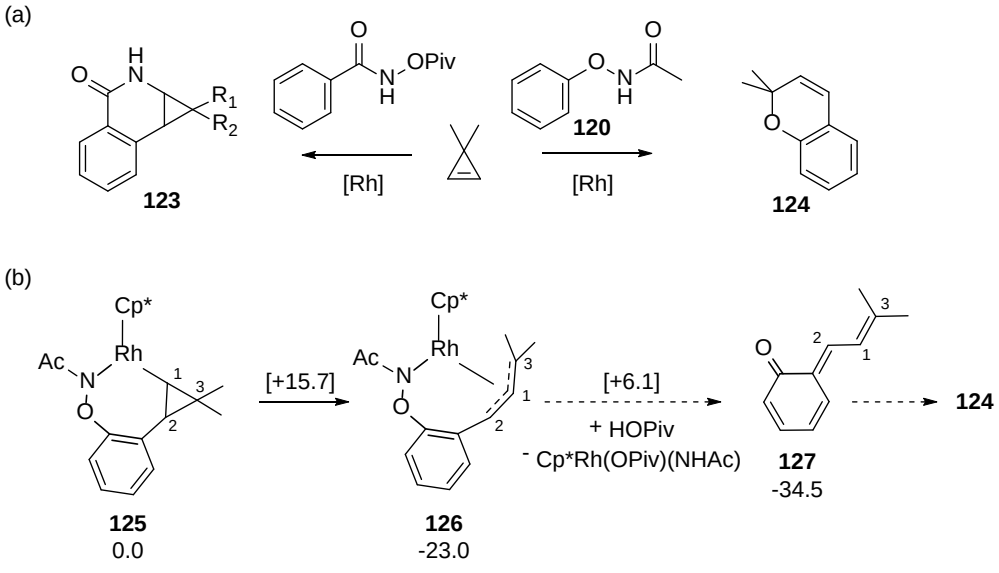

Figure 51. (a) Different outcomes of the reactions of 3,3-dimethylcycloprop-1-ene *with N*-phenoxyacetamide and *N*-pivaloxybenzamide at [Rh(OPiv)$_2$Cp*]. Adapted with permission from Ref. 188. Copyright 2015 American Chemical Society; (b) Key steps in the formation of *2H*-chromene **124** with relative free energies in kcal/mol.' Adapted with permission from Ref. 189. Copyright 2016 American Chemical Society

Ammonium groups are also effective internal oxidants via loss of amine by C-N bond cleavage. Using M06(MeCN) and B3LYP-D3(MeCN) calculations Lan, Wan and Li modelled the [Rh(OAc)$_2$Cp*]-catalysed formation of a benzocyclopentanone from an acetophenone ammonium cation and α-diazoesters (Figure 52).[190] Active catalyst [Rh(OAc)$_2$Cp*] interacts with the ammonium salt to form a C-bound enolate intermediate from which rate determining C-H activation proceeds with a barrier of 26.3 kcal/mol (B3LYP-D3); barriers via the O-bound enolate were 2-3 kcal/mol higher. The reaction proceeds via diazoester coordination, N_2 loss and carbene insertion to give **128**. NEt_3 loss from **128** has a computed barrier of 20.7 kcal/mol (B3LYP-D3) and leads, after coordination of OAc, to **129**. The Rh(V)-carbene intermediate, **129**, is isoelectronic with the Rh(V)-nitrene species mentioned previously (e.g. $\mathbf{V_{OPiv}}$, Figure 44(c)). Insertion of the carbene moiety followed by protonolysis complete the cycle. Overall aryl C-H activation is rate-limiting and this is consistent with a significant k_H/k_D KIE observed experimentally.

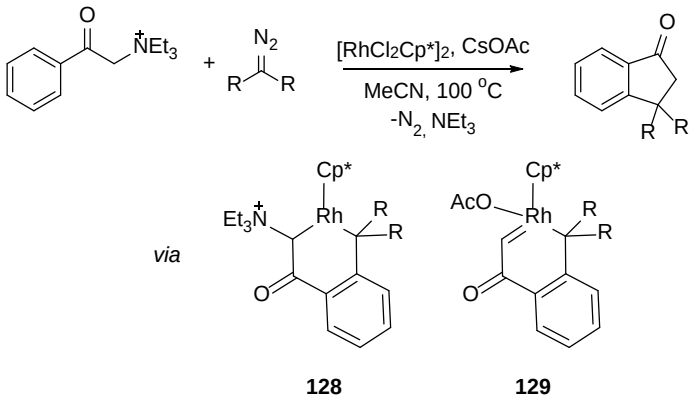

Figure 52. Rh-catalysed benzocyclopentanone formation from the coupling of α-diazoesters (R = $CO_2{}^i$Pr) with benzophenone ammonium salts.[190] Adapted with permission from Ref. 43. Copyright 2016, John Wiley and Sons.

Internal oxidation by N-N bond cleavage of 2-acetyl-1-arylhydrazines, **130**, has been exploited in the Rh(III)-catalysed synthesis of indoles as studied by Lin with M06(DCE, D3) calculations (Figure 53).[191] After deprotonation to form **Int130a**, the terminal NAc group directs a two-step C-H activation with an overall $\Delta G^{\ddagger}$ of 18.8 kcal/mol. HOAc/PhCCPh exchange then gives **Int130b**, from which alkyne insertion leads to **Int130c** *via* a transition state at 29.2 kcal/mol. A facile 1,2-Rh shift followed by HOAc-assisted H^+ transfer then accesses **Int130e** which can undergo ring closure by C-N reductive coupling to give the Rh(I) species, **Int130f**. Reoxidation then occurs via N-N bond cleavage to regenerate a Rh(III) species, **Int130g**. H_2NAc is then displaced by HOAc with a second equivalent of HOAc protonating the Rh-N bond to release the indole and regenerate the catalyst. Experimentally the reaction proceeds at 70 ^{o}C and a k_H/k_D KIE of 2.3 is observed and it is proposed that the computed reverible (*i.e.* endothermic) C-H activation would affect the overall rate as a pre-equilibrium prior to rate-limiting alkyne insertion. Calculations suggest that the -NH(NHAc) group is a weaker oxidant than-NH(OAc); C-N bond coupling with alkynes is therefore possible, while that with alkenes is inaccessible. Li and Liao drew similar conclusions in their work.[192]

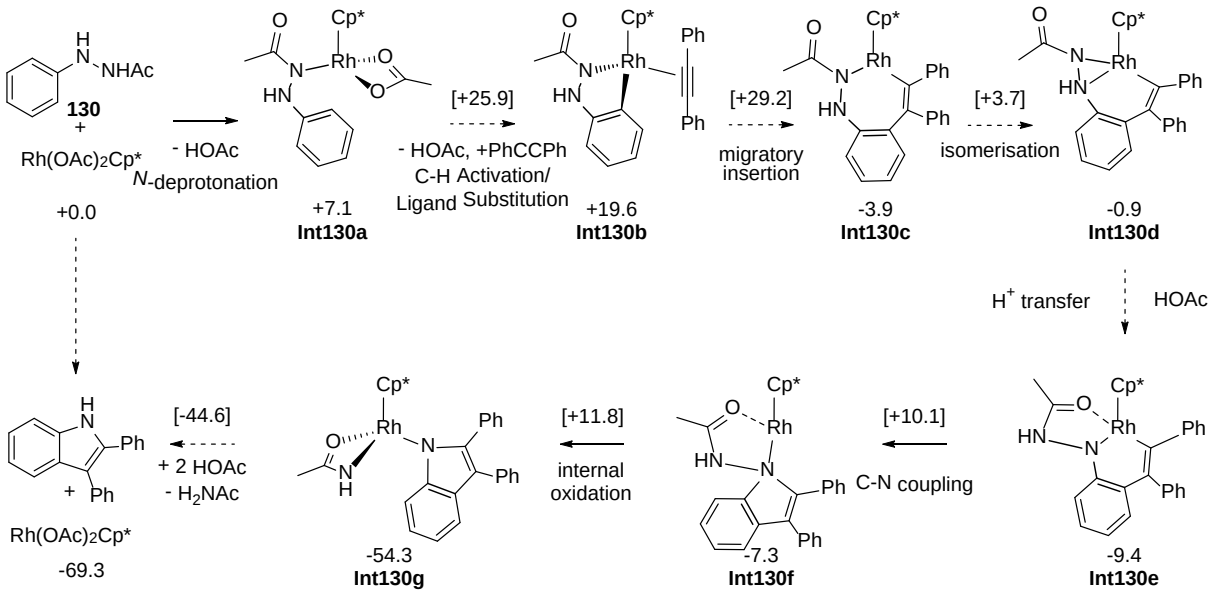

Figure 53. Key stationary points for [Rh(OAc)$_2$Cp*]-catalysed indole formation via the coupling of 2-acetyl-1-arylhydrazine, **130**, with diphenylacetylene. Free energies are indicated in kcal/mol.[191] Adapted with permission from Ref. 43. Copyright 2016, John Wiley and Sons.

Liu and Bi considered the coupling of alkynes with pyrazolone, **131**, to form the 2,3-diphenyl-1H-indole derivative **132**, a further example of a reaction that involves oxidative cleavage of a substrate N-N bond (see Figure 54(a); M06(PhBr)//B3LYP calculations)).[193] **131** lacks a heteroatom-H bond, however, deprotonation of the backbone CH_2 group via **TS131a** is found to be accessible and, upon HOAc release, frees up a coordination site for the (now anionic) substrate to bind. Unlike most *N*-H or *O*-H deprotonations, this initial C(sp^3)-H deprotonation proves less kinetically accessible ($\Delta G^{\ddagger}$ = 19.7 kcal/mol, Figure 54(b)) than the following directed AMLA/CMD C-H activation via **TS131b** ($\Delta G^{\ddagger}$ = 17.4 kcal/mol). Non-directed *ortho*-C-H activation via **TS131c** is also disfavored ($\Delta G^{\ddagger}$ = 25.1 kcal/mol). Insertion of PhCCPh then forms **Int131a**, a 7-membered rhodacycle which undergoes C-N bond formation to a zwitterionic Rh(I) intermediate **Int131b** (Figure 54(c)). N-N oxidative cleavage occurs at this point to give Rh(III)-nitrene **Int131c** which reacts with 2 equiv of HOAc to release the indole product and regenerate [Rh(OAc)$_2$Cp*]. The N-N cleavage transition state is rate-determining with

$\Delta G^{\ddagger}_{span}$ = 31.1 kcal/mol relative to **Int131a**. An alternative process via a Rh(V)-nitrene formed upon N-N cleavage in **Int131a** has a barrier in excess of 50 kcal/mol.

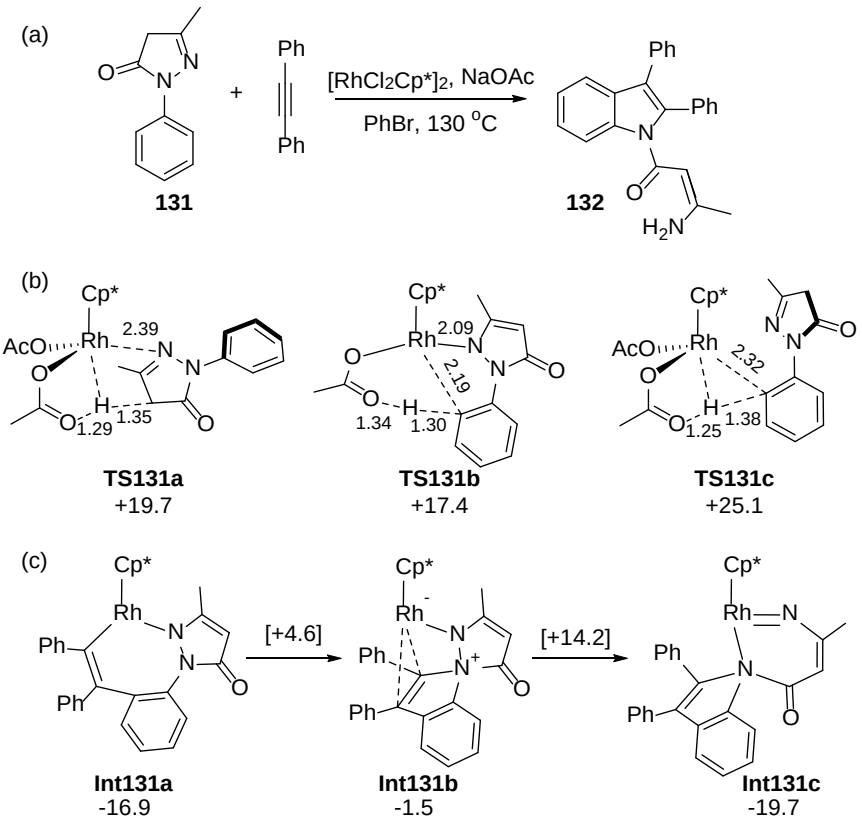

Figure 54. (a) Rh-catalysed coupling of alkynes with pyrazolone **131**; (b) Geometries of alternative C-H activation transition states with selected distances in Å; (c) Key stationary points associated with the alkyne insertion and N-N bond cleavage steps. Free energies are indicated in kcal/mol. Adapted with permission from Ref. 193. Copyright 2015 The Royal Society of Chemistry.

Huang has provided a further variation of the internal oxidant theme in a study of the redox neutral Rh(III)-catalyzed formation of 1-aminoindolines, **134**, via the intermolecular annulation of aryl-substituted diazenecarboxylates, **133** (see Figure 55).[194] M06-2X(DCE)//M06 calculations showed the alternative N^1- or N^2-bound [Rh(OAc)(**133**)Cp*]$^+$ precursors to be similar in energy, but that AMLA/CMD C-H activation is more accessible from the N^2-bound form ($\Delta G^{\ddagger}$ = 19.4 kcal/mol *cf*. 27.8 kcal/mol via the *N*^{1}-bound isomer which gives a strained 4-membered metallacycle). Ethene insertion forms a 7-membered rhodacycle, **Int133a**. At this point neither C-N reductive coupling nor

β-H transfer onto N^2 (via a Rh-H intermediate) are accessible. Instead **Int133a** rearranges to **Int133b** in which N^1 is bound to the metal center. Reductive coupling is now accessible ($\Delta G^{\ddagger}$ = 11.1 kcal/mol) with the assistance of the electronically flexible *N*-Boc moiety that gives a formally anionic *O*-bound ligand and thus maintains the Rh(III) oxidation state in **Int133c**. Protonation with HOAc releases the coupled product and regenerates the {Rh(OAc)} catalyst. With acrylonitrile a 2,1-insertion is kinetically preferred.

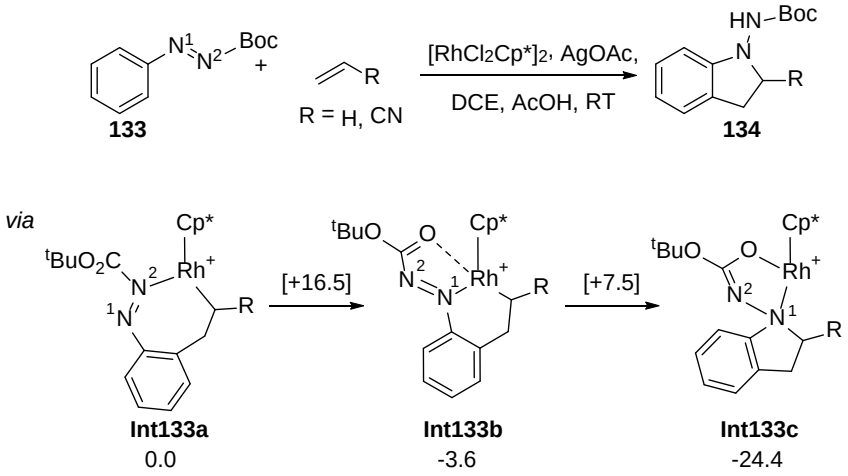

Figure 55. Rh(III)-catalyzed intermolecular annulation of aryl-substituted diazenecarboxylates, **133**, with alkenes. Key stationary points are indicated with free energies (kcal/mol) quoted relative to **Int133a** set to 0.0 kcal/mol. Adapted with permission from Ref. 194. Copyright 2016 American Chemical Society.

The cleavage of an N-S bond to effect the redox neutral Rh(III)-catalyzed annulation of *N*-t-butylsulfinylimine, **135**, with ethyl acrylate to give *1H*-isoindoles, **136**, has been modelled by Lan and Li with M11L(DCE)//B3LYP calculations (see Figure 56).[195] $[Rh(OAc)(HOAc)Cp^*]^+$ is considered as the active species in this study which, after HOAc/**135** substitution, allows for an *N*-directed AMLA/CMD C-H activation with $\Delta G^{\ddagger}$ = 25.8 kcal/mol and ΔG = +1.6 kcal/mol. The reaction proceeds via HOAc/ethyl acrylate exchange, insertion and β-H transfer to form a hydrido alkene intermediate **Int135a**. Deprotonation of this hydride by the –S(O)^{t}Bu moiety releases HOS^{t}Bu and forms a cationic Rh(III)-imide complex **Int135b**. C-N bond formation proceeds via insertion of the alkene into the Rh-imide

bond which generates a 2° Rh-alkyl, **Int135c**. A HOAc-promoted 1,2[Rh]-shift to a 3° alkyl (i.e forming a Rh-C^1 bond) then permits a second alkene insertion. For the first insertion the endothermic C-H activation is rate-limiting and so consistent with the observation of H/D exchange in the absence of alkene and a significant k_H/k_D KIE. $\Delta G^{\ddagger}_{span}$ for the second insertion appears to be somewhat larger at 29.7 kcal/mol.

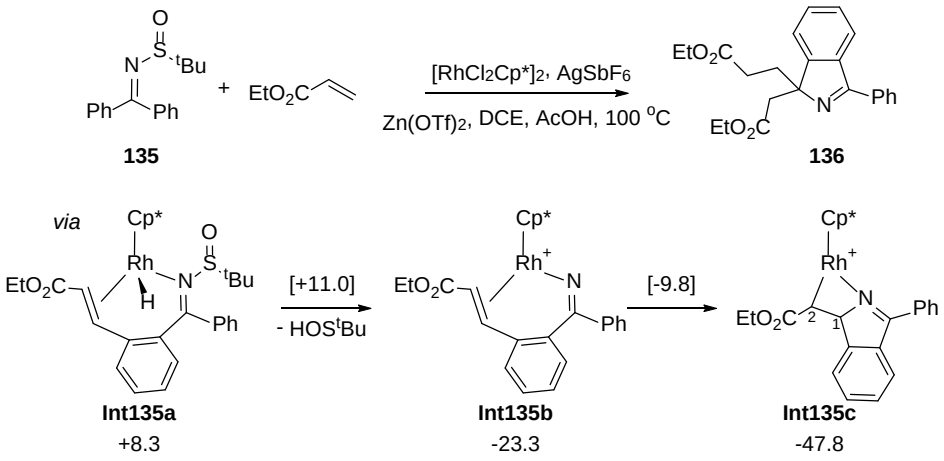

Figure 56. Key stationary points for the Rh(III)-catalyzed annulation of *N*-t-butylsulfinylimine, **135**, with ethyl acrylate; free energies (kcal/mol) and are quoted relative to the reactants at 0.0 kcal/mol. Adapted with permission from Ref. 195. Copyright 2016 American Chemical Society.

6.1.2. Catalytic Heterocycle Formation with External Oxidants. In the absence of an internal oxidant this role is played by metal salts, typically $Cu(OAc)_2.H_2O$ or AgOAc. In computational studies these are often assumed to act after the reductive coupling event. Attempts have been made to model this reoxidation, but this is challenging due to the speciation of these metal salts (and their reduced equivalents) in solution. In principle, oxidation of the metal center could occur at any point in the reaction mechanism and computational studies highlighting this possibility are now appearing, especially prior to the final reductive coupling step. The assumption that oxidation occurs after product release (or at least does not impinge on the rate-determining step within catalysis) could be probed experimentally by checking for product formation in the absence of the oxidant.

Davies and Macgregor modelled the oxidative coupling of 5-methyl-3-phenylpyrazole, **137**, and 4-octyne at [Rh(OAc)$_2$Cp*] using BP86(DCE) and BP86(DCE, D3) calculations (Figure 57).[196] Experimentally, H/D exchange occurs both in the absence (40% *ortho*-deuteration) and in the presence of alkyne (7% incorporation). C-H activation is therefore reversible, but the reduced D-incorporation in presence of alkyne also indicates that protonolysis of the initial cyclometallated intermediate **Int137b** (via **TS137a**) and the onward reaction via HOAc/alkyne exchange and migratory insertion (via **TS137b**) have similar rates. This feature was only captured upon inclusion of the D3 dispersion correction, the major effect of which was to make the HOAc/^{n}PrCC^{n}Pr substitution step much more accessible (ΔG: BP86(DCE) = +6.8 kcal/mol; BP86(DCE, D3) = -1.5 kcal/mol). The different bulk of the two ligands involved in this process make it particularly sensitive to the dispersion correction. Similar results were found with other approaches that incorporate dispersion effects (e.g. M06 or B97D, or the addition of a D3 correction to other pure or hybrid functionals).

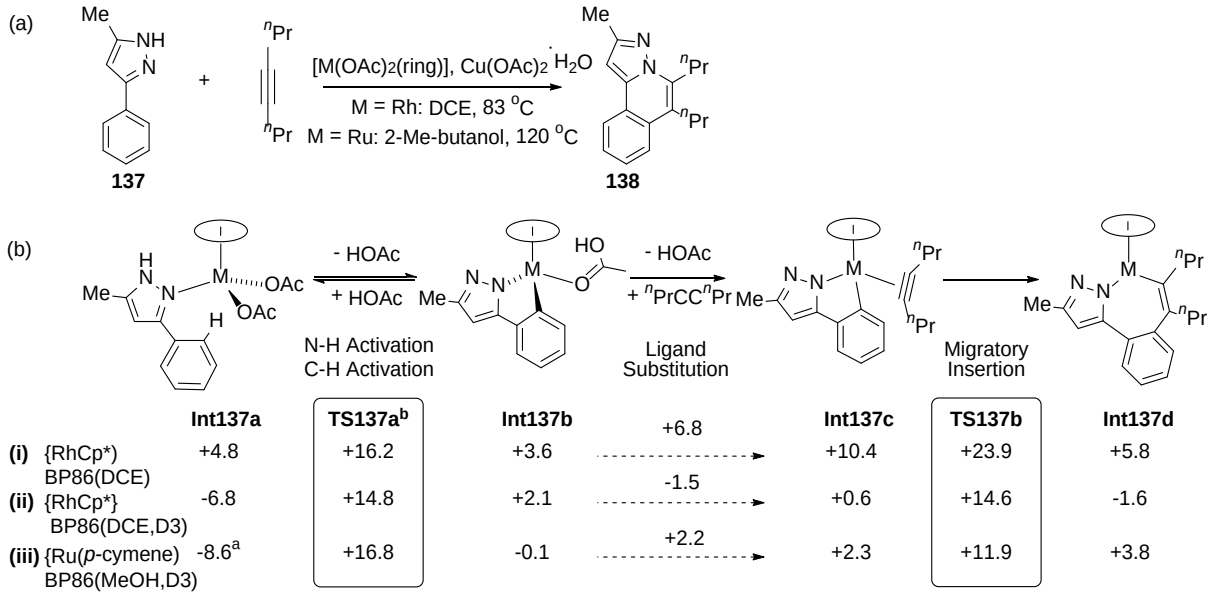

Figure 57. (a) Rh- and Ru-catalysed oxidative coupling of 4-octyne and 3-phenylpyzazole, **137**, to form pyrazoloisoquinoline, **138**. (b) Selected stationary points for (i) {RhCp*} (BP86(DCE)), (ii) {RhCp*} (BP86(DCE, D3)) and (iii) {Ru(*p*-cymene)} (BP86(MeOH, D3)) with free energies (kcal/mol) quoted relative to the reactants set to 0.0 kcal/mol in each case.[196] [a]-8.6 kcal/mol is the most stable

point on the computed profile and corresponds to the *N*-deprotonated form of **137**. [b] **TS137a** is the highest point in a multi-step process that links **Int137a** to **Int137b**. Adapted with permission from Ref. 43. Copyright 2016, John Wiley and Sons.

Useful insight was gained by comparing the behavior of the [Ru(OAc)$_2$(*p*-cymene)] system and so this is discussed here. Rate-limiting C-H activation was found for both metals, with a higher free energy span computed for Ru (25.4 kcal/mol) over Rh (21.8 kcal/mol), this being in qualitative agreement with the higher temperatures required experimentally for Ru (120 ^{o}C in 2-methylbutanol compared to 83 ^{o}C in DCE for Rh). For Rh a k_H/k_D KIE of 2.7 ± 0.5 is observed and the calculations mirror this via a two-step C-H activation process in which the C-H bond cleavage transition state, **TS137a$_{Rh}$** (Figure 58), is the highest point; a corresponding KIE of 5.5 was computed. In contrast for Ru, calculations defined a single-step C-H activation via **TS137a$_{Ru}$** which is characterized by the κ^2-κ^1 displacement of OAc. As a result **TS137a$_{Ru}$** features minimal C-H bond stretching and a small computed KIE of only 1.2, consistent with the value of 1.1 ± 0.2 determined experimentally. This study shows that the absence of a marked k_H/k_D KIE does not *necessarily* indicate that C-H activation is not rate-limiting, and that this result may arise if the C-H activation transition state has a very early geometry.

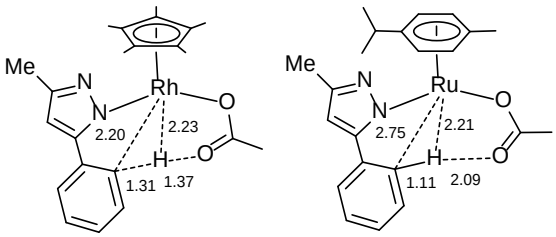

k_H/k_D (exp) = 2.7 ± 0.5
k_H/k_D (calc) = 5.5
TS137a$_{Rh}$

k_H/k_D (exp) = 1.1 ± 0.2
k_H/k_D (calc) = 1.2
TS137a$_{Ru}$

Figure 58. Rate-limiting transition states for the C-H activation of 5-methyl-3-phenylpyrazole at {Rh(OAc)Cp*} (**TS137a$_{Rh}$**) and {Ru(OAc)(*p*-cymene)} (**TS137a$_{Ru}$**). Key distances are shown in Å along with the experimental and computed k_H/k_D KIEs.[196] Adapted with permission from Ref. 43. Copyright 2016, John Wiley and Sons.

Davies and Macgregor have also considered the C–N and C–C oxidative coupling of alkynes with 1-phenylpyrazole, **138**, using BP86(D3, solvent)//BP86 calculations.[197] This substrate lacks a protic hydrogen and so access to an AMLA/CMD directed C-H activation requires initial OAc/**138** substitution to form cationic [Rh(κ^2-OAc)(**138**)Cp*]$^+$. In addition, non-directed (intermolecular) C-H activations were also defined at a neutral [Rh(κ^1-OAc)$_2$Cp*] moiety for both the *ortho*-C-H and the pyrazole C5-H positions (*cf*. **TS131c**, Figure 54). The involvement of charged intermediates makes the barriers to the directed C-H activation highly solvent-dependent, whereas those for the non-directed processes are not significantly affected by solvent choice (see Figure 59). With ethanol and DCE solvents the directed process and subsequent reaction with ^{n}PrCC^{n}Pr lead to **139**, where the C-N coupling is rate-limiting (EtOH: $\Delta G^{\ddagger}_{span}$ = 22.2 kcal/mol, ΔG = -3.2 kcal/mol). In contrast, with PhCCPh the energetics of C-N coupling are less favorable ($\Delta G^{\ddagger}$ = 27.3 kcal/mol, ΔG = +3.3 kcal/mol) and, consistent with this, the corresponding 7-membered rhodacycle does not undergo this coupling experimentally. Once formed, **139** can react via non-directed C5-H activation followed by C-C coupling with either alkyne to form **140**. In contrast, the initial reaction of **138** in xylene proceeds via a non-directed process to give **141**. The reaction in xylene stops at this point;[198] however, more polar solvents do permit a directed C-H activation to occur after which C-N coupling produces **140**. Computed barriers to C-X reductive coupling are lower for X = C than when X = N, and coupling is also facilitated in the 'strapped' substrates **139** and **141** by the extra strain this induces in the 7-membered rhodacycles. With 2-phenylpyridine the initial directed C-H activation is readily accessible ($\Delta G^{\ddagger}$ = 8.8 kcal/mol in EtOH) and insertion can then occur with both alkynes. Non-directed C-H activation of the backbone positions is then inaccessible due to the lower acidity of these positions ($\Delta G^{\ddagger}$ = 28 kcal/mol) and no further coupling is observed.

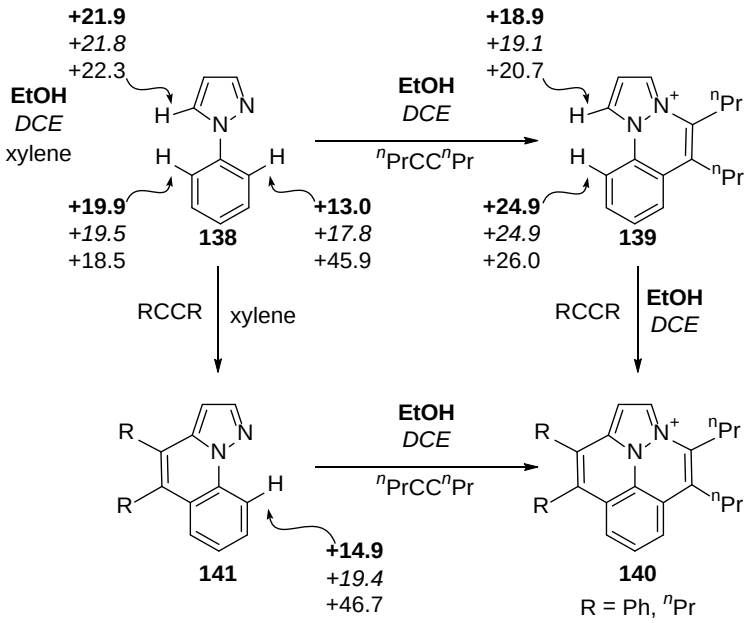

Figure 59. Different products emerging from the Rh(III)-catalysed coupling of 1-phenylpyrazole, **138**, with 4-octyne. Overall barriers for C-H activation at the indicated sites are provided in kcal/mol, computed in EtOH (bold) DCE (italics) and xylene (plain text). Adapted with permission from Ref. 197. Copyright 2015 American Chemical Society.

Several other studies have investigated the formation of *N*-heterocycles through the Rh(III)-catalysed oxidative coupling with alkynes. Mascareñas and Gulías have modelled the intramolecular annulation of an *N*-alkynyl-tethered benzamide **142a** to give a tricyclic isoquinolone **142b** with B3LYP(MeOH) calculations (Figure 60(a)).[199] *N*-deprotonation and AMLA/CMD C-H activation at $[Rh(OAc)_2Cp^*]$ permit an intramolecular insertion that, unusually, occurs preferentially into the Rh-N bond rather than the Rh-C bond. This is the rate determining process and corresponds to a large $\Delta G^{\ddagger}_{span}$ of 36.4 kcal/mol; experimentally the reaction proceeds at 110 °C. Rodríguez, Arrayás and Carretero have assessed competing C-H functionalisation of *N*-benzyl-2-picolinamides with alkynes.[200] Starting from **143** (Figure 60(b), the Cl analogue of which was characterised experimentally) M06 calculations define reaction profiles with similar barriers for combined pyridine

dissociation and AMLA/CMD activation at the heteroaryl C-H[a] bond ($\Delta G^{\ddagger}$ = 38.1 kcal/mol) and the aryl C-H[b] bond ($\Delta G^{\ddagger}$ = 39.0 kcal/mol). The similar barriers are consistent with H/D exchange at both positions experimentally, although the computed barriers are rather high for the conditions employed (1,4-dioxane/D_2O, 120 °C). Subsequent alkyne insertion is more accessible after C-H[a] activation and leads to an isoquinolone product. Finally, Wu, Zhang and Wang modelled the formation of the tetracyclic species **144** via the coupling of 2,3-diphenylindole with PhCCPh at [$Rh(OAc)_2Cp^*$] (Figure 60(c)).[201] M06(MeOH)//B3LYP calculations indicate rate-limting alkyne insertion with $\Delta G^{\ddagger}_{span}$ = 24.2 kcal/mol, consistent with a small k_H/k_D KIE of 1.1 determimed experimentally.

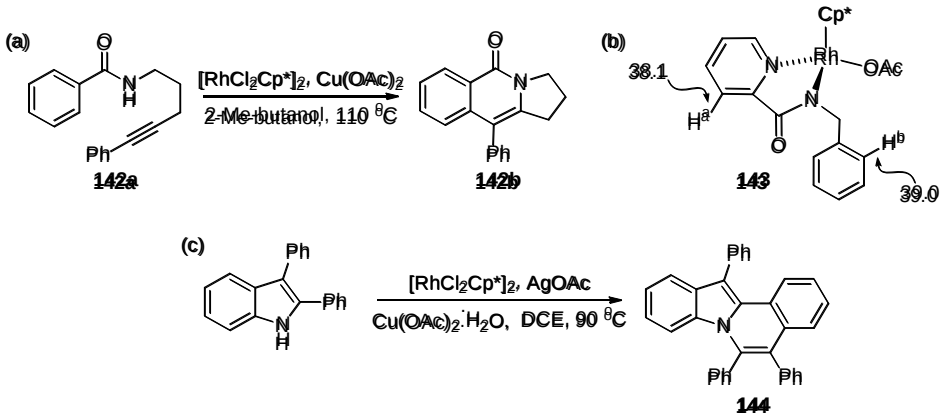

Figure 60. Rh(III)-catalysed reactions forming *N*-heterocycles: (a) formation a tricyclic isoquinolone, **142b**; adapted from Ref. 199. (b) Common precursor to competing C-H activations in *N*-benzyl-2-picolimamide with overall barriers indicated in kcal/mol;[200] (c) Formation of tetracyclic species **144**. Adapted with permission from Ref. 201. Copyright 2014 American Chemical Society.

The non-innocence of the oxidant in determining the outcome of the [$RhCl_2Cp^*]_2$-catalysed coupling of MeCCPh with benzoic acid has been highlighted by Maseras.[202] In the presence of $Cu(OAc)_2.H_2O$ this reaction forms the isocoumarin product **149** whereas with AgOAc extrusion of CO_2 occurs and coupling with a second alkyne gives the naphthalene derivative **147** (Figure 61). B97D(*o*-xylene) calculations on the intermediate rhodacycle **145** show that, in isolation, CO_2 extrusion ($\Delta G^{\ddagger}$ = 8.2

kcal/mol) to **146** is more accessible than C-O coupling ($\Delta G^{\ddagger}$ = 13.0 kcal/mol). However, the copper acetate additive is proposed to intervene in the form of a $[CuCl(OAc)(H_2O)]_2$ dimer that forms the bridged adduct **148** (ΔG = -15.3 kcal/mol). **148** is computed as a triplet with significant spin density computed at each of the formally Cu(II) centers. C-O bond coupling then proceeds with a barrier of 15.9 kcal/mol, making this process more accessible than CO_2 extrusion direct from **145**. Moreover, the computed spin densities in **TS148** show a transfer of charge toward the Cu centers and are consistent with a degree of Rh(IV) character in the transition state. This "cooperative reductive elimination" highlights further ways in which additives may impinge on C-H functionalisation.

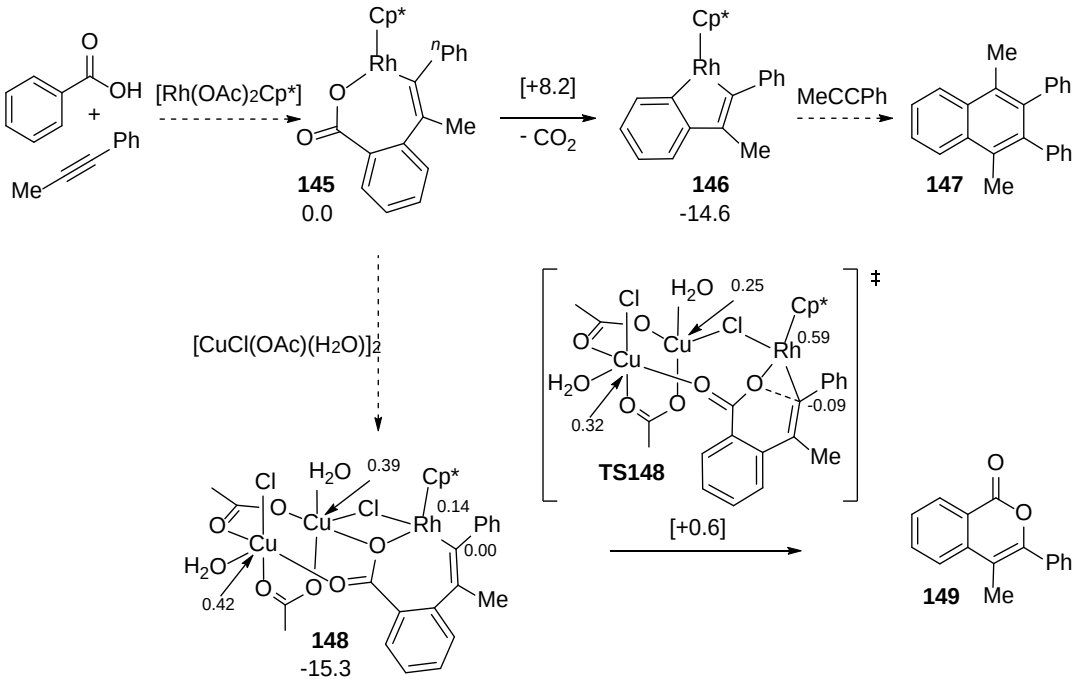

Figure 61. Key steps in the Rh-catalysed reaction of MeCCPh with benzoic acid. Computed free energies are provided in kcal/mol relative to species **145** set to 0.0 kcal/mol, with computed spin densities indicated for structures **148** and **TS148**. Adapted with permission from Ref. 202. Copyright 2016 John Wiley and Sons.

The oxidative coupling of benzoic acids with alkynes at $[Ir(OAc)_2Cp^*]$ has been modelled by Ison using BP86(MeOH) calculations (Figure 62(a)).[203] *O*-deprotonation gives $[Ir(\kappa^2\text{-}OAc)(\kappa^1\text{-}O_2CPh)Cp^*]$ from which AMLA/CMD C-H activation proceeds with $\Delta G^{\ddagger}$ = 19.5 kcal/mol and ΔG = +11.1 kcal/mol.

HOAc/4-octyne substitution then leads to a rate-limiting alkyne insertion with $\Delta G^{\ddagger}_{span}$ = 30.9 kcal/mol. It is likely this barrier would be affected by the inclusion of dispersion effects since, as detailed above, the HOAc/alkyne substitution step is particularly sensitive to these effects.[196] Upon insertion, C-O reductive coupling gives an Ir(I) intermediate in which the isocoumarin product is bound in an η^4 fashion. Oxidation with two equivalents of 'AgOAc' is then proposed to occur in two steps, the first giving an Ir(II)OAc species, atomic 'Ag' and releasing the organic product, the second then regenerating the Ir(III)$(OAc)_2$ catalyst. A related Rh-catalysed coupling of phenylphosphonates and alkynes to give phosphaisocoumarins, **150**, was reported by Zhao based on B3LYP(^{t}BuOH, D3) calculations.[204]

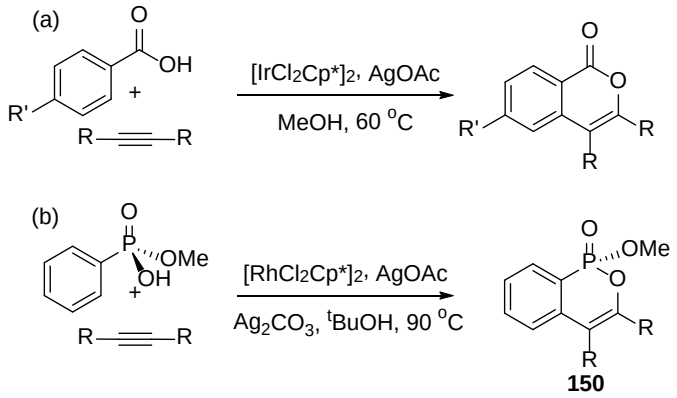

Figure 62. (a) Ir-catalysed isocoumarin formation (computational study: R = Me, R' = H);[203] (b) Rh-catalysed phosphaisocoumarin formation (computational study: R = Me).[204] Adapted with permission from Ref. 43. Copyright 2016, John Wiley and Sons.

The Rh(III)-catalysed asymmetric spiroannulation of 3-chloro-1-phenyl-2-naphthol, **151**, with PhCCPh has been studied by Zheng and You based on a [$Rh(OAc)_2$Cp'] active species, where Cp' is a chiral 1,1'-binaphthalene-based ligand (see Figure 63(a)).[205] B3LYP(toluene, D3)//ωB97X-D calculations (with optimisations in toluene) indicate *O*-deprotonation of the naphthol to have a computed barrier of 17.4 kcal/mol and to be endergonic by 10.5 kcal/mol; however, it is proposed that the stoichiometric base, 'K_2CO_3', can drive this forward thermodynamically by removing HOAc as a '$K_2(HCO_3)OAc$' cluster, making the deprotonation exergonic by 16.5 kcal/mol. A two-step AMLA/CMD

C-H activation then proceeds with $\Delta G^{‡}$ = 17.3 kcal/mol and ΔG = +10.6 kcal/mol, this step again being promoted by removal of HOAc by 'K_2CO_3' (ΔG = -18.9 kcal/mol). This represents the lowest of four diastereomeric pathways to form the 6-membered cyclometallated intermediate **Int151a** which was found to readily interconvert between its four diastereomers. The enantiomeric induction occurs in the subsequent alkyne binding and (irreversible) insertion steps for which a preference for the *pro*-S pathway is computed ($\Delta\Delta G^{‡}$ = 2.9 kcal/mol). This forms intermediate **Int151b** which then accesses a $C^1\cdots C^3$ bond coupling ($\Delta G^{‡}$ = 14.8 kcal/mol; ΔG = +6.9 kcal/mol) that installs the chiral quaternary carbon of the dearomatized product bound in **Int151c**. This is distinctly favored over the alternative C-O reductive coupling ($\Delta G^{‡}$ = 30.4 kcal/mol). Exergonic re-oxidation by '$[Cu(OAc)_2]_2$' then reforms [$Rh(OAc)_2Cp$'] and releases the product (**152**) along with '$[Cu(OAc)]_2$'. As formulated, $\Delta G^{‡}_{span}$ for this process is the C-H activation step at 17.3 kcal/mol, although this value does assume facile and rapid deprotonation after the initial *O*-deprotonation; if this did not occur then the energy span for the sequential *O*-deprotonation/C-H activation would be 28.8 kcal/mol. The 2.9 kcal/mol preference in the enantio-determining alkyne insertion step agrees well with an experimental enantiomeric ratio of 97:3 in favor of the *S*-product and this preference is linked to a destabilising O⋯O interaction between the substrate and one methoxy substituent on the chiral ligand in the higher energy *pro*-R transition state. With MeCCPh, insertion with Ph adjacent to the metal is preferred and this is postulated to be assisted by favorable π–π interactions between the alkyne phenyl group and the 2-naphthol ring. Huang has reported a related study on the Rh(III)-catalysed coupling of 2-$H_2C{=}CRC_6H_4OH$ (**153**, R = H, Me) with PhCCPh (Figure 63(b)).[170] These form a 6-membered rhodacycle analogous to **Int151a** in Figure 63(a) and with R = Me B3LYP(MeCN, D3) calculations suggest that C-C coupling and spiroannulation to **154** is kinetically favored by 3.9 kcal/mol over C-O reductive coupling that would give the benzooxepine product **155**. In contrast, when R = H, C-O coupling has the lower barrier by 2.1 kcal/mol. This swap is in accord with experimental observations and is thought to relate to increased steric hindrance in the C-O bond forming transition state when R = Me. In this case an additional metallacyclopropene intermediate

was located on the C-C bond formation pathway and a related mechanism was also invoked for the Ru-catalysed spiroannulation of naphthols and alkynes (see Section 8.1).

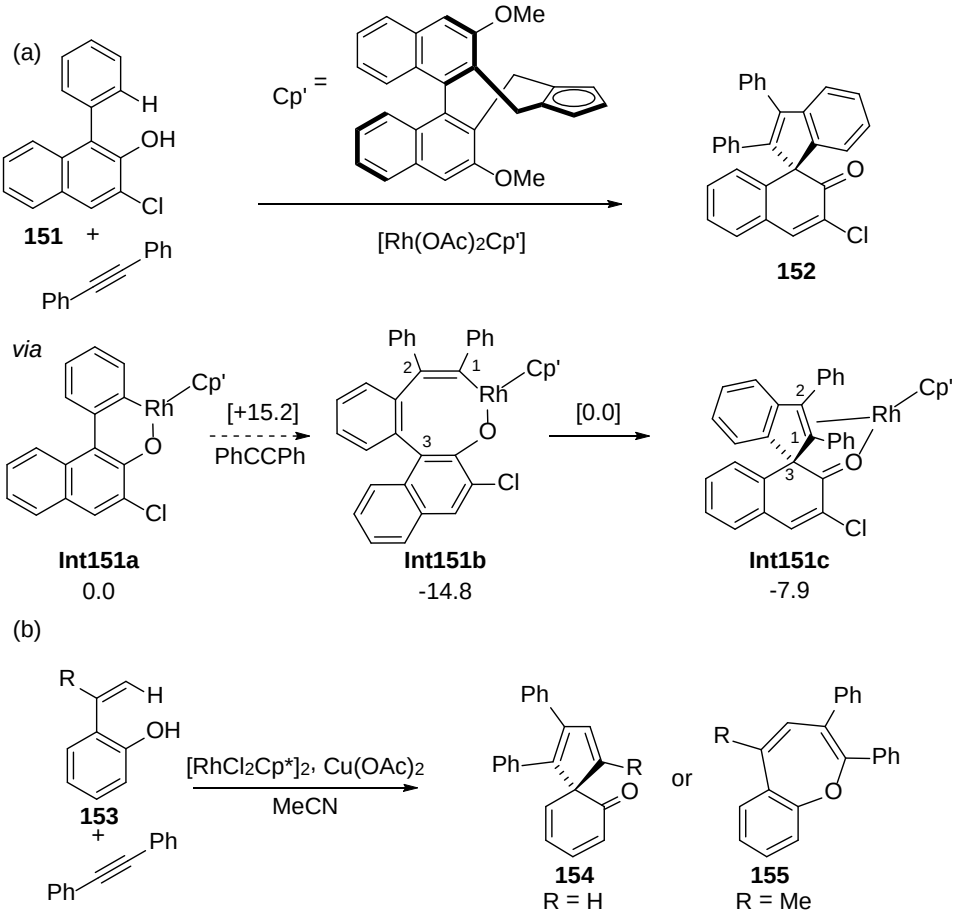

Figure 63. (a) Spiroannulation of 3-chloro-1-phenyl-2naphthol, **151**, with PhCCPh at a [Rh(OAc)$_2$Cp'] active species. Key stationary points are indicated with free energies (kcal/mol) quoted relative to **Int151a** plus free PhCCPh set to 0.0 kcal/mol. Adapted with permission from Ref. 205. Copyright 2016 American Chemical Society. (b) Competing outcomes of the reaction of 2-H_2C=CRC_6H_4OH, **153**, with PhCCPh. Adapted with permission from Ref. 170. Copyright 2016 John Wiley and Sons.

The mechanism of Rh(III)-catalysed C-H functionalization of quinoline *N*-oxide, **19**, with PhCCPh to form **156** has been studied by Li and Lan with M11L(1,4-dioxane)//B3LYP calculations (Figure 64).[206] In this case a new heterocyclic ring is not formed, but the mechanism is closely related to the others covered in this section and so is discussed here. Starting from the cationic solvent adduct, [Rh(κ^2-

OAc)(1,4-dioxane)Cp*]$^+$ in which the exchange of OAc by 1,4-dioxane is assumed, substitution of 1,4-dioxane by **19** then allows the *N*-oxide oxygen to act as a directing group for an AMLA/CMD C-H activation ($\Delta G^‡$ = +23.3 kcal/mol; ΔG = +7.4 kcal/mol). HOAc/PhCCPh substitution and migratory insertion into the Rh-C bond forms rhodacycle **Int19a** which then undergoes C-O bond forming reductive coupling to give tricyclic species, **Int19b** ($\Delta G^‡$ = +24.6 kcal/mol; ΔG = +0.4 kcal/mol). Rather than dissociate, **Int19b** accesses a very facile N-O oxidative cleavage to form **Int19c**, thus completing a net O atom transfer from N to C via Rh. Rearrangement of **Int19c** to **Int19d** allows product release via protonation with HOAc with an overall barrier of 23.4 kcal/mol. This final step is endergonic and regenerates the [Rh(OAc)(1,4-dioxane)Cp*]$^+$ active species; as such the energy span in this case links **Int19d** to the reductive coupling transition state in the subsequent cycle and has a value of 29.5 kcal/mol. With MeCCPh insertion is favoured such that the Ph group is adjacent to Rh.

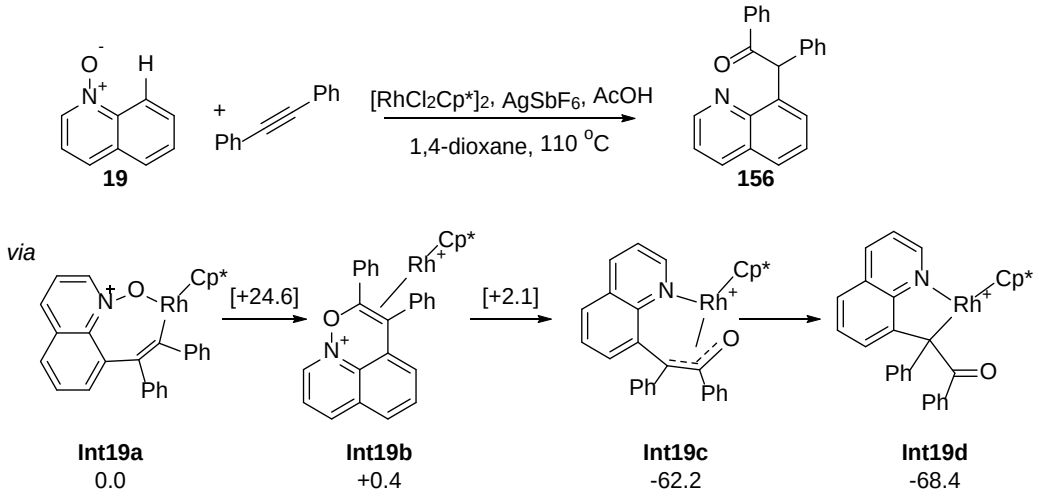

Figure 64. Rh(III)-catalysed alkenylation of quinoline *N*-oxide, **19**, with PhCCPh to form **156**. Key stationary points are indicated with free energies (kcal/mol) quoted relative to **Int19a** set to 0.0 kcal/mol. Adapted with permission from Ref. 206. Copyright 2015 John Wiley and Sons.

Related mechanisms have been characterised by Yu for the enantioselective indoline formation from phenylnitrones and PhCCPh,[207] and by Zhou, Yang and Zhu for the coupling of 1-naphthylamine *N*-oxides, **157**, with diazo compounds to give 1H-benzo[*g*]indolines **158** (Figure 65).[208] The latter

reaction requires activation of both a C(sp^2)-H and a C(sp^3)-H bond and M06(DCE) calculations indicate an initial C(sp^2)-H activation is preferred via a [Rh(OAc)(κ^1-*O*-**157**)Cp*]$^+$ precursor and an overall barrier of $\Delta G^‡$ = 28.4 kcal/mol. α-diazomalonate addition and loss of N_2 forms a Rh-carbene which inserts into the Rh-aryl bond to form the 6-membered rhodacycle **Int157a**. C(sp^3)-H activation then occurs via an external CMD in which acetate removes a proton that is geminal to the agostic C-H bond via **TS157** with a barrier of 20.1 kcal/mol. A transition state for a non-metal assisted C(sp^3)-H deprotonation proved to be 13.6 kcal/mol less accessible. **Int157b** features a κ^3-*O,C,C*-ligand but direct C-C coupling at this point has a significant barrier of 47.5 kcal/mol. Instead N-O bond cleavage is postulated to form a Rh=O species, **Int157c** ($\Delta G^‡$ = 31.9 kcal/mol, ΔG = -1.0 kcal/mol), protonolysis of which releases an iminium cation that undergoes off-metal intramolecular C-C bond formation. Protonation of the Rh=O unit by HOAc is assumed to regenerate [Rh(OAc)$_2$Cp*]. Overall N_2 loss from the diazocarbene is rate determining and equates to a computed $\Delta G^‡_{span}$ of 34.0 kcal/mol, rather large given that experimentally catalysis proceeds efficiently at 60 °C.

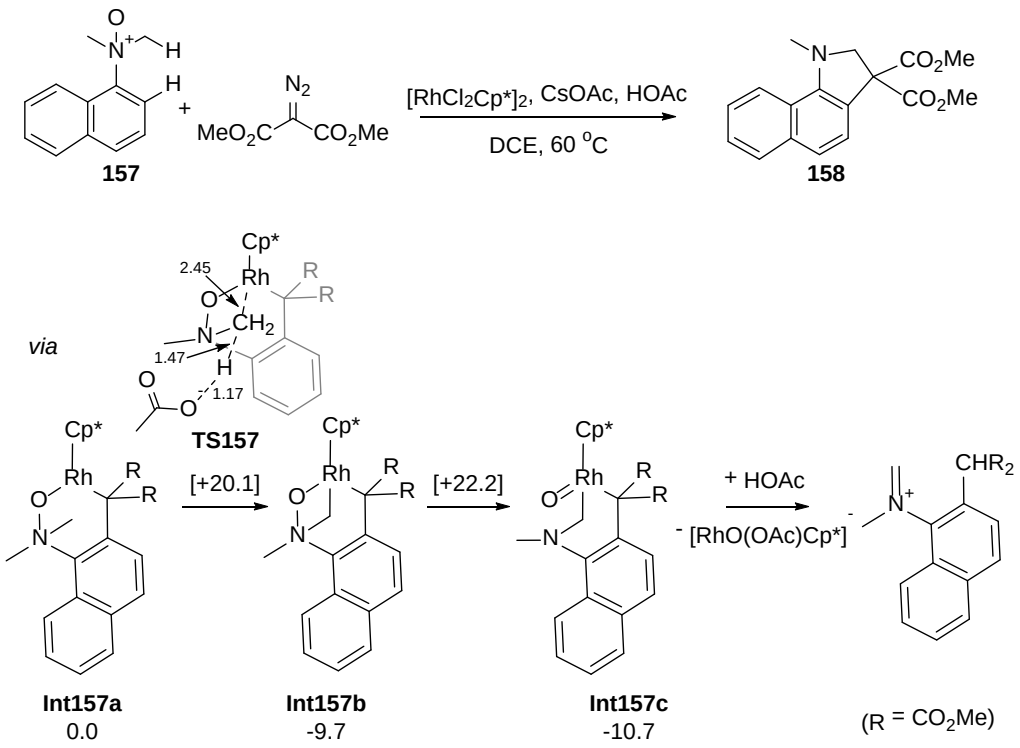

Figure 65. Rh(III)-catalysed coupling of 1-naphthylamine *N*-oxide, **157**, with an α-diazocarbene to give *1H*-benzo[g]indoline **158**. Key stationary points are indicated with free energies (kcal/mol) quoted relative to **Int157a** set to 0.0 kcal/mol. Adapted with permission from Ref. 208. Copyright 2015 John Wiley and Sons.

Lan and Huang have studied the Rh(III)-catalysed oxidative cyclocarbonylation of ketimines, **159**, to give 3-methylene-isoindolin-1-one **160** using M11-L(toluene)//B3LYP calculations (see Figure 66).[209] The ketimine is proposed to access the cycle as its enamine tautomer, **159***, allowing facile *N*-deprotonation and AMLA/CMD C(sp^2)-H bond activation to form cyclometallated **Int159a** ($\Delta G^{\ddagger}$ = 28.8 kcal/mol). This then tautomerises on the metal to give **Int159a*** with subsequent migratory insertion of CO into the Rh-aryl bond. Coordination of a second CO molecule precedes facile C-N bond coupling to form the product, **160,** and $[Rh(CO)_2Cp^*]$. The latter is assumed to be re-oxidised to $[Rh(OAc)_2Cp^*]$ by $[Cu(OAc)_2]$.

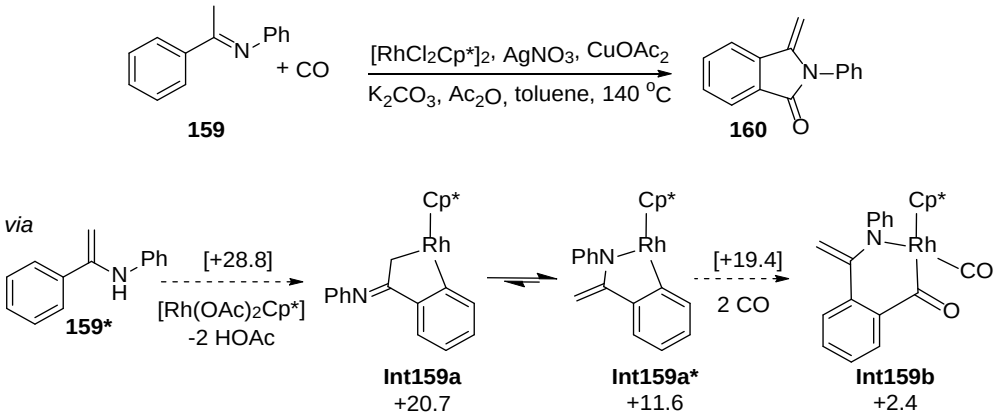

Figure 66. Rh(III)-catalysed oxidative cyclocarbonylation of ketimine **159**. Key stationary points are indicated with free energies (kcal/mol) quoted relative to $[Rh(OAc)_2Cp^*]$ and the reactants set to 0.0 kcal/mol. Adapted with permission from Ref. 209. Copyright 2016 American Chemical Society.

6.1.3. Direct Functionalisation. Rh(III)-catalysed direct functionalisation, the net replacement of a C-H bond by a C-R group, has been modelled with a variety of coupling partners. Studies of alkenylation are most prevalent and an example has already been mentioned in Section 6.1.1 as an

alternative outcome of the reaction of benzamides fitted with an internal oxidant (see Figure 44).[179] C-C bond formation has been modelled with diazocarbenes, allyl and aryl precursors, although direct arylation is far less common than in Pd catalysis. Direct C-C bond formation is also seen in the reactions of *N*-oxides with alkynes, and these were covered in Section 6.1.2 due to the mechanistic similarity of this process with heterocycle formation (see Figure 64).

One of the first computational studies of direct alkenylation came from Huang and Fu who used a M06(THF)//B3LYP protocol to model the Rh(III)-catalyzed oxidative Heck coupling of aryl carbamates with alkenes (see Figure 67, where THF presents a similar dielectric to the tetrahydropyran (THP) solvent used experimentally).[210] The reaction of *m*-tolyldimethylcarbamate, **161**, with ethyl acrylate was assumed to proceed from a 16e $[Rh(OAc)Cp^*]^+$ precursor with the substrate binding *via* the carbamate oxygen (**Int161a**, 0.0 kcal/mol). This then reacts preferentially at the less hindered *ortho*-position via a one-step C-H activation with a computed barrier of 22.2 kcal/mol. Loss of HOAc gives the 6-membered metallacycle, **Int161b**, at +7.9 kcal/mol, which then undergoes 2,1-insertion with ethyl acrylate with an overall barrier of 11.9 kcal/mol to produce the 8-membered rhodacycle, **Int161c**, at -5.5 kcal/mol. β-H transfer to Rh(I)-H intermediate, **Int161d**, is endergonic ($\Delta G^{\ddagger}$ = 16.9 kcal/mol; ΔG =+17.0 kcal/mol), with product release presumed to occur in the presence of the $Cu(OAc)_2$ oxidant. Rate-limiting C-H activation is therefore proposed, and while this would be consistent with an intramolecular k_H/k_D KIE of 3.1 the computed $\Delta G^{\ddagger}_{span}$ of 22.2 kcal/mol is perhaps rather low for the experimental conditions (24 hours at 110 °C).[211] One possible reason for this may be that the energetic cost of OAc dissociation from $[Rh(OAc)_2Cp^*]$ to form the unsaturated $[Rh(OAc)Cp^*]^+$ precursor has not been taken into account. An alternative mechanism featuring initial C-H activation of the ethyl acrylate was also modelled but found to have a higher barrier in excess of 25.1 kcal/mol.

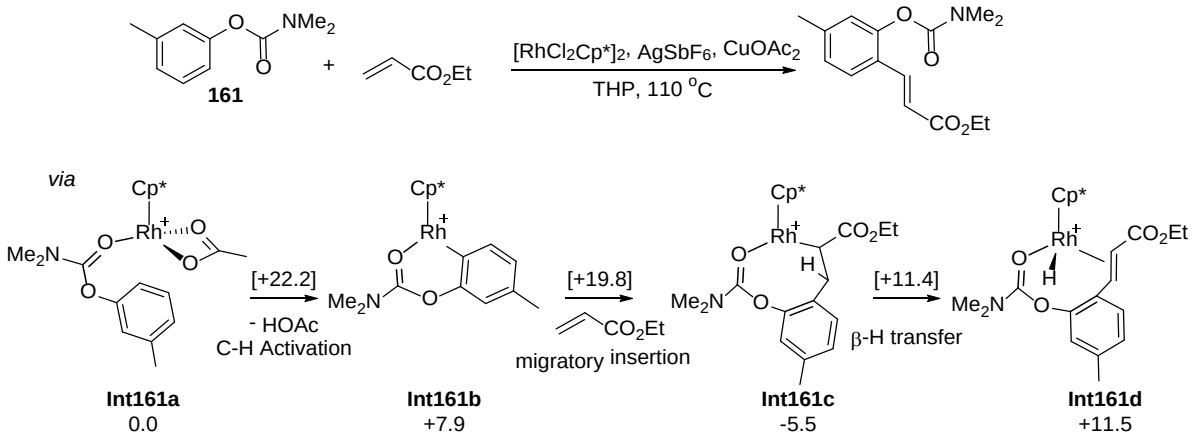

Figure 67. The Rh-catalysed reaction of ethyl acrylate with *m*-tolyldimethylcarbamate, **161**, with selected stationary points; free energies (kcal/mol) are quoted relative to **Int161a** set to 0.0 kcal/mol.[210] Adapted with permission from Ref. 43. Copyright 2016, John Wiley and Sons.

Davies and Macgregor have also modelled the related couplings of 5-methyl-3-phenylpyrazole, **137**, with methyl acrylate and styrene at [Rh(OAc)$_2$Cp*] (Figure 68(a), BP86-D3(DCE) calculations).[212] Starting from alkene analogues of the previously discussed cyclometallated intermediate (**137c**, Figure 57),[196] 2,1-insertion was computed to be preferred for both alkenes, with a slightly lower barrier for methyl acrylate than for styrene (approximately 20 kcal/mol and 23 kcal/mol respectively). The rhodacyclic products are sufficiently flexible that β-H transfer can occur to give both the *cis* and *trans* alkene products, with the experimentally observed *trans* isomers (**162**) being favoured both kinetically and thermodynamically. For methyl acrylate the overall barriers for C-H activation and the subsequent alkene insertion were computed to be similar, whereas with styrene insertion is clearly rate-limiting. Huang and Wang modelled the reaction of dimethyl-2-vinylcyclopropane-1,1-dicarboxylate with *N*-methoxybenzamide (Figure 68(b), M06(CF_3CH_2OH) calculations). This proceeds by a reversible C-H activation with a barrier of 21.4 kcal/mol followed by rate-limiting 2,1-insertion with a free energy span of 26.1 kcal/mol.[213] In this case further reaction via β-H elimination and ring opening of the cyclopropane forms **163**. The coupling of allyl carbonate at a cyclometallated *N*-sulfonyl ketimine has also been modelled, although the C-H activation step was not itself considered in this case.[214]

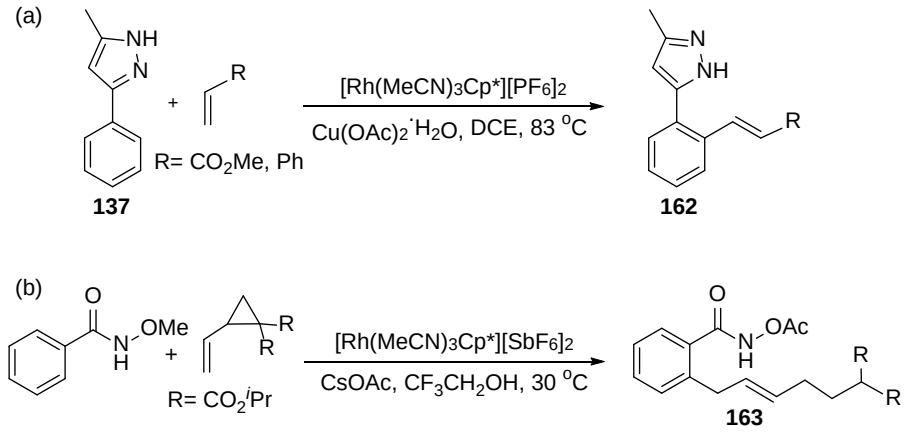

Figure 68. Rh-catalysed alkenylations: (a) 5-methyl-3-phenylpyrazole, **137**, with H_2C=CHR (R = Ph, CO_2Me);[212] (b) *N*-methoxybenzamide with dimethyl-2-vinylcyclopropane-1,1-dicarboxylate.[213] Adapted with permission from Ref. 43. Copyright 2016, John Wiley and Sons.

Li and Liao have also modelled the reactions of *N*-phenoxyacetamide, **120**, with styrene and *N*-tosylhydrazone to give the 1,2 and 1,1-diarylalkenes **164** and **165** respectively, see Figure 69.[192] M06(solvent) calculations provide similar profiles in both EtOH and toluene for the initial cyclometallation to give the common intermediate **166**. With styrene a 2,1-insertion is followed by the mechanism outlined in Figure 44(b), i.e. β-H transfer and N-H reductive coupling to Rh(I) amine intermediate **Int164a**, followed by N-O oxidative cleavage with transfer of the NHAc group onto Rh (**Int164b**) and protonolysis by HOAc to release **164**. The oxidative cleavage is rate-determining with $\Delta G^{\ddagger}_{span}$ = 28.8 kcal/mol, and this process is shown to be kinetically favored by 3.1 kcal/mol over formation of a Rh(V)-nitrene species. The endothermicity of the initial cyclometallation is proposed to contribute to the observed k_H/k_D KIE seen experimentally. In the presence of base *N*-tosylhydrazone forms an α-diazocarbene and this species reacts with intermediate **166** to form **Int165a** and, after insertion, the stable 6-membered rhodacycle, **Int165b**. The most accessible pathway then involves NAc transfer to Rh to form a Rh(V)-nitrene, **Int165c**, which rearranges to give the Rh(III) species **Int165d** that features a methylenecyclohexadienone moiety. H^+ transfer from the Me group to nitrogen reinstates aromaticity in **Int165e**, and protonation releases the alkenylated

product **165**. The internal oxidation is again rate-determining with $\Delta G^{\ddagger}_{span}$ = 21.1 kcal/mol. A Rh(III)-Rh(I)-Rh(III) pathway is therefore favored with styrene, but a Rh(III)-Rh(V)-Rh(III) pathway dominates with *N*-tosylhydrazone.

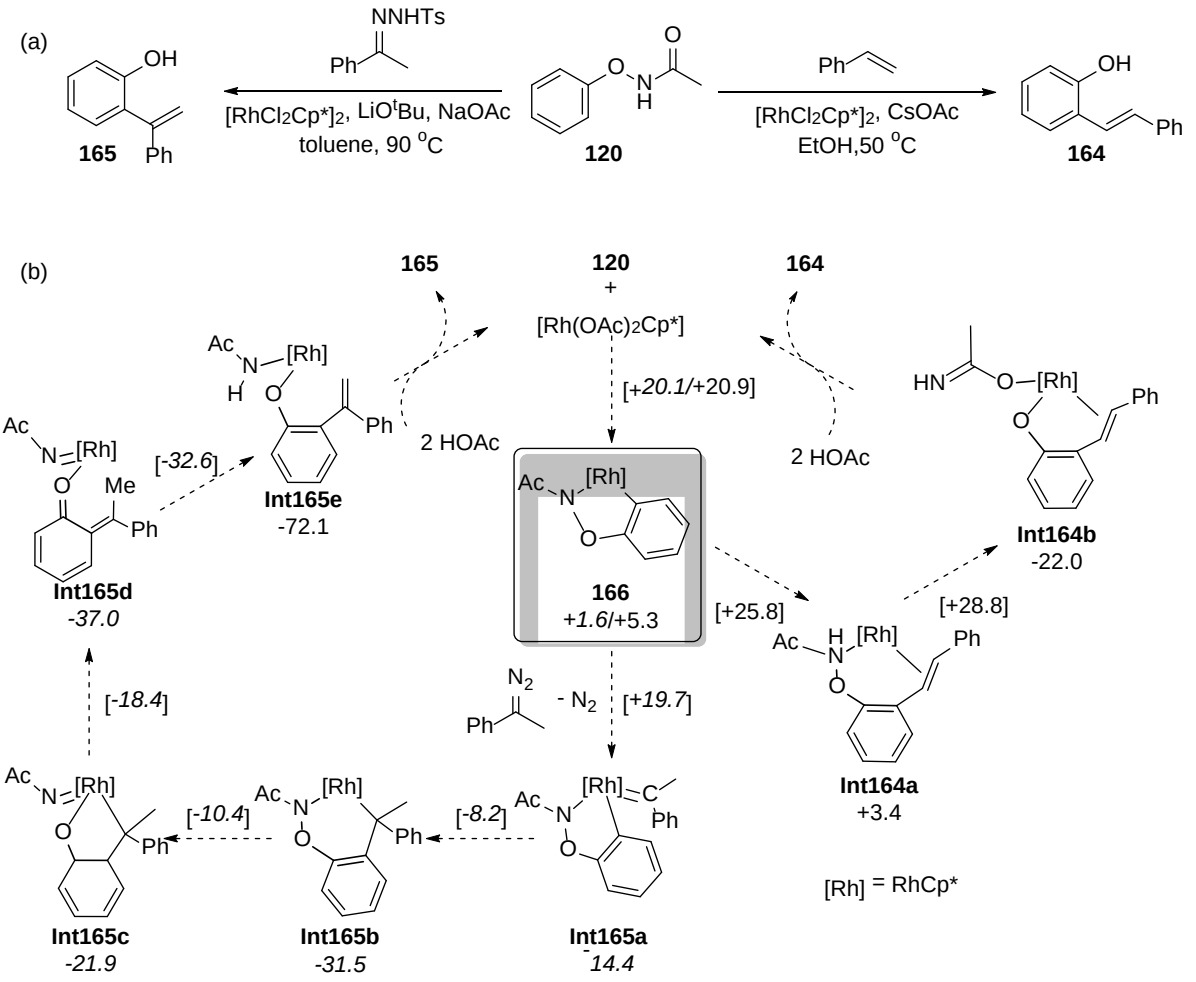

Figure 69. (a) Reactions of *N*-phenoxyacetamide, **120**, with styrene and *N*-tosylhydrazone to give diarylalkenes **164** and **165** respectively; [Rh] = RhCp*; (b) key stationary points with free energies (kcal/mol) quoted relative to $[Rh(OAc)_2Cp^*]$ plus the organic reactants set to 0.0 kcal/mol. Adapted with permission from Ref. 192. Copyright 2016 The Royal Society of Chemistry.

Zhao and Wang[215] have used PBE0(PhBr, D3BJ) calculations to model the direct arylation of $PhC(O)N^iPr_2$ with bromobenzene as reported by Glorius (**167** to **168**, Figure 70).[216] Starting from a $[Rh(\kappa^2\text{-OPiv})(\kappa\text{-}O\text{-}\mathbf{167})Cp^*]^+$ precursor an AMLA/CMD *ortho*-C-H bond activation occurs in one step ($\Delta G^{\ddagger}$ = 20 kcal/mol; ΔG = +10.6 kcal/mol). HOPiv/PhBr exchange forms an adduct in which the PhBr

binds in a η^1-fashion through the *para*-C. Several possible *para*-C-H activation pathways were then considered, with non-pivalate-assisted processes (oxidative addition or H-transfer onto either the benzamide oxygen or the Cp* ligand) being ruled out. Instead deprotonation of the *para*-C-H bond via an external pivalate was computed to have a barrier of only 6.9 kcal/mol and forms [Rh(**167'**)PhCp*]. C-C coupling then proceeds with a barrier of 28.0 kcal/mol. The authors designate this C-H activation reaction as an S_E3 process, similar to that proposed by Jutand,[217,218] although no specific computational evidence is presented to support this and the calculated transition state geometry resembles an external CMD. Further calculations show *meta*-C-H activation is slightly less accessible ($\Delta G^{\ddagger}$ = 29.2 kcal/mol) and experimentally a 2.8:1 meta:para selectivity is seen; computed k_H/k_D KIEs of around 3.6 also compare well with experimental values.

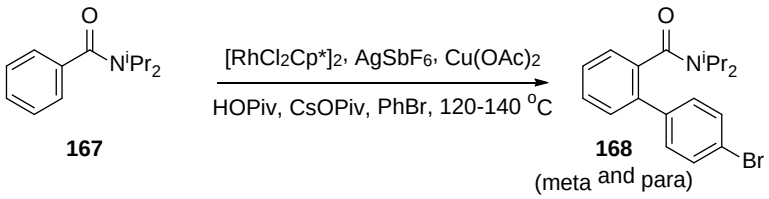

167 **168** (meta and para)

Figure 70. Rh(III)-catalysed direct arylation of PhC(O)N^{i}Pr$_2$ with bromobenzene modelled by Zhao and Wang. Adapted with permission from Ref. 215. Copyright 2015 American Chemical Society.

Lan and Li have modelled the Rh(III)-catalysed amination of benzo*[h]*quinoline, **bzq**, with anthranils, **169**, using M11-L(DCE)//B3LYP calculations (Figure 71).[219] Starting from a 16e [Rh(OPiv)Cp*]$^+$ precursor, binding of **bzq** followed by an AMLA/CMD C-H activation proceeds with a barrier of 14.8 kcal/mol and, after HOAc/anthracil (with R = R' = H) exchange, leads to key intermediate **Int169a** at -2.0 kcal/mol. Of several pathways that were considered, amination via N-O bond cleavage and formation of the Rh(V)-nitrene intermediate **Int169b** proved most accessible. Nitrene insertion into the Rh-aryl bond proceeds with an overall barrier (relative to **Int169a**) of 21.8 kcal/mol. Protonolysis of the resultant amide by HOPiv releases the final product. Analogues of **Int169a** and **Int169c** were

characterised experimentally with R = Cl, R' = Ph. With this substrate the computed barrier (in $CHCl_3$) for the conversion of **Int169a** to **Int169c** is 27.9 kcal/mol and this compares favorably with an experimental value of 24.9 kcal/mol.

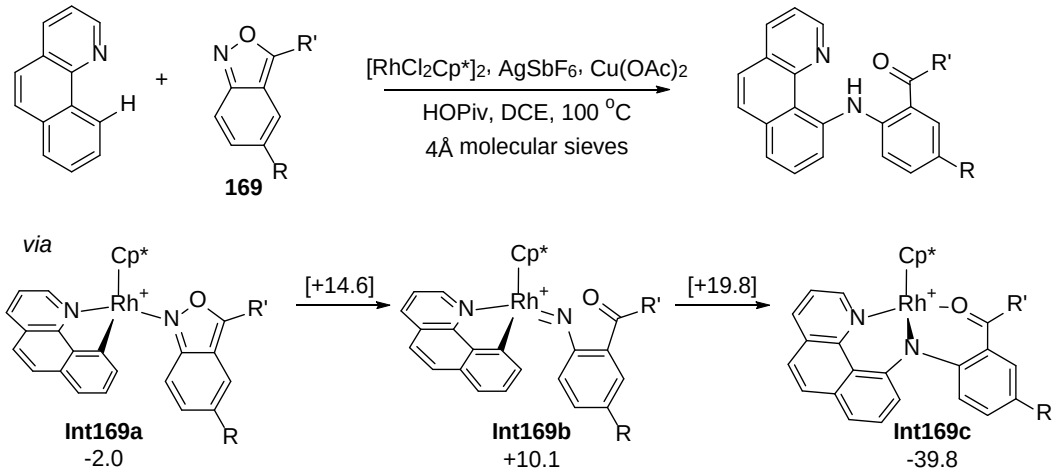

Figure 71. Rh(III)-catalysed amination of **bzq** with anthranils, **169**. Key stationary points (with R = R' = H) are indicated with free energies (kcal/mol) quoted relative to the reactants set to 0.0 kcal/mol. Adapted with permission from Ref. 219. Copyright 2016 John Wiley and Sons.

6.2 Intramolecular C(sp^3)-H Bond Activation

Relatively few computational studies on carboxylate-assisted intramolecular C(sp^3)-H activation at Rh or Ir have been reported, although one example, the external CMD of an C(sp^3)-H bond in 1-naphthylamine N-oxide (**157**, Figure 65) modelled by Zhou, Yang and Zhu, has already been mentioned.[208] Morokuma has considered the $[RhCl_2Cp^*]_2$-catalyzed C(sp^3)-H bond functionalisation of 8-methylquinoline (**8mq**) with alkynes (Figure 72).[220] Experimentally,[221] H/D exchange occurs in the absence of alkyne when $Cu(OAc)_2$ is present, but is not observed when the alkyne is available. This indicates rate-limiting C-H activation which is confirmed by a significant k_H/k_D KIE of 4.0. The cyclometallated intermediate [Rh(**8mq'**)ClCp*] was also isolated experimentally. Initial B3LYP-D3(DMF) calculations were based on the formation of a contact ion-pair, [Rh(κ^1-OAc)(**8mq**)Cp*]OAc,

that features a C(sp^3)-H···Rh agostic interaction. From here an external CMD was found to be most accessible and proceeds to form [Rh(**8mq'**)(κ^1-OAc)Cp*].HOAc with $\Delta H^{\ddagger}$ = 10.7 kcal/mol and ΔH = -21.6 kcal/mol. These energetics are, however, incompatible with reversible H/D exchange. Instead the authors propose that $Cu(OAc)_2$ is present in DMF as *trans*-[$Cu(\kappa^1\text{-}OAc)_2(DMF)_2$] and that, as a result, there is no free acetate available in solution. C-H activation is therefore postulated to occur at [Rh(Cl)(**8mq**)Cp*]$^+$ with *trans*-[$Cu(\kappa^1\text{-}OAc)_2(DMF)_2$] acting as an external base via one of the acetate C=O groups. The computed energetics of this step ($\Delta H^{\ddagger}$ = 26.4 kcal/mol; ΔH = -0.8 kJ/mol) would be consistent with reversible C-H activation. Subsequent alkyne insertion proceeds after Cl^- dissociation from the cyclometaled intermediate. One feature of this study is the high exothermicity computed for Cl/OAc exchange: for example [Rh(**8mq'**)(OAc)Cp*] is 17.3 kcal/mol more stable than [Rh(**8mq'**)ClCp*], although only the latter species is observed experimentally even in the presence of excess OAc. This also contrasts with other experimental studies that suggest Cl/OAc exchange in MeOH to be near to equilibrium;[174] computationally the energetics of anion exchange have also been shown to be sensitive to the inclusion of diffuse functions in the basis set.[172] Further exploration of these issues would therefore be of interest. A related work by Wang considered a directed C(sp^3)-H activation of **8mq** at [$Rh(OAc)_2$Cp*], but without prior OAc loss. B3LYP(DMF) calculations provide a barrier of over 50 kcal/mol, confirming the importance of creating a vacant site at the metal center for formation of the M-aryl bond.[222]

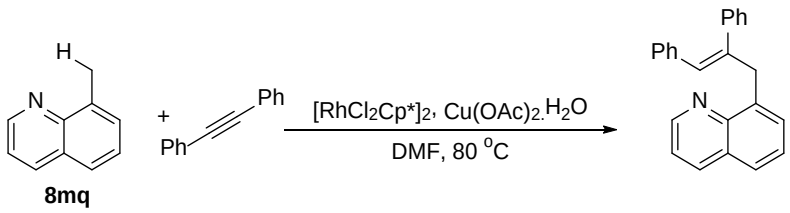

Figure 72. Rh(III)-catalyzed C(sp^3)-H bond functionalisation of 8-methylquinoline, **8mq**, with PhCCPh. Adapted with permission from Ref. 220. Copyright 2015 John Wiley and Sons

A study of intramolecular C(sp^3)-H activation involving the Ir(III)-catalysed direct arylation of ketoximes has been reported by Xia and Shi who used M06(cyclohexane, D3) calculations to model the reaction of butan-2-one-*O*-methyl oxime, **170** (R = H), with Ph_2IOTf (see Figure 73).[223] Of a number of cationic [Ir(X)(κ-*N*-**170**)Cp*]$^+$ precursors considered (X = κ^1-*N*-NTf_2, κ^2-OPiv or κ^2-OTf) the most accessible AMLA/CMD pathway for β-C(sp^3)-H bond activation was for X = OTf ($\Delta G^‡$ = 24.1 kcal/mol, ΔG = +13.0 kcal/mol, relative to a [Ir(κ^1-*N*-NTf)(κ-*O*-Ph_2IOTf)Cp*]$^+$ precursor). Oxidation with Ph_2IX was computed to be most accessible when X = NTf_2, with Ph^+ transfer to the Ir center proceeding with a barrier of only 9.4 kcal/mol, followed by addition of the NTf_2 anion to form intermediate **Int170**. C-C coupling then readily occurs with a barrier of 9.1 kcal/mol. The overall computed reaction profile implies rate-limiting C-H activation with $\Delta G^‡_{span}$ = 24.1 kcal/mol, consistent with a reported k_H/k_D of 4.0. The alternative sequence involving initial Ph^+ transfer and then C-H activation was ruled out. No reaction with the substrate **170** when R = Me is observed experimentally and calculations show not only increased barriers for the C-H activation at [Ir(OTf)(κ-*N*-**170**)Cp*]$^+$ but also that Ph^+ transfer would become rate-limiting in these cases, with $\Delta G^‡_{span}$ = 32.8 kcal/mol and 37.1 kcal/mol for β-C-H and γ-C-H functionalisation respectively.

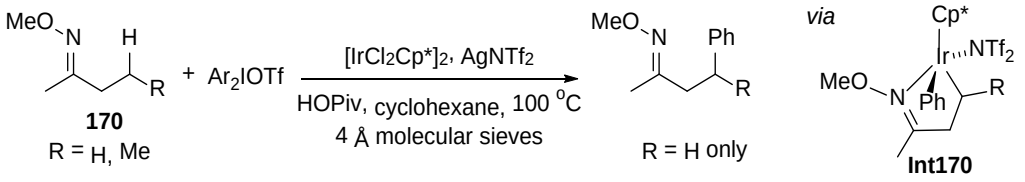

Figure 73. Ir(III)-catalysed direct arylation of ketoximes with Ar_2IOTf (Ar = Ph in the computational study). Adapted with permission from Ref. 223. Copyright 2015 American Chemical Society.

To this point examples of carboxylate-assisted intramolecular C-H activation at Rh and Ir have depended on a heteroatom directing group. A variation on this theme has been eluciated by Bera in a joint experimental and computational study of the acetate-induced activation of the allylic C(sp^3)-H

bonds in the cyclooctadiene (COD) ligand.[224] This process, in which one of the C=C double bonds may be viewed as a directing group, is seen in the reaction of $[Ir(\mu\text{-OAc})(COD)]_2$ with 3-(pyrid-2-yl)-imidazolium bromides that leads to the unexpected product **171** in which the COD has isomerised to a C–H activated κ^1-η^3-binding mode (see Figure 74). In contrast, the methoxide-bridged precursor gave the un-isomerised product **172**. B3LYP calculations indicated initial C-H activation of the imidazolium C2-H bond occurs via a concerted oxidative addition and gives a hydrido alkene intermediate **173**. This features a κ^2-OAc ligand that then undergoes a two-step acetate-assisted C-H activation via an agostic intermediate from which allylic C-H bond cleavage proceeds via **TS173** with an overall barrier of 18.1 kcal/mol. The subsequent insertion of the second alkene moiety into the Ir-H bond in **174** then leads to the formation of the observed product **171**. The short Ir···H and Ir···C contacts in **TS173** suggest this allylic C-H activation is a genuine AMLA/CMD-type process in which metal and intramolecular base work in concert to effect the C-H bond cleavage.

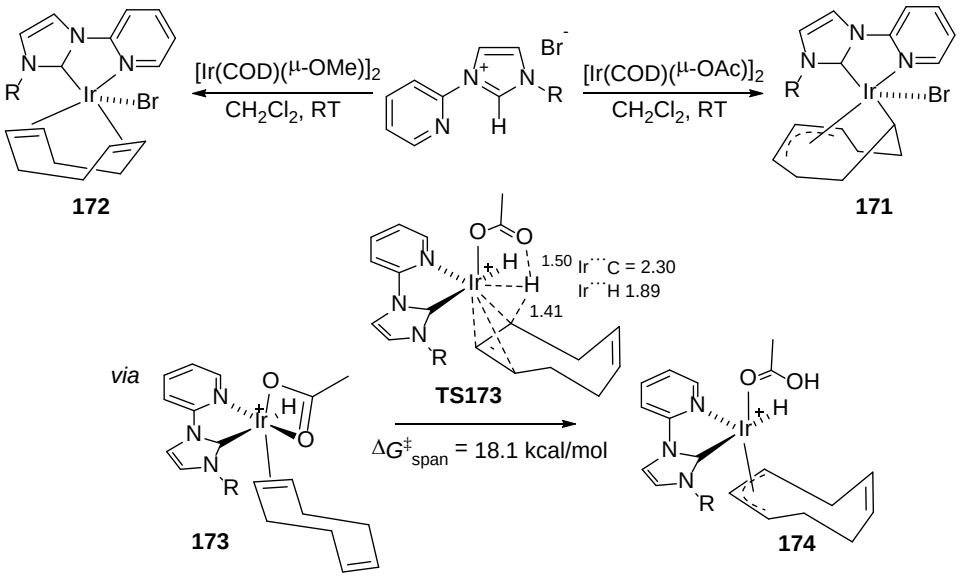

Figure 74. Reactions of $[Ir(\mu\text{-X})(COD)]_2$ (X = OMe, OAc) with 3-(pyrid-2-yl)-imidazolium bromides (exp: R = mesityl; calc: R = Me); key stationary points in the COD isomerisation highlighting C(sp^3)-H activation transition state **TS173** with selected distances in Å. Adapted with permission from Ref. 224. Copyright 2015 American Chemical Society.

Further mechanistic studies on this carboxylate-induced COD isomerisation were performed by Kunz on the related [Ir(C^C)(COD)]$^+$ system, **175**, where C^C is a chelating bis-NHC ligand (see Figure 75).[225] Experimental studies showed that formation of the isomerised product **176** requires donor solvents such as MeCN and is catalysed by acid. Intermediate **177** was also isolated in CH_2Cl_2 when R = CF_3 and shown to react on to form **176** in MeCN. Moreover, H/D exchange was shown to occur exclusively at the four H_{endo} positions. BP86-D3 calculations on **177** (with R = CH_3) indicate that, after an initial isomerisation, alkene insertion into the Ir-H bond can form agostic intermediate **Int177** with an overall barrier of 12.7 kcal/mol and ΔG = +8.1 kcal/mol. A facile AMLA/CMD allylic C-H activation with a barrier of 2.7 kcal/mol then leads, after HOAc/MeCN substitution, to **176** (ΔG = -10.8 kcal/mol *cf*. **177**). The observation of H/D exchange at the *endo* positions is consistent with C-H activation being an intramolecular AMLA/CMD and argues against an external CMD. The alternative C-H activation/alkene insertion sequence (operative in the Bera system[224]) was ruled out in this case as the initial allylic C-H activation has a high barrier of 28.4 kcal/mol.

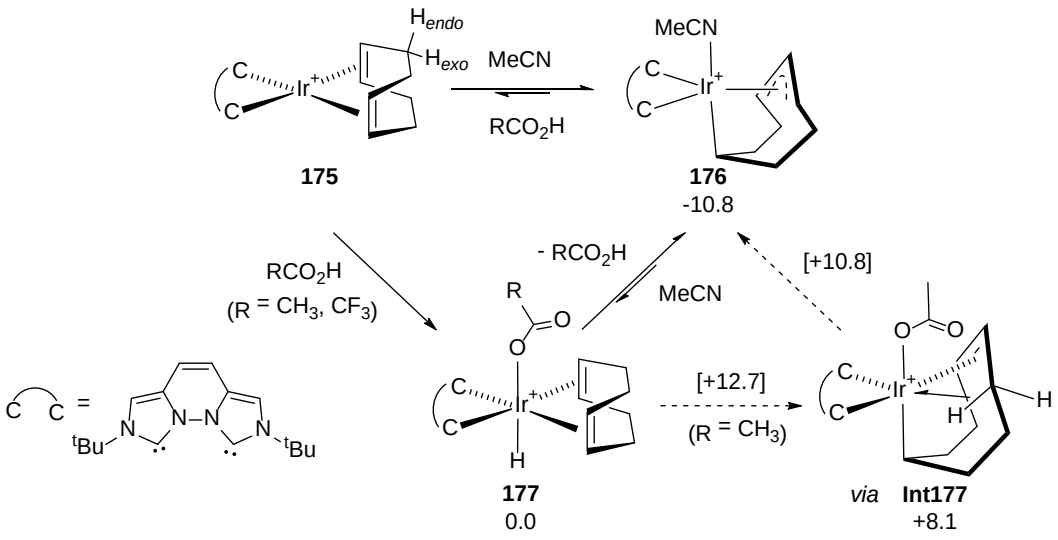

Figure 75. Carboxylate-induced COD isomerisation in [(C^C)IrCOD]$^+$, **175**, with key stationary points and free energies (kcal/mol) relative to **177** set to 0.0 kcal/mol. Adapted with permission from Ref. 225. Copyright 2015 American Chemical Society.

[Rh(C^C)I_2(OAc)] complexes (where C^C = bidentate 'normal' and 'abnormal' NHCs linked by a –$(CH_2)_3$- unit) exhibit C(sp^3)-H activation of the linker's central CH_2 group. This process occurs more readily with the abnormal NHCs, and BP86(MeCN) calculations suggest these induce an easier pre-dissociation of iodide, rather than having any direct effect on the AMLA/CMD C-H activation step.[226]

6.3 Intermolecular C(sp^2)-H Activation

Following on from their pioneering work on the C-H activation of benzene[63] Periana and Goddard revisited the *cis*-[Ir(acac)$_2$(κ^2-O_2CR)] system (R = CH_3, CF_3) to rationalise observed differences in the H/D exchange reactions of benzene. With R = CH_3 multiple H/D exchange gives higher $C_6H_{6-n}D_n$ species, whereas with R = CF_3 only a single H/D exchange event occurs to form C_6H_5D.[227] B3LYP(HOAc) calculations indicate that when R = CH_3 the reaction proceeds via the rate-limiting formation of *cis*-[Ir(acac)$_2$(κ^1-O_2CR)(η^2-C_6H_6)] ($\Delta H^{\ddagger}$ = 23 kcal/mol, see Figure 76). Subsequently AMLA/CMD C-H activation occurs via a transition state at +21 kcal/mol. H/D exchange at the resultant HOAc ligand and a reversal of these steps would then generate C_6H_5D. However, in this case further C-H activation is shown to be more accessible than arene loss ($\Delta\Delta H^{\ddagger}$ = 2 kcal/mol), and so several H/D exchange events occur before the arene eventually dissociates. In contrast when R = CF_3 (calculated in TFAH), the initial addition of C_6H_6 is much easier ($\Delta H^{\ddagger}$ = 5 kcal/mol) and the C-H activation transition state lies above this at 10 kcal/mol. Hence, only a single H/D exchange occurs as the arene will readily dissociate as C_6H_5D. A computed difference of 13 kcal/mol between the two overall barriers agrees well with experiment, although the computed values are both *ca*. 5 kcal/mol too low.

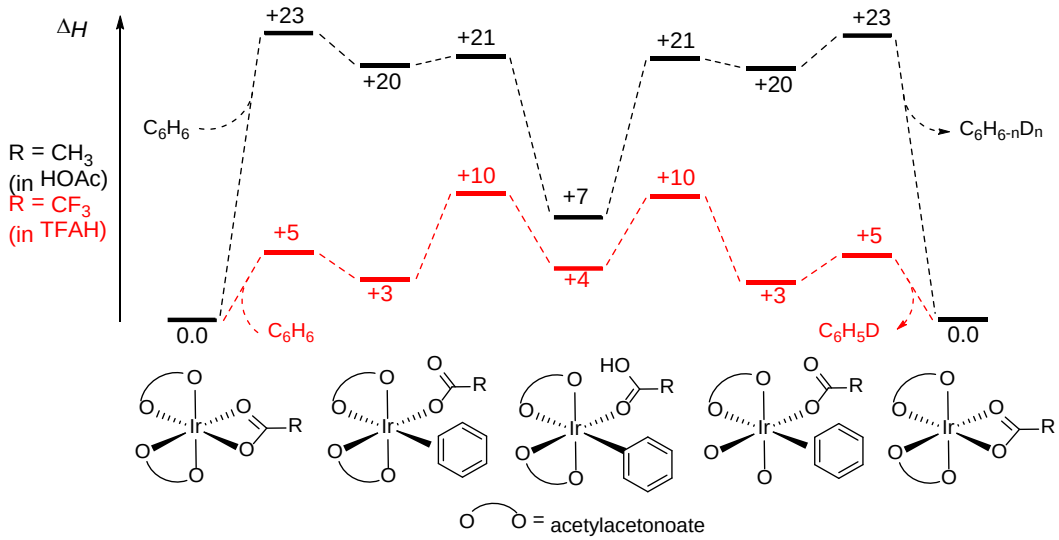

Figure 76. Computed reaction profiles (kcal/mol) for H/D exchange of benzene at *cis*-[Ir(acac)$_2$(κ^2-O_2CR)] (R = CH_3, CF_3). Adapted with permission from Ref. 227. Copyright 2015 American Chemical Society.

H/D exchange of benzene has also been reported by Gunnoe and Goddard at [(N,N)Rh(TFA)(TFAH)] complexes, where N,N = bidentate diazobutadiene (**178a**) or bis(2-oxazolin-2-yl) ligands (**178b**).[228] (M06(TFAH)//B3LYP) calculations showed similar overall barriers for an initial oxidative addition or for TFAH/benzene substitution and an AMLA/CMD C-H activation. For **178a** (the most active species experimentally) $\Delta G^{\ddagger}_{span}$ is computed to be 30.9 kcal/mol at 498 K and is consistent with an observed turnover number of 450 after two hours at 423 K ($\Delta G^{\ddagger}_{span}$ ≈ 27.4 kcal/mol). Jones has modelled both the C(sp^2)-H and C(sp^3)-H activation reactions of isopropylbenzene at [M(bdmpza)Cl_3]$^-$ complexes (M = Rh, Ir; bdmpza = *bis*-(3,5-dimethylpyrazol-1-yl)acetate and this will be discussed below in Section 6.4.[229]

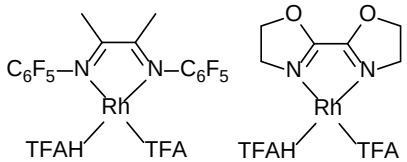

178a **178b**

Gorelsky and Woo have compared the C-H activation of benzene at [Ir(Ph)(κ^2-CO_3^-)(PMe_3)(py)] with that of the heterocycles 2-methoxythiophene, 2,3-dimethylfuran and *N*-methylindole. B3LYP(toluene) calculations showed that the lowest energy C-H activation pathway involved isomerisation of square-pyramidal [Ir(κ^2-CO_3^-)(Ph)(PMe_3)(py)] with an axial Ph ligand to a structure featuring an axial pyridine which forms an η^2-C-H adduct with the approaching benzene molecule (ΔG = +26.7 kcal/mol). C-H activation thus places the new phenyl group trans to the low trans influence pyridine. Unusually, assistance by the carbonate ligand is achieved whilst maintaining a κ^2-binding mode throughout and so proceeds via a 4-membered AMLA/CMD transition state (**TS179**, Figure 77). Similar transition states were located for the heterocycle substrates and the computed reactivity and selectivity patterns were consistent with experimental observations.[230] Lapointe and Gorelsky also modelled the C-H activation of benzene at [Ir(CO_3^-)(PMe_3)Cp*] and [Rh(OAc)(PMe_3)Cp*] as part of their analysis of the CMD process at Pd centres.[137]

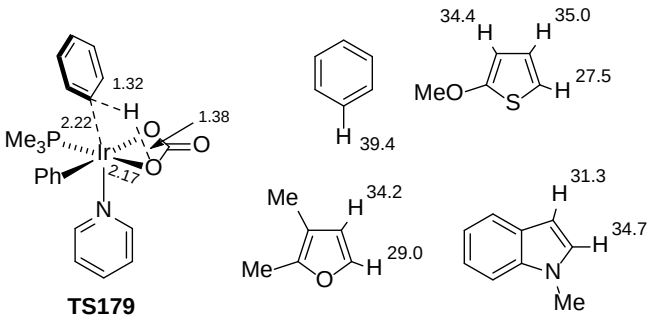

Figure 77. Computed transition state for C-H activation of benzene at [Ir(κ^2-CO_3^-)(Ph)(PMe_3)(py)] with selected distances in Å; computed barriers for the C-H activation of (hetero)arene substrates at [Ir(κ^2-CO_3^-)(Ph)(PMe_3)(py)] are also indicated in kcal/mol. Adapted with permission from Ref. 230. Copyright 2011 John Wiley and Sons.

A comparison of the C-H activation of benzene and ethene at an [Ir(κ^2-OAc)(PMe_3)Cp]$^+$ model species was presented by Davies and Macgregor using BP86 calculations.[231] Both substrates undergo a two-step C-H activation in which the initial κ^2-κ^1-displacement of OAc is rate-limiting with overall barriers of 28.4 kcal/mol and 26.3 kcal/mol respectively. With benzene an η^2-adduct is formed at +22.9

kcal/mol from which C-H activation has a barrier of 5.2 kcal/mol to give $[Ir(Ph)(HOAc)(PMe_3)Cp]^+$ at +16.6 kcal/mol. A similar profile was characterised with ethene, albeit with a more stable η^2-adduct (+9.9 kcal/mol) that increases the barrier to C-H activation to 15.0 kcal/mol. $[Ir(C_2H_3)(HOAc)(PMe_3)Cp]^+$ is formed at +10.7 kcal/mol.

6.4 Intermolecular C(sp^3)-H Activation

Goddard and Periana have investigated the C-H activation of methane at the $Ir(TFA)_2(NNC)$ complex **180** in TFAH (where NNC is a cyclometallated 6-Ph-2,2'-bipyridine ligand), a key step in catalytic formation of CF_3CO_2Me (Figure 78).[232] B3LYP(TFAH) calculations indicate complementary energetics between the κ^2-κ^1-displacement step (ΔH = +14.9/+3.9 kcal/mol trans to TFA/N^2) and the subsequent C-H cleavage step ($\Delta H^{\ddagger}$ = 7.2/19.3 kcal/mol; all values computed at 453 K). Thus the overall barrier via **TS180a** (+22.1 kcal/mol) is lower with Ir-Me bond formation trans to TFA and forms **181** at +16.8 kcal/mol. This compares with overall barriers of 23.2 kcal/mol with Ir-Me bond formation trans to N^2 via **TS180b** to give **182**, and 24.2 kcal/mol for H transfer onto the aryl ring of the NNC ligand.

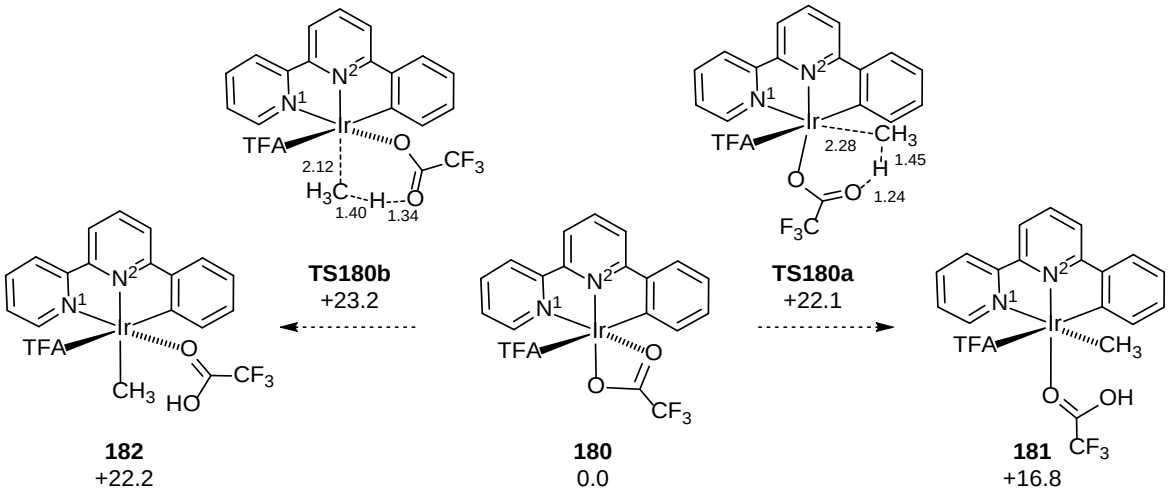

Figure 78. Key stationary points in the C-H activation of methane at the $Ir(TFA)_2(NNC)$ complex **180**; relative enthalpies computed at 453 K are given in kcal/mol and selected distances in Å. Adapted with permission from Ref. 232. Copyright 2009 The Royal Society of Chemistry.

Jones has demonstrated that [M(bdmpza)Cl_3]$^-$ complexes (M = Rh, Ir; bdmpza = *bis*-(3,5-dimethylpyrazol-1-yl)acetate) induce H/D exchange at both the arene C(sp^2)-H and the β-alkyl C(sp^3)-H bonds of alkylbenzenes in TFAH.[229] B3LYP(HOAc) calculations were employed to model H/D exchange processes in *iso*-propylbenzene, starting from [Rh(bdmpza)(κ^2-O_2CCF_3)($C_6H_5{}^iPr$)]$^+$, **183** (Figure 79) featuring the arene bound in an η^2-C-H fashion through one *ortho*-C-H bond. **183** is a precursor to both *ortho*-C(sp^2)-H activation ($\Delta G^‡$ = 23.2 kcal/mol) and β-alkyl-C(sp^3)-H activation ($\Delta G^‡$ = +32.3 kcal/mol) and these computed values agree well with experiment. Activation of the α-C-H bond is much less accessible ($\Delta G^‡$ = 44.1 kcal/mol), and indeed no H/D exchange was observed at that site. All three processes go *via* similar AMLA/CMD transition states which differ primarily in their computed Rh···C distances (C(sp^2)-H: 2.16 Å; β-C(sp^3)-H: 2.29 Å; α-C(sp^3)-H: 2.39 Å). Competing C(sp^2)-H and C(sp^3)-H bond activation of α-pyridinium and α-imidazolium esters (e.g. **184**) at [$IrCl_2Cp^*$]$_2$/NaOAc was modelled by Cross.[233] M06(CH_2Cl_2)//B3LYP calculations characterised a non-directed C-H activation process initiated from H-bonded adducts formed at the {Ir(κ^1-OAc)$_2$Cp*} fragment. The observed C(sp^3)-H activation was computed to be favored kinetically over the thermodynamically more stable C(sp^2)-H activation, albeit with rather large barriers in excess of 40 kcal/mol.

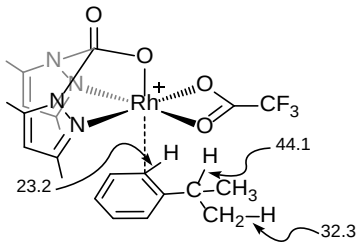

183

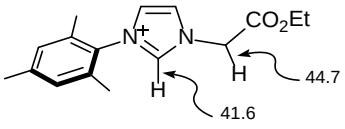

184

Figure 79. Competing C-H activation processes at [Rh(bdmpza)(κ^2-O_2CCF_3)($C_6H_5{}^iPr$)]$^+$(**183**)[229] and α-imidazolium ester (**184**);[233] computed free energy barriers are indicated in kcal/mol. Adapted with permission from Ref.44. Copyright 2016 Springer International Publishing.

As part of their drive to develop new catalysts for CH_4 to CH_3OH conversion, Nielsen, Goddard and Gunnoe have assessed the C-H activation of methane at a range of Rh-complexes featuring various bi- and tri-dentate ligands. Initial work[234] adopted an M06//B3LYP protocol for reactions in both water and TFAH and indicated an amidinate ligand with three C_6F_5 substituents (as in **185**) in TFAH solvent gave the most accessible C-H activation ($\Delta G^{\ddagger}$ = 27.6 kcal/mol relative to **185** and a free proton). The mechanism entailed TFAH/CH_4 exchange and an AMLA/CMD C-H activation involving one of the TFA ligands. The electron withdrawing amidinate ligand promotes this reaction by enhancing σ-donation from the methane C-H bond. Computed Rh-Me bond strengths were a good indicator of the trend in the C-H activation barrier heights. Functionalization of the Rh-Me complex (*via* nucleophilic attack of TFA at the bound methyl group) had a barrier of 36.8 kcal/mol. This result is solvent-dependent, however, with the relative energies of the C-H activation and nucleophilic attack transition states swapping when re-computed with a model formed in water ($\Delta G^{\ddagger}$ = +35.0 and 33.3 kcal/mol respectively).

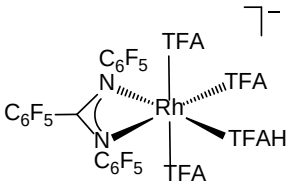

185

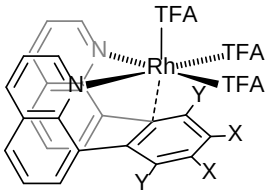

186

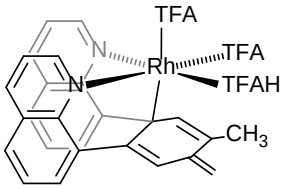

187

In a later study the reactivity of a variety of [Rh(TFA)$_3$(bis(quinolinyl)benzene)] complexes, **186**, was assessed. In this case the parent system (X = Y = H) gave the lowest barriers for both H_3C-H bond activation and the subsequent functionalization with TFA ($\Delta G^{\ddagger}$ = 33.4 kcal/mol and 35.8 kcal/mol respectively).[235] Experimental studies highlighted H/D exchange in the Me substituents of an *o*-xylene-based ligand (Y = H, X = Me)[236] and M06(TFAH)//B3LYP calculations showed this unusual 'remote' C(sp^3)-H bond activation proceeds *via* deprotonation by a Rh-bound TFA ligand. This results in dearomatization of the xylyl moiety and concomitant metalation at the *para* position giving **187** at +4.8 kcal/mol. $\Delta H^{\ddagger}$ was calculated to be 22.4 kcal/mol, and compares with an experiment value of 21

± 2 kcal/mol. Nielsen and Goldman have also studied H/D exchange at the benzylic position of mesitylene at $[Ir(O_2CR)_2(H_2O)(Phebox)]$ complexes (R = CH_3, CF_3, see Figure 80).[237] B3LYP(mesitylene) calculations define pathways where C-H activation via **TS188** is rate-limiting and these provide a lower barrier in the case of the TFA system, consistent with the somewhat greater H/D exchange activity seen experimentally in that case (130 °C, 12 hrs in mesitylene). This study also highlighted a background H/D exchange at the mesitylene aryl positions in the absence of catalyst. This phenomenon was also identified by Goddard and Gunnoe who performed experimental and computational (M06(TFAH)) studies that demonstrate proton-catalysed H/D exchange in acidic media via a Wheland intermediate.[238] This study highlights that care is required when interpreting the observation of arene H/D exchange in acidic media.

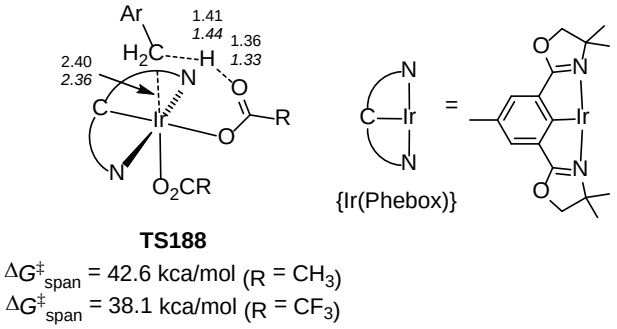

TS188

$\Delta G^{\ddagger}_{span}$ = 42.6 kca/mol (R = CH_3)

$\Delta G^{\ddagger}_{span}$ = 38.1 kca/mol (R = CF_3)

Figure 80. Computed transition states for C(sp^3)-H activation of mesitylene at $[Ir(O_2CR)_2(H_2O)(Phebox)]$ complexes (R = CH_3, CF_3); with selected distances in Å. Adapted with permission from Ref. 237. Copyright 2015 American Chemical Society.

7. Cobalt

The first computational study of a carboxylate-assisted C-H activation at Co was reported by Matsunaga and Kanai in their 2014 study of the {Co(III)Cp*}-catalysed formation of pyrroloindolones via coupling of alkynes *with N*-dimethylcarbamoyl-indole, **189**.[239] B3LYP calculations probing C-H activation at the 2-position indicated the presence of two different agostic intermediates on a very flat energy profile. The highest lying transition state equates to a rearrangement between these two

species and corresponds to an overall barrier of 20.5 kcal/mol. The C-H cleavage transition state, **[1]TS189**, is only slightly more stable at +19.4 kcal/mol and the geometry of this species is shown in Figure 81. H^+-transfer onto the Co-bound oxygen is a much higher energy process ($\Delta G^{\ddagger}$ = +36.5 kcal/mol). These free energies are relative to a [Co(OAc)(κ-*O*-**189**)Cp*]$^+$ precursor in its singlet state. However, a spin triplet precursor is computed to be just 1.0 kcal/mol less stable with C-H activation on the triplet surface proceeding in a single step via **[3]TS189** with a barrier of 20.9 kcal/mol. **[3]TS189** features a somewhat later geometry than **[1]TS189** with a longer C···H distance (1.35 Å), as well as a noticeable elongation of the Rh-O bond to the carbamoyl directing group. C-H activation is endergonic with ΔG = +12.0 kcal/mol (singlet) or +15.6 kcal/mol (triplet), and this accords with H/D exchange being seen experimentally but without the observation of any cyclometalated intermediates. The proximity of the two surfaces emphasizes the importance of taking into account different spin states with a first row transition metal. The greater activity of the {CoCp*} catalysts over {RhCp*} species observed experimentally was attributed to a higher computed polarity of the Co-C bond that is suggested to promote the final reductive coupling step. In a subsequent study the C-H allylation of *N*-pyrimidin-2-yl indole with allylic alcohols was modelled with B3LYP(D3) calculations, although in this case the C-H activation step was not considered computationally.[240]

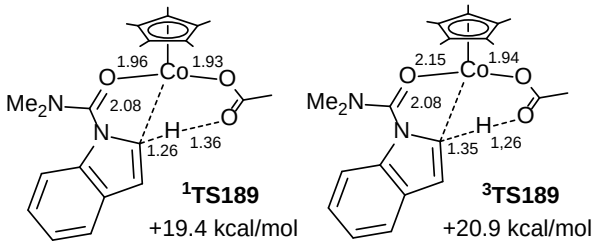

Figure 81. Transition states for C2-H activation of *N*-dimethylcarbamoylindole, **189**, at [Co(OAc)$_2$Cp*], computed in the singlet (**[1]TS189**) and triplet (**[3]TS189**) states; free energies are in kcal/mol and selected distances are in Å.[239] Adapted with permission from Ref.44. Copyright 2016 Springer International Publishing.

Wei and Niu have characterised an AMLA/CMD C-H activation with an acrylamide containing a bidentate aminopyridine-*N*-oxide directing group at both Co(II) and Co(III) metal centres, where these were computed with the M06-L functional with optimisation in MeOH solvent as a doublet and as a singlet respectively (see ^{2}**190**$^{-}$ and ^{1}**190**).[241] C-H activation in both species proceeds in a single step (^{2}**190**$^{-}$: $\Delta G^{\ddagger}$ = 28.0 kcal/mol, ΔG = +14.0 kcal/mol; ^{1}**190**: $\Delta G^{\ddagger}$ = 37.0 kcal/mol, ΔG = +12.0 kcal/mol) and the magnitude of these barriers lead the authors to propose an alternative mechanism based on a single electron transfer process to be operative in this case. Alkyne insertion and C-N reductive coupling from the resultant 7-membered cobaltacycle was studied by Macgregor and Ackermann at a related Co(II) species, **191**, using BP86(TFE, BJD3) calculations.[242] This study did not consider the C-H activation step, but does highlight the accessibility of higher spin states for both the Co(II) and Co(III) oxidation states. Prior oxidation to Co(III) greatly facilitates C-N coupling with amide nitrogen which proceeds on the triplet surface.

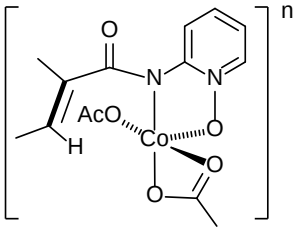

^{2}**190**$^{-}$ (Co(II): n = -1)
^{1}**190** (Co(III): n = 0)

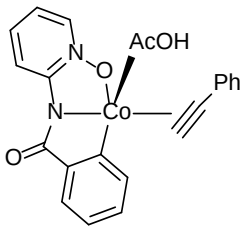

191

C(sp^{3})-H bond activation has also been modelled at a Co(III) centre by Sundararaju as part of a mechanistic study on the alkenylation of 8-methylquinoline (**8mq**) with alkynes.[243] The proposed precursor to C-H activation is an ion-pair [Co(OAc)(**8mq**)Cp*]OAc. B3LYP-D3 calculations indicate a barrier of only 2.5 kcal/mol for an external CMD where a C-H bond geminal to an agostic C-H bond is deprotonated, and this is clearly favoured by 11.4 kcal/mol over an intramolecular AMLA/CMD process. The C-H activation is exergonic (ΔG = -22.1 kcal/mol) consistent with the absence of any H/D exchange experimentally. This large exergonicity is relatively unusual for the C-H activation step at Group 9 centers and it would be of interest to confirm this result when the effects of solvent and

a larger basis set are included. The analogous process at [Rh(OAc)(**8mq**)Cp*]OAc was discussed in Section 6.3).[220]

8. Group 8

Compared to the extensive work on Groups 9 and 10 species relatively few computational studies on carboxylate-assisted C-H activation at Group 8 systems have been published. Moreover, those that are available are almost exclusively concerned with Ru, and we are only aware of one study on Os and none on Fe. The following discussion of Group 8 systems is therefore split into two sections, the first on intramolecular carboxylate-assisted C-H activation and the second on intermolecular carboxylate-assisted C-H activation.

8.1 Intramolecular C-H Activation

Roithova has reported a combined ESI-MS and DFT study analysing the products of the reaction of 2-phenylpyridine (**ppy**) with $[RuCl_2(\eta\text{-}C_6H_6)]_2$ in MeCN in the presence of HOAc and NEt_3.[71] A parent ion at *m*/*z* 394 is assigned to $[Ru(\kappa^2\text{-}OAc)(\mathbf{ppy})(\eta\text{-}C_6H_6)]^+$ on the basis of a comparison of observed and computed infrared spectra. Collision-induced dissociation (CID) of HOAc occurs with an energy of 27.0 ± 0.7 kcal/mol, indicating facile C-H activation in the CID experiment. A parent ion at *m*/*z* 394 was also seen with 3-phenylpyridine; in this case CID was dominated by loss of the 3-phenylpyridine moiety although evidence for some HOAc loss (hence C-H activation) was also seen, albeit with a much higher energy of 40.9 ± 0.7 kcal/mol. B3LYP(D2) calculations characterise a $[Ru(\kappa^1\text{-}OAc)(\mathbf{ppy})(\eta\text{-}C_6H_6)]^+$ intermediate at +14.3 kcal/mol which undergoes AMLA/CMD C-H activation with a minimal further barrier of 1.0 kcal/mol. The overall C-H activation process is endothermic (ΔH = +3.3 kcal/mol). B3LYP(D2) gives a computed HOAc dissociation enthalpy from $[Ru(\kappa^2\text{-}OAc)(\mathbf{ppy})(\eta\text{-}C_6H_6)]^+$ of 33.9 kcal/mol, hence somewhat overestimated compared to experiment.

As described in Section 6.1.2 Davies and Macgregor have modeled the oxidative coupling of 5-methyl-3-phenylpyrazole, **137**, with 4-octyne at both $[Ru(OAc)_2(p\text{-cymene})]$ and $[Rh(OAc)_2Cp^*]$ (see

Figure 82).[196] For the Ru system the key details are a computed $\Delta G^{\ddagger}_{span}$ of 25.4 kcal/mol which encompasses both *N*-deprotonation and a one-step rate-limiting AMLA/CMD C-H activation. The low experimental k_H/k_D KIE of 1.1 ± 0.2 was reproduced computationally (1.2) and could be reconciled by the very early geometry of the transition state: this equated to the κ^2-κ^1 displacement of OAc and so exhibits minimal C-H bond elongation. This study emphasized the importance of treating dispersion effects and this was also highlighted by Chen in a benchmarking study based on C-H bond cleavage in a [Ru(κ^1-O_2CH)(κ^1-O_2CPh)(η-C_6H_6)] model system. B3LYP-D3 and ωB97X-D gave the overall best performance against the results of high level CCSD(T)-F12 calculations.[175]

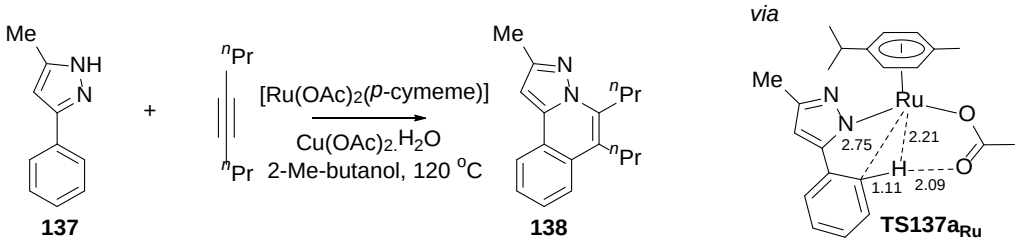

137 **138** **TS137a$_{Ru}$**

Figure 82. Ru-catalysed oxidative coupling of 3-phenylpyrazole, **137**, and 4-octyne to form a pyrazoloisoquinoline, **138**; the rate-determining transition state is shown with key distances in Å. Adapted with permission from Ref. 196. Copyright 2014 American Chemical Society.

The range of species that have been shown computationally to participate as internal bases in the AMLA/CMD process has been extended by Ackermann who reported an M06L(toluene) study on the cyclometalation of **ppy** at a model [Ru(Cl)(PMe_2=O)(**ppy**)(η-C_6H_6)] species.[244] This is the first step in a catalytic arylation process and involves initial chloride dissociation to form an ion pair with a vacant site for C-H activation. This then proceeds with assistance by the dimethylphosphinite oxygen, passing through a 5-membered AMLA-5/CMD transition state **TS192**. The overall barrier is 24.7 kcal/mol and the cyclometalated product, which features a *P*-bound dimethylphosphinous acid ligand is exergonic by 4.8 kcal/mol. As part of their survey of the factors promoting the activation of *N*,*N*-bidentate directing groups (see Section 4.1), Huang, Wang and Chen included the C(sp^2)-H bond activation reactions of *N*-(quinolin-8-yl)benzamide (**31**) and *N*-(pyridin-2-ylmethyl)-benzamide (**32**) at

a model $[Ru(OAc)_2(PH_3)_3]$ species.[92] A related study considered C(sp^3)-H activation[93] with similar trends to those computed with $[Ni(OAc)_2]$ and $[Pd(OAc)_2]$ being seen in both cases.

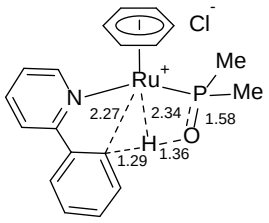

TS192
(distances in Å)

M06(MeOH) calculations were used by Lledós and Urriolabeitia to model the oxidative coupling of 2-butyne with benzylamines, **193**, at $[Ru(OAc)_2(p\text{-cymene})]_2$ (Figure 83).[245] Starting from $[Ru(OAc)_2(p\text{-cymene})]$ OAc/amine substitution initially forms a contact ion-pair, **Int193a**, in which the displaced acetate H-bonds to the amine. From here external CMD via **TS193** at 24.6 kcal/mol was computed to be 2.3 kcal/mol more accessible than an alternative intramolecular AMLA/CMD process. Displacement of OAc by 2-butyne gives **Int193c**, which undergoes insertion to give a 7-membered ruthenacycle that can rebind OAc to give the saturated intermediate **Int193d**. The most accessible pathway for C-N bond formation necessitates both loss of OAc and *N*-decoordination such that the liberated amine can act as a nucleophile at the bound Ru-alkenyl. OAc remains H-bonded to the amine during this process, which has an overall barrier (relative to **Int193d**) of 28.8 kcal/moland leads to a protonated 1,2-dihydroisoquinoline bound to a Ru(0) metal centre (**Int193e**). Oxidation of both these components completes the cycle and releases the isoquinoline product (although these steps were not modelled). Overall, no unique rate-determining process could be defined, the Gibbs energy barrier to C-H activation (25-27 kcal/mol) being only slightly lower than those for insertion and C-N bond formation (each *ca*. 29 kcal/mol). Experimentally, the reaction required heating to *ca.* 100 ^{o}C. Related profiles were also computed for 1-naphthylmethyl, 2-methylallylamine and 2-thiophenemethylamine. Zhang and Rao have also compared the alternative intramolecular

AMLA/CMD C-H activations of *N*-methyl-*N*-phenylbenzamide, **21**, at a [Ru(TFA)(κ-*O*-**21**)(*p*-cymene)]$^+$ intermediate (see Section 4.1) with M06(HOAc)//B3LYP calculations.[79]

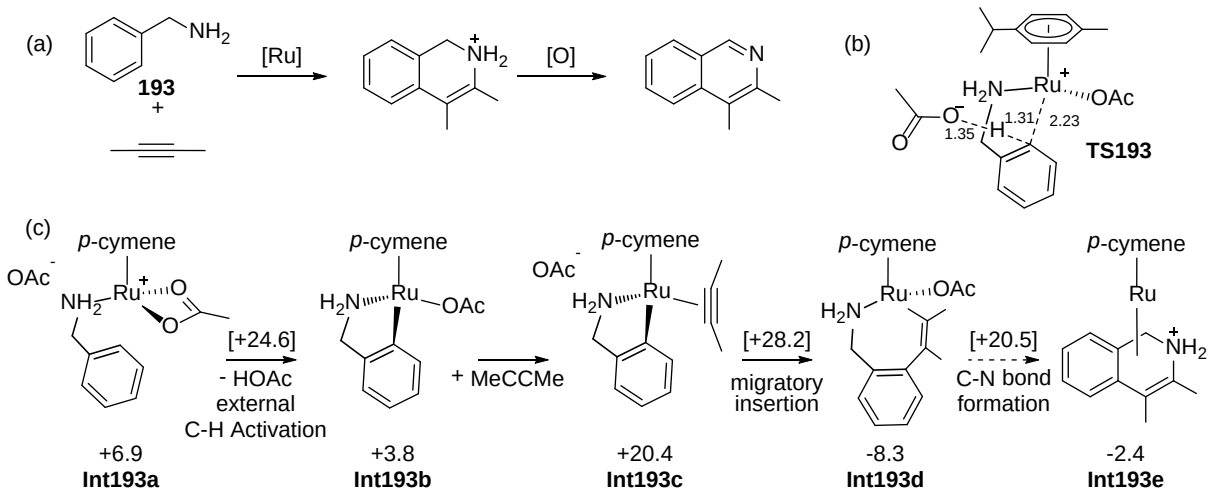

Figure 83. (a) Ru-catalysed oxidative coupling of 2-butyne with benzylamine, **193**, to form 3,4-dimethylisoquinoline; (b) transition state for C-H activation *via* an external CMD with key distances in Å; (c) Selected stationary points with free energies in (kcal/mol) quoted relative to the reactants at 0.0 kcal/mol.[245] Adapted with permission from Ref. 43. Copyright 2016, John Wiley and Sons.

The coupling of 1-phenyl-2-naphthol, **194**, with PhCCMe has been modelled by Huang using B3LYP(D3, 1,4-dioxane) calculations (see Figure 84).[170] Initial *O*-deprotonation proceeds with an overall barrier of 18.6 kcal/mol and is approximately thermoneutral (ΔG = +0.4 kcal/mol), although the loss of HOAc (modelled via reaction with 'K_2CO_3' to form 'KOAc' and '$KHCO_3$') drives this forward thermodynamically (ΔG = - 18.7 kcal/mol). A one-step AMLA/CMD C-H activation of a phenyl *ortho*-C-H bond then has a barrier of 23.9 kcal/mol and is initially rather endergonic (ΔG = +18.2 kcal/mol). However, loss of HOAc via reaction with 'K_2CO_3' is again considered to drive this through to give in this case the 16e cyclometallated intermediate, **Int194a**, at -19.7 kcal/mol. Alkyne insertion into the Ru-C bond produces a 8-membered ruthenaacycle **Int194b** in which the Ph substituent is adjacent to Ru; the transition state for the alternative regioselectivity is 5.4 kcal/mol higher in energy. Both direct C^1-C^3 bond formation ($\Delta G^‡$ = 39.3 kcal/mol) and C-O reductive coupling ($\Delta G^‡$ = 55.7 kcal/mol)

are disfavored from **Int194b**. Instead, rearrangement to a metallacyclopropene intermediate **Int194c** ($\Delta G^{\ddagger}$ = 17.0 kcal/mol) provides a low energy route to the spiroannulated product that is bound to Ru in **Int194d**. The initial C-H activation is rate-limiting ($\Delta G^{\ddagger}_{span}$ = 23.9 kcal/mol) and the degree of C-H elongation in this structure (C···H = 1.35 A) suggests it would be consistent with the significant k_H/k_D KIE observed experimentally.

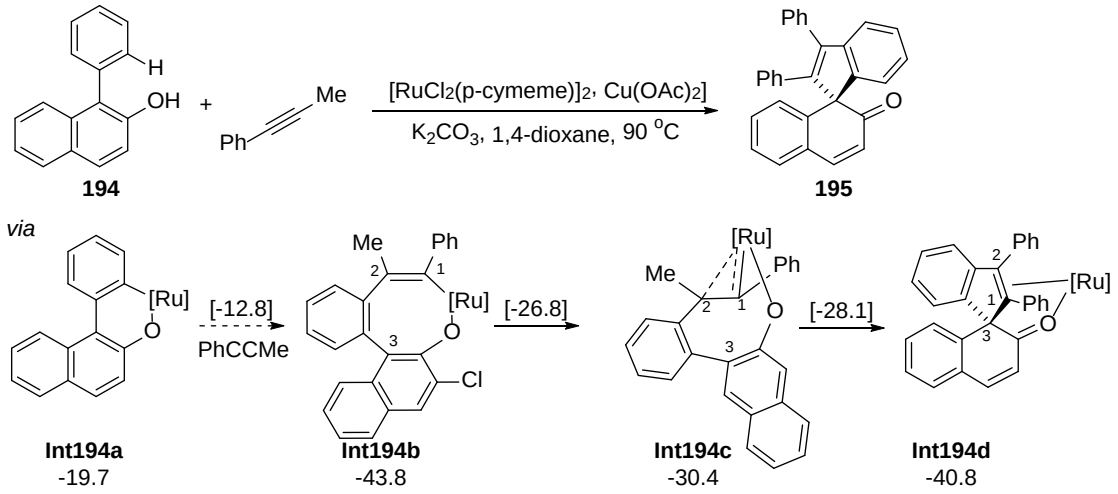

Figure 84. Ru(II)-catalysed spiroannulation of 1-phenyl-2-naphthol, **194**, with PhCCMe; [Ru] = Ru(*p*-cymene) giving **195**. Selected stationary points are indicated with free energies (kcal/mol) quoted relative to the reactants at 0.0 kcal/mol. Adapted with permission from Ref. 170. Copyright 2016 John Wiley and Sons.

Yu and Wang have studied the mechanism of the formal dehydrative [4 + 2] cycloaddition of enamides with alkynes to form substituted pyridines (see Figure 85(a)).[246] Using M06(toluene)//B3LYP calculations, adducts of the form [Ru(κ^1-OAc)$_2$(**196**)(η^6-C_6H_6)] were located in which **196** (with R^1 = H and R^2 = R^3 = Me, Figure 85(b)) is bound either through the carbonyl oxygen (set to 0.0 kcal/mol) or the C=C double bond (at +1.0 kcal/mol). A non-directed CMD activation of the alkenyl C-H bond proceeds from the latter with an overall barrier of 18.2 kcal/mol to give, after HOAc loss, a 6-membered ruthenacycle **Int196a**, at +3.8 kcal/mol. Decoordination of the carbonyl moiety permits MeCCPh to bind and the subsequent insertion generates **Int196b** at -8.2 kcal/mol.

The transition state with Ph adjacent to Ru is 4.4 kcal/mol below that for insertion with Me beside Ru. Rearrangement of **Int196b** allows insertion of the carbonyl group into the Ru-C(Ph) bond to give **Int196c**. These steps correspond to an energetic span of 29.1 kcal/mol. Protonolysis then releases **Int196d** that undergoes off-metal dehydration to give the pyridine product **197**.

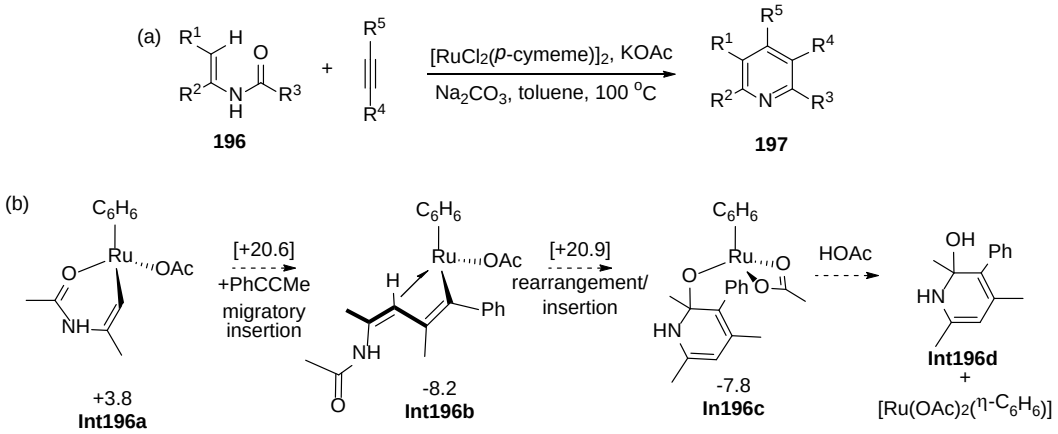

Figure 85. (a) Ru(II)-catalysed dehydrative [4 + 2] cycloaddition of enamides, **196**, with alkynes to form substituted pyridines; (b) selected stationary points with free energies in kcal/mol quoted relative to [Ru(OAc)$_2$(κ-*O*-**196**)(η-C$_6$H$_6$)] (with R^1 = H and R^2 = R^3 = Me) set to 0.0 kcal/mol. Adapted with permission from Ref. 246. Copyright 2015 American Chemical Society.

McMullin, Williams and Frost have used BP86(2-Me-THF, D3BJ) calculations to study the [RuCl$_2$(*p*-cymene)]$_2$-catalysed alkenylation reaction of 3-phenyl-2-oxazolidinone, **198**, with methyl acrylate, with free energies reported at 120 °C and corrected for concentration effects (see Figure 86).[247] Starting from a cationic carbonyl-bound [Ru(κ^2-OAc)(κ-*O*-**198**)(*p*-cymene)]$^+$ adduct at 0.0 kcal/mol, the lowest energy pathway involves a two-step AMLA/CMD C-H activation ($\Delta G^{\ddagger}$ = 13.4 kcal/mol, ΔG = +4.0 kcal/mol) with the κ^2- κ^1-OAc displacement transition state lying 1.4 kcal/mol above that for C-H bond cleavage. HOAc/methyl acrylate substitution accesses a 2,1-insertion with a barrier of 13.5 kcal/mol and gives an 8-membered ruthenacycle **Int198a** at -4.7 kcal/mol. Barriers for the alternative 1,2-insertions are ca. 5 kcal/mol higher. β-H transfer then proceeds via initial rearrangement to a β-agostic intermediate **Int198b** from which β-H transfer occurs with a minimal

barrier to form **Int198c** at +2.1 kcal/mol in which the trans-alkenylation product, **199**, is bound to the Ru center. The energetic span therefore corresponds to the formation of the agostic intermediate prior to the β-H transfer with $\Delta G^{\ddagger}_{span}$ = 15.3 kcal/mol and this step has a negligible computed k_H/k_D KIE. Experimentally a KIE of around 2 is observed, however, and the factors that may impact this are discussed.

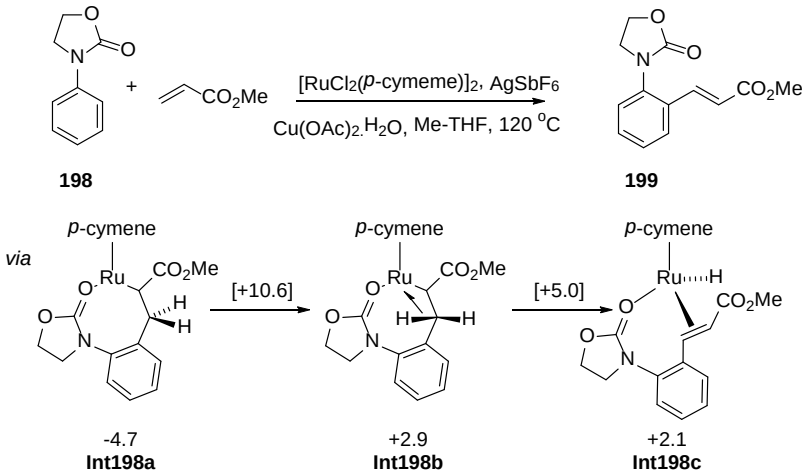

Figure 86. Ru(II)-catalysed alkenylation of 3-phenyl-2-oxazolidinone, **198**, with methyl acrylate along with selected stationary points (free energies in kcal/mol quoted relative to the [Ru(κ^2-OAc)(κ-*O*-**198**)(*p*-cymene)]$^+$ at 0.0 kcal/mol). Adapted with permission from Ref. 247. Copyright 2016 American Chemical Society.

Prabhu has studied the *ortho*-C-H functionalisation of acetophenone, **200**, with *N*-substituted maleimides, **201** (see Figure 87(a)).[248] Using an M06(DCE)//B3LYP protocol with optimisation (with R = Me) including the effects of DCE solvent, an initial [Ru(κ^1-OAc)$_2$(κ-*O*-**200**)(η-C$_6$H$_6$)] adduct **Int200a** is located at 4.0 kcal/mol above the separated reactants (see Figure 87(b)). From here an AMLA/CMD C-H activation is characterised with unusually, both OAc ligands remaining bound to the metal center, rather than dissociation of one OAc ligand to form a cationic intermediate. Instead an η^6-η^2 slippage of the benzene ligand occurs during the C-H activation (see **TS200**) to permit the new Ru-C bond to form. This process has a modest overall barrier of 17.4 kcal/mol and entails HOAc dissociation to give **Int200b** at +0.9 kcal/mol in which the benzene has reverted to an η^6-binding

mode. Insertion of *N*-methylmaleimide into the Ru-aryl bond (again with η^6-η^2 benzene slippage) then forms **Int200c** at -20.5 kcal/mol. The rigid bicyclic structure of this species does not permit β-H transfer and so an alkenylation product is not formed. Instead protonolysis by HOAc is accessible ($\Delta G^{\ddagger}$ = 21.5 kcal/mol, ΔG = -9.3 kcal/mol) and gives **Int200d**, which upon release of **202** regenerates the $[Ru(OAc)_2(\eta\text{-}C_6H_6)]$ active species.

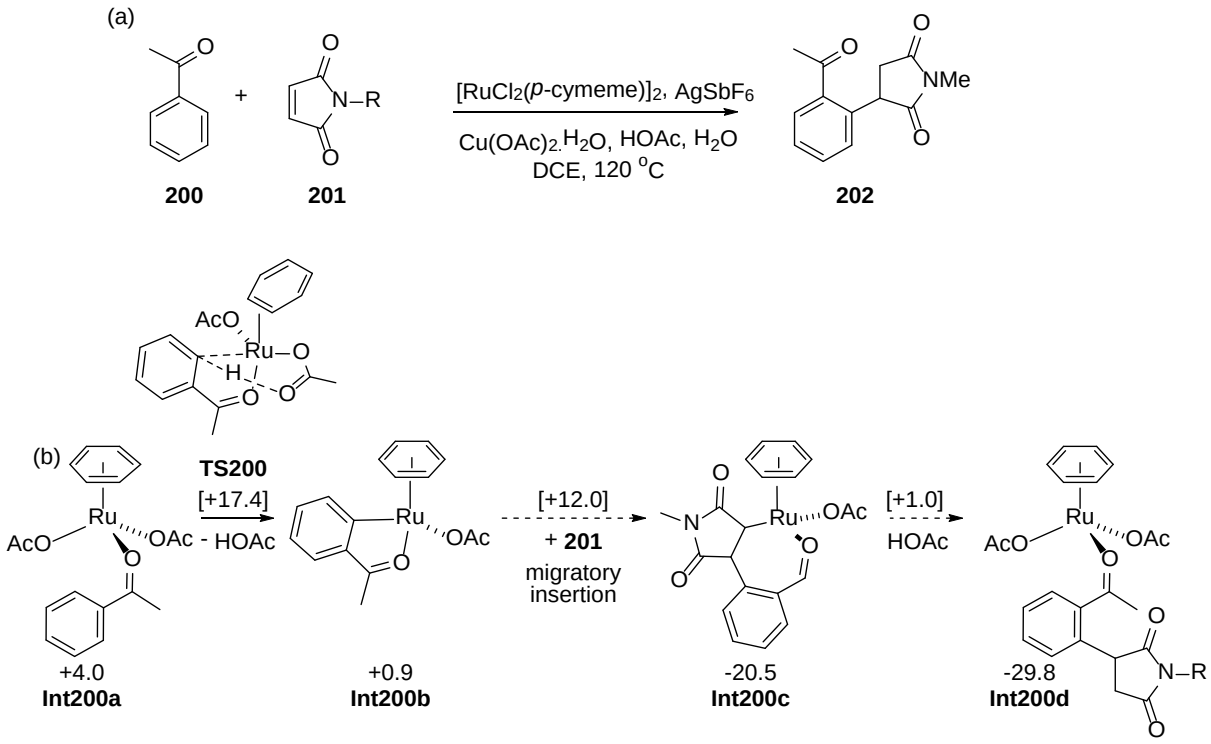

Figure 87. (a) Ru(II)-catalysed *ortho*-C-H functionalisation of acetophenone, **200**, with *N*-substituted maleimides, **201**; (b) selected stationary points (kcal/mol, relative to $[Ru(OAc)_2(\eta\text{-}C_6H_6)]$ and the free reactants set to 0.0 kcal/mol). Adapted with permission from Ref. 248. Copyright 2016 American Chemical Society.

The direct arylation of a bidentate 8-aminoquinoline substrate, **203**, has been modelled by Lan using M11-L(toluene)//B3LYP calculations (see Figure 88).[249] The reaction is postulated to proceed via displacement of the *p*-cymene ligand by **203** followed by *N*-deprotonation. A carbonate-assisted AMLA/CMD C-H activation ($\Delta G^{\ddagger}$ = 20.6 kcal/mol, ΔG = -1.5 kcal/mol) then produces **Int203** from

which oxidative addition of PhBr proceeds with $\Delta G^{\ddagger}_{span}$ = 34.2 kcal/mol. This energetic span is made up of HCO_3^-/PhBr exchange (ΔG = +28.1 kcal/mol) followed by a relatively facile Ph-Br activation step ($\Delta G^{\ddagger}$ = 6.1 kcal/mol). The high endergonicity of HCO_3^- loss may reflect the low polarity of the toluene solvent. Facile C-C reductive coupling and protonolysis with an incoming substrate molecule releases the product **204**. The alternative sequence (i.e. initial PhBr oxidative addition followed by introduction of **203**) was computed to have a significantly higher barrier.

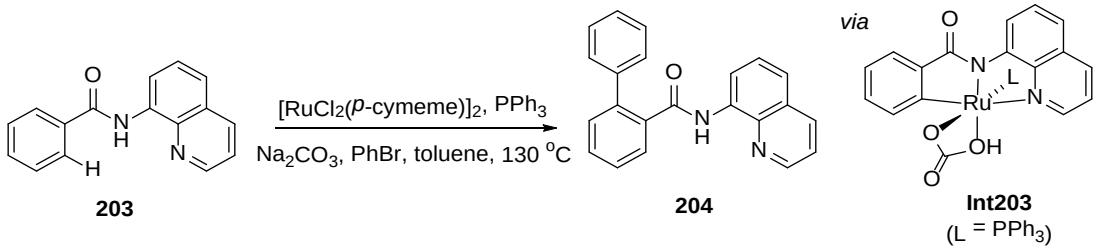

Figure 88. Ru(II)-catalysed direct arylation of **203** with PhBr. Adapted with permission from Ref. 249. Copyright 2016 American Chemical Society.

Houk and Grubbs have carried out detailed studies on the cyclometallation reactions of 2nd generation Grubbs' catalysts bearing bulky NHC ligands.[250] Starting from **205a**, C-H activation requires two Cl/OPiv substitutions to give **205b**, as well as displacement of the axial benzylidene oxygen to access **206** (Figure 89). M06(THF)//B3LYP calculations then show C-H activation proceeds via an AMLA/CMD mechanism to give **207**. The computed overall barrier (relative to **205b**) and k_H/k_D KIE (23.5 kcal/mol and 6.5 respectively) are in good agreement with experimental values (22.2 ± 0.1 kcal/mol and 8.1 ± 1.7). Alternative C-H activation mechanisms at a mixed OPiv/Cl complex, involving an equatorial OPiv, or with OPiv acting as an external base all proved less accessible. The presence of two OPiv ligands is important as one of these can act as a κ^2-spectator that stabilizes the Ru centre. The positioning of the active OPiv in an axial site also accounts for the diastereoselectivity of this C(sp^3)-H bond activation. In comparison, C(sp^3)-H activation of the mesityl substituent is less accessible ($\Delta G^{\ddagger}$ = 27.7 kcal/mol) as the required rotation around the N-Mes bond is hindered by the NHC backbone. C(sp^3)-H activation of an *N*-^{t}Bu substituent is, on the other hand, predicted to be

accessible ($\Delta G^{\ddagger}$ = 15.2 kcal/mol). Further calculations on analogues of **205b** with X = OAc, $PhCO_2^-$ showed the overall barrier to C-H activation to increase as the basicity of the carboxylate is reduced.

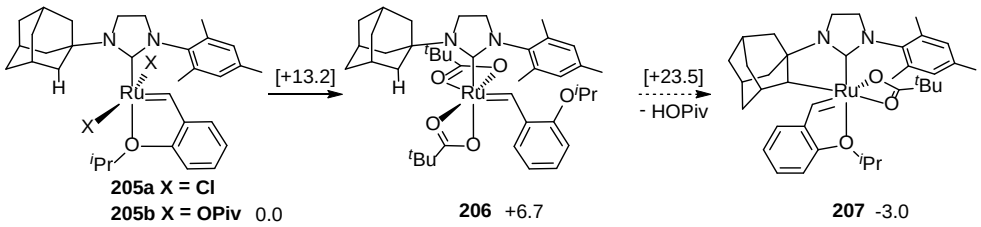

Figure 89. C(sp^3)-H activation in a Grubbs' catalyst with computed free energies in kcal/mol.[250] Adapted with permission from Ref.44. Copyright 2016 Springer International Publishing.

These cyclometalated systems proved to be highly effective as *Z*-selective alkene metathesis catalysts and this prompted a systematic study of the formation of a range of analogous cyclometallated species at the equivalent *bis*-OPiv Ru fragments **205$_L$** (see Figure 90).[251] Moving from methylene C-H activation in the 1-adamantyl system (**205$_A$**, $\Delta G^{\ddagger}$ = 23.5 kcal/mol) to the more hindered methine C-H bond in the 2-adamantyl analogues **205$_B$** (with Ar= Mes or DIPP) resulted in increased barriers of ca. 28 kcal/mol. For the norbornyl substituent in **205$_C$**, *endo*-C-H activation to form a 5-membered ruthenacycle ($\Delta G^{\ddagger}$ = 22.5 kcal/mol) is favored over the formation of a 6-membered species via C-H activation at the methyl substituent ($\Delta G^{\ddagger}$ = 27.7 kcal/mol) or the remote *exo*-C-H bond ($\Delta G^{\ddagger}$ = 32.0 kcal/mol). In contrast, formation of a 4-membered product is accessible with the acyclic diaminocarbene ligand in **205$_D$** as the more open architecture of this ligand allows for deformation in the C-H activation process. C-H activation of ligand **205$_E$** is inaccessible, however, and this is proposed to be due to both the formation of a 6-membered ruthenacycle and a stabilisation in the ground state due to a lack of steric encumbrance around the sulfur centre. The origin of the *Z*-selectivity was also considered although this is beyond the scope of this review.[252]

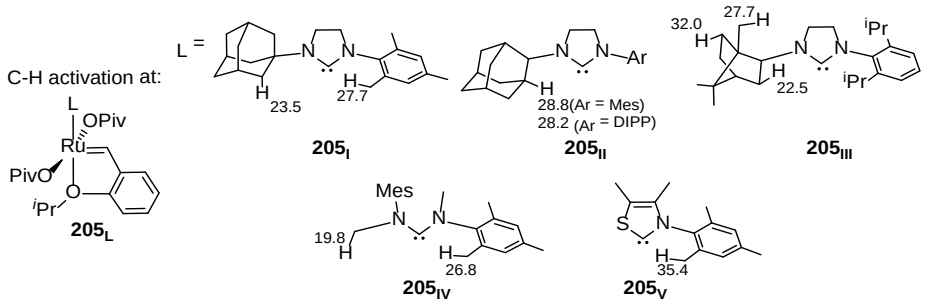

Figure 90. Different NHC ligands used in the study of intramolecular C(sp^3)-H activation at species **205_L**; overall barriers are reported in kcal/mol at the varuious sites indicated. Adapted with permission from Ref. 251. Copyright 2015 American Chemical Society.

8.2 Intermolecular C-H Activation

Hölscher and Leitner have used calculations in the design of catalysts for benzene carboxylation based on Ru(PCNCP)($O_2CPh)_2$ complexes, where PCNCP is a tridentate pincer ligand (see Figure 91).[253] Surprisingly, this was found experimentally to prefer a *fac*-coordination mode over the targeted *mer*-geometry and this was confirmed with M06L(benzene) calculations that found the *fac*-isomer to be 6.1 kcal/mol more stable. The computed reaction profiles then illustrate the importance of both the carboxylate κ^2-κ^1-displacement and the C-H cleavage steps in contributing to the overall barrier to C-H activation. For the *fac*-isomer κ^2-κ^1-displacement is relatively easy ($\Delta G^{\ddagger}$ = 19.6 kcal/mol) as the Ru-O bond is labilized by being opposite the relatively high trans influence phosphine. By the same token C-H cleavage step is then difficult ($\Delta G^{\ddagger}$ = 22.8 kcal/mol) as the new Ru-Ph bond must now develop trans to the phosphine. For the *mer*-isomer κ^2-κ^1-displacement with Ru-O dissociation trans to pyridine is now much harder ($\Delta G^{\ddagger}$ = 25.5 kcal/mol) but the subsequent C-H bond cleavage is easier ($\Delta G^{\ddagger}$ = 13.5 kcal/mol). After loss of benzoic acid, CO_2 insertion via transition states at 26.7 kcal/mol (*fac*) and 29.6 kcal/mol (*mer*) complete the cycle. Overall for the *fac*-isomer the C-H cleavage step is therefore rate-limiting ($\Delta G^{\ddagger}_{span}$ = 38.7 kcal/mol) while for the mer-isomer this is the κ^2-κ^1-displacement step ($\Delta G^{\ddagger}_{span}$ = 25.5 kcal/mol, where this is relative to the *mer*-isomer at +6.1 kcal/mol). Moving to PONOP analogues (i.e. swapping the CH_2 linkers with O)

makes the *mer*-isomer 0.1 kcal/mol more stable than the *fac* due to the ability of the O linker to participate in conjugation with the central pyridine ring. Free energy spans of 31.9 kcal/mol and 26.3 kcal/mol are computed for the *fac*- and *mer*-isomers respectively. Earlier B97-D calculations on the *mer*-isomers indicated barriers were also affected by the phosphine substituents (R = 1-pyrrolidinyl < Ph < ^{t}Bu) and could also be reduced by introducing electron withdrawing substituents *para* to the pyridyl nitrogen of the tridentate ligand.[254]

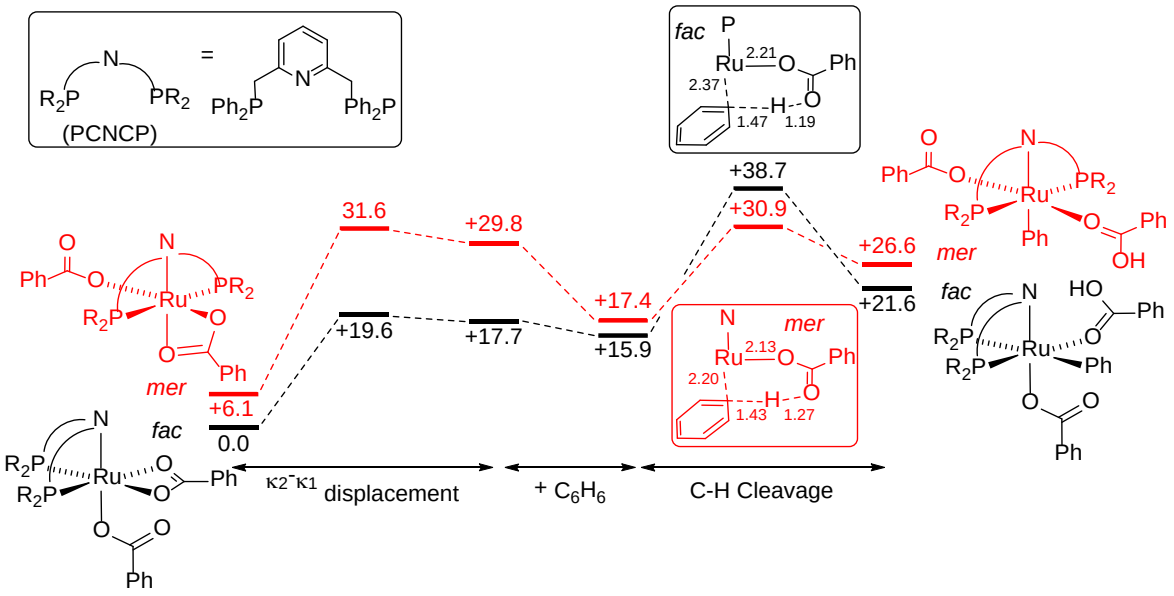

Figure 91. Computed reaction profiles (kcal/mol) for C-H activation of benzene at *fac*- and *mer*-Ru(PCNCP)(O_2CPh)$_2$ complexes; details of the computed C-H activation transition states are provided with selected distances in Å. Adapted with permission from Ref. 253. Copyright 2014, The Royal Society of Chemistry.

The carboxylate-assisted activation of the C(sp)-H bond in phenylacetylene has been modelled by Lynam and Slattery as a key step in the alkyne/vinylidene isomerisation at [Ru(OAc)$_2$(PPh$_3$)$_2$].[255] PBE0//BP86 calculations characterise the formation of an initial π-bound adduct, *trans*-[Ru(κ^1-OAc)(κ^2-OAc)(HCCPh)(PPh$_3$)$_2$] from which an alternate C-H σ-complex lies only 1 kcal/mol higher in

energy. Facile AMLA/CMD C-H activation then proceeds via **TS206** to form *trans*-[Ru(κ^2-OAc)(CCPh)(HOAc)(PPh_3)$_2$] ($\Delta G^{\ddagger}$ = 1.2 kcal/mol; ΔG = -8.4 kcal/mol). The HOAc thus formed can then deliver a proton to the β-carbon of the acetylide to form a vinylidene ligand in an overall process that the authors term a 'ligand-assisted proton shuttle' (LAPS).

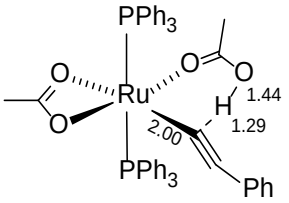

TS206

One example of AMLA/CMD C-H activation at osmium has been reported, in Nielsen and Periana's study of catalytic H/D exchange of benzene at complexes bearing neutral tridentate PyBox ligands, L.[256] Using M06(HOAc)//B3LYP calculations a chloro-bridged dimer, [Os(μ-Cl)(OAc)L]$_2$ was proposed as the resting state in acetic acid and this first breaks up into [OsCl(κ^2-OAc)L] monomers (ΔG = +5.6 kcal/mol). κ^2-κ^1-displacement of OAc by benzene costs a further 19.2 kcal/mol before AMLA/CMD C-H activation proceeds through a 6-membered transition state at +32.0 kcal/mol to form [OsCl(HOAc)(Ph)L] at +18.4 kcal/mol.

9. Discussion

Over the period of this review (late-2009 to mid-2016) the body of computational work on carboxylate-assisted C-H activation at Group 8-10 metal centers has reinforced the AMLA/CMD concepts that were developed at the end of the last decade. In this view a Lewis acidic metal center and an intramolecular basic ligand combine to facilitate C-H bond cleavage via C-H deprotonation. More recently variations of this pattern have been proposed: in particular, an external base may also perform the deprotonation ('external CMD') or a protic solvent molecule may act as a base before relaying a proton to a remote, terminal carboxylate. Both electron-rich and electron-deficient aromatic substrates can react via an AMLA/CMD pathway and the carboxylate-assisted activation of

C(sp^3)-H bonds is readily accommodated within this framework. The AMLA/CMD concept also extends to other chelating bases that can play the role of the intramolecular base. It is even operative in main group systems: for example $Tl(OTf)_3$ activates simple alkanes via this mechanism.[257,258] To date, when a carboxylate (or related base) has been shown to facilitate an AMLA/CMD C-H activation there has been no clear computational evidence to implicate a Wheland intermediate. The traditional S_EAr mechanism therefore appears not to be involved in these carboxylate-assisted C-H bond activations.

Carboxylate-assisted C-H activation generally entails two processes: first the creation of a vacant site at which a new M-C bond can form, and then the cleavage of the C-H bond. The commonly used metal precursors are saturated complexes such as 16e $[Pd(OAc)_2]$ or 18e $[M(OAc)_2Cp^*]$ (M = Rh, Ir) or $[Ru(OAc)_2(arene)]$ all of which feature κ^2-OAc ligands. The energetics of the κ^2-κ^1 displacement of OAc or the dissociation of an OAc anion can therefore contribute significantly to the overall barrier for C-H activation. With substrates featuring a protic directing group the reaction is often initiated with a proton transfer onto a bound OAc ligand to form HOAc. This can then more readily dissociate from the metal center and thus facilitate the overall C-H activation process. This strategy contributes to the efficacy of the commonly used bidentate directing groups such as 2-amidoquinoline, as well as MPAA co-ligands. With non-protic directing groups OAc/substrate exchange is normally required resulting in the formation of cationic organometallic intermediates and a dissociated OAc anion. Polar solvents may therefore facilitate this process and, computationally, modelling the energetics of anion dissociation requires care, as this has been shown to be highly basis set dependent. Within the context of catalysis these OAc protonation and exchange steps are often central to the generation (and regeneration) of the active species and it is therefore important that these routine processes are fully taken into account in any computational model.

A clear trend in recent computational work is the modelling of full catalytic cycles that incorporate a carboxylate-assisted C-H activation. This also reflects experimental developments where catalytic C-

H functionalisation is increasingly exploited as a practical tool in organic synthesis. A significant proportion of the articles summarised here combine computational and experimental results and often include the full molecular structure of the catalyst and substrates used experimentally in the computational model. The large size of these models makes a treatment of dispersion effects mandatory for the computation of reasonable energetics. The advent of dispersion-corrected DFT has highlighted the initially counterintuitive observation that the introduction of bulky substituents can be a stabilising factor.[259] Apparently simple processes such as ligand dissociation or substitution reactions are therefore particularly sensitive to the methodology adopted and the energetics of these steps can have a significant effect on the overall shape of a reaction profile.

The use of large models, coupled to the routine treatment of implicit solvation, entropy and temperature effects have allowed computation to reflect more closely the conditions used in experiment. Among the most insightful studies are those that feature a two-way dialogue between computation and experiment, i.e. where computation is used not only to rationalise experimental observations but also where experimental data are used to test the validity of the computational methods and/or chemical models used in the calculations. Substrate H/D exchange is commonly used to provide insight into the C-H activation process. The observation of H/D exchange implies an endergonic carboxylate-assisted C-H activation to form (in the case of acetate) an HOAc adduct, followed by an efficient H/D exchange with solvent and deuteration of the M-C bond (i.e. the reverse of the initial C-H activation). However, other processes may intervene to trap out the initial HOAc adduct, for example substitution of HOAc by another species (ligand, solvent molecule or substrate) or deprotonation of HOAc to form a more stable OAc adduct. Indeed several studies have postulated that this is the role played by the stoichiometric bases, generally carbonate salts, that are present in experimental catalytic protocols.[124, 145, 170] If these alternative processes are efficient then H/D exchange may not be observed experimentally, even though the initial C-H activation process is endergonic. Intimate knowledge of these ligand exchange and deprotonation steps from

computation would therefore be extremely valuable, although these are challenging to calculate, not least because of the difficulty in modelling inorganic salts in organic solution (see below).

Another widely used experimental technique is the determination of k_H/k_D KIEs. Such data can be misinterpreted[260] and so insight from computation is particularly useful. In many cases the computed energy surfaces associated with carboxylate-assisted C-H activation are rather flat and may feature an agostic intermediate, in particular for intramolecular AMLA/CMD C-H activation. The two transition states around this intermediate equate to the κ^2- κ^1 displacement of OAc and the subsequent C-H bond cleavage. The former generally exhibits little C-H elongation and so if it is higher in energy then only a small (if any) k_H/k_D KIE would be anticipated. Thus the lack of a significant k_H/k_D KIE experimentally does not necessarily mean that the C-H activation process is not rate-limiting. As pointed out by Hartwig[260] the position of the C-H activation transition state relative to the overall rate-determining transition state is also important. The ability of computation to place the energetics of a C-H activation process into the context of an overall reaction profile is therefore invaluable. For example, AMLA/CMD transition states that contribute to a pre-equilibrium prior to the rate-limiting step may still contribute to a significant KIE if they exhibit significant C-H bond elongation.

Another strength of computational modelling lies in its ability to define the details of a catalytic cycle. Ideally, these multi-step processes can then be interpreted in terms of the energetic span model. However, computation often reveals the difficulties in identifying a single “rate determining step” within a catalytic cycle: several components within a cycle may have a similar energetic span and this can complicate the chemical interpretation; moreover the presence of multiple pre-equilibria that are subject to concentration effects exacerbates the situation. As a result it may be difficult to equate experimental observations such as a given selectivity or a k_H/k_D KIE to a single transition state or barrier. One recent development is to tackle these problems through the use of kinetic modelling. Here a kinetic model is constructed on the basis of the computed profile that also

supplies the necessary energies to provide an overall rate of reaction. This approach also allows concentration effects to be taken into account. Those studies that have applied kinetic modelling to processes featuring a carboxylate-assisted C-H activation show a lot of promise, and have highlighted the very subtle relationship between the computed energetics and the observed outcomes.[115,180] The availability of reliable computed energetics is therefore essential. One aspect of this, as discussed by several authors here,[157,125,87,254,256] is the well-known difficulty of using free energies computed in the gas-phase to interpret reactions that, experimentally, proceed in solution.

Two further important aspects of catalysis based on carboxylate-assisted C-H activation that are only now beginning to be tackled are the roles played by additives and oxidants. Both classes of species are often simple inorganic metal salts and the speciation of these salts in organic solvents needs some clarification. Experimental insight into this issue would be particularly valuable. To date some computational studies have adopted cluster models in which ions are solvated by a small number of explicit solvent molecules.[90] Alternatively M_2CO_3 or CsF additives are simply described in calculations as molecular ion-pairs. Such models may exaggerate the effect of these species as the ionic charges are not screened by the effects of an explicit solvent shell. The different solubility of inorganic salts in organic solvents may also affect reactivity and this concentration effect is difficult to capture computationally.

Generally, most studies assume that, if necessary, reoxidation of the metal catalyst can readily occur after the product release steps. However, in principle the required oxidation may occur at any point in the mechanism and this may be probed experimentally by checking whether products are formed in stoichiometric reactions in the absence of oxidant. Computationally, the modelling of metal salts as oxidants presents similar difficulties to those described above for additives and in this case both the oxidised and reduced forms must be modelled. Dioxygen is perhaps the best defined oxidant from a computational point of view and, experimentally, air would be an ideal oxidant. The extensive computational studies on the mode of action of internal oxidants in Rh catalysis have highlighted the

importance of understanding the exact nature of the oxidant (e.g. *N*-OMe versus *N*-O_2CR) and how the timing of the oxidation within the cycle can control the outcome of the process. This body of work also showcases the power of computational chemistry to provide insight into complex catalytic processes.

10. Conclusions and Outlook

Computational studies have played a central role in developing the fundamental understanding of carboxylate-assisted C-H activation and, more recently, showing how this process contributes to practical catalytic cycles for C-H functionalisation. This field has matured to the extent that it now provides a practical tool in organic synthesis for the production of fine chemicals and can sit beside more traditional strategies based on cross-coupling reactions. However, many opportunities still exist: the goal of completely replacing the atom inefficient cross-coupling strategies is not yet realised, while practical schemes for the catalytic upgrading of simple hydrocarbons to more valuable fuels or feedstocks are also not yet in hand. Future computational studies will surely play a role in defining likely catalysts and conditions to achieve these important goals. Recently there has been a drive to use more widely available 1st row transition metals as catalysts. Such systems can access a range of different spin-states, the computational assessment of which is challenging due to the functional sensitivity of spin-state energetics.

As well as supporting experimental developments, computational chemistry itself remains a developing field. Much of the work in this review represents the state of the art, however challenges remain. Chief amongst these are the computation of accurate energetics that can feed into the quantitative understanding - and ultimately the prediction - of reactivity. This implies the accurate modelling of free energies and the use of more sophisticated chemical models that better reflect the complex reaction conditions that are used experimentally. Progress in these areas may ultimately rely on molecular dynamics techniques and real advances have already been made in applying these methods to organometallic chemistry and homogeneous catalysis.[261,262] Nevertheless such methods

require significant computational resources and do not yet represent a practical tool for widespread use.

Whether developing these new methodologies or pursuing state of the art static calculations, a close dialogue between experiment and computation remains vital. Improved mechanistic insight demands input from experiment in the form of quantitative experimental data. This may take the form of kinetic data on the overall process (orders of reaction and activation parameters), but also the quantification of the thermodynamics associated with key equilibria that are often challenging to compute. The isolation of intermediates and the characterisation of individual steps would also be ideal for the benchmarking of computational data and would provide a stringent test for computational chemists to assess their methodologies and chemical models. With this approach the role of computation in integrating carboxylate-assisted C-H activation into ever-more ambitious catalytic schemes and the role of experiment in enhancing developments in computation both have a vibrant future.

11. Acknowledgements. We thank the EPSRC for financial support through awards EP/J002712/1 and EP/J021911/1 (SAM) and EP/J002917/1 and EP/J021709/1 (DLD) and EUCOST Action CA15106 "C-H Activation in Organic Synthesis (CHAOS)".

12. References.

(1) Balcells, D.; Clot, E.; Eisenstein, O. C-H Bond Activation in Transition Metal Species from a Computational Perspective, *Chem. Rev.* **2010**, *110*, 749-823.

(2) Lapointe, D.; Fagnou, K. Overview of the Mechanistic Work on the Concerted Metallation-Deprotonation Pathway, *Chem. Lett.* **2010**, *39*, 1119-1126.

(3) Boutadla, Y.; Davies, D. L.; Macgregor, S. A.; Poblador-Bahamonde, A. I. Mechanisms of C-H Bond Activation: Rich Synergy between Computation and Experiment, *Dalton Trans.* **2009**, 5820-5831.

(4) Vastine, B. A.; Hall, M. B. The Molecular and Electronic Structure of Carbon-Hydrogen Bond Activation and Transition Metal Assisted Hydrogen Transfer, *Coord. Chem. Rev.* **2009**, *253*, 1202-1218.

(5) Pascual, S.; de Mendoza, P.; Braga, A. A. C.; Maseras, F.; Echavarren, A. M. Bidentate Phosphines as Ligands in the Palladium-Catalyzed Intramolecular Arylation: The Intermolecular Base-Assisted Proton Abstraction Mechanism, *Tetrahedron* **2008**, *64*, 6021-6029.

(6) Perutz, R. N.; Sabo-Etienne, S. The Sigma-Cam Mechanism: Sigma Complexes as the Basis of Sigma-Bond Metathesis at Late-Transition-Metal Centers, *Angew. Chem. Int. Ed.* **2007**, *46*, 2578-2592.

(7) Grimme, S.; Ehrlich, S.; Goerigk, L. Effect of the Damping Function in Dispersion Corrected Density Functional Theory, *J. Comput. Chem.* **2011**, *32*, 1456-1465.

(8) Grimme, S.; Antony, J.; Ehrlich, S.; Krieg, H. A Consistent and Accurate Ab Initio Parametrization of Density Functional Dispersion Correction (DFT-D) for the 94 Elements H-Pu, *J. Chem. Phys.* **2010**, *132*, 154104.

(9) Grimme, S. Semiempirical GGA-Type Density Functional Constructed with a Long-Range Dispersion Correction, *J. Comput. Chem.* **2006**, *27*, 1787-1799.

(10) Chai, J.-D.; Head-Gordon, M. Long-Range Corrected Hybrid Density Functionals with Damped Atom-Atom Dispersion Corrections, *Phys. Chem. Chem. Phys.* **2008**, *10*, 6615-6620.

(11) Zhao, Y.; Truhlar, D. The M06 Suite of Density Functionals for Main Group Thermochemistry, Thermochemical Kinetics, Noncovalent Interactions, Excited States, and Transition Elements: Two New Functionals and Systematic Testing of Four M06-Class Functionals and 12 Other Functionals, *Theor. Chem. Acc.* **2008**, *120*, 215-241.

(12) Jacobsen, H.; Cavallo, L. On the Accuracy of DFT Methods in Reproducing Ligand Substitution Energies for Transition Metal Complexes in Solution: The Role of Dispersive Interactions, *ChemPhysChem* **2012**, *13*, 562-569.

(13) Ahlquist, M. S. G.; Norrby, P.-O. Dispersion and Back-Donation Gives Tetracoordinate [Pd(PPh_3)$_4$], *Angew. Chem. Int. Ed.* **2011**, *50*, 11794-11797.

(14) McMullin, C. L.; Jover, J.; Harvey, J. N.; Fey, N. Accurate Modelling of Pd(0) + PhX Oxidative Addition Kinetics, *Dalton Trans.* **2010**, *39*, 10833-10836.

(15) Minenkov, Y.; Occhipinti, G.; Jensen, V. R. Metal–Phosphine Bond Strengths of the Transition Metals: A Challenge for DFT, *J. Phys. Chem. A* **2009**, *113*, 11833-11844.

(16) Sieffert, N.; Bühl, M. Noncovalent Interactions in a Transition-Metal Triphenylphosphine Complex: A Density Functional Case Study, *Inorg. Chem.* **2009**, *48*, 4622-4624.

(17) Zhao, Y.; Truhlar, D. G. Attractive Noncovalent Interactions in the Mechanism of Grubbs Second-Generation Ru Catalysts for Olefin Metathesis, *Org. Lett.* **2007**, *9*, 1967-1970.

(18) High-level wavefunction methods promise the accurate treatment of these long-range electron correlation effects, however, such methods are generally still too computationally demanding for routine use on large model systems. The situation is ongoing, however, with the emergence of efficient algorithms capable of capturing the accuracy of coupled-cluster theory at reasonable computational cost; see for example Ref. 19

(19) Sparta, M.; Riplinger, C.; Neese, F. Mechanism of Olefin Asymmetric Hydrogenation Catalyzed by Iridium Phosphino-Oxazoline: A Pair Natural Orbital Coupled Cluster Study, *J. Chem. Theor. Comput.* **2014**, *10*, 1099-1108.

(20) Gensch, T.; Hopkinson, M. N.; Glorius, F.; Wencel-Delord, J. Mild Metal-Catalyzed C-H Activation: Examples and Concepts, *Chem. Soc. Rev.* **2016**, *45*, 2900-2936.

(21) Hartwig, J. F. Evolution of C–H Bond Functionalization from Methane to Methodology, *J. Am. Chem. Soc.* **2016**, *138*, 2-24.

(22) Zhu, R.-Y.; Farmer, M. E.; Chen, Y.-Q.; Yu, J.-Q. A Simple and Versatile Amide Directing Group for C−H Functionalizations, *Angew. Chem. Int. Ed.* **2016**, *55*, 10578-10599.

(23) Liu, C.; Yuan, J.; Gao, M.; Tang, S.; Li, W.; Shi, R.; Lei, A. Oxidative Coupling between Two Hydrocarbons: An Update of Recent C–H Functionalizations, *Chem. Rev.* **2015**, *115*, 12138-12204.

(24) Song, G.; Li, X. Substrate Activation Strategies in Rhodium(III)-Catalyzed Selective Functionalization of Arenes, *Acc. Chem. Res.* **2015**, *48*, 1007-1020.

(25) Yang, L.; Huang, H. Transition-Metal-Catalyzed Direct Addition of Unactivated C–H Bonds to Polar Unsaturated Bonds, *Chem. Rev.* **2015**, *115*, 3468-3517.

(26) Zhang, F.; Spring, D. R. Arene C-H Functionalisation Using a Removable/Modifiable or a Traceless Directing Group Strategy, *Chem. Soc. Rev.* **2014**, *43*, 6906-6919.

(27) Kozhushkov, S. I.; Ackermann, L. Ruthenium-Catalyzed Direct Oxidative Alkenylation of Arenes through Twofold C-H Bond Functionalization, *Chem. Sci.* **2013**, *4*, 886-896.

(28) Arockiam, P. B.; Bruneau, C.; Dixneuf, P. H. Ruthenium(II)-Catalyzed C–H Bond Activation and Functionalization, *Chem. Rev.* **2012**, *112*, 5879-5918.

(29) Patureau, F. W.; Wencel-Delord, J.; Glorius, F. Cp*Rh-Catalyzed C–H Activations: Versatile Dehydrogenative Cross-Couplings of Csp^2 C–H Positions with Olefins, Alkynes, and Arenes, *Aldrichimica Acta* **2012**, *45*, 31-41.

(30) Song, G.; Wang, F.; Li, X. C-C, C-O and C-N Bond Formation Via Rhodium(III)-Catalyzed Oxidative C-H Activation, *Chem. Soc. Rev.* **2012**, *41*, 3651-3678.

(31) Ackermann, L. Carboxylate-Assisted Transition-Metal-Catalyzed C–H Bond Functionalizations: Mechanism and Scope, *Chem. Rev.* **2011**, *111*, 1315-1345.

(32) Cho, S. H.; Kim, J. Y.; Kwak, J.; Chang, S. Recent Advances in the Transition Metal-Catalyzed Twofold Oxidative C-H Bond Activation Strategy for C-C and C-N Bond Formation, *Chem. Soc. Rev.* **2011**, *40*, 5068-5083.

(33) Satoh, T.; Miura, M. Oxidative Coupling of Aromatic Substrates with Alkynes and Alkenes under Rhodium Catalysis, *Chem. – Eur. J.* **2010**, *16*, 11212-11222.

(34) Balcells, D.; Clot, E.; Eisenstein, O.; Nova, A.; Perrin, L. Deciphering Selectivity in Organic Reactions: A Multifaceted Problem, *Acc. Chem. Res.* **2016**, *49*, 1070-1078.

(35) Perrin, L.; Carr, K. J. T.; McKay, D.; McMullin, C. L.; Macgregor, S. A.; Eisenstein, O. Modelling and Rationalizing Organometallic Chemistry with Computation: Where Are We?, *Struct. Bond.* **2016**, *167*, 1-37.

(36) Sperger, T.; Sanhueza, I. A.; Schoenebeck, F. Computation and Experiment: A Powerful Combination to Understand and Predict Reactivities, *Acc. Chem. Res.* **2016**, *49*, 1311-1319.

(37) Cheng, G.-J.; Zhang, X.; Chung, L. W.; Xu, L.; Wu, Y.-D. Computational Organic Chemistry: Bridging Theory and Experiment in Establishing the Mechanisms of Chemical Reactions, *J. Am. Chem. Soc.* **2015**, *137*, 1706-1725.

(38) Jindal, G.; Kisan, H. K.; Sunoj, R. B. Mechanistic Insights on Cooperative Catalysis through Computational Quantum Chemical Methods, *ACS Catal.* **2015**, *5*, 480-503.

(39) Bonney, K. J.; Schoenebeck, F. Experiment and Computation: A Combined Approach to Study the Reactivity of Palladium Complexes in Oxidation States 0 to IV, *Chem. Soc. Rev.* **2014**, *43*, 6609-6638.

(40) Guan, W.; Sayyed, F. B.; Zeng, G.; Sakaki, S. σ-Bond Activation of Small Molecules and Reactions Catalyzed by Transition-Metal Complexes: Theoretical Understanding of Electronic Processes, *Inorg. Chem.* **2014**, *53*, 6444-6457.

(41) Lupp, D.; Christensen, N. J.; Fristrup, P. Synergy between Experimental and Theoretical Methods in the Exploration of Homogeneous Transition Metal Catalysis, *Dalton Trans.* **2014**, *43*, 11093-11105.

(42) Pahls, D. R.; Allen, K. E.; Goldberg, K. I.; Cundari, T. R. Understanding the Effect of Ancillary Ligands on Concerted Metalation–Deprotonation by (^{dm}Phebox)Ir(OAc)$_2$(H_2O) Complexes: A DFT Study, *Organometallics* **2014**, *33*, 6413-6419.

(43) Carr, K. J. T.; Macgregor, S. A.; McMullin, C. L. In *Transition Metal-Catalyzed Heterocycle Synthesis Via C–H Activation*; Wiley-VCH Verlag GmbH & Co. KGaA, 2016.

(44) Carr, K. J. T.; Macgregor, S. A.; McMullin, C. L. In *C-H Bond Activation and Catalytic Functionalization I*; Dixneuf, P. H., Doucet, H., Eds.; Springer International Publishing: Switzerland, 2016.

(45) Kozuch, S.; Shaik, S. How to Conceptualize Catalytic Cycles? The Energetic Span Model, *Acc. Chem. Res.* **2011**, *44*, 101-110.

(46) Biswas, B.; Sugimoto, M.; Sakaki, S. C-H Bond Activation of Benzene and Methane by M(η^2-$O_2CH)_2$ (M = Pd or Pt). A Theoretical Study, *Organometallics* **2000**, *19*, 3895-3908.

(47) Ziatdinov, V. R.; Oxgaard, J.; Mironov, O. A.; Young, K. J. H.; Goddard, W. A.; Periana, R. A. Carboxylic Solvents and O-Donor Ligand Effects on CH Activation by Pt(II), *J. Am. Chem. Soc.* **2006**, *128*, 7404-7405.

(48) Davies, D. L.; Donald, S. M. A.; Macgregor, S. A. Computational Study of the Mechanism of Cyclometalation by Palladium Acetate, *Journal of the American Chemical Society* **2005**, *127*, 13754-13755.

(49) Ryabov, A. D.; Sakodinskaya, I. K.; Yatsimirsky, A. K. Kinetics and Mechanism of Ortho-Palladation of Ring-Substituted *N,N*-Dimethylbenzylamines, *J.Chem. Soc. Dalton Trans.* **1985**, 2629-2638.

(50) Kragten, D. D.; van Santen, R. A.; Neurock, M.; Lerou, J. J. A Density Functional Study of the Acetoxylation of Ethylene to Vinyl Acetate Catalyzed by Palladium Acetate, *J. Phys. Chem. A* **1999**, *103*, 2756-2765.

(51) García-Cuadrado, D.; Braga, A. A. C.; Maseras, F.; Echavarren, A. M. Proton Abstraction Mechanism for the Palladium-Catalyzed Intramolecular Arylation, *J. Am. Chem. Soc.* **2006**, *128*, 1066-1067.

(52) García-Cuadrado, D.; de Mendoza, P.; Braga, A. A. C.; Maseras, F.; Echavarren, A. M. Proton-Abstraction Mechanism in the Palladium-Catalyzed Intramolecular Arylation: Substituent Effects, *J. Am. Chem. Soc.* **2007**, *129*, 6880-6886.

(53) Lafrance, M.; Gorelsky, S. I.; Fagnou, K. High-Yielding Palladium-Catalyzed Intramolecular Alkane Arylation: Reaction Development and Mechanistic Studies, *J. Am. Chem. Soc.* **2007**, *129*, 14570-14571.

(54) Chaumontet, M.; Piccardi, R.; Audic, N.; Hitce, J.; Peglion, J.-L.; Clot, E.; Baudoin, O. Synthesis of Benzocyclobutenes by Palladium-Catalyzed C-H Activation of Methyl Groups: Method and Mechanistic Study, *J. Am. Chem. Soc.* **2008**, *130*, 15157-15166.

(55) Aguilar, D.; Bielsa, R.; Contel, M.; Lledós, A.; Navarro, R.; Soler, T.; Urriolabeitia, E. P. Regioselective Ortho Palladation of Stabilized Iminophosphoranes in Exo Positions: Scope, Limitations, and Mechanistic Insights, *Organometallics* **2008**, *27*, 2929-2936.

(56) Lafrance, M.; Rowley, C. N.; Woo, T. K.; Fagnou, K. Catalytic Intermolecular Direct Arylation of Perfluorobenzenes, *J. Am. Chem. Soc.* **2006**, *128*, 8754-8756.

(57) Gorelsky, S. I.; Lapointe, D.; Fagnou, K. Analysis of the Concerted Metalation-Deprotonation Mechanism in Palladium-Catalyzed Direct Arylation across a Broad Range of Aromatic Substrates, *J. Am. Chem. Soc.* **2008**, *130*, 10848-10849.

(58) Lafrance, M.; Fagnou, K. Palladium-Catalyzed Benzene Arylation: Incorporation of Catalytic Pivalic Acid as a Proton Shuttle and a Key Element in Catalyst Design, *J. Am. Chem. Soc.* **2006**, *128*, 16496-16497.

(59) Lapointe, D.; Markiewicz, T.; Whipp, C. J.; Toderian, A.; Fagnou, K. Predictable and Site-Selective Functionalization of Poly(Hetero)Arene Compounds by Palladium Catalysis, *J. Org. Chem.* **2011**, *76*, 749-759.

(60) Boutadla, Y.; Davies, D. L.; Macgregor, S. A.; Poblador-Bahamonde, A. I. Computational and Synthetic Studies on the Cyclometallation Reaction of Dimethylbenzylamine with $[IrCl_2Cp^*]_2$: Role of the Chelating Base, *Dalton Trans.* **2009**, 5887-5893.

(61) Davies, D. L.; Donald, S. M. A.; Al-Duaij, O.; Macgregor, S. A.; Polleth, M. Electrophilic C-H Activation at {Cp*Ir}: Ancillary-Ligand Control of the Mechanism of C-H Activation, *J. Am. Chem. Soc.* **2006**, *128*, 4210-4211.

(62) Davies, D. L.; Donald, S. M. A.; Al-Duaij, O.; Fawcett, J.; Little, C.; Macgregor, S. A. N−H Versus C−H Activation of a Pyrrole Imine at {Cp*Ir}: A Computational and Experimental Study, *Organometallics* **2006**, *25*, 5976-5978.

(63) Ess, D. H.; Bischof, S. M.; Oxgaard, J.; Periana, R. A.; Goddard, W. A., III Transition State Energy Decomposition Study of Acetate-Assisted and Internal Electrophilic Substitution C-H Bond Activation by $(Acac\text{-}O,O)_2ir(X)$ Complexes (X = Ch_3COO, OH), *Organometallics* **2008**, *27*, 6440-6445.

(64) Ess, D. H.; Gunnoe, T. B.; Cundari, T. R.; Goddard, W. A.; Periana, R. A. Ligand Lone-Pair Influence on Hydrocarbon C−H Activation: A Computational Perspective, *Organometallics* **2010**, *29*, 6801-6815.

(65) Oxgaard, J.; Tenn, W. J., III; Nielsen, R. J.; Periana, R. A.; Goddard, W. A., III Mechanistic Analysis of Iridium Heteroatom C-H Activation: Evidence for an Internal Electrophilic Substitution Mechanism, *Organometallics* **2007**, *26*, 1565-1567.

(66) Oxgaard, J.; Muller, R. P.; Goddard, W. A.; Periana, R. A. Mechanism of Homogeneous Ir(III) Catalyzed Regioselective Arylation of Olefins, *J. Am. Chem. Soc.* **2004**, *126*, 352-363.

(67) Ess, D. H.; Nielsen, R. J.; Goddard III, W. A.; Periana, R. A. Transition-State Charge Transfer Reveals Electrophilic, Ambiphilic, and Nucleophilic Carbon−Hydrogen Bond Activation, *J. Am. Chem. Soc.* **2009**, *131*, 11686-11688.

(68) Cundari, T. R.; Grimes, T. V.; Gunnoe, T. B. Activation of Carbon-Hydrogen Bonds via 1,2-Addition across M-X (X = OH or NH_2) Bonds of d^6 Transition Metals as a Potential Key Step in Hydrocarbon Functionalization: A Computational Study, *J. Am. Chem. Soc.* **2007**, *129*, 13172-13182.

(69) Özdemir, I.; Demir, S.; Çetinkaya, B.; Gourlaouen, C.; Maseras, F.; Bruneau, C.; Dixneuf, P. H. Direct Arylation of Arene C-H Bonds by Cooperative Action of NHcarbene-Ruthenium(II) Catalyst and Carbonate via Proton Abstraction Mechanism, *J. Am. Chem. Soc.* **2008**, *130*, 1156-1157.

(70) The situation has some parallels with the variations in the detailed reaction profiles computed for classical S_EAr processes, see B. Galabov, B.; Nalbantova, D.; Schleyer, P. v. R.; Schaefer, H. F. *Acc. Chem. Res*. **2016**, *49*, 1191-1199

(71) Gray, A.; Tsybizova, A.; Roithova, J. Carboxylate-Assisted C-H Activation of Phenylpyridines with Copper, Palladium and Ruthenium: A Mass Spectrometry and DFT Study, *Chem. Sci.* **2015**, *6*, 5544-5553.

(72) Laga, E.; García-Montero, A.; Sayago, F. J.; Soler, T.; Moncho, S.; Cativiela, C.; Martínez, M.; Urriolabeitia, E. P. Cyclopalladation and Reactivity of Amino Esters through C-H Bond Activation: Experimental, Kinetic, and Density Functional Theory Mechanistic Studies, *Chem. – Eur. J.* **2013**, *19*, 17398-17412.

(73) Zhang, L.; Fang, D.-C. DFT Studies on the Directing Group Dependent Arene-Alkene Cross-Couplings: Arene Activation vs. Alkene Activation, *Org. Biomol. Chem.* **2015**, *13*, 7950-7960.

(74) Korenaga, T.; Suzuki, N.; Sueda, M.; Shimada, K. Ligand Effect on Direct Arylation by CMD Process, *J. Organomet. Chem.* **2015**, *780*, 63-69.

(75) Aullón, G.; Chat, R.; Favier, I.; Font-Bardia, M.; Gómez, M.; Granell, J.; Martínez, M.; Solans, X. Cyclometallation of Amino-Imines on Palladium Complexes. The Effect of the Solvent on the Experimental and Calculated Mechanism, *Dalton Trans.* **2009**, 8292-8300.

(76) Granell, J.; Martínez, M. Kinetico-Mechanistic Studies of Cyclometalating C-H Bond Activation Reactions on Pd(II) and Rh(II) Centres: The Importance of Non-Innocent Acidic Solvents in the Process, *Dalton Trans.* **2012**, *41*, 11243-11258.

(77) Roiban, G.-D.; Serrano, E.; Soler, T.; Aullón, G.; Grosu, I.; Cativiela, C.; MartÍnez, M.; Urriolabeitia, E. P. Regioselective Orthopalladation of (Z)-2-Aryl-4-Arylidene-5(4H)-Oxazolones: Scope, Kinetico-Mechanistic, and Density Functional Theory Studies of the C-H Bond Activation, *Inorg. Chem.* **2011**, *50*, 8132-8143.

(78) Stephens, D. E.; Lakey-Beitia, J.; Atesin, A. C.; Ateşin, T. A.; Chavez, G.; Arman, H. D.; Larionov, O. V. Palladium-Catalyzed C8-Selective C-H Arylation of Quinoline *N*-Oxides:

Insights into the Electronic, Steric, and Solvation Effects on the Site Selectivity by Mechanistic and DFT Computational Studies, *ACS Catal.* **2015**, *5*, 167-175.

(79) Sun, Y.-H.; Sun, T.-Y.; Wu, Y.-D.; Zhang, X.; Rao, Y. A Diversity-Oriented Synthesis of Bioactive Benzanilides Via a Regioselective C(sp^2)-H Hydroxylation Strategy, *Chem. Sci.* **2016**, *7*, 2229-2238.

(80) Anand, M.; Sunoj, R. B. Role of Explicit Solvents in Palladium(II)-Catalyzed Alkoxylation of Arenes: An Interesting Paradigm for Preferred Outer-Sphere Reductive Elimination over Inner-Sphere Pathway, *Organometallics* **2012**, *31*, 6466-6481.

(81) Anand, M.; Sunoj, R. B. Palladium(II)-Catalyzed Direct Alkoxylation of Arenes: Evidence for Solvent-Assisted Concerted Metalation Deprotonation, *Org. Lett.* **2011**, *13*, 4802-4805.

(82) Rauf, W.; Brown, J. M. Palladium-Catalysed Directed C-H Activation by Anilides and Ureas; Water Participation in a General Base Mechanism, *Org. Biomol. Chem.* **2016**, *14*, 5251-5257.

(83) Szabó, F.; Daru, J.; Simkó, D.; Nagy, T. Z.; Stirling, A.; Novák, Z. Mild Palladium-Catalyzed Oxidative Direct Ortho-C-H Acylation of Anilides under Aqueous Conditions, *Adv. Synth. Catal.* **2013**, *355*, 685-691.

(84) Haines, B. E.; Berry, J. F.; Yu, J.-Q.; Musaev, D. G. Factors Controlling Stability and Reactivity of Dimeric Pd(II) Complexes in C-H Functionalization Catalysis, *ACS Catal.* **2016**, *6*, 829-839.

(85) Musaev, D. G.; Figg, T. M.; Kaledin, A. L. Versatile Reactivity of Pd-Catalysts: Mechanistic Features of the Mono-*N*-Protected Amino Acid Ligand and Cesium-Halide Base in Pd-Catalyzed C-H Bond Functionalization, *Chem. Soc. Rev.* **2014**, *43*, 5009-5031.

(86) Ishikawa, A.; Nakao, Y.; Sato, H.; Sakaki, S. Pd(II)-Promoted Direct Cross-Coupling Reaction of Arenes Via Highly Regioselective Aromatic C-H Activation: A Theoretical Study, *Dalton Trans.* **2010**, *39*, 3279-3289.

(87) Canty, A. J.; Ariafard, A.; Sanford, M. S.; Yates, B. F. Mechanism of Pd-Catalyzed Ar–Ar Bond Formation Involving Ligand-Directed C–H Arylation and Diaryliodonium Oxidants: Computational Studies of Orthopalladation at Binuclear Pd(II) Centers, Oxidation to Form

Binuclear Palladium(III) Species, and Ar···Ar Reductive Coupling, *Organometallics* **2013**, *32*, 544-555.

(88) Yoo, E. J.; Ma, S.; Mei, T. S.; Chan, K. S. L.; Yu, J. Q. Pd-Catalyzed Intermolecular C-H Amination with Alkylamines, *J. Am. Chem. Soc.* **2011**, *133*, 7652-7655.

(89) Anand, M.; Sunoj, R. B.; Schaefer, H. F., III Non-Innocent Additives in a Palladium(II)-Catalyzed C-H Bond Activation Reaction: Insights into Multimetallic Active Catalysts, *J. Am. Chem. Soc.* **2014**, *136*, 5535-5538.

(90) Anand, M.; Sunoj, R. B.; Schaefer, H. F., III Palladium-Silver Cooperativity in an Aryl Amination Reaction through C-H Functionalization, *ACS Catal.* **2016**, *6*, 696-708.

(91) Yang, Y.-F.; Cheng, G.-J.; Liu, P.; Leow, D.; Sun, T.-Y.; Chen, P.; Zhang, X.; Yu, J.-Q.; Wu, Y.-D.; Houk, K. N. Palladium-Catalyzed Meta-Selective C-H Bond Activation with a Nitrile-Containing Template: Computational Study on Mechanism and Origins of Selectivity, *J. Am. Chem. Soc.* **2014**, *136*, 344-355.

(92) Tang, H.; Zhou, B.; Huang, X.-R.; Wang, C.; Yao, J.; Chen, H. Origins of Selective C(sp^2)–H Activation Using Transition Metal Complexes with *N,N*-Bidentate Directing Groups: A Combined Theoretical–Experimental Study, *ACS Catal.* **2014**, *4*, 649-656.

(93) Tang, H.; Huang, X.-R.; Yao, J.; Chen, H. Understanding the Effects of Bidentate Directing Groups: A Unified Rationale for sp^2 and sp^3 C-H Bond Activations, *J. Org. Chem.* **2015**, *80*, 4672-4682.

(94) Cross, W. B.; Hope, E. G.; Lin, Y.-H.; Macgregor, S. A.; Singh, K.; Solan, G. A.; Yahya, N. *N*,*N*-Chelate-Control on the Regioselectivity in Acetate-Assisted C-H Activation, *Chem. Commun.* **2013**, *49*, 1918-1920.

(95) Chapman, M. R.; Pask, C. M.; Ariafard, A.; Willans, C. E. Σ-Alkenyl *Endo*-Palladacycle Formation Via Regiospecific Functionalisation of an Unreactive Nhc-Tethered C(sp^2)-H Bond, *Chem. Commun.* **2015**, *51*, 5513-5515.

(96) Zhang, L.; Fang, D.-C. Catalytic C-H Activation/C-C Coupling Reaction: DFT Studies on the Mechanism, Solvent Effect, and Role of Additive, *J. Org. Chem.* **2013**, *78*, 2405-2412.

(97) Musaev, D. G.; Kaledin, A.; Shi, B.-F.; Yu, J.-Q. Key Mechanistic Features of Enantioselective C–H Bond Activation Reactions Catalyzed by [(Chiral Mono-*N*-Protected Amino Acid)–Pd(II)] Complexes, *J. Am. Chem. Soc.* **2012**, *134*, 1690-1698.

(98) Haines, B. E.; Musaev, D. G. Factors Impacting the Mechanism of the Mono-*N*-Protected Amino Acid Ligand-Assisted and Directing-Group-Mediated C–H Activation Catalyzed by Pd(II) Complex, *ACS Catal.* **2015**, *5*, 830-840.

(99) Cheng, G.-J.; Yang, Y.-F.; Liu, P.; Chen, P.; Sun, T.-Y.; Li, G.; Zhang, X.; Houk, K. N.; Yu, J.-Q.; Wu, Y.-D. Role of *N*-Acyl Amino Acid Ligands in Pd(II)-Catalyzed Remote C-H Activation of Tethered Arenes, *J. Am. Chem. Soc.* **2014**, *136*, 894-897.

(100) Zhang, X.; Chung, L. W.; Wu, Y.-D. New Mechanistic Insights on the Selectivity of Transition-Metal-Catalyzed Organic Reactions: The Role of Computational Chemistry, *Acc. Chem. Res.* **2016**, *49*, 1302–1310.

(101) Cheng, G.-J.; Chen, P.; Sun, T.-Y.; Zhang, X.; Yu, J.-Q.; Wu, Y.-D. A Combined IM-MS/DFT Study on Pd(MPAA) -Catalyzed Enantioselective C-H Activation: Relay of Chirality through a Rigid Framework, *Chem. – Eur. J.* **2015**, *21*, 11180-11188.

(102) Maji, A.; Bhaskararao, B.; Singha, S.; Sunoj, R. B.; Maiti, D. Directing Group Assisted Meta-Hydroxylation by C-H Activation, *Chem. Sci.* **2016**, *7*, 3147-3153.

(103) Zhou, M.-J.; Yang, T. L.; Dang, L. Theoretical Studies on Palladium-Mediated Enantioselective C-H Iodination, *J. Org. Chem.* **2016**, *81*, 1006-1020.

(104) Haines, B. E.; Xu, H.; Verma, P.; Wang, X.-C.; Yu, J.-Q.; Musaev, D. G. Mechanistic Details of Pd(II)-Catalyzed C–H Iodination with Molecular I_2: Oxidative Addition vs Electrophilic Cleavage, *J. Am. Chem. Soc.* **2015**, *137*, 9022-9031.

(105) Liu, L.; Yuan, H.; Fu, T. T.; Wang, T.; Gao, X.; Zeng, Z. P.; Zhu, J.; Zhao, Y. F. Double Role of the Hydroxy Group of Phosphoryl in Palladium(II)-Catalyzed Ortho-Olefination: A Combined Experimental and Theoretical Investigation, *J. Org. Chem.* **2014**, *79*, 80-87.

(106) Li, X.; Pan, J.; Song, S.; Jiao, N. Pd-Catalyzed Dehydrogenative Annulation Approach for the Efficient Synthesis of Phenanthridinones, *Chem. Sci.* **2016**, *7*, 5384-5389.

(107) Gu, H.; Qiu, Z.; Zhang, Z.; Li, J.; Yan, B. A Mechanistic Study of $Pd(OAc)_2$-Catalyzed Intramolecular C-H Functionalization Reaction Involving CO/Isonitrile Insertion, *Dalton Trans.* **2015**, *44*, 9839-9846.

(108) Dang, Y.; Deng, X.; Guo, J.; Song, C.; Hu, W.; Wang, Z.-X. Unveiling Secrets of Overcoming the "Heteroatom Problem" in Palladium-Catalyzed Aerobic C-H Functionalization of Heterocycles: A DFT Mechanistic Study, *J. Am. Chem. Soc.* **2016**, *138*, 2712-2723.

(109) Lian, B.; Zhang, L.; Chass, G. A.; Fang, D.-C. $Pd(OAc)_2$-Catalyzed C–H Activation/C–O Cyclization: Mechanism, Role of Oxidant—Probed by Density Functional Theory, *J. Org. Chem.* **2013**, *78*, 8376-8385.

(110) Holstein, P. M.; Vogler, M.; Larini, P.; Pilet, G.; Clot, E.; Baudoin, O. Efficient Pd^0-Catalyzed Asymmetric Activation of Primary and Secondary C-H Bonds Enabled by Modular Binepine Ligands and Carbonate Bases, *ACS Catal.* **2015**, *5*, 4300-4308.

(111) Kefalidis, C. E.; Baudoin, O.; Clot, E. DFT Study of the Mechanism of Benzocyclobutene Formation by Palladium-Catalysed C(sp^3)-H Activation: Role of the Nature of the Base and the Phosphine, *Dalton Trans.* **2010**, *39*, 10528-10535.

(112) Rousseaux, S.; Davi, M.; Sofack-Kreutzer, J.; Pierre, C.; Kefalidis, C. E.; Clot, E.; Fagnou, K.; Baudoin, O. Intramolecular Palladium-Catalyzed Alkane C-H Arylation from Aryl Chlorides, *J. Am. Chem. Soc.* **2010**, *132*, 10706-10716.

(113) Häller, L. J. L.; Page, M. J.; Macgregor, S. A.; Mahon, M. F.; Whittlesey, M. K. Activation of an Alkyl C-H Bond Geminal to an Agostic Interaction: An Unusual Mode of Base-Induced C-H Activation, *J. Am. Chem. Soc.* **2009**, *131*, 4604-4605.

(114) Janody, S.; Jazzar, R.; Comte, A.; Holstein, P. M.; Vors, J.-P.; Ford, M. J.; Baudoin, O. Synthesis of 1-Indanols and 1-Indanamines by Intramolecular Palladium(0)-Catalyzed C(sp^3)-H Arylation: Impact of Conformational Effects, *Chem. – Eur. J.* **2014**, *20*, 11084-11090.

(115) Kefalidis, C. E.; Davi, M.; Holstein, P. M.; Clot, E.; Baudoin, O. Mechanistic Study of the Selectivity of Olefin Versus Cyclobutene Formation by Palladium(0)-Catalyzed Intramolecular C(sp^3)–H Activation, *J. Org. Chem.* **2014**, *79*, 11903-11910.

(116) Gutiérrez-Bonet, Á.; Juliá-Hernández, F.; de Luis, B.; Martin, R. Pd-Catalyzed C(sp^3)–H Functionalization/Carbenoid Insertion: All-Carbon Quaternary Centers Via Multiple C–C Bond Formation, *J. Am. Chem. Soc.* **2016**, *138*, 6384-6387.

(117) Zhang, Q.; Yu, H.-Z.; Fu, Y. Mechanistic Study of Palladium-Catalyzed Chemoselective C(sp^3)–H Activation of Carbamoyl Chloride, *Organometallics* **2013**, *32*, 4165-4173.

(118) Solé, D.; Pérez-Janer, F.; Zulaica, E.; Guastavino, J. F.; Fernández, I. Pd-Catalyzed A-Arylation of Sulfones in a Three-Component Synthesis of 3-[2-(Phenyl/Methylsulfonyl)Ethyl]Indoles, *ACS Catal.* **2016**, *6*, 1691-1700.

(119) Smalley, A. P.; Gaunt, M. J. Mechanistic Insights into the Palladium-Catalyzed Aziridination of Aliphatic Amines by C-H Activation, *J. Am. Chem. Soc.* **2015**, *137*, 10632-10641.

(120) Zhang, Y.; Qi, Z.-H.; Ruan, G.-Y.; Zhang, Y.; Liu, W.; Wang, Y. Mechanism of Pd-Catalyzed C(sp^3)-H Activation of Aliphatic Amines: An Insight from DFT Calculations, *RSC Advances* **2015**, *5*, 71586-71592.

(121) Giri, R.; Lan, Y.; Liu, P.; Houk, K. N.; Yu, J.-Q. Understanding Reactivity and Stereoselectivity in Palladium-Catalyzed Diastereoselective sp^3 C–H Bond Activation: Intermediate Characterization and Computational Studies, *J. Am. Chem. Soc.* **2012**, *134*, 14118-14126.

(122) Katayev, D.; Larionov, E.; Nakanishi, M.; Besnard, C.; Kündig, E. P. Palladium–N-Heterocyclic Carbene (NHC)-Catalyzed Asymmetric Synthesis of Indolines through Regiodivergent C(sp^3)-H Activation: Scope and DFT Study, *Chem. – Eur. J.* **2014**, *20*, 15021-15030.

(123) Larionov, E.; Nakanishi, M.; Katayev, D.; Besnard, C.; Kündig, E. P. Scope and Mechanism of Asymmetric C(sp^3)-H/C(Ar)-X Coupling Reactions: Computational and Experimental Study, *Chem. Sci.* **2013**, *4*, 1995-2005.

(124) Rousseaux, S.; Gorelsky, S. I.; Chung, B. K. W.; Fagnou, K. Investigation of the Mechanism of C(sp^3)-H Bond Cleavage in Pd(0)-Catalyzed Intramolecular Alkane Arylation Adjacent to Amides and Sulfonamides, *J. Am. Chem. Soc.* **2010**, *132*, 10692-10705.

(125) Jiang, J.; Yu, J.-Q.; Morokuma, K. Mechanism and Stereoselectivity of Directed C(sp^3)-H Activation and Arylation Catalyzed by Pd(II) with Pyridine Ligand and Trifluoroacetate: A Computational Study, *ACS Catal.* **2015**, *5*, 3648-3661.

(126) Wei, Y.; Tang, H.; Cong, X.; Rao, B.; Wu, C.; Zeng, X. Pd(II)-Catalyzed Intermolecular Arylation of Unactivated C(sp^3)-H Bonds with Aryl Bromides Enabled by 8-Aminoquinoline Auxiliary, *Org. Lett.* **2014**, *16*, 2248-2251.

(127) Dang, Y.; Qu, S.; Nelson, J. W.; Pham, H. D.; Wang, Z.-X.; Wang, X. The Mechanism of a Ligand-Promoted C(sp^3)-H Activation and Arylation Reaction via Palladium Catalysis: Theoretical Demonstration of a Pd(II)/Pd(IV) Redox Manifold, *J. Am. Chem. Soc.* **2015**, *137*, 2006-2014.

(128) Poveda, A.; Alonso, I.; Fernández-Ibáñez, M. A. Experimental and Computational Studies on the Mechanism of the Pd-Catalyzed C(sp^3)-H γ-Arylation of Amino Acid Derivatives Assisted by the 2-Pyridylsulfonyl Group, *Chem. Sci.* **2014**, *5*, 3873-3882.

(129) Chen, F.-J.; Zhao, S.; Hu, F.; Chen, K.; Zhang, Q.; Zhang, S.-Q.; Shi, B.-F. Pd(II)-Catalyzed Alkoxylation of Unactivated C(sp^3)-H and C(sp^2)-H Bonds Using a Removable Directing Group: Efficient Synthesis of Alkyl Ethers, *Chem. Sci.* **2013**, *4*, 4187-4192.

(130) Wang, M.; Yang, Y.; Fan, Z.; Cheng, Z.; Zhu, W.; Zhang, A. Pd-Catalyzed α-Selective C(sp^3)-H Acetoxylation of Amides through an Unusual Cyclopalladation Mechanism, *Chem. Commun.* **2015**, *51*, 3219-3222.

(131) Duarte, F. J. S.; Poli, G.; Calhorda, M. J. Mechanistic Study of the Direct Intramolecular Allylic Amination Reaction Catalyzed by Palladium(II), *ACS Catal.* **2016**, *6*, 1772-1784.

(132) Jindal, G.; Sunoj, R. B. Importance of Ligand Exchanges in Pd(II)-Bronsted Acid Cooperative Catalytic Approach to Spirocyclic Rings, *J. Am. Chem. Soc.* **2014**, *136*, 15998-16008.

(133) Engelin, C.; Jensen, T.; Rodriguez-Rodriguez, S.; Fristrup, P. Mechanistic Investigation of Palladium-Catalyzed Allylic C-H Activation, *ACS Catal.* **2013**, *3*, 294-302.

(134) van Zeist, W.-J.; Bickelhaupt, F. M. The Activation Strain Model of Chemical Reactivity, *Org. Biomol. Chem.* **2010**, *8*, 3118-3127.

(135) Gorelsky, S. I. Origins of Regioselectivity of the Palladium-Catalyzed (Aromatic)C-H Bond Metalation-Deprotonation, *Coord. Chem. Rev.* **2013**, *257*, 153-164.

(136) Gorelsky, S. I. Tuning the Regioselectivity of Palladium-Catalyzed Direct Arylation of Azoles by Metal Coordination, *Organometallics* **2012**, *31*, 794-797.

(137) Gorelsky, S. I.; Lapointe, D.; Fagnou, K. Analysis of the Palladium-Catalyzed (Aromatic)C-H Bond Metalation-Deprotonation Mechanism Spanning the Entire Spectrum of Arenes, *J. Org. Chem.* **2012**, *77*, 658-668.

(138) Tan, Y.; Hartwig, J. F. Assessment of the Intermediacy of Arylpalladium Carboxylate Complexes in the Direct Arylation of Benzene: Evidence for C-H Bond Cleavage by "Ligandless" Species, *J. Am. Chem. Soc.* **2011**, *133*, 3308-3311.

(139) Guihaumé, J.; Clot, E.; Eisenstein, O.; Perutz, R. N. Importance of Palladium-Carbon Bond Energies in Direct Arylation of Polyfluorinated Benzenes, *Dalton Trans.* **2010**, *39*, 10510-10519.

(140) Petit, A.; Flygare, J.; Miller, A. T.; Winkel, G.; Ess, D. H. Transition-State Metal Aryl Bond Stability Determines Regioselectivity in Palladium Acetate Mediated C-H Bond Activation of Heteroarenes, *Org. Lett.* **2012**, *14*, 3680-3683.

(141) Tang, S.-Y.; Yu, H.-Z.; You, W.-L.; Guo, Q.-X. Mechanistic Study of Palladium-Catalyzed Oxidative C-H/C-H Coupling of Polyfluoroarenes with Simple Arenes, *Chinese J. Chem. Phys.* **2013**, *26*, 415-423.

(142) Ricci, P.; Krämer, K.; Cambeiro, X. C.; Larrosa, I. Arene-Metal π-Complexation as a Traceless Reactivity Enhancer for C-H Arylation, *J. Am. Chem. Soc.* **2013**, *135*, 13258-13261.

(143) Campeau, L.-C.; Bertrand-Laperle, M.; Leclerc, J.-P.; Villemure, E.; Gorelsky, S.; Fagnou, K. C2, C5, and C4 Azole *N*-Oxide Direct Arylation Including Room-Temperature Reactions, *J. Am. Chem. Soc.* **2008**, *130*, 3276-3277.

(144) Potavathri, S.; Pereira, K. C.; Gorelsky, S. I.; Pike, A.; LeBris, A. P.; DeBoef, B. Regioselective Oxidative Arylation of Indoles Bearing *N*-Alkyl Protecting Groups: Dual C-H Functionalization via a Concerted Metalation-Deprotonation Mechanism, *J. Am. Chem. Soc.* **2010**, *132*, 14676-14681.

(145) Sun, H.-Y.; Gorelsky, S. I.; Stuart, D. R.; Campeau, L.-C.; Fagnou, K. Mechanistic Analysis of Azine *N*-Oxide Direct Arylation: Evidence for a Critical Role of Acetate in the $Pd(OAc)_2$ Precatalyst, *J. Org. Chem.* **2010**, *75*, 8180-8189.

(146) Tan, Y.; Barrios-Landeros, F.; Hartwig, J. F. Mechanistic Studies on Direct Arylation of Pyridine *N*-Oxide: Evidence for Cooperative Catalysis between Two Distinct Palladium Centers, *J. Am. Chem. Soc.* **2012**, *134*, 3683-3686.

(147) Gorelsky, S. I. Reactivity and Regioselectivity of Palladium-Catalyzed Direct Arylation in Noncooperative and Cooperative Processes, *Organometallics* **2012**, *31*, 4631-4634.

(148) Liégault, B.; Petrov, I.; Gorelsky, S. I.; Fagnou, K. Modulating Reactivity and Diverting Selectivity in Palladium-Catalyzed Heteroaromatic Direct Arylation through the Use of a Chloride Activating/Blocking Group, *J. Org. Chem.* **2010**, *75*, 1047-1060.

(149) Wakioka, M.; Nakamura, Y.; Hihara, Y.; Ozawa, F.; Sakaki, S. Factors Controlling the Reactivity of Heteroarenes in Direct Arylation with Arylpalladium Acetate Complexes, *Organometallics* **2013**, *32*, 4423-4430.

(150) Wakioka, M.; Nakamura, Y.; Hihara, Y.; Ozawa, F.; Sakaki, S. Effects of PAr_3 Ligands on Direct Arylation of Heteroarenes with Isolated $[Pd(2,6\text{-}Me_2C_6H_3)(M\text{-}O_2CMe)(PAr_3)]_4$ Complexes, *Organometallics* **2014**, *33*, 6247-6252.

(151) Zhu, Y.-S.; Shi, B.; Fang, R.; Wang, X.; Jing, H. Palladium-Catalyzed Microwave-Assisted Direct Arylation of Imidazo[2,1-*b*]Thiazoles with Aryl Bromides: Synthesis and Mechanistic Study, *Org. Biomol. Chem.* **2014**, *12*, 5773-5780.

(152) Ueda, K.; Yanagisawa, S.; Yamaguchi, J.; Itami, K. A General Catalyst for the β-Selective C-H Bond Arylation of Thiophenes with Iodoarenes, *Angew. Chem. Int. Ed.* **2010**, *49*, 8946-8949.

(153) Yanagisawa, S.; Ueda, K.; Sekizawa, H.; Itami, K. Programmed Synthesis of Tetraarylthiophenes through Sequential C-H Arylation, *J. Am. Chem. Soc.* **2009**, *131*, 14622-14623.

(154) Steinmetz, M.; Ueda, K.; Grimme, S.; Yamaguchi, J.; Kirchberg, S.; Itami, K.; Studer, A. Mechanistic Studies on the Pd-Catalyzed Direct C-H Arylation of 2-Substituted Thiophene Derivatives with Arylpalladium Bipyridyl Complexes, *Chem. – Asian. J.* **2012**, *7*, 1256-1260.

(155) Tang, S.-Y.; Guo, Q.-X.; Fu, Y. Mechanistic Origin of Ligand-Controlled Regioselectivity in Pd-Catalyzed C-H Activation/Arylation of Thiophenes, *Chem. – Eur. J.* **2011**, *17*, 13866-13876.

(156) Sanhueza, I. A.; Wagner, A. M.; Sanford, M. S.; Schoenebeck, F. On the Role of Anionic Ligands in the Site-Selectivity of Oxidative C-H Functionalization Reactions of Arenes, *Chem. Sci.* **2013**, *4*, 2767-2775.

(157) Choi, H.; Min, M.; Peng, Q.; Kang, D.; Paton, R. S.; Hong, S. Unraveling Innate Substrate Control in Site-Selective Palladium-Catalyzed C-H Heterocycle Functionalization, *Chem. Sci.* **2016**, *7*, 3900-3909.

(158) Xi, P.; Yang, F.; Qin, S.; Zhao, D.; Lan, J.; Gao, G.; Hu, C.; You, J. Palladium(II)-Catalyzed Oxidative C-H/C-H Cross-Coupling of Heteroarenes, *J. Am. Chem. Soc.* **2010**, *132*, 1822-1824.

(159) Yang, N.; Dong, L.; Su, Z.; Hu, C. Theoretical Study on the Mechanism of $Pd(OAc)_2$ Catalyzed Dehydrogenative Cross-Coupling of Two Heteroarenes, *RSC Advances* **2013**, *3*, 20772-20781.

(160) Meir, R.; Kozuch, S.; Uhe, A.; Shaik, S. How Can Theory Predict the Selectivity of Palladium-Catalyzed Cross-Coupling of Pristine Aromatic Molecules?, *Chem. – Eur. J.* **2011**, *17*, 7623-7631.

(161) Cong, X.; Tang, H.; Wu, C.; Zeng, X. Role of Mono-*N*-Protected Amino Acid Ligands in Palladium(II)-Catalyzed Dehydrogenative Heck Reactions of Electron-Deficient (Hetero)Arenes: Experimental and Computational Studies, *Organometallics* **2013**, *32*, 6565-6575.

(162) Zhang, S.; Shi, L.; Ding, Y. Theoretical Analysis of the Mechanism of Palladium(II) Acetate-Catalyzed Oxidative Heck Coupling of Electron-Deficient Arenes with Alkenes: Effects of the Pyridine-Type Ancillary Ligand and Origins of the Meta-Regioselectivity, *J. Am. Chem. Soc.* **2011**, *133*, 20218-20229.

(163) Zhang, S.; Chen, Z.; Qin, S.; Lou, C.; Senan, A. M.; Liao, R.-Z.; Yin, G. Non-Redox Metal Ion Promoted Oxidative Coupling of Indoles with Olefins by the Palladium(Ii) Acetate Catalyst through Dioxygen Activation: Experimental Results with DFT Calculations, *Org. Biomol. Chem.* **2016**, *14*, 4146-4157.

(164) Zhou, Y.-P.; Wang, M.-Y.; Fang, S.; Chen, Y.; Liu, J.-Y. DFT Studies on the Mechanism of Palladium Catalyzed Arylthiolation of Unactive Arene to Diaryl Sulfide, *RSC Advances* **2016**, *6*, 18300-18307.

(165) Munz, D.; Meyer, D.; Strassner, T. Methane CH Activation by Palladium Complexes with Chelating Bis(NHC) Ligands: A DFT Study, *Organometallics* **2013**, *32*, 3469-3480.

(166) Munz, D.; Strassner, T. Catalytic Hydrocarbon Oxidation by Palladium-Bis-NHC-Complexes, *Top. Catal.* **2014**, *57*, 1372-1376.

(167) Munz, D.; Strassner, T. On the Mechanism of the Palladium Bis(NHC) Complex Catalyzed CH Functionalization of Propane: Experiment and DFT Calculations, *Chem. – Eur. J.* **2014**, *20*, 14872-14879.

(168) Lu, Q.; Yu, H.; Fu, Y. Mechanistic Study of Chemoselectivity in Ni-Catalyzed Coupling Reactions between Azoles and Aryl Carboxylates, *J. Am. Chem. Soc.* **2014**, *136*, 8252-8260.

(169) Xu, H.; Muto, K.; Yamaguchi, J.; Zhao, C.; Itami, K.; Musaev, D. G. Key Mechanistic Features of Ni-Catalyzed C–H/C–O Biaryl Coupling of Azoles and Naphthalen-2-yl Pivalates, *J. Am. Chem. Soc.* **2014**, *136*, 14834-14844.

(170) Zhang, M.; Huang, G. Mechanism and Selectivity of RuII- and RhIII-Catalyzed Oxidative Spiroannulation of Naphthols and Phenols with Alkynes through a C−H Activation/Dearomatization Strategy, *Chem. – Eur. J.* **2016**, *22*, 9356–9365.

(171) Ahlquist, M.; Periana, R. A.; Goddard III, W. A. C-H Activation in Strongly Acidic Media. The Co-Catalytic Effect of the Reaction Medium, *Chem. Commun.* **2009**, 2373-2375.

(172) Carr, K. J. T.; Davies, D. L.; Macgregor, S. A.; Singh, K.; Villa-Marcos, B. Metal Control of Selectivity in Acetate-Assisted C-H Bond Activation: An Experimental and Computational Study of Heterocyclic, Vinylic and Phenylic C(sp^2)-H Bonds at Ir and Rh, *Chem. Sci.* **2014**, *5*, 2340-2346.

(173) Li, J.; Hu, W.; Peng, Y.; Zhang, Y.; Li, J.; Zheng, W. Theoretical Study on Iridacycle and Rhodacycle Formation via C–H Activation of Phenyl Imines, *Organometallics* **2014**, *33*, 2150-2159.

(174) Li, L.; Brennessel, W. W.; Jones, W. D. C−H Activation of Phenyl Imines and 2-Phenylpyridines with $[Cp^*MCl_2]_2$ (M = Ir, Rh): Regioselectivity, Kinetics, and Mechanism, *Organometallics* **2009**, *28*, 3492-3500.

(175) Sun, Y.; Hu, L.; Chen, H. Comparative Assessment of DFT Performances in Ru- and Rh-Promoted σ-Bond Activations, *J. Chem. Theor. Comput.* **2015**, *11*, 1428-1438.

(176) Lloret, J.; Estevan, F.; Lahuerta, P.; Hirva, P.; Pérez-Prieto, J.; Sanaú, M. Dirhodium(II) Compounds with Bridging Thienylphosphines: Studies on Reversible P,C/P,S Coordination, *Chem. – Eur. J.* **2009**, *15*, 7706-7716.

(177) Guimond, N.; Gorelsky, S. I.; Fagnou, K. Rhodium(III)-Catalyzed Heterocycle Synthesis Using an Internal Oxidant: Improved Reactivity and Mechanistic Studies, *J. Am. Chem. Soc.* **2011**, *133*, 6449-6457.

(178) Zhao, L.; Fang, D.-C. A Theoretical Probe of Mechanistic Trichotomy in Rh-III-Catalyzed Annulation with Alkyne Mida Boronates: Roles of Salt, Solvent, and Coupling Partner, *Eur. J. Org. Chem.* **2015**, 4772-4781.

(179) Xu, L.; Zhu, Q.; Huang, G.; Cheng, B.; Xia, Y. Computational Elucidation of the Internal Oxidant-Controlled Reaction Pathways in Rh(III)-Catalyzed Aromatic C–H Functionalization, *J. Org. Chem.* **2012**, *77*, 3017-3024.

(180) Wodrich, M. D.; Ye, B.; Gonthier, J. F.; Corminboeuf, C.; Cramer, N. Ligand-Controlled Regiodivergent Pathways of Rhodium(III)-Catalyzed Dihydroisoquinolone Synthesis: Experimental and Computational Studies of Different Cyclopentadienyl Ligands, *Chem. – Eur. J.* **2014**, *20*, 15409-15418.

(181) Guo, W.; Zhou, T.; Xia, Y. Mechanistic Understanding of the Aryl-Dependent Ring Formations in Rh(III)-Catalyzed C-H Activation/Cycloaddition of Benzamides and Methylenecyclopropanes by DFT Calculations, *Organometallics* **2015**, *34*, 3012-3020.

(182) Wu, S.; Zeng, R.; Fu, C.; Yu, Y.; Zhang, X.; Ma, S. Rhodium-Catalyzed C-H Functionalization-Based Approach to Eight-Membered Lactams, *Chem. Sci.* **2015**, *6*, 2275-2285.

(183) Xing, Z.; Huang, F.; Sun, C.; Zhao, X.; Liu, J.; Chen, D. Density Functional Theory Study of Rh(III)-Catalyzed C–H Activations and Intermolecular Annulations between Benzamide Derivatives and Allenes, *Inorg. Chem.* **2015**, *54*, 3958-3969.

(184) Du, L.; Xu, Y.; Yang, S.; Li, J.; Fu, X. Computational Insights into the Rhodium(III)-Catalyzed Coupling of Benzamides and 1,6-Enynes Via a Tunable Arylative Cyclization, *J. Org. Chem.* **2016**, *81*, 1921-1929.

(185) Zhou, T.; Guo, W.; Xia, Y. Rh-V-Nitrenoid as a Key Intermediate in Rh-III-Catalyzed Heterocyclization by CH Activation: A Computational Perspective on the Cycloaddition of Benzamide and Diazo Compounds, *Chem. – Eur. J.* **2015**, *21*, 9209-9218.

(186) Yang, Y.-F.; Houk, K. N.; Wu, Y.-D. Computational Exploration of RhIII/RhV and RhIII/RhI Catalysis in Rhodium(III)-Catalyzed C–H Activation Reactions of *N*-Phenoxyacetamides with Alkynes, *J. Am. Chem. Soc.* **2016**, *138*, 6861-6868.

(187) Li, J.; Qiu, Z. DFT Studies on the Mechanism of the Rhodium(III)-Catalyzed C-H Activation of *N*-Phenoxyacetamide, *J. Org. Chem.* **2015**, *80*, 10686-10693.

(188) Guo, W.; Xia, Y. Mechanistic Understanding of the Divergent Reactivity of Cyclopropenes in Rh(III)-Catalyzed C–H Activation/Cycloaddition Reactions of N-Phenoxyacetamide and N-Pivaloxybenzamide, *J. Org. Chem.* **2015**, *80*, 8113-8121.

(189) Chen, J.; Guo, W.; Xia, Y. Computational Revisit to the Beta-Carbon Elimination Step in Rh(III)-Catalyzed C-H Activation/Cycloaddition Reactions of *N*-Phenoxyacetamide and Cyclopropenes, *J. Org. Chem.* **2016**, *81*, 2635-2638.

(190) Yu, S.; Liu, S.; Lan, Y.; Wan, B.; Li, X. Rhodium-Catalyzed C–H Activation of Phenacyl Ammonium Salts Assisted by an Oxidizing C–N Bond: A Combination of Experimental and Theoretical Studies, *J. Am. Chem. Soc.* **2015**, *137*, 1623-1631.

(191) Chen, W.-J.; Lin, Z. Rhodium(III)-Catalyzed Hydrazine-Directed C–H Activation for Indole Synthesis: Mechanism and Role of Internal Oxidant Probed by DFT Studies, *Organometallics* **2015**, *34*, 309-318.

(192) Qiu, Z.; Deng, J.; Zhang, Z.; Wu, C.; Li, J.; Liao, X. Mechanism of the Rhodium(III)-Catalyzed Alkenylation Reaction of *N*-Phenoxyacetamide with Styrene or *N*-Tosylhydrazone: A Computational Study, *Dalton Trans.* **2016**, *45*, 8118-8126.

(193) Wu, W.; Liu, Y.; Bi, S. Mechanistic Insight into Conjugated N-N Bond Cleavage by Rh(III)-Catalyzed Redox-Neutral C-H Activation of Pyrazolones, *Org. Biomol. Chem.* **2015**, *13*, 8251-8260.

(194) Ajitha, M. J.; Huang, K.-W. Mechanism and Regioselectivity of Rh(III)-Catalyzed Intermolecular Annulation of Aryl-Substituted Diazenecarboxylates and Alkenes: DFT Insights, *Organometallics* **2016**, *35*, 450-455.

(195) Wang, Q.; Li, Y.; Qi, Z.; Xie, F.; Lan, Y.; Li, X. Rhodium(III)-Catalyzed Annulation between *N*-Sulfinyl Ketoimines and Activated Olefins: C-H Activation Assisted by an Oxidizing N-S Bond, *ACS Catal.* **2016**, *6*, 1971-1980.

(196) Algarra, A. G.; Cross, W. B.; Davies, D. L.; Khamker, Q.; Macgregor, S. A.; McMullin, C. L.; Singh, K. Combined Experimental and Computational Investigations of Rhodium- and Ruthenium-Catalyzed C-H Functionalization of Pyrazoles with Alkynes, *J. Org. Chem.* **2014**, *79*, 1954-1970.

(197) Davies, D. L.; Ellul, C. E.; Macgregor, S. A.; McMullin, C. L.; Singh, K. Experimental and DFT Studies Explain Solvent Control of C-H Activation and Product Selectivity in the Rh(III)-Catalyzed Formation of Neutral and Cationic Heterocycles, *J. Am. Chem. Soc.* **2015**, *137*, 9659-9669.

(198) Zhang, X.-S.; Chen, K.; Shi, Z.-J. Transition Metal-Catalyzed Direct Nucleophilic Addition of C-H Bonds to Carbon-Heteroatom Double Bonds, *Chem. Sci.* **2014**, *5*, 2146-2159.

(199) Quiñones, N.; Seoane, A.; García-Fandiño, R.; Luis Mascareñas, J.; Gulías, M. Rhodium(III)-Catalyzed Intramolecular Annulations Involving Amide-Directed C-H Activations: Synthetic Scope and Mechanistic Studies, *Chem. Sci.* **2013**, *4*, 2874-2879.

(200) Martínez, A. M.; Echavarren, J.; Alonso, I.; Rodríguez, N.; Gómez Arrayás, R.; Carretero, J. C. RhI/RhIII Catalyst-Controlled Divergent Aryl/Heteroaryl C-H Bond Functionalization of Picolinamides with Alkynes, *Chem. Sci.* **2015**, *6*, 5802-5814.

(201) Sun, H.; Wang, C.; Yang, Y.-F.; Chen, P.; Wu, Y.-D.; Zhang, X.; Huang, Y. Synthesis of Indolo[2,1-*a*]Isoquinolines via a Triazene-Directed C–H Annulation Cascade, *J. Org. Chem.* **2014**, *79*, 11863-11872.

(202) Funes-Ardoiz, I.; Maseras, F. Cooperative Reductive Elimination: The Missing Piece in the Oxidative-Coupling Mechanistic Puzzle, *Angew. Chem. Int. Ed.* **2016**, *55*, 2764-2767.

(203) Frasco, D. A.; Lilly, C. P.; Boyle, P. D.; Ison, E. A. Cp*Ir-III-Catalyzed Oxidative Coupling of Benzoic Acids with Alkynes, *ACS Catal.* **2013**, *3*, 2421-2429.

(204) Liu, L.; Wu, Y.; Wang, T.; Gao, X.; Zhu, J.; Zhao, Y. Mechanism, Reactivity, and Selectivity in Rh(III)-Catalyzed Phosphoryl-Directed Oxidative C-H Activation/Cyclization: A DFT Study, *J. Org. Chem.* **2014**, *79*, 5074-5081.

(205) Zheng, C.; Zheng, J.; You, S.-L. A DFT Study on Rh-Catalyzed Asymmetric Dearomatization of 2-Naphthols Initiated with C-H Activation: A Refined Reaction Mechanism and Origins of Multiple Selectivity, *ACS Catal.* **2016**, *6*, 262-271.

(206) Li, Y.; Liu, S.; Qi, Z.; Qi, X.; Li, X.; Lan, Y. The Mechanism of N-O Bond Cleavage in Rhodium-Catalyzed C-H Bond Functionalization of Quinoline *N*-Oxides with Alkynes: A Computational Study, *Chem. – Eur. J.* **2015**, *21*, 10131-10137.

(207) Liu, T.; Zheng, X.-W.; Han, L.-L.; Li, Y.-P.; Han, S.-M.; Yu, Z.-Y. Mechanistic Insight into the Selective Cyclization of Arylnitrones to Indolines via Rh(III) Catalyst: A Theoretical Study, *RSC Advances* **2016**, *6*, 23265-23271.

(208) Zhou, B.; Chen, Z.; Yang, Y.; Ai, W.; Tang, H.; Wu, Y.; Zhu, W.; Li, Y. Redox-Neutral Rhodium-Catalyzed C-H Functionalization of Arylamine N-Oxides with Diazo Compounds: Primary C(sp^3)-H/C(sp^2)-H Activation and Oxygen-Atom Transfer, *Angew. Chem. Int. Ed.* **2015**, *54*, 12121-12126.

(209) Gao, B.; Liu, S.; Lan, Y.; Huang, H. Rhodium-Catalyzed Cyclocarbonylation of Ketimines via C-H Bond Activation, *Organometallics* **2016**, *35*, 1480-1487.

(210) Zhang, Q.; Yu, H.-Z.; Li, Y.-T.; Liu, L.; Huang, Y.; Fu, Y. Computational Study on Mechanism of Rh(III)-Catalyzed Oxidative Heck Coupling of Phenol Carbamates with Alkenes, *Dalton Trans.* **2013**, *42*, 4175-4184.

(211) Gong, T.-J.; Xiao, B.; Liu, Z.-J.; Wan, J.; Xu, J.; Luo, D.-F.; Fu, Y.; Liu, L. Rhodium-Catalyzed Selective C–H Activation/Olefination of Phenol Carbamates, *Org. Lett.* **2011**, *13*, 3235-3237.

(212) Algarra, A. G.; Davies, D. L.; Khamker, Q.; Macgregor, S. A.; McMullin, C. L.; Singh, K.; Villa-Marcos, B. Combined Experimental and Computational Investigations of Rhodium-Catalysed C-H Functionalisation of Pyrazoles with Alkenes, *Chem. – Eur. J.* **2015**, *21*, 3087-3096.

(213) Wu, J.-Q.; Qiu, Z.-P.; Zhang, S.-S.; Liu, J.-G.; Lao, Y.-X.; Gu, L.-Q.; Huang, Z.-S.; Li, J.; Wang, H. Rhodium(III)-Catalyzed C-H/C-C Activation Sequence: Vinylcyclopropanes as Versatile Synthons in Direct C-H Allylation Reactions, *Chem. Commun.* **2015**, *51*, 77-80.

(214) Mei, S.-T.; Wang, N.-J.; Ouyang, Q.; Wei, Y. Rhodium-Catalysed Direct C-H Allylation of *N*-Sulfonyl Ketimines with Allyl Carbonates, *Chem. Commun.* **2015**, *51*, 2980-2983.

(215) Zhao, D.; Li, X.; Han, K.; Li, X.; Wang, Y. Theoretical Investigations on Rh(III)-Catalyzed Cross-Dehydrogenative Aryl-Aryl Coupling via C-H Bond Activation, *J. Phys. Chem. A* **2015**, *119*, 2989-2997.

(216) Wencel-Delord, J.; Nimphius, C.; Patureau, F. W.; Glorius, F. [RhIIICp*]-Catalyzed Dehydrogenative Aryl-Aryl Bond Formation, *Angew. Chem. Int. Ed.* **2012**, *51*, 2247-2251.

(217) Fabre, I.; von Wolff, N.; Le Duc, G.; Flegeau, E. F.; Bruneau, C.; Dixneuf, P. H.; Jutand, A. Autocatalytic Intermolecular Versus Intramolecular Deprotonation in CH Bond Activation of Functionalized Arenes by Ruthenium(II) or Palladium(II) Complexes, *Chem. – Eur. J.* **2013**, *19*, 7595-7604.

(218) Flegeau, E. F.; Bruneau, C.; Dixneuf, P. H.; Jutand, A. Autocatalysis for C-H Bond Activation by Ruthenium(II) Complexes in Catalytic Arylation of Functional Arenes, *J. Am. Chem. Soc.* **2011**, *133*, 10161-10170.

(219) Yu, S.; Tang, G.; Li, Y.; Zhou, X.; Lan, Y.; Li, X. Anthranil: An Aminating Reagent Leading to Bifunctionality for Both C(sp^3)−H and C(sp^2)−H under Rhodium(III) Catalysis, *Angew. Chem. Int. Ed.* **2016**, *55*, 8696–8700.

(220) Jiang, J.; Ramozzi, R.; Morokuma, K. Rh-III-Catalyzed C(sp^3)-H Bond Activation by an External Base Metalation/Deprotonation Mechanism: A Theoretical Study, *Chem. – Eur. J.* **2015**, *21*, 11158-11164.

(221) Liu, B.; Zhou, T.; Li, B.; Xu, S.; Song, H.; Wang, B. Rhodium(III)-Catalyzed Alkenylation Reactions of 8-Methylquinolines with Alkynes by C(sp^3)-H Activation, *Angew. Chem. Int. Ed.* **2014**, *53*, 4191-4195.

(222) Huang, X.; Wang, M.; Wang, L.; Wang, J. How Rhodium (III) Complexes Catalyze Alkenylation of C(sp^3)-H Bond of 8-Methyquinolines, *J. Organomet. Chem.* **2015**, *787*, 1-7.

(223) Gao, P.; Guo, W.; Xue, J.; Zhao, Y.; Yuan, Y.; Xia, Y.; Shi, Z. Iridium(III)-Catalyzed Direct Arylation of C–H Bonds with Diaryliodonium Salts, *J. Am. Chem. Soc.* **2015**, *137*, 12231-12240.

(224) Rahaman, S. M. W.; Dinda, S.; Sinha, A.; Bera, J. K. A Noninnocent Cyclooctadiene (COD) in the Reaction of an "Ir(COD)(OAc)" Precursor with Imidazolium Salts, *Organometallics* **2013**, *32*, 192-201.

(225) Raible, B.; Gierz, V.; Kunz, D. Identifying and Rationalizing the Conditions for the Isomerization of 1,5-Cyclooctadiene in Iridium Complexes by Experimental and Theoretical Mechanistic Studies, *Organometallics* **2015**, *34*, 2018-2027.

(226) Krüger, A.; Häller, L. J. L.; Müller-Bunz, H.; Serada, O.; Neels, A.; Macgregor, S. A.; Albrecht, M. Smooth C(Alkyl)-H Bond Activation in Rhodium Complexes Comprising Abnormal Carbene Ligands, *Dalton Trans.* **2011**, *40*, 9911-9920.

(227) Bischof, S. M.; Ess, D. H.; Meier, S. K.; Oxgaard, J.; Nielsen, R. J.; Bhalla, G.; Goddard, W. A., III; Periana, R. A. Benzene C-H Bond Activation in Carboxylic Acids Catalyzed by *O*-Donor Iridium(III) Complexes: An Experimental and Density Functional Study, *Organometallics* **2010**, *29*, 742-756.

(228) Webster-Gardiner, M. S.; Fu, R.; Fortman, G. C.; Nielsen, R. J.; Gunnoe, T. B.; Goddard, W. A., III Arene C-H Activation Using Rh(I) Catalysts Supported by Bidentate Nitrogen Chelates, *Catal. Sci. Tech.* **2015**, *5*, 96-100.

(229) Rhinehart, J. L.; Manbeck, K. A.; Buzak, S. K.; Lippa, G. M.; Brennessel, W. W.; Goldberg, K. I.; Jones, W. D. Catalytic Arene H/D Exchange with Novel Rhodium and Iridium Complexes, *Organometallics* **2012**, *31*, 1943-1952.

(230) García-Melchor, M.; Gorelsky, S. I.; Woo, T. K. Mechanistic Analysis of Iridium(III) Catalyzed Direct C-H Arylations: A DFT Study, *Chem. – Eur. J.* **2011**, *17*, 13847-13853.

(231) Davies, D. L.; Macgregor, S. A.; Poblador-Bahamonde, A. I. Computational Study of Ethene Hydroarylation at Ir(κ^2-OAc)(PMe_3)Cp, *Dalton Trans.* **2010**, *39*, 10520-10527.

(232) Young, K. J. H.; Oxgaard, J.; Ess, D. H.; Meier, S. K.; Stewart, T.; Goddard, I. I. I. W. A.; Periana, R. A. Experimental Realization of Catalytic CH_4 Hydroxylation Predicted for an Iridium NNC Pincer Complex, Demonstrating Thermal, Protic, and Oxidant Stability, *Chem. Commun.* **2009**, 3270-3272.

(233) Cross, W. B.; Razak, S.; Singh, K.; Warner, A. J. C(sp^3)-H Activation without a Directing Group: Regioselective Synthesis of *N*-Ylide or *N*-Heterocyclic Carbene Complexes Controlled by the Choice of Metal and Ligand, *Chem. – Eur. J.* **2014**, *20*, 13203-13209.

(234) Fu, R.; Nielsen, R. J.; Goddard, W. A., III; Fortman, G. C.; Gunnoe, T. B. DFT Virtual Screening Identifies Rhodium-Amidinate Complexes as Potential Homogeneous Catalysts for Methane-to-Methanol Oxidation, *ACS Catal.* **2014**, *4*, 4455-4465.

(235) Fu, R.; O'Reilly, M. E.; Nielsen, R. J.; Goddard, W. A., III; Gunnoe, T. B. Rhodium Bis(Quinolinyl)Benzene Complexes for Methane Activation and Functionalization, *Chem. – Eur. J.* **2015**, *21*, 1286-1293.

(236) O'Reilly, M. E.; Fu, R.; Nielsen, R. J.; Sabat, M.; Goddard, W. A., III; Gunnoe, T. B. Long-Range C-H Bond Activation by Rh-III-Carboxylates, *J. Am. Chem. Soc.* **2014**, *136*, 14690-14693.

(237) Zhou, M.; Johnson, S. I.; Gao, Y.; Emge, T. J.; Nielsen, R. J.; Goddard, W. A., III; Goldman, A. S. Activation and Oxidation of Mesitylene C-H Bonds by (Phebox)Iridium(III) Complexes, *Organometallics* **2015**, *34*, 2879-2888.

(238) Munz, D.; Webster-Gardiner, M.; Fu, R.; Strassner, T.; Goddard, W. A., III; Gunnoe, T. B. Proton or Metal? The H/D Exchange of Arenes in Acidic Solvents, *ACS Catal.* **2015**, *5*, 769-775.

(239) Ikemoto, H.; Yoshino, T.; Sakata, K.; Matsunaga, S.; Kanai, M. Pyrroloindolone Synthesis Via a Cp*Co-III-Catalyzed Redox-Neutral Directed C-H Alkenylation/Annulation Sequence, *J. Am. Chem. Soc.* **2014**, *136*, 5424-5431.

(240) Suzuki, Y.; Sun, B.; Sakata, K.; Yoshino, T.; Matsunaga, S.; Kanai, M. Dehydrative Direct C-H Allylation with Allylic Alcohols under Cp*Co-III Catalysis, *Angew. Chem. Int. Ed.* **2015**, *54*, 9944-9947.

(241) Guo, X.-K.; Zhang, L.-B.; Wei, D.; Niu, J.-L. Mechanistic Insights into Cobalt(II/III)-Catalyzed C-H Oxidation: A Combined Theoretical and Experimental Study, *Chem. Sci.* **2015**, *6*, 7059-7071.

(242) Mei, R.; Wang, H.; Warratz, S.; Macgregor, S. A.; Ackermann, L. Cobalt-Catalyzed Oxidase C-H/N-H Alkyne Annulation: Mechanistic Insights and Access to Anticancer Agents, *Chem. – Eur. J.* **2016**, *22*, 6759-6763.

(243) Sen, M.; Emayavaramban, B.; Barsu, N.; Premkumar, J. R.; Sundararaju, B. Cp*Co(III)-Catalyzed C(sp^3)-H Bond Activation: A Highly Stereoselective and Regioselective Alkenylation of 8-Methylquinoline with Alkynes, *ACS Catal.* **2016**, *6*, 2792-2796.

(244) Zell, D.; Warratz, S.; Gelman, D.; Garden, S. J.; Ackermann, L. Single-Component Phosphinous Acid Ruthenium(II) Catalysts for Versatile C−H Activation by Metal–Ligand Cooperation, *Chem. – Eur. J.* **2016**, *22*, 1248-1252.

(245) Ruiz, S.; Villuendas, P.; Ortuño, M. A.; Lledós, A.; Urriolabeitia, E. P. Ruthenium-Catalyzed Oxidative Coupling of Primary Amines with Internal Alkynes through C-H Bond Activation: Scope and Mechanistic Studies, *Chem. – Eur. J.* **2015**, *21*, 8626–8636.

(246) Wu, J.; Xu, W.; Yu, Z.-X.; Wang, J. Ruthenium-Catalyzed Formal Dehydrative 4+2 Cycloaddition of Enamides and Alkynes for the Synthesis of Highly Substituted Pyridines: Reaction Development and Mechanistic Study, *J. Am. Chem. Soc.* **2015**, *137*, 9489-9496.

(247) Leitch, J. A.; Wilson, P. B.; McMullin, C. L.; Mahon, M. F.; Bhonoah, Y.; Williams, I. H.; Frost, C. G. Ruthenium(II)-Catalyzed C–H Functionalization Using the Oxazolidinone Heterocycle as a Weakly Coordinating Directing Group: Experimental and Computational Insights, *ACS Catal.* **2016**, *6*, 5520-5529.

(248) Bettadapur, K. R.; Lanke, V.; Prabhu, K. R. Ru (II)-Catalyzed C-H Activation: Ketone-Directed Novel 1,4-Addition of Ortho C-H Bond to Maleimides, *Org. Lett.* **2015**, *17*, 4658-4661.

(249) Shan, C.; Luo, X.; Qi, X.; Liu, S.; Li, Y.; Lan, Y. Mechanism of Ruthenium-Catalyzed Direct Arylation of C-H Bonds in Aromatic Amides: A Computational Study, *Organometallics* **2016**, *35*, 1440-1445.

(250) Cannon, J. S.; Zou, L.; Liu, P.; Lan, Y.; O'Leary, D. J.; Houk, K. N.; Grubbs, R. H. Carboxylate-Assisted C(sp^3)–H Activation in Olefin Metathesis-Relevant Ruthenium Complexes, *J. Am. Chem. Soc.* **2014**, *136*, 6733-6743.

(251) Herbert, M. B.; Suslick, B. A.; Liu, P.; Zou, L.; Dornan, P. K.; Houk, K. N.; Grubbs, R. H. Cyclometalated *Z*-Selective Ruthenium Metathesis Catalysts with Modified *N*-Chelating Groups, *Organometallics* **2015**, *34*, 2858-2869.

(252) Liu, P.; Xu, X.; Dong, X.; Keitz, B. K.; Herbert, M. B.; Grubbs, R. H.; Houk, K. N. *Z*-Selectivity in Olefin Metathesis with Chelated Ru Catalysts: Computational Studies of Mechanism and Selectivity, *J. Am. Chem. Soc.* **2012**, *134*, 1464-1467.

(253) Stoychev, S. D.; Conifer, C. M.; Uhe, A.; Hölscher, M.; Leitner, W. A DFT Study of Ruthenium Pincer Carboxylate Complexes as Potential Catalysts for the Direct Carboxylation of Arenes with CO_2 - Meridional Versus Facial Coordination, *Dalton Trans.* **2014**, *43*, 11180-11189.

(254) Uhe, A.; Hölscher, M.; Leitner, W. Carboxylation of Arene C-H Bonds with CO_2: A DFT-Based Approach to Catalyst Design, *Chem. – Eur. J.* **2012**, *18*, 170-177.

(255) Johnson, D. G.; Lynam, J. M.; Slattery, J. M.; Welby, C. E. Insights into the Intramolecular Acetate-Mediated Formation of Ruthenium Vinylidene Complexes: A Ligand-Assisted Proton Shuttle (LAPS) Mechanism, *Dalton Trans.* **2010**, *39*, 10432-10441.

(256) Young, K. J. H.; Lokare, K. S.; Leung, C. H.; Cheng, M.-J.; Nielsen, R. J.; Petasis, N. A.; Goddard, W. A., III; Periana, R. A. Synthesis of Osmium and Ruthenium Complexes Bearing Dimethyl (S,S)-2,2 '-(Pyridine-2,6-Diyl)-Bis-(4,5-Dihydrooxazol-4-Carboxylate) Ligand and Application to Catalytic H/D Exchange, *J. Mol. Cat. A* **2011**, *339*, 17-23.

(257) Gustafson, S. J.; Fuller, J. T.; Devarajan, D.; Snyder, J.; Periana, R. A.; Hashiguchi, B. G.; Konnick, M. M.; Ess, D. H. Contrasting Mechanisms and Reactivity of Tl(III), Hg(II), and Co(III) for Alkane C–H Functionalization, *Organometallics* **2015**, *34*, 5485-5495.

(258) Hashiguchi, B. G.; Konnick, M. M.; Bischof, S. M.; Gustafson, S. J.; Devarajan, D.; Gunsalus, N.; Ess, D. H.; Periana, R. A. Main-Group Compounds Selectively Oxidize Mixtures of Methane, Ethane, and Propane to Alcohol Esters, *Science* **2014**, *343*, 1232-1237.

(259) Grimme, S.; Schreiner, P. R. Steric Crowding Can Stabilize a Labile Molecule: Solving the Hexaphenylethane Riddle, *Angew. Chem. Int. Ed.* **2011**, *50*, 12639-12642.

(260) Simmons, E. M.; Hartwig, J. F. On the Interpretation of Deuterium Kinetic Isotope Effects in C-H Bond Functionalizations by Transition-Metal Complexes, *Angew. Chem. Int. Ed.* **2012**, *51*, 3066-3072.

(261) Vidossich, P.; Lledos, A.; Ujaque, G. First-Principles Molecular Dynamics Studies of Organometallic Complexes and Homogeneous Catalytic Processes, *Acc. Chem. Res.* **2016**, *49*, 1271-1278.

(262) Vidossich, P.; Lledos, A.; Ujaque, G. Realistic Simulation of Organometallic Reactivity in Solution by Means of First-Principles Molecular Dynamics, *Struct. Bond.* **2016**, *167*, 81-106.

Biographies

David (Dai) Davies completed his undergraduate (1980) and postgraduate studies (1984) at Bristol University working with Prof S.A.R. Knox and was then a NATO postdoctoral fellow at Caltech with Prof J. E. Bercaw. He was appointed to a lectureship at the University of Leicester in 1985, was promoted to senior lecturer in 1999 to Reader in 2007 and full Professor in 2013. His research interests are across a broad range of chemistry including (i) C-H activation and functionalisation particularly from a mechanistic viewpoint (ii) synthesis and applications of luminescent organometallic complexes; (iii) development of new ionic liquids and deep eutectic solvents. Much of his work has involved close collaboration with computational chemists which have contributed significantly to his understanding.

Stuart A. Macgregor completed his undergraduate (1988) and postgraduate studies (1992) at the University of Edinburgh, the latter working with Lesley Yellowlees and Alan Welch on the structural and electrochemical properties of metallaboranes. He was awarded a NATO Western European Fellowship to work with Odile Eisenstein at the Université de Paris-Sud in Orsay, near Paris, where he first encountered density functional theory. He then spent two years at the Australian National University before returning to Edinburgh in 1997 to take up a Lectureship at Heriot-Watt University in 1997. He was promoted to Reader in 2006 and full Professor in 2009 and served as Head of the Institute of Chemical Sciences from 2010 to 2014. His research uses computational chemistry to model the chemical structure and reactivity of transition metal systems, with an emphasis on challenging or unusual bond activation processes and how such reactions can contribute to homogeneous catalysis and metal-mediated organic synthesis. His work is performed in close collaboration with experimentalists.

Claire L. McMullin completed her undergraduate degree at the University of Bristol in 2007, spending her Erasmus year at Universität Heidelberg. She continued her postgraduate studies at the University of Bristol, focusing on using computational chemistry to investigate reaction mechanisms

and crystallography under the guidance of Natalie Fey and Guy Orpen. After spending a year in America working with Tom Cundari at the University of North Texas investigating a range of organometallic systems with DFT methods, Claire returned to the UK in 2012 to work with Stuart Macgregor and Dai Davies on the C-H functionalization of phenyl-pyrazoles. Since 2015, Claire is the computational teaching fellow at the University of Bath.

Table of contents (TOC) graphic: